The characteristic based split (CBS) scheme for laminar and turbulent incompressible flow simulations.

Liu, Chun-Bin

The Characteristic Based Split (CBS) scheme for laminar and turbulent incompressible flow simulations

Chun-Bin Liu

Thesis submitted to the University of Wales Swansea
in candidature for the degree of Doctor of Philosophy

September 2005

Civil and Computational Engineering Centre
School of Engineering
University of Wales Swansea
Singleton Park, Swansea SA2 8PP
Wales, United Kingdom

APPENDIX 3 : Specimen Layout for Declaration/Statements page to be included in Higher Degree Theses

DECLARATION

This work has not previously been accepted in substance for any degree and is not being concurrently submitted in candidature for any degree.

Signed .... (candidate)

Date ....28/09/2005..

STATEMENT 1

This thesis is the result of my own investigations, except where otherwise stated.

Other sources are acknowledged by footnotes giving explicit references. A bibliography is appended.

Signed .... (candidate)

Date ....28/09/2005..

STATEMENT 2

I hereby give consent for my thesis, if accepted, to be available for photocopying and for inter-library loan, and for the title and summary to be made available to outside organisations.

Signed .... (candidate)

Date ....28/09/2005..

Contents

List of Figures

List of Tables

Acknowledgments

I express my sincere and deep gratitude to my supervisor Dr. P. Nithiarasu for his support, advice and constructive criticism during the course of this work.

I am also grateful to all the staff of the School of Engineering of University of Wales Swansea for their help.

Words of thanks would fail to express my indebtedness to H.-W. Lin. She has always been a great girlfriend and unfailing support.

Last but not least, thanks to my parents. What I have accomplished in life is the result of their unconditional love and years of sacrifice.

Nomenclature

Upper-case Roman

A	total area of a linear triangular element
A^i	triangle formed by an arbitrary point in the element ($i = 1,2,3$ nodes)
$\mathbf{B}$	3×6 (2-dimensional) or 6×12 (3-dimensional) matrix of strain shape function
C_D	constant turbulence lengthscale
$\mathbf{C_u}$	6×6 (2-dimensional) or 12×12 (3-dimensional) matrix of reducible continuity
$\left[C_u^{i,j}\right]$	coefficients of $\mathbf{C_u}$ matrix (i row; j column)
$\mathbf{C}_{\mathbf{u}\kappa}$	6×6 (2-dimensional) or 12×12 (3-dimensional) matrix of the isotropic turbulence for the intermediate momentum
$\left[C_{u\kappa}^{i,j}\right]$	coefficients of $\mathbf{C}_{\mathbf{u}\kappa}$ matrix (i row; j column)
$\mathbf{C}_\kappa$	3×3 (2-dimensional) or 4×4 (3-dimensional) matrix of $\tilde{\mathbf{K}}$ being transported by the velocity in a convective action
$\left[C_\kappa^{i,j}\right]$	coefficients of $\mathbf{C}_\kappa$ matrix (i row; j column)
$\mathbf{C}_\varepsilon$	3×3 (2-dimensional) or 4×4 (3-dimensional) matrix of $\tilde{\mathbf{E}}$ being transported by the velocity in a convective action
$\left[C_\varepsilon^{i,j}\right]$	coefficients of $\mathbf{C}_\varepsilon$ matrix (i row; j column)
$\mathbf{C}_{\tilde{\nu}}$	3×3 (2-dimensional) or 4×4 (3-dimensional) matrix of $\tilde{\tilde{\nu}}$ being transported by the velocity in a convective action
$\left[C_{\tilde{\nu}}^{i,j}\right]$	coefficients of $\mathbf{C}_{\tilde{\nu}}$ matrix (i row; j column)
D	diameter of the circular cylinder
E_{u_i}	error magnitude of velocity
E_p	error magnitude of pressure
E_i^κ	energy flux of the turbulent kinetic energy equation
E_i^ε	energy flux of the isotropic dissipation rate equation

$\mathbf{E}$	symmetric matrix $= \mathbf{G}\mathbf{M}_u^{-1}\mathbf{G}^{\mathrm{T}} - \iota\mathbf{H}$
$\tilde{\mathbf{E}}$	3×1 (2-dimensional) or 4×1 (3-dimensional) vector of nodal '$\varepsilon\rho$'
G	gravitational potential
G_{ij}	shear stress generation of transport $\overline{u_i'u_j'}$ equation
$\mathbf{G}$	3×6 (2-dimensional) or 4×12 (3-dimensional) gradient operator matrix
$\left[G^{i,j}\right]$	coefficients of $\mathbf{G}$ matrix (i row; j column)
$\mathbf{H}$	3×3 (2-dimensional) or 4×4 (3-dimensional) symmetric matrix for the pressure equation in step2
$\left[H^{i,j}\right]$	coefficients of $\mathbf{H}$ matrix (i row; j column)
$\mathbf{I_o}$	diagonal matrix for a linear (newtonian) isotropic fluid
$\mathbf{J}$	Jacobian matrix of transformation
K	turbulent kinetic energy times density $= \kappa\rho$
$\tilde{\mathbf{K}}$	3×1 (2-dimensional) or 4×1 (3-dimensional) vector of nodal '$\kappa\rho$'
$\mathbf{K_u}$	6×6 (2-dimensional) or 12×12 (3-dimensional) symmetric matrix of the characteristic-Galerkin stabilizing term for the intermediate momentum
$\left[K_u^{i,j}\right]$	coefficients of $\mathbf{K_u}$ matrix (i row; j column)
$\mathbf{K}_\tau$	6×6 (2-dimensional) or 12×12 (3-dimensional) symmetric, viscous diffusion matrix for the intermediate momentum
$\left[K_\tau^{i,j}\right]$	coefficients of $\mathbf{K}_\tau$ matrix (i row; j column)
$\mathbf{K}_\kappa$	3×3 (2-dimensional) or 4×4 (3-dimensional) symmetric, viscous diffusion matrix for the transport equation of turbulent kinetic energy
$\left[K_\kappa^{i,j}\right]$	coefficients of $\mathbf{K}_\kappa$ matrix (i row; j column)
$\mathbf{K}_{\mathbf{u}\kappa}$	3×3 (2-dimensional) or 4×4 (3-dimensional) symmetric matrix of the characteristic-Galerkin stabilizing term for the transport equation of turbulent kinetic energy
$\left[K_{u\kappa}^{i,j}\right]$	coefficients of $\mathbf{K}_{\mathbf{u}\kappa}$ matrix (i row; j column)
$\mathbf{K}_\varepsilon$	3×3 (2-dimensional) or 4×4 (3-dimensional) symmetric, viscous diffusion matrix for the transport equation of dissipation rate
$\left[K_\varepsilon^{i,j}\right]$	coefficients of $\mathbf{K}_\varepsilon$ matrix (i row; j column)

$\mathbf{K_{u\varepsilon}}$ 3 × 3 (2-dimensional) or 4 × 4 (3-dimensional) symmetric matrix of the characteristic-Galerkin stabilizing term for the transport equation of dissipation rate

$\left[K_{u\varepsilon}^{i,j}\right]$ coefficients of $\mathbf{K_{u\varepsilon}}$ matrix (i row; j column)

$\mathbf{K}_{\hat{\nu}}$ 3 × 3 (2-dimensional) or 4 × 4 (3-dimensional) symmetric, viscous diffusion matrix for the modified turbulent eddy kinematic viscosity

$\left[K_{\hat{\nu}}^{i,j}\right]$ coefficients of $\mathbf{K}_{\hat{\nu}}$ matrix (i row; j column)

$\mathbf{K}_{\mathbf{u}\hat{\nu}}$ 3 × 3 (2-dimensional) or 4 × 4 (3-dimensional) symmetric matrix of the characteristic-Galerkin stabilizing term for the modified turbulent eddy kinematic viscosity

$\left[K_{u\hat{\nu}}^{i,j}\right]$ coefficients of $\mathbf{K}_{\mathbf{u}\hat{\nu}}$ matrix (i row; j column)

L reference length

L lengthscale of the turbulence

L^i non-dimensional area coordinates ($i = 1, 2, 3$ nodes)

M^i non-dimensional volume coordinates ($i = 1, ..., 4$ nodes)

$\mathbf{M_u}$ 6 × 6 (2-dimensional) or 12 × 12 (3-dimensional) lumped symmetric matrix for the velocity

$\left[M_u^{i,j}\right]$ coefficients of $\mathbf{M_u}$ matrix (i row; j column)

$\mathbf{M_p}$ 3 × 3 (2-dimensional) or 4 × 4 (3-dimensional) lumped symmetric matrix for the pressure

$\left[M_p^{i,j}\right]$ coefficients of $\mathbf{M_p}$ matrix (i row; j column)

$\mathbf{M}_\kappa$ 3 × 3 (2-dimensional) or 4 × 4 (3-dimensional) lumped symmetric matrix for the turbulent kinetic energy

$\left[M_\kappa^{i,j}\right]$ coefficients of $\mathbf{M}_\kappa$ matrix (i row; j column)

$\mathbf{M}_\varepsilon$ 3 × 3 (2-dimensional) or 4 × 4 (3-dimensional) lumped symmetric matrix for the dissipation rate

$\left[M_\varepsilon^{i,j}\right]$ coefficients of $\mathbf{M}_\varepsilon$ matrix (i row; j column)

$\mathbf{M}_{\hat{\nu}}$ 3 × 3 (2-dimensional) or 4 × 4 (3-dimensional) lumped symmetric matrix for the modified turbulent eddy kinematic viscosity

$\left[M_{\hat{\nu}}^{i,j}\right]$	coefficients of $\mathbf{M}_{\hat{\nu}}$ matrix (i row; j column)
N^i	shape functions ($i = 1, ..., 4$ nodes)
$\mathbf{N_p}$	1×3 (2-dimensional) or 1×4 (3-dimensional) vector of shape functions for the pressure
$\mathbf{N_u}$	2×6 (2-dimensional) or 3×12 (3-dimensional) matrix of shape functions for the velocity
$\mathbf{N}_\kappa$	1×3 (2-dimensional) or 1×4 (3-dimensional) vector of shape functions for the turbulent kinetic energy
$\mathbf{N}_\varepsilon$	1×3 (2-dimensional) or 1×4 (3-dimensional) vector of shape functions for the dissipation rate
$\mathbf{N}_{\hat{\nu}}$	1×3 (2-dimensional) or 1×4 (3-dimensional) vector of shape functions for the modified turbulent eddy kinematic viscosity
P	pressure
P_{ij}	production of turbulent kinetic energy
$\tilde{\mathbf{P}}$	3×1 (2-dimensional) or 4×1 (3-dimensional) vector of nodal pressures
Q	source/reaction term of the convection-diffusion equation
R_κ, R_t	turbulent Reynolds numbers
Re	Reynolds number
S	magnitude of the vorticity
S_{ij}	mean strain-rate tensor
$\tilde{S}$	dimensionless strain parameter
$\hat{S}$	function for using the Spalart-Allmaras model
$\mathbf{S}$	strain matrix operator
T	time interval
U_j	momentum of fluid particles per unit volume $= \rho u_j$ ($j = 1, 2, 3$ directions)
U_o	characteristic velocity scale of the largest eddy
$U_j^\star$	intermediate auxiliary variable ($j = 1, 2, 3$ directions)
$\tilde{\mathbf{U}}_\mathbf{j}$	vector of nodal U_j ($j = 1, 2, 3$ directions)
$\tilde{\mathbf{U}}$	6×1 (2-dimensional) or 12×1 (3-dimensional) vector of nodal

	momentum per unit volume
V	total volume of a linear tetrahedral element
V^i	tetrahedron formed by an arbitrary point in the element ($i = 1, ..., 4$ nodes)
X	normalized viscosity

Lower-case Roman

b_{ij}	normalized Reynolds stress anisotropy tensor
c	speed of sound
c_1, c_2, c_3	constants for the non-linear $\kappa - \varepsilon$ model
c_{b1}, c_{b2}	constants for the Spalart-Allmaras model
c_{w1}	function for the Spalart-Allmaras model
c_{w2}, c_{w3}	constants for the Spalart-Allmaras model
$c_{\hat{\nu}1}$	constants for the Spalart-Allmaras model
c_μ	constant for the turbulent eddy kinematic viscosity
c_ε, $c_{\varepsilon1}$, $c_{\varepsilon2}$, $c_{\varepsilon3}$	constants for the dissipation rate equation
d^t_{ij}	turbulent stress diffusion of transport $\overline{u'_i u'_j}$ equation
d^ν_{ij}	viscous diffusion of transport $\overline{u'_i u'_j}$ equation
e	reference artificial compressibility parameter
$\|e\|_{L_2}$	L_2 norm of velocity residual by root mean square (RMS) errors
f_j	body force ($j = 1, 2, 3$ directions)
f_b	near wall function
$f_{\varepsilon1}$, $f_{\varepsilon2}$	wall damping functions for the production and source terms of the dissipation rate equation
f_μ	wall damping function for the turbulent eddy kinematic viscosity
f_w	near-wall damping function
$f_{\hat{\nu}1}$, $f_{\hat{\nu}2}$	functions used in the Spalart-Allmaras model
$\mathbf{f}_1$, $\mathbf{f}_2$	vectors from the forcing terms
$\mathbf{f_u}$	6×1 (2-dimensional) or 12×1 (3-dimensional) vector of the deviatoric shear stresses

$\left[f_u^{i,j}\right]$	coefficients of $\mathbf{f_u}$ vector (i row; j column)
$\mathbf{f_p}$	3×1 (2-dimensional) or 4×1 (3-dimensional) vector of the pressure
$\left[f_p^{i,j}\right]$	coefficients of $\mathbf{f_p}$ vector (i row; j column) including Dirichlet boundary condition
$\mathbf{f}_{\kappa\boldsymbol{\Omega}}$	3×1 (2-dimensional) or 4×1 (3-dimensional) vector of generation and source terms of the turbulent kinetic energy equation
$\left[f_{\kappa\Omega}^{i,j}\right]$	coefficients of $\mathbf{f}_{\kappa\boldsymbol{\Omega}}$ vector (i row; j column)
$\mathbf{f}_{\kappa\boldsymbol{\Gamma}}$	3×1 (2-dimensional) or 4×1 (3-dimensional) forcing vector of the turbulent kinetic energy equation
$\left[f_{\kappa\Gamma}^{i,j}\right]$	coefficients of $\mathbf{f}_{\kappa\boldsymbol{\Gamma}}$ vector (i row; j column)
$\mathbf{f}_{\hat{\nu}\boldsymbol{\Omega}}$	3×1 (2-dimensional) or 4×1 (3-dimensional) vector of second diffusion term in the modified turbulent eddy kinematic viscosity equation
$\left[f_{\hat{\nu}\Omega}^{i,j}\right]$	coefficients of $\mathbf{f}_{\hat{\nu}\boldsymbol{\Omega}}$ vector (i row; j column)
$\mathbf{f}_{\hat{\nu}\boldsymbol{\Omega}^*}$	3×1 (2-dimensional) or 4×1 (3-dimensional) vector of production and destruction terms of the modified turbulent eddy kinematic viscosity equation
$\left[f_{\hat{\nu}\Omega^*}^{i,j}\right]$	coefficients of $\mathbf{f}_{\hat{\nu}\boldsymbol{\Omega}^*}$ vector (i row; j column)
$\mathbf{f}_{\hat{\nu}\boldsymbol{\Gamma}}$	3×1 (2-dimensional) or 4×1 (3-dimensional) forcing vector of the modified turbulent eddy kinematic viscosity equation
$\left[f_{\hat{\nu}\Gamma}^{i,j}\right]$	coefficients of $\mathbf{f}_{\hat{\nu}\boldsymbol{\Gamma}}$ vector (i row; j column)
g	function for the Spalart-Allmaras model
h	local element size
l_m	mixing length
l^s	lengthscale
l_o	characteristic lengthscale of the largest eddy
$\mathbf{m}$	two- or three-dimensional strain/stress vectors
$\mathbf{n}$	components of the outward normal to the boundaries
n_i	outward normal to boundary ($i = 1, 2, 3$ directions)

p	modified pressure
$\bar{p}$	mean (time-averaged) modified pressure
$\bar{p}^*$	dimensionless mean (time-averaged) modified pressure
$\tilde{\mathbf{p}}$	3×1 (2-dimensional) or 4×1 (3-dimensional) vector of nodal pressure
p'	fluctuating modified pressure
r	function for the Spalart-Allmaras model
t	time
t^*	dimensionless time
t_{ref}	time of the reference particle
$\mathbf{t_d}$	2×1 (2-dimensional) or 3×1 (3-dimensional) vector of interface traction corresponding to the deviatoric stresses
$\mathbf{t_p}$	interface traction corresponding to the pressure
u	characteristic velocity
u^s	velocity scale
u^+	mean velocity normalized by the friction velocity $\equiv \bar{u}_1/u_\tau$
u_∞	free stream velocity
u_τ	friction velocity $= \sqrt{\tau_w/\rho}$
u_i	velocity components ($i = 1, 2, 3$ directions)
$\bar{u}_i$	mean (time-averaged) velocity ($i = 1, 2, 3$ directions)
$\bar{u}_i^*$	dimensionless mean (time-averaged) velocity ($i = 1, 2, 3$ directions)
$\overline{u_i'u_j'}$	Reynolds stresses ($i = 1, 2, 3$ and $j = 1, 2, 3$ directions)
u'_i	fluctuating velocity ($i = 1, 2, 3$ directions)
$\breve{u}_i$	average value of u_i along the characteristics ($j = 1, 2, 3$ directions)
$\tilde{\mathbf{u}}_\mathbf{j}$	vector of nodal velocities ($j = 1, 2, 3$ directions)
$\tilde{\mathbf{u}}$	6×1 (2-dimensional) or 12×1 (3-dimensional) vector of nodal velocities
v_{conv}	convective velocity
v_{diff}	diffusive velocity
w	weighting function
x_i	Cartesian coordinates ($i = 1, 2, 3$ directions)

x_1^i, x_2^i, x_3^i	global Cartesian coordinates ($i = 1, ..., 4$ nodes)
x_i^*	dimensionless Cartesian coordinates ($i = 1, 2, 3$ directions)
$\hat{x}_i$	characteristic direction ($i = 1, 2, 3$ directions)
y	distance from the nearest wall
y^+	dimensionless distance from the wall normalized by the viscous lengthscale $\equiv x_2/\delta_\nu = u_\tau x_2/\nu$

Upper-case Greek

Γ	boundary of the domain Ω
ΔE	E quantity between levels $n+1$ and n
ΔK	K quantity between levels $n+1$ and n
Δp	pressure between levels $n+1$ and n
$\Delta\tilde{\mathbf{p}}$	3×1 (2-dimensional) or 4×1 (3-dimensional) vector of nodal pressure between levels $n+1$ and n
Δt	local (or pseudo) time step between levels $n+1$ and n
Δt_{conv}	(local) time step calculation using convective velocity
Δt_{diff}	(local) time step calculation using diffusive velocity
Δt_{temp}	external (local) time step calculation for temporal stability
Δt_{spat}	internal (local) time step calculation for spatial stability
$\Delta U_j^\star$	intermediate impulse per unit volume $= U_j^\star - U_j^n$ ($j = 1, 2, 3$ directions)
ΔU_j^τ	impulse per unit volume between levels $n+1$ and n ($j = 1, 2, 3$ directions) based on the real time step
ΔU_j	impulse per unit volume between levels $n+1$ and n ($j = 1, 2, 3$ directions)
$\Delta\tilde{\mathbf{U}}_\mathbf{j}^\star$	vector of nodal $\Delta U_j^\star$ ($j = 1, 2, 3$ directions)
$\Delta\tilde{\mathbf{U}}^\star$	6×1 (2-dimensional) or 12×1 (3-dimensional) vector of nodal $\mathbf{\Delta U}^\star$
$\Delta\tilde{\mathbf{U}}_\mathbf{j}$	vector of nodal ΔU_j between levels $n+1$ and n ($j = 1, 2, 3$ directions)
$\Delta\tilde{\mathbf{U}}$	6×1 (2-dimensional) or 12×1 (3-dimensional) vector of nodal $\mathbf{\Delta U}$ between levels $n+1$ and n
$\Delta\tilde{\mathbf{U}}^\tau$	6×1 (2-dimensional) or 12×1 (3-dimensional) vector of nodal $\mathbf{\Delta U}^\tau$

	for real time
$\Delta\hat{\nu}$	modified turbulence viscosity between levels $n+1$ and n
$\Delta\tau$	real time step between levels $n+1$ and n
$\Delta\phi$	scalar-dependent variable between levels $n+1$ and n
Λ	limited condition number of preconditioned conjugate gradient
Ξ_1, Ξ_2, ..., Ξ_7	the constitutive stress/vorticity terms of the cubic formulation
Π_{ij}	second-order closure function
Φ_{ij}	pressure-strain correlation of transport $\overline{u_i'u_j'}$ equation
Ψ	penalty function
Ω	any problem domain
$\tilde{\Omega}$	dimensionless vorticity parameter
Ω_{ij}, $\hat{\Omega}_{ij}$	mean vorticity tensor

Lower-case Greek

α_1, α_2, ..., α_7	coefficients of the constitutive stress/vorticity terms of the cubic form
α_{ijkl}	fourth rank tensor
α	diffusion coefficient
β	artificial compressibility parameter
γ_1, γ_2, ..., γ_7	coefficients of Π_{ij} form
δ	distance travelled by the particle
δ_ν	viscous lengthscale $= \nu/u_\tau$
δ_{ij}	Kronecker delta
ϵ	scalar turbulent dissipation rate $= \varepsilon_{ii}/2$
ε	isotropic dissipation rate of the turbulent kinetic energy
ε^*	dimensionless isotropic dissipation rate of the turbulent kinetic energy
$\tilde{\varepsilon}$	vector of nodal ε
ε_{ij}	dissipative correlation of second-rank tensor of transport $\overline{u_i'u_j'}$ equation
ε_{ii}	scalar turbulent dissipation rate
ε_{ij}^D	deviatoric of ε_{ij}

ζ	non-dimensional local coordinates system
η	non-dimensional local coordinates system
θ, θ_1, θ_2	parameters for different schemes (eg. explicit, semi-implicit or implicit)
ι	ratio of Δt_{spat} to Δt_{temp}
κ	(scalar) turbulent kinetic energy $= \overline{u'_j u'_j}/2$
κ^*	dimensionless turbulent kinetic energy
$\tilde{\kappa}$	vector of nodal κ
λ_{min}, λ_{max}	the smallest and largest eigenvalues
ϑ_1, ϑ_2, ϑ_3	scalar function of the general isotropic tensor of rank four
μ	dynamic viscosity
μ^*	dimensionless dynamic viscosity
μ_t	turbulent eddy dynamic viscosity
μ_t^*	dimensionless turbulent eddy dynamic viscosity
ν	kinematic viscosity
ν_t	turbulent eddy kinematic viscosity
$\hat{\nu}$	modified turbulent eddy kinematic viscosity
$\hat{\nu}^*$	dimensionless modified turbulent eddy kinematic viscosity
$\tilde{\hat{\nu}}$	vector of nodal $\hat{\nu}$
ξ	non-dimensional local coordinates system
ρ	density
$\bar{\rho}$	mean (time-averaged) density
ρ'	fluctuating density
ρ_∞	free stream density
ρ^*	dimensionless density
σ_{vn}	von Neumann number
$\sigma_{v\kappa}$	von Kármán number
σ_κ	diffusion Prandtl number for the turbulent kinetic energy
σ_ε	diffusion Prandtl number for the dissipation rate of the turbulence energy
$\sigma_{\hat{\nu}}$	diffusion Prandtl number for the modified turbulent kinematic viscosity

τ	turbulence timescale $=\varepsilon/\kappa$
τ_o	characteristic timescale of the largest eddy
τ_{ij}	viscous shear stress tensor
τ_{ij}^*	dimensionless viscous shear stress tensor
τ_{ij}^R	Reynolds stresses $\equiv -\rho\overline{u_i'u_j'}$
τ_{ij}^{R*}	dimensionless Reynolds stresses
τ_w	wall shear stress
ϕ	scalar-dependent variable
ψ_i	instantaneous quantities
$\bar{\psi}_i$	mean (time-averaged) quantities
ψ_i'	random quantities
ω	turbulence frequency $= \kappa/\varepsilon$

Symbols

$conv$	convection
$diff$	diffusion
$temp$	temporal
$spat$	spatial
max	maximum
min	minimum
∂_i	partial differentiation with respect to x_i ($i = 1, 2, 3$ directions)
$det(\mathbf{J})$	determinant of $\mathbf{J}$
∇	gradient operator $\equiv \mathbf{e}_i\partial_i$ in which $\mathbf{e}_i$ is a unit vector
∇^T	divergence operator
∇^2	Laplacian operator $= \nabla \cdot \nabla = \delta_{ij}\partial_i\partial_j$

Subscripts

ie	number of the local element
ip	number of the node

n	n time step level or iteration level
$n+(1/2)$	$n+(1/2)$ time step level or iteration level
$n+1$	$n+1$ time step level or iteration level

Superscripts

m	real time step level
n	n time step level or iteration level
$n+(1/2)$	$n+(1/2)$ time step level or iteration level
$n+1$	$n+1$ time step level or iteration level
$n-1$	$n-1$ time step level or iteration level

Summary

In this thesis, the matrix free Characteristic Based Split (**CBS**) scheme based on an artificial compressibility (**AC**) method and the semi-implicit CBS scheme are presented for laminar and turbulent incompressible flows. Numerical simulations of steady and unsteady state incompressible flow problems have been carried out on structured and unstructured meshes of linear triangular and tetrahedral elements. The standard Galerkin method was used for spatial discretization of the governing equations in their semi-discrete CBS form. Four different Reynolds average Navier-Stokes (**RANS**) turbulence models have been studied in detail. They are the one-equation linear $\kappa - l$ model of Wolfshtein, the one-equation Spalart-Allmaras model, the two-equation linear $\kappa - \varepsilon$ model with two different low Reynolds number treatments (Lam-Bremhorst damping functions and Fan-Lakshminarayana-Barnett damping functions), and the two-equation nonlinear near-wall $\kappa - \varepsilon$ model with Kimura-Hosoda's parameters. The results of standard steady flow in a channel, inside a lid-driven cavity, over a backward facing step, around a stationary sphere and through an upper human airway are adequately predicted. In addition to steady state flow problems, unsteady Reynolds-averaged Navier-Stokes (**URANS**) model was employed to solve vortex shedding behind a circular cylinder using a dual-time stepping technique. The two- and three-dimensional results presented show that both the CBS-AC matrix free procedure and semi-implicit CBS formulation are accurate and efficient.

Chapter 1

Introduction

1.1 General remarks on the CBS scheme

It is well known that generally direct finite element formulations without any stabilization may result in violent oscillations if employed to solve incompressible flow equations. The instability due to the non-linear convective acceleration terms, which make the fluid mechanics equations non-self-adjoint, leads to a system of non-symmetric equations. Unless the velocity is very small, for instance creeping flows, spatial oscillations due to central-type spatial discretization of convective acceleration will occur. Thus the spatial discretization derived by the standard Galerkin method (or Bubnov-Galerkin method) [1, 2]–the shape functions are used as weighting–is not valid here though this gives minimum error in the energy and the L_2 norms for self-adjoint problems. On the other hand, the incompressible limit, Ladyshenskaya-Babuška-Brezzi (**LBB**) conditions [3, 4, 5], introduces instability if equal order interpolations for velocity and pressure are used. Therefore, use of simple linear triangular elements result in highly oscillatory solutions when the viscous flows of incompressible fluids is solved using equal order interpolations [6]. The violation of this condition often results in numerically unphysical oscillations in the pressure field. However, second order terms introduced into the discrete governing equations ensures that stable solution is obtained in this study.

There are several stable approximations available to deal with the steady-state situations which reduce/eliminate oscillations resulted from standard discretization of convective acceleration terms. For the steady-state convection-diffusion equation with a scalar variable, generally treatments include the Streamline Upwind Petrov-Galerkin (**SUPG**) method [7], the Galerkin Least Squares (**GLS**) method [8, 9], the Finite Increment Calculus (**FIC**) method [10] and the Subgrid Scale (**SGS**) method [11]. The methods available to stabilize oscillation via transient formulation include the Characteristic-Galerkin (**CG**) method [12, 13, 14, 15, 16] and the Taylor-Galerkin (**TG**) method [17, 18]. In this study, the CG procedure is employed to solve the Navier-Stokes equations and the Reynolds average Navier-Stokes (**RANS**) equations.

The SUPG approximation can be employed by taking the weighting functions different from the interpolation (shape) functions. This non-standard weighting in the discrete form was to introduce consistent stabilization to solve convection dominated problems. The Galerkin process based on a least square residual minimization also permits non-self adjoint operators to be treated. The process of adding the higher order terms via the GLS formulation can stabilize oscillations. Indeed the concept of the extra terms are often known as 'artificial or balancing diffusion'. The FIC procedure directly obtains the balancing diffusion in the governing differential equations via higher-order approximations using Taylor series.

In this thesis a combination of time discretization in the characteristic direction along with standard Galerkin spatial approximation is used to deal with incompressible flow equations. Its derivation involves a Taylor series expansion in a semi-discrete system along the problem characteristics to obtain second order accuracy in time. The extra higher order terms can either be derived in conservation or non-conservation form for any scalar convected quantity. The TG scheme gives similar form of convection stabilization for scalar convection-diffusion problems. The TG method is the finite element counterpart of the Lax-Wendroff type [19] developed in the finite difference context.

In order to circumvent unphysical pressure oscillation, the development of stable procedures in which the LBB condition is stabilized have been proposed and being widely used [6]. The Characteristic Based Split (**CBS**) algorithm [13, 15, 16] based on firstly removing all the pressure gradient terms from the Navier-Stokes equations leads to a non-singular solution for any interpolating shape functions used for velocity and pressure. In the second step, the pressure is obtained from the continuity equation and finally the intermediate velocity variables obtained from the first step are corrected to get the final velocity values.

For the solution of both compressible and incompressible flows, CBS scheme was initially presented by Zienkiewicz and Codina [13]. Also, CBS scheme has been extended to investigate other applications, for example solid dynamics [20], shallow water flows [16, 21], thermal and porous medium flows [16, 22, 23, 24, 25]. However, recently it has been combined with the standard Artificial Compressibility (**AC**) method [26] to obtain an efficient and accurate explicit matrix free procedure [27, 28].

Such a matrix free CBS-AC scheme, via a dual time stepping technique [27, 29] gives a transient numerical solution for unsteady flow problems. This method has been implemented to solve turbulent incompressible flows using RANS and unsteady RANS (**URANS**) in this thesis. Several articles have been published on the artificial compressibility formulation for turbulent flow calculations in the past [30]-[49]. It is noticed that all the referred papers use either finite difference or finite volume method for spatial discretization and many of reported studies use additional dissipation model to get a stable pressure solution.

The semi-implicit CBS scheme, which requires a matrix solution procedure [6], [50]-[53] for the implicit solution of the pressure Poisson equation, has also been implemented along with one of the RANS models.

1.2 Strategies of turbulence modelling and simulations

In the study of turbulent flows, one of the first methods that was designed for directly solving the time-dependent Navier-Stokes equations is called Direct Numerical Simulation (**DNS**) by which all the relevant scales are resolved without any turbulence model equation or averaged variable. For the high-Reynolds-number flows, the DNS method is intractable to resolve all lengthscales and timescales between the largest and smallest range in the turbulent velocity field. Thus, the Large Eddy Simulation (**LES**) approach in which the filtering operation and the space-averaged equation of fluid flow is the alternative. The effect of the larger and easily-resolvable scales on the turbulent motions are computed by LES procedures using the Smagorinsky SGS stress model [54, 55], the dynamic SGS eddy viscosity model [56, 57, 59], the least squares dynamic SGS closure model [58, 59], the monotone integrated large eddy simulation (**MILES**) approach [60]-[63] and the variational multiscale model [64, 65, 66] etc. Thus the (filtered) Navier-Stokes equations which provide adequate dissipation of turbulent kinetic energy is responsible for the energy transfer between the large resolved scales and the SGS eddies.

In the Smagorinsky model, the eddy viscosity based on the application of the mixing length hypothesis is employed to be proportional to the SGS lengthscale, through the universal Smagorinsky constant, and the turbulent velocity scale imposed by the second-order symmetric tensor of the filtered strain-rate. To correct asymptotic behaviour in the near-wall region of a boundary layer in different flow regimes, the concept of the so-called 'double filter levels' leads to SGS stress tensor in which Smagorinsky constant is replaced by an algebraic equation. It is known as the dynamic eddy viscosity model which can dynamically obtain the constant that is a function of space and time. A potentially important modification of the dynamic mode is made by a least squares approach to avoid the denominator become zero. Except for the above explicit SGS stress models, one of the implicit numerical filters is so-called the MILES approach, wherein the inherent numerical dissipation based on the flux corrected transport scheme [67] or the piecewise parabolic method [68] in the SGS model is used. In the multiscale formulation, the SGS stress is modelled by the fluctuating rate-of-strain rather than the filtering rate-of-strain which represents a missing effect based on unresolved subgrid scales on resolved scales (space-averaged) within the filtered Navier-Stokes equations. In brief, LES is used to simulate the large-scale motion on which the effect of small scales is modeled.

RANS models are developed using time-averaged quantities resulting from the decomposition of mean and fluctuating parts [69]. It extends the classical time-averaged approaches that involve the numerical solution of the Reynolds equations to determine the mean velocity field. The mixing-length hypothesis [70] in which velocity scale is defined based on the turbulent kinetic energy was suggested by Kolmogorov and Prandtl [71, 72] for solving the transport equation. Here the turbulent eddy viscosity formulation is replaced with the absolute values of the mean velocity gradient. It implicates that the turbulent eddy viscosity is a scalar in this turbulence-energy hypothesis. This RANS model is called the one-equation model because it has just one turbulence quantity—turbulent kinetic energy—for transport. The one-equation model of Wolfshtein [73] based on length scale of dissipation and viscosity is employed to account for the near wall effects in this work.

The two-equation model belongs to the RANS model as well. This model uses two turbulence quantities. The turbulent kinetic energy κ is taken as one of the variables. Another is determined by several quantities, for instance, turbulence dissipation rate ε [74, 75], turbulence frequency $\omega = \kappa/\varepsilon$ [76] and turbulence timescale $\tau = \varepsilon/\kappa$ [77]. However, several investigators have applied the linear $\kappa - \varepsilon$ model to develop nonlinear eddy-viscosity models (**NLEVMs**) in the constitutive stress—strain/vorticity equation for practical engineering turbulent flows during the past two decade [78]-[84].

One of the hybrid techniques, detached eddy simulation (**DES**) approach, was suggested by Spalart et al. [85, 86, 87] in order to combine the most beneficial results of RANS and LES. The closure is based on a modification to the Spalart-Allmaras model such that the whole boundary layer uses the RANS model and separated regions away from boundary layers use LES at external flows.

In this thesis, the linear $\kappa - \varepsilon$ model is used to demonstrate the use of both the matrix free CBS-AC scheme and semi-implicit CBS scheme. The low-Reynolds-number approximations, the Lam-Bremhorst model [88] and Fan-Lakshminarayana-Barnett model [89], for predicting wall-bounded turbulence are also demonstrated in this thesis. Especially, the unsteady turbulent boundary layers with correct asymptotic behaviour in the near-wall region had been improved by Fan et al's work. For the nonlinear $\kappa - \varepsilon$ mode, the Kimura-Hosoda formulation [84] was presented in the Reynolds stress tensor. In majority of the turbulent cases studied in this thesis, the Spalart-Allmaras model [90] has been used as a one-equation turbulence model for transport of the turbulent eddy kinematic viscosity.

It is not very clear when computing power will be sufficient enough to carry out LES calculations on practical engineering problems. One prediction (Spalart) suggests that it will be in the year 2045 before a reasonable size engineering problem is solved using LES.

It is also not clear how LES is going to develop itself as an unstructured mesh method. Thus this thesis is devoted to develop unstructured mesh based matrix free method for RANS calculations. Through examples it is proved that sufficiently accurate turbulent flow calculations can be carried out on fully unstructured meshes.

This thesis describes the RANS modelling using a matrix free scheme in detail. Various governing equations and their origins are summarized along with the finite element solution procedure. The accuracy and efficiency of the matrix free scheme is demonstrated through several laminar and turbulent incompressible flow problems. The semi-implicit form of the CBS scheme is also implemented for the sake of comparison. In the following section, the contents of the present work is described in same detail.

1.3 Organisation of the thesis

This research aims at using the matrix free CBS-AC scheme and semi-implicit CBS scheme to solve both laminar and turbulent incompressible flow problems using the structured, unstructured and hybrid meshes.

Chapters 2 to 3 deal with the mathematical models and turbulence formulations for incompressible flows. Applying the Reynolds decomposition to split into mean and fluctuating values of Naiver-Stokes equations are explained in Chapter 2 followed by a discussion on the derivation of several turbulence transport equations. In Chapter 3, various turbulence RANS models are explained in detail.

Chapter 4 covers CBS algorithm in detail using an explicit discretization technique. A combination of the artificial compressibility method and the dual time stepping process are used here to solve unsteady problems with the matrix free form while the pressure Poisson equation of the semi-implicit scheme is solved using a conjugate gradient method. Two- and three-dimensional matrix coefficients resulting from the weak formulation has been obtained by the rules of linear algebra and shown in Appendices A and B. Chapter 4 also presents how CBS scheme avoids LBB condition.

Chapters 5 to 6 present numerical experiments of steady and transient laminar flow calculations. Many two- and three-dimensional benchmark problems have been presented in Chapter 5. The steady and unsteady incompressible flow calculation inside a two-dimensional non-rectangular double driven cavity at a Reynolds number range of 50 and 10000 are described in Chapter 6.

In Chapters 7 to 8 numerical solutions of turbulent incompressible flow problems are evaluated by the one- and two-equation turbulence models. The first benchmark problem is the turbulent incompressible flow through a two-dimensional rectangular channel at Re=12300. The other steady state problems studied are the turbulent two- and three-dimensional flow past a backward facing step at Re=3025 and the model upper human airway at a moderate Reynolds number. The application of URANS is investigated by solving the vortex shedding behind a circular cylinder at Re=10000. All two dimensional turbulent flow problems are presented in Chapter 7. Three dimensional RANS and URANS turbulence calculations are shown in Chapter 8.

The conclusions derived from the present study are described in Chapter 9. This chapter also gives same ideas for future research.

Chapter 2

The turbulent mean-flow equations

2.1 The Navier-Stokes equations

The mass conservation based on time rate of decrease of mass inside the control volume is equal to net mass flow out control surface. It leads to the conservation form of the continuity equation which can be expressed as

$$-\frac{\partial \rho}{\partial t} = \frac{\partial (\rho u_i)}{\partial x_i} \tag{2.1}$$

where ρ is the density, u_i are the velocity components, x_i are Cartesian coordinates.

The constitutive relation for the deviatoric stress components τ_{ij} for Newtonian fluids is given as

$$\tau_{ij} = \mu \left(\frac{\partial u_i}{\partial x_j} + \frac{\partial u_j}{\partial x_i} - \frac{2}{3} \frac{\partial u_k}{\partial x_k} \delta_{ij} \right) \tag{2.2}$$

where μ is the dynamic viscosity, δ_{ij} is the Kroneker delta.

The general momentum equations based on the Newton's second law $(ma_i = F_i)$ is

$$\rho \frac{Du_j}{Dt} = -\frac{\partial P}{\partial x_j} + \frac{\partial \tau_{ij}}{\partial x_i} + \rho f_j \tag{2.3}$$

where Du_j/Dt are the acceleration of the moving fluid element, P is the pressure, $-\partial_j P + \partial_i \tau_{ij}$ are the net surface force per unit volume, f_j are the body force which is the gravity acting on the fluid element.

By substituting Equation (2.2) into the general momentum Equation (2.3), the momentum equation in differential form of Cartesian tensor notation can be given as

$$\frac{\partial u_j}{\partial t} + \frac{\partial (u_j u_k)}{\partial x_k} = -\frac{1}{\rho}\frac{\partial p}{\partial x_j} + \frac{\partial}{\partial x_i}\left[\nu\left(\frac{\partial u_i}{\partial x_j} + \frac{\partial u_j}{\partial x_i} - \frac{2}{3}\frac{\partial u_k}{\partial x_k}\delta_{ij}\right)\right] \tag{2.4}$$

where $\nu \equiv \mu/\rho$ is the kinematic viscosity, and the modified pressure p includes pressure and a constant gravitational field, that is $p = P + G$.

2.2 The Reynolds averaged Navier-Stokes equations

The Reynolds averaged Navier-Stokes equations can be derived by the Reynolds decomposition. The decomposition of the instantaneous quantities ψ_i as a function of time at a fixed point in a turbulent flow into its time-averaging value $\bar{\psi}_i$ and the random quantities ψ_i' (see Figure 2.1), i.e.

$$\psi_i' \equiv \psi_i - \bar{\psi}_i \tag{2.5}$$

and definitions of the mean values for velocities and modified pressure in a turbulent flow [91] are

$$\bar{u}_i = \frac{1}{T}\int_0^T u_i dt; \qquad \bar{p} = \frac{1}{T}\int_0^T p dt$$

and

$$\bar{u}_i' = \frac{1}{T}\int_0^T u_i' dt = \bar{p}' = \frac{1}{T}\int_0^T p' dt \equiv 0 \tag{2.6}$$

where T is time interval. Substituting Equation (2.5) with definitions of the mean velocity values we obtain the Reynolds stress

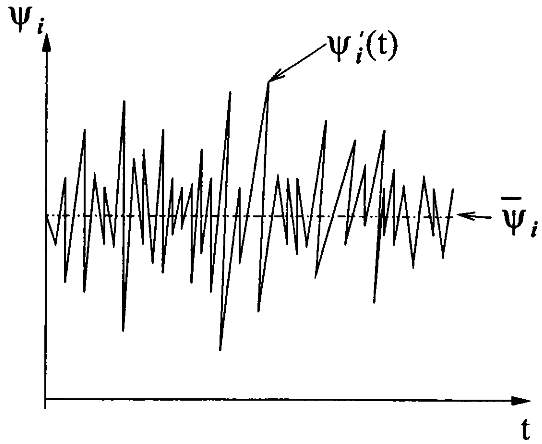

Figure 2.1: Description of the instantaneous quantities.

$$
\begin{aligned}
\overline{u'_i u'_j} &= \frac{1}{T}\int_0^T u'_i u'_j dt \\
&= \overline{u_i u_j} - \overline{\bar{u}_i \bar{u}_j + \bar{u}_i u'_j + \bar{u}_j u'_i} \\
&= \overline{u_i u_j} - \bar{u}_i \bar{u}_j + \bar{u}_i \bar{u}'_j + \bar{u}_j \bar{u}'_i \\
&= \overline{u_i u_j} - \bar{u}_i \bar{u}_j
\end{aligned}
\tag{2.7}
$$

It is assumed that the turbulent velocity and modified pressure are differentiable. It also takes the mean commutative law of the derivative by integration during an interval of time T and derivatives with respect to time or space can be interchanged.

$$
\begin{aligned}
\overline{\frac{\partial \bar{u}_j}{\partial t}} &= \frac{\partial \bar{u}_j}{\partial t}\left(\frac{1}{T}\int_0^T dt\right) = \frac{\partial \bar{u}_j}{\partial t} \\
\overline{\frac{\partial u_j}{\partial x_k}} &= \frac{\partial}{\partial x_k}\left(\frac{1}{T}\int_0^T u_j dt\right) = \frac{\partial \bar{u}_j}{\partial x_k} \\
\overline{\frac{\partial \bar{u}_j}{\partial x_k}} &= \frac{\partial}{\partial x_k}\left(\bar{u}_j \frac{1}{T}\int_0^T dt\right) = \frac{\partial \bar{u}_j}{\partial x_k} \\
\overline{\frac{\partial p}{\partial x_j}} &= \frac{\partial}{\partial x_j}\left(\frac{1}{T}\int_0^T p dt\right) = \frac{\partial \bar{p}}{\partial x_j}
\end{aligned}
\tag{2.8}
$$

and also

$$\overline{\frac{\partial u_j'}{\partial x_k}} = \frac{\partial}{\partial x_k}\left(\frac{1}{T}\int_0^T u_j' dt\right) = \frac{\partial \bar{u}_j'}{\partial x_k} = 0 \tag{2.9}$$

The differential conservation form of the mean-continuity equation can be written as

$$\overline{\frac{\partial \rho}{\partial t} + \frac{\partial \rho u_i}{\partial x_i}} = \frac{\partial \bar{\rho}}{\partial t} + \frac{\partial \bar{\rho}\bar{u}_i}{\partial x_i} + \frac{\partial \overline{\rho' u_i'}}{\partial x_i} = 0 \tag{2.10}$$

For incompressible flow, Equation (2.10) becomes

$$\frac{\partial \bar{u}_i}{\partial x_i} = 0 \tag{2.11}$$

Equation (2.11) is the continuity equation for incompressible turbulent flow given in terms of time-averaging quantities.

The mean of substantial derivative in conservative form can be written as [92]

$$\overline{\frac{Du_j}{Dt}} = \overline{\frac{\partial u_j}{\partial t} + \frac{\partial u_j u_k}{\partial x_k}} = \frac{\partial \bar{u}_j}{\partial t} + \frac{\partial}{\partial x_k}\left(\bar{u}_j \bar{u}_k + \overline{u_j' u_k'}\right) \tag{2.12}$$

Therefore, we obtain the mean-momentum equation

$$\frac{\partial \bar{u}_j}{\partial t} + \frac{\partial \left(\bar{u}_j \bar{u}_k\right)}{\partial x_k} = -\frac{1}{\rho}\frac{\partial \bar{p}}{\partial x_j} + \frac{\partial}{\partial x_i}\left[\nu\left(\frac{\partial \bar{u}_i}{\partial x_j} + \frac{\partial \bar{u}_j}{\partial x_i} - \frac{2}{3}\frac{\partial \bar{u}_k}{\partial x_k}\delta_{ij}\right)\right] - \frac{\partial \overline{u_j' u_k'}}{\partial x_k} \tag{2.13}$$

The above equation is well known as the Reynolds equation. Obviously, it differs from Equation (2.4). The extra last term is referred to as the Reynolds stresses. Both the mean flow quantities and the Reynolds stresses are unknown so some transport models are required in the turbulence regime.

2.3 The turbulent kinetic energy equation

According to the turbulent eddy viscosity hypothesis of Boussinesq [93], the deviatoric Reynolds stress tensor $-\overline{u_i' u_j'} + (2/3)\kappa\delta_{ij}$ is proportional to the mean strain-rate tensor [92]

$$-\overline{u_i'u_j'} + \frac{2}{3}\kappa\delta_{ij} = \frac{1}{2}\alpha_{ijkl}\left(\frac{\partial \bar{u}_k}{\partial x_l} + \frac{\partial \bar{u}_l}{\partial x_k}\right)$$
$$= \nu_t\left(\frac{\partial \bar{u}_i}{\partial x_j} + \frac{\partial \bar{u}_j}{\partial x_i} - \frac{2}{3}\frac{\partial \bar{u}_k}{\partial x_k}\delta_{ij}\right) \qquad (2.14)$$

where $\alpha_{ijkl} \equiv \delta_{ij}\delta_{kl}\vartheta_1 + \delta_{ik}\delta_{jl}(\vartheta_2 + \vartheta_3) + \delta_{il}\delta_{jk}(\vartheta_2 - \vartheta_3)$; ϑ_1, ϑ_2 and ϑ_3 are scalars [94], ν_t is the turbulent eddy kinematic viscosity that is the positive scalar coefficient and the turbulent kinetic energy (per unit mass) is $\kappa \equiv (1/2)\overline{u_i'u_i'}$.

In the above equation, the isotropic part of the Reynolds stress tensor is $(2/3)\kappa\delta_{ij}$. According to the Boussinesq's turbulent eddy viscosity hypothesis, the relation between the stress and the mean rate of strain for the Newtonian fluid is determined by the turbulent kinetic energy κ.

Because the turbulent kinetic energy κ is a scalar quantity of considerable importance, the transport equation of the turbulent kinetic energy is derived here. First, by subtracting Equation (2.13) from Equation (2.4), we have the fluctuating velocity u_j' equation, i.e.

$$\frac{\partial u_j'}{\partial t} + \frac{\partial}{\partial x_k}\left(\bar{u}_j u_k' + u_j'\bar{u}_k + u_j'u_k'\right) = -\frac{1}{\rho}\frac{\partial p'}{\partial x_j} + \frac{\partial}{\partial x_i}\left[\nu\left(\frac{\partial u_i'}{\partial x_j} + \frac{\partial u_j'}{\partial x_i} - \frac{2}{3}\frac{\partial u_k'}{\partial x_k}\delta_{ij}\right)\right] + \frac{\partial \overline{u_j'u_k'}}{\partial x_k} \qquad (2.15)$$

Then each term is multiplied by u_j' and using the chain rule

$$\frac{\partial}{\partial t}\left(\frac{u_j'u_j'}{2}\right) + \frac{\partial}{\partial x_k}\left(\bar{u}_k\frac{u_j'u_j'}{2}\right) = -u_j'u_k'\frac{\partial \bar{u}_j}{\partial x_k} - \frac{\partial}{\partial x_k}\left(\frac{u_k'u_j'u_j'}{2}\right) - \frac{\partial}{\partial x_j}\left(\frac{u_j'p'}{\rho}\right) +$$
$$+ \frac{p'}{\rho}\frac{\partial u_j'}{\partial x_j} + \nu\frac{\partial}{\partial x_i}\left[u_j'\left(\frac{\partial u_i'}{\partial x_j} + \frac{\partial u_j'}{\partial x_i} - \frac{2}{3}\frac{\partial u_k'}{\partial x_k}\delta_{ij}\right)\right] -$$
$$- u_j'\bar{u}_j\frac{\partial u_k'}{\partial x_k} - \nu\left(\frac{\partial u_i'}{\partial x_j} + \frac{\partial u_j'}{\partial x_i} - \frac{2}{3}\frac{\partial u_k'}{\partial x_k}\delta_{ij}\right)\frac{\partial u_j'}{\partial x_i} +$$
$$+ \frac{\partial}{\partial x_k}\left(u_j'\overline{u_j'u_k'}\right) - \overline{u_j'u_k'}\frac{\partial u_j'}{\partial x_k} \qquad (2.16)$$

Continuing in this way, by taking mean values on both sides of Equation (2.16) and considering each of these terms independently one obtains for incompressible flow.

$$\overline{\frac{\partial}{\partial t}\left(\frac{u'_j u'_j}{2}\right)} + \overline{\frac{\partial}{\partial x_k}\left(\bar{u}_k\frac{u'_j u'_j}{2}\right)} = \overline{-u'_j u'_k\frac{\partial \bar{u}_j}{\partial x_k}} - \overline{\frac{\partial}{\partial x_k}\left(\frac{u'_k u'_j u'_j}{2}\right)} - \overline{\frac{\partial}{\partial x_j}\left(\frac{u'_j p'}{\rho}\right)} + $$
$$+ \overline{\frac{\partial}{\partial x_k}\left(u'_j\overline{u'_j u'_k}\right)} + \overline{\frac{\partial}{\partial x_i}\left[\nu u'_j\left(\frac{\partial u'_i}{\partial x_j} + \frac{\partial u'_j}{\partial x_i} - \frac{2}{3}\frac{\partial u'_k}{\partial x_k}\delta_{ij}\right)\right]} -$$
$$- \overline{\nu\left(\frac{\partial u'_i}{\partial x_j} + \frac{\partial u'_j}{\partial x_i} - \frac{2}{3}\frac{\partial u'_k}{\partial x_k}\delta_{ij}\right)\frac{\partial u'_j}{\partial x_i}} - \overline{u'_j u'_k}\frac{\partial u'_j}{\partial x_k} \tag{2.17}$$

Since $\bar{u}_k$, $\partial\bar{u}_j/\partial x_k$ and $\overline{u'_j u'_k}$ are constants with respect to time, finally, the turbulent kinetic energy equation can be expressed as

$$\underbrace{\frac{\partial}{\partial t}\left(\frac{\overline{u'_j u'_j}}{2}\right) + \frac{\partial}{\partial x_k}\left(\bar{u}_k\frac{\overline{u'_j u'_j}}{2}\right)}_{Convective\ \ acceleration} = \underbrace{-\frac{\partial}{\partial x_k}\left(\frac{\overline{u'_k u'_j u'_j}}{2}\right) - \frac{\partial}{\partial x_j}\left(\frac{\overline{u'_j p'}}{\rho}\right)}_{Diffusion} +$$
$$+ \underbrace{\frac{\partial}{\partial x_i}\left[\overline{\nu u'_j\left(\frac{\partial u'_i}{\partial x_j} + \frac{\partial u'_j}{\partial x_i} - \frac{2}{3}\frac{\partial u'_k}{\partial x_k}\delta_{ij}\right)}\right]}_{Viscous\ \ diffusion} + \underbrace{\left(-\overline{u'_j u'_k}\frac{\partial \bar{u}_j}{\partial x_k}\right)}_{Generation} -$$
$$- \underbrace{\overline{\nu\left(\frac{\partial u'_i}{\partial x_j} + \frac{\partial u'_j}{\partial x_i} - \frac{2}{3}\frac{\partial u'_k}{\partial x_k}\delta_{ij}\right)\frac{\partial u'_j}{\partial x_i}}}_{Dissipation\ \ rate} \tag{2.18}$$

2.4 The isotropic dissipation rate equation

For the high Reynolds number flows, an exact equation for the isotropic dissipation rate of the turbulent kinetic energy is obtained by using the isotropic second-rank tensor in the viscous diffusion terms and by differentiating Equation (2.15) with respect to x_m. The result may be written as

$$\frac{\partial}{\partial t}\left(\frac{\partial u'_j}{\partial x_m}\right) + \frac{\partial}{\partial x_k}\left(\frac{\partial u'_j u'_k}{\partial x_m}\right) = -\frac{\partial}{\partial x_k}\left(\frac{\partial \bar{u}_j u'_k}{\partial x_m}\right) - \frac{\partial}{\partial x_k}\left(\frac{\partial u'_j \bar{u}_k}{\partial x_m}\right) - \frac{1}{\rho}\frac{\partial}{\partial x_j}\left(\frac{\partial p'}{\partial x_m}\right) +$$
$$+ \nu\frac{\partial^2}{\partial x_i^2}\left(\frac{\partial u'_j}{\partial x_m}\right) + \frac{\partial}{\partial x_k}\left(\frac{\partial \overline{u'_j u'_k}}{\partial x_m}\right) \tag{2.19}$$

Then it is assumed that the velocity gradients are continuous and multiplying through out by $2\nu\partial u'_j/\partial x_m$ and using the product rule of the derivative and the chain rule. We have for an incompressible fluid

$$
\begin{aligned}
2\frac{\partial}{\partial t}\left(\frac{\nu}{2}\frac{\partial u_j'}{\partial x_m}\frac{\partial u_j'}{\partial x_m}\right) &= -2\nu\frac{\partial u_j'}{\partial x_m}\frac{\partial}{\partial x_m}\left(u_k'\frac{\partial \bar{u}_j}{\partial x_k}\right) - 2\nu\frac{\partial u_j'}{\partial x_m}\frac{\partial}{\partial x_m}\left(\bar{u}_k\frac{\partial u_j'}{\partial x_k}\right) - \\
&- 2\nu\frac{\partial u_j'}{\partial x_m}\frac{\partial u_k'}{\partial x_m}\frac{\partial u_j'}{\partial x_k} - u_k'\nu\frac{\partial}{\partial x_k}\left(\frac{\partial u_j'}{\partial x_m}\frac{\partial u_j'}{\partial x_m}\right) - \\
&- \frac{2\nu}{\rho}\frac{\partial}{\partial x_j}\left(\frac{\partial u_j'}{\partial x_m}\frac{\partial p'}{\partial x_m}\right) + 2\nu^2\frac{\partial}{\partial x_i}\left[\frac{\partial}{\partial x_i}\left(\frac{1}{2}\frac{\partial u_j'}{\partial x_m}\frac{\partial u_j'}{\partial x_m}\right)\right] - \\
&- 2\nu^2\left[\frac{\partial}{\partial x_i}\left(\frac{\partial u_j'}{\partial x_m}\right)\right]^2 + 2\nu\frac{\partial u_j'}{\partial x_m}\frac{\partial}{\partial x_m}\left(\frac{\partial \overline{u_j'u_k'}}{\partial x_k}\right) \qquad (2.20)
\end{aligned}
$$

However, taking the time averaged values on both sides of the equation, the dissipation rate equation of the turbulent kinetic energy becomes

$$
\begin{aligned}
\frac{\partial}{\partial t}\left(\nu\overline{\frac{\partial u_j'}{\partial x_m}\frac{\partial u_j'}{\partial x_m}}\right) &= -\frac{\partial}{\partial x_k}\left(\bar{u}_k\nu\overline{\frac{\partial u_j'}{\partial x_m}\frac{\partial u_j'}{\partial x_m}}\right) - \\
&- \frac{2\nu}{\rho}\frac{\partial}{\partial x_j}\overline{\left(\frac{\partial u_j'}{\partial x_m}\frac{\partial p'}{\partial x_m}\right)} - 2\overline{\left[\nu\frac{\partial}{\partial x_i}\left(\frac{\partial u_j'}{\partial x_m}\right)\right]^2} - \\
&- \frac{\partial}{\partial x_k}\left(\overline{u_k'\nu\frac{\partial u_j'}{\partial x_m}\frac{\partial u_j'}{\partial x_m}}\right) - 2\nu\overline{\frac{\partial u_j'}{\partial x_m}\frac{\partial u_k'}{\partial x_m}\frac{\partial u_j'}{\partial x_k}} - \\
&- 2\nu\left(\overline{\frac{\partial u_j'}{\partial x_m}\frac{\partial u_k'}{\partial x_m}}\right)\frac{\partial \bar{u}_j}{\partial x_k} - 2\nu\left(\overline{\frac{\partial u_j'}{\partial x_m}\frac{\partial u_j'}{\partial x_k}}\right)\frac{\partial \bar{u}_k}{\partial x_m} - \\
&- 2\nu\overline{u_k'\frac{\partial u_j'}{\partial x_m}}\frac{\partial}{\partial x_m}\left(\frac{\partial \bar{u}_j}{\partial x_k}\right) + \\
&+ \nu\frac{\partial}{\partial x_i}\left[\frac{\partial}{\partial x_i}\left(\nu\overline{\frac{\partial u_j'}{\partial x_m}\frac{\partial u_j'}{\partial x_m}}\right)\right] \qquad (2.21)
\end{aligned}
$$

In the above equation, the isotropic dissipation rate $\nu\overline{\partial_m u_j'\partial_m u_j'}$ is introduced by a second-order symmetric tensor. The result may be written as

$$\underbrace{\frac{\partial}{\partial t}\left[\overline{\nu\left(\frac{\partial u'_m}{\partial x_j}+\frac{\partial u'_j}{\partial x_m}-\frac{2}{3}\frac{\partial u'_l}{\partial x_l}\delta_{mj}\right)\frac{\partial u'_j}{\partial x_m}}\right]}_{\text{(i)}}+\underbrace{\frac{\partial}{\partial x_k}\left[\bar{u}_k\overline{\nu\left(\frac{\partial u'_m}{\partial x_j}+\frac{\partial u'_j}{\partial x_m}-\frac{2}{3}\frac{\partial u'_l}{\partial x_l}\delta_{mj}\right)\frac{\partial u'_j}{\partial x_m}}\right]}_{\text{(ii)}}$$

$$=\underbrace{-\frac{2\nu}{\rho}\frac{\partial}{\partial x_j}\overline{\left(\frac{\partial u'_j}{\partial x_m}\frac{\partial p'}{\partial x_m}\right)}}_{\text{(iii}-1)}\underbrace{-\frac{\partial}{\partial x_k}\left[\overline{u'_k\nu\left(\frac{\partial u'_m}{\partial x_j}+\frac{\partial u'_j}{\partial x_m}-\frac{2}{3}\frac{\partial u'_l}{\partial x_l}\delta_{mj}\right)\frac{\partial u'_j}{\partial x_m}}\right]}_{\text{(iii}-2)}+$$

$$+\underbrace{\nu\frac{\partial}{\partial x_i}\left\{\frac{\partial}{\partial x_i}\left[\overline{\nu\left(\frac{\partial u'_m}{\partial x_j}+\frac{\partial u'_j}{\partial x_m}-\frac{2}{3}\frac{\partial u'_l}{\partial x_l}\delta_{mj}\right)\frac{\partial u'_j}{\partial x_m}}\right]\right\}}_{\text{(iii}-2)}-$$

$$\underbrace{-2\nu\left(\overline{\frac{\partial u'_j}{\partial x_m}\frac{\partial u'_k}{\partial x_m}}\right)\frac{\partial \bar{u}_j}{\partial x_k}-2\nu\left(\overline{\frac{\partial u'_j}{\partial x_m}\frac{\partial u'_j}{\partial x_k}}\right)\frac{\partial \bar{u}_k}{\partial x_m}}_{\text{(iv)}}-$$

$$\underbrace{-2\nu\overline{\frac{\partial u'_j}{\partial x_m}\frac{\partial u'_k}{\partial x_m}\frac{\partial u'_j}{\partial x_k}}-2\overline{\left[\nu\frac{\partial}{\partial x_i}\left(\frac{\partial u'_j}{\partial x_m}\right)\right]^2}}_{\text{(v)}}\underbrace{-2\nu\overline{u'_k\frac{\partial u'_j}{\partial x_m}}\frac{\partial}{\partial x_m}\left(\frac{\partial \bar{u}_j}{\partial x_k}\right)}_{\text{(vi)}} \tag{2.22}$$

Equation (2.22) is called as the isotropic dissipation rate equation of the turbulent kinetic energy and each term is identified as follows: (**i**) Time rate of increase of the dissipation rate of the turbulent kinetic energy. (**ii**) Convective acceleration of the dissipation rate of turbulent kinetic energy by mean flow. (**iii − 1**) Viscous diffusion of the dissipation rate of turbulent kinetic energy by pressure fluctuation. Following Hanjalić and Launder [95], this term contains higher order derivative of the mean or fluctuating velocity field (fourth-order tensor) which is neglected. (**iii − 2**) Viscous diffusion of the dissipation rate of turbulent kinetic energy by velocity fluctuations. (**iv**) Production of the dissipation rate of turbulent kinetic energy by time-averaged velocity gradients. (**v**) Destruction of the dissipation rate of turbulent kinetic energy. (**vi**) Viscous diffusion of the dissipation rate of turbulent kinetic energy for lower-Reynolds-number flows.

The moment approximation is to provide reasonable closing procedure in terms of multiple correlations of velocity fluctuations and the dissipation rate [95, 96]. These terms may be respectively written as

$$-\frac{\partial}{\partial x_k}\left[\overline{u'_k\nu\left(\frac{\partial u'_m}{\partial x_j}+\frac{\partial u'_j}{\partial x_m}-\frac{2}{3}\frac{\partial u'_l}{\partial x_l}\delta_{mj}\right)\frac{\partial u'_j}{\partial x_m}}\right]$$

$$=\frac{\partial}{\partial x_k}\left\{\left[\frac{c_\varepsilon\frac{\overline{u'_ju'_j}}{2}\overline{u'_ku'_m}}{\overline{\nu\left(\frac{\partial u'_m}{\partial x_j}+\frac{\partial u'_j}{\partial x_m}-\frac{2}{3}\frac{\partial u'_l}{\partial x_l}\delta_{mj}\right)\frac{\partial u'_j}{\partial x_m}}}\right]\frac{\partial}{\partial x_m}\left[\overline{\nu\left(\frac{\partial u'_m}{\partial x_j}+\frac{\partial u'_j}{\partial x_m}-\frac{2}{3}\frac{\partial u'_l}{\partial x_l}\delta_{mj}\right)\frac{\partial u'_j}{\partial x_m}}\right]\right\} \tag{2.23}$$

$$-2\nu\left(\overline{\frac{\partial u'_j}{\partial x_m}\frac{\partial u'_k}{\partial x_m}}+\overline{\frac{\partial u'_m}{\partial x_k}\frac{\partial u'_m}{\partial x_j}}\right)\frac{\partial \bar{u}_j}{\partial x_k} = -\left[\frac{c_{\varepsilon 1}\overline{\nu\left(\frac{\partial u'_m}{\partial x_j}+\frac{\partial u'_j}{\partial x_m}-\frac{2}{3}\frac{\partial u'_l}{\partial x_l}\delta_{mj}\right)\frac{\partial u'_j}{\partial x_m}}\,\overline{u'_ju'_k}}{\frac{\overline{u'_ju'_j}}{2}}\right]\frac{\partial \bar{u}_j}{\partial x_k} \tag{2.24}$$

$$-2\left\{\nu\overline{\frac{\partial u'_j}{\partial x_m}\frac{\partial u'_k}{\partial x_m}\frac{\partial u'_j}{\partial x_k}}+\overline{\left[\nu\frac{\partial}{\partial x_i}\left(\frac{\partial u'_j}{\partial x_m}\right)\right]^2}\right\} = -\frac{c_{\varepsilon 2}\left[\overline{\nu\left(\frac{\partial u'_m}{\partial x_j}+\frac{\partial u'_j}{\partial x_m}-\frac{2}{3}\frac{\partial u'_l}{\partial x_l}\delta_{mj}\right)\frac{\partial u'_j}{\partial x_m}}\right]^2}{\frac{\overline{u'_ju'_j}}{2}} \tag{2.25}$$

and

$$-2\nu\overline{u'_k\frac{\partial u'_j}{\partial x_m}}\frac{\partial}{\partial x_m}\left(\frac{\partial \bar{u}_j}{\partial x_k}\right) = c_{\varepsilon 3}\nu\frac{\frac{\overline{u'_ju'_j}}{2}\overline{u'_iu'_k}}{\overline{\nu\left(\frac{\partial u'_m}{\partial x_j}+\frac{\partial u'_j}{\partial x_m}-\frac{2}{3}\frac{\partial u'_l}{\partial x_l}\delta_{mj}\right)\frac{\partial u'_j}{\partial x_m}}}\left(\frac{\partial^2\bar{u}_j}{\partial x_i\partial x_m}\right)\left(\frac{\partial^2\bar{u}_j}{\partial x_k\partial x_m}\right) \tag{2.26}$$

where c_ε, $c_{\varepsilon 1}$, $c_{\varepsilon 2}$ and $c_{\varepsilon 3}$ are constants.

Equation (2.26) may be replaced with suitable wall damping functions, so the final form of the simulated dissipation rate equation of turbulent kinetic energy can thus be expressed as

$$\begin{aligned}
&\underbrace{\frac{\partial}{\partial t}\left[\nu\overline{\left(\frac{\partial u'_m}{\partial x_j}+\frac{\partial u'_j}{\partial x_m}-\frac{2}{3}\frac{\partial u'_l}{\partial x_l}\delta_{mj}\right)\frac{\partial u'_j}{\partial x_m}}\right]+\frac{\partial}{\partial x_k}\left[\bar{u}_k\nu\overline{\left(\frac{\partial u'_m}{\partial x_j}+\frac{\partial u'_j}{\partial x_m}-\frac{2}{3}\frac{\partial u'_l}{\partial x_l}\delta_{mj}\right)\frac{\partial u'_j}{\partial x_m}}\right]}_{Convection} \\
&= \underbrace{\frac{\partial}{\partial x_i}\left\{\nu\frac{\partial}{\partial x_i}\left[\nu\overline{\left(\frac{\partial u'_m}{\partial x_j}+\frac{\partial u'_j}{\partial x_m}-\frac{2}{3}\frac{\partial u'_l}{\partial x_l}\delta_{mj}\right)\frac{\partial u'_j}{\partial x_m}}\right]\right\}}_{Viscous\ diffusion}+ \\
&+\underbrace{\frac{\partial}{\partial x_k}\left\{\left[\frac{c_\varepsilon\frac{\overline{u'_ju'_j}}{2}\overline{u'_ku'_m}}{\nu\overline{\left(\frac{\partial u'_m}{\partial x_j}+\frac{\partial u'_j}{\partial x_m}-\frac{2}{3}\frac{\partial u'_l}{\partial x_l}\delta_{mj}\right)\frac{\partial u'_j}{\partial x_m}}}\right]\frac{\partial}{\partial x_m}\left[\nu\overline{\left(\frac{\partial u'_m}{\partial x_j}+\frac{\partial u'_j}{\partial x_m}-\frac{2}{3}\frac{\partial u'_l}{\partial x_l}\delta_{mj}\right)\frac{\partial u'_j}{\partial x_m}}\right]\right\}}_{Viscous\ diffusion}- \\
&-\underbrace{\left[\frac{c_{\varepsilon 1}\nu\overline{\left(\frac{\partial u'_m}{\partial x_j}+\frac{\partial u'_j}{\partial x_m}-\frac{2}{3}\frac{\partial u'_l}{\partial x_l}\delta_{mj}\right)\frac{\partial u'_j}{\partial x_m}}\,\overline{u'_ju'_k}}{\frac{\overline{u'_ju'_j}}{2}}\right]\frac{\partial \bar{u}_j}{\partial x_k}}_{Production}-\underbrace{\frac{c_{\varepsilon 2}\left[\nu\overline{\left(\frac{\partial u'_m}{\partial x_j}+\frac{\partial u'_j}{\partial x_m}-\frac{2}{3}\frac{\partial u'_l}{\partial x_l}\delta_{mj}\right)\frac{\partial u'_j}{\partial x_m}}\right]^2}{\frac{\overline{u'_ju'_j}}{2}}}_{Source}
\end{aligned} \tag{2.27}$$

The above equation contains three different constants which are described in Chapter 3.

2.5 The Reynolds stresses equation

For an incompressible turbulent flow, the exact transport equation for the Reynolds stresses $\overline{u'_ju'_l}$ is obtained from the fluctuating velocity Equation (2.15) based on second-rank isotropic tensor in the viscous diffusion terms.

Each term in the fluctuating velocity u'_j equation is multiplied by u'_l that gives

$$u'_l\frac{\partial u'_j}{\partial t}+u'_l\frac{\partial \bar{u}_ju'_k}{\partial x_k}+u'_l\frac{\partial u'_j\bar{u}_k}{\partial x_k}+u'_l\frac{\partial u'_ju'_k}{\partial x_k}=-\frac{u'_l}{\rho}\frac{\partial p'}{\partial x_j}+\nu u'_l\frac{\partial^2 u'_j}{\partial x_i^2}+u'_l\frac{\partial \overline{u'_ju'_k}}{\partial x_k} \tag{2.28}$$

The same equation for the velocity component u'_l is multiplied by u'_j can be written as

$$u'_j\frac{\partial u'_l}{\partial t}+u'_j\frac{\partial \bar{u}_lu'_k}{\partial x_k}+u'_j\frac{\partial u'_l\bar{u}_k}{\partial x_k}+u'_j\frac{\partial u'_lu'_k}{\partial x_k}=-\frac{u'_j}{\rho}\frac{\partial p'}{\partial x_l}+\nu u'_j\frac{\partial^2 u'_l}{\partial x_i^2}+u'_j\frac{\partial \overline{u'_lu'_k}}{\partial x_k} \tag{2.29}$$

By adding Equations (2.28) and (2.29) and using the differential rule,

$$\begin{aligned} \frac{\partial u'_j u'_l}{\partial t} + u'_l u'_k \frac{\partial \bar{u}_j}{\partial x_k} &= -u'_j u'_k \frac{\partial \bar{u}_l}{\partial x_k} - \frac{\partial \bar{u}_k u'_j u'_l}{\partial x_k} - \frac{\partial u'_j u'_l u'_k}{\partial x_k} - \\ &- \frac{1}{\rho}\frac{\partial p' u'_l}{\partial x_j} + \frac{p'}{\rho}\frac{\partial u'_l}{\partial x_j} - \frac{1}{\rho}\frac{\partial p' u'_j}{\partial x_l} + \frac{p'}{\rho}\frac{\partial u'_j}{\partial x_l} + \\ &+ \nu \frac{\partial^2 u'_l u'_j}{\partial x_i^2} - 2\nu \frac{\partial u'_l}{\partial x_i}\frac{\partial u'_j}{\partial x_i} + u'_l \frac{\partial \overline{u'_j u'_k}}{\partial x_k} + u'_j \frac{\partial \overline{u'_l u'_k}}{\partial x_k} \end{aligned} \tag{2.30}$$

Taking mean values on both sides in the above equation, the transport equation of the Reynolds stresses may be written in the form [95, 97]

$$\begin{aligned} \underbrace{\frac{\partial \overline{u'_j u'_l}}{\partial t} + \frac{\partial}{\partial x_k}\left(\bar{u}_k \overline{u'_j u'_l}\right)}_{Convection} &= \underbrace{-\frac{\partial \overline{u'_j u'_l u'_k}}{\partial x_k} - \frac{1}{\rho}\left(\frac{\partial \overline{p' u'_l}}{\partial x_j} + \frac{\partial \overline{p' u'_j}}{\partial x_l}\right) + \nu \frac{\partial^2 \overline{u'_l u'_j}}{\partial x_i^2}}_{Diffusion} - \\ &- \underbrace{\overline{u'_l u'_k}\frac{\partial \bar{u}_j}{\partial x_k} - \overline{u'_j u'_k}\frac{\partial \bar{u}_l}{\partial x_k}}_{Generation} + \\ &+ \underbrace{\overline{\frac{p'}{\rho}\left(\frac{\partial u'_l}{\partial x_j} + \frac{\partial u'_j}{\partial x_l}\right)}}_{Redistribution} - \underbrace{2\nu \overline{\frac{\partial u'_l}{\partial x_i}\frac{\partial u'_j}{\partial x_i}}}_{Destruction} \end{aligned} \tag{2.31}$$

The above equation is referred to as second-order or second-moment closure for turbulence transport models since it is derived by taking a second moment of the fluctuating Navier-Stokes equations. It is solved for the individual Reynolds stresses. The right-hand side of Equation (2.31) contains several correlations between turbulence quantities and their fluctuating and time-averaged components. In this work, the Reynolds stress equation of the one-point velocity correlation is used to build up the foundation of the constitutive anisotropic Reynolds stress equation of the nonlinear $\kappa - \varepsilon$ model [84, 98, 99]. However, it is noted that both κ-equation and ε-equation may be written in the canonical form of the exact Reynolds-stress-transport, i.e.

$$\begin{aligned} \underbrace{\frac{D\overline{u'_i u'_j}}{Dt}}_{Convection} &= \textbf{Diffusion} + \textbf{Production (Generation)} + \\ &+ \textbf{Dissipation / Destruction (Source)} \end{aligned} \tag{2.32}$$

2.6 Summary

In this chapter, various time-averaged equations for the turbulent incompressible flow are discussed. The turbulent kinetic energy, the energy dissipation rate and the Reynolds stresses equations are derived from the governing equations of fluid dynamics–the Navier-Stokes equations which represent the fundamental physical principle of fluid flow. Further details on the turbulence equations are given in the following chapter.

Chapter 3

Turbulence models

3.1 Introduction

It is obvious from the previous chapter that the quantity to be modelled is the Reynolds stress tensor $\overline{u_i'u_j'}$. In this chapter, various available options are outlined. The Boussinesq hypothesis for Reynolds stresses will be assumed here. Both two- and one-equation models are explained in the following sections.

3.2 The two-equation model: linear $\kappa - \varepsilon$ formulation

From the Navier-Stokes equations and the Reynolds averaged Navier-Stokes equations in Chapter 2, we obtain the turbulent kinetic energy Equation (2.18) of which the energy flux may be written as

$$E_i^\kappa = \frac{\overline{u_i'u_j'u_j'}}{2} + \frac{\overline{u_i'p'}}{\rho} - \overline{\nu u_j' \left(\frac{\partial u_i'}{\partial x_j} + \frac{\partial u_j'}{\partial x_i} - \frac{2}{3}\frac{\partial u_k'}{\partial x_k}\delta_{ij} \right)} \tag{3.1}$$

The energy flux E_i^κ is approximated by the generalized gradient diffusion hypothesis resulting from Daly and Harlow [100] and simplified by Pope [92] to give

$$E_i^\kappa = -\left(\nu + \frac{\nu_t}{\sigma_\kappa}\right)\frac{\partial \kappa}{\partial x_i} \tag{3.2}$$

Thus, the first transport equation for the turbulent kinetic energy κ is of the form

$$\frac{\partial \kappa}{\partial t} + \frac{\partial \kappa \bar{u}_i}{\partial x_i} = \frac{\partial}{\partial x_i}\left(\nu + \frac{\nu_t}{\sigma_\kappa}\right)\frac{\partial \kappa}{\partial x_i} + \frac{1}{\rho}\tau_{ij}^R \frac{\partial \bar{u}_i}{\partial x_j} - \varepsilon \tag{3.3}$$

where the diffusion Prandtl number for the turbulent kinetic energy is $\sigma_\kappa = 1.0$, the dissipation rate is $\varepsilon = \overline{\nu(\partial_j u'_i + \partial_i u'_j - (2/3)\partial_k u'_k \delta_{ij})\partial_i u'_j}$ and the Reynolds stresses are $\tau_{ij}^R = -\rho\overline{u'_i u'_j}$.

From Equation (2.27), the energy flux of the dissipation rate equation may be expressed as

$$E_i^\varepsilon = \left[-\nu + \frac{c_\varepsilon \frac{\overline{u'_j u'_j}}{2}\left(-\overline{u'_k u'_i}\right)}{\overline{\nu\left(\frac{\partial u'_i}{\partial x_j} + \frac{\partial u'_j}{\partial x_i} - \frac{2}{3}\frac{\partial u'_k}{\partial x_k}\delta_{ij}\right)\frac{\partial u'_j}{\partial x_i}}} \right] \frac{\partial}{\partial x_i}\left[\overline{\nu\left(\frac{\partial u'_i}{\partial x_j} + \frac{\partial u'_j}{\partial x_i} - \frac{2}{3}\frac{\partial u'_k}{\partial x_k}\delta_{ij}\right)\frac{\partial u'_j}{\partial x_i}} \right] \tag{3.4}$$

which is modelled with the generalized gradient diffusion hypothesis as

$$E_i^\varepsilon = -\left(\nu + \frac{\nu_t}{\sigma_\varepsilon}\right)\frac{\partial \varepsilon}{\partial x_i} \tag{3.5}$$

The transport equation for calculating the turbulence energy dissipation rate ε can generally be written in the following form

$$\frac{\partial \varepsilon}{\partial t} + \frac{\partial \varepsilon \bar{u}_i}{\partial x_i} = \frac{\partial}{\partial x_i}\left(\nu + \frac{\nu_t}{\sigma_\varepsilon}\right)\frac{\partial \varepsilon}{\partial x_i} + c_{\varepsilon 1}\frac{\varepsilon}{\kappa\rho}\tau_{ij}^R\frac{\partial \bar{u}_i}{\partial x_j} - c_{\varepsilon 2}\frac{\varepsilon^2}{\kappa} \tag{3.6}$$

where the constants are $c_{\varepsilon 1} = 1.44$ and $c_{\varepsilon 2} = 1.92$ are proposed by Launder and Sharma [101]. The diffusion Prandtl number for the dissipation rate is $\sigma_\varepsilon = 1.3$ and the turbulent eddy kinematic viscosity as [74]

$$\nu_t = c_\mu \frac{\kappa^2}{\varepsilon} \tag{3.7}$$

where $c_\mu = 0.09$.

The above linear $\kappa - \varepsilon$ model belongs to the class of two-equation models, in which closure transport equations are solved for two turbulence quantities κ and ε. The Reynolds stresses τ_{ij}^R or $-\overline{u'_i u'_j}$ are calculated by a linear strain relation from Boussinesq hypothesis [93] which ignores anisotropic effects.

For near-wall treatment, the coefficients c_μ, $c_{\varepsilon 1}$ and $c_{\varepsilon 2}$ are multiplied by the turbulence damping functions f_μ, $f_{\varepsilon 1}$ and $f_{\varepsilon 2}$ respectively.

These functions, firstly, was used by Lam and Bremhorst [88]. The dissipation rate ε employed by Gibson et al. [102] is given as

$$\varepsilon = 0.2274\,[1 - exp\,(-0.01189 R_\kappa)]^2\,\frac{(0.8548)\,\kappa^2}{\nu_t} \tag{3.8}$$

Comparison of the above equation with Equation (3.7) gives a simpler relationship for f_μ in terms of turbulent Reynolds numbers R_κ and R_t

$$f_\mu = [1 - exp\,(-0.0165 R_\kappa)]^2 \left(1 + \frac{20.5}{R_t}\right) \tag{3.9}$$

where both the turbulent Reynolds numbers are defined as $R_t = \kappa^2/\nu\varepsilon$ and $R_\kappa = \sqrt{\kappa}y/\nu$ in which y is the distance from the nearest wall.

By avoiding the destruction term, $2\nu\,(\partial\sqrt{\kappa}/\partial x_2)^2$, in the transport equation of the turbulent kinetic energy to yield reasonable prediction in the near wall region [74, 103], $f_{\varepsilon 1}$ is increased to a larger value rather than constant or equal to unity. Thus $f_{\varepsilon 1}$ is modelled with the following form

$$f_{\varepsilon 1} = 1 + \left(\frac{0.05}{f_\mu}\right)^3 \tag{3.10}$$

The damping function $f_{\varepsilon 2}$ was suggested by Jones and Launder's work [74, 103] modified and is written as

$$f_{\varepsilon 2} = 1 - exp\left(-R_t^2\right) \tag{3.11}$$

The above equation tends to zero as the turbulent Reynolds number R_t tends to zero. Also, it makes sure that the dissipation rate ε is not infinite even if the turbulent kinetic energy κ is equal to zero on the solid walls.

Another wall function used in the present work as given by Fan et al. [89]. Here, the development of low Reynolds number functions to account for the near-wall damping effects, the function f_w is introduced by Speziale et al. [77] and the experimental data resulting from Patel et al. [104] were used to formulate expression in terms of R_κ, i.e.

$$f_w = 1 - exp\left\{-\frac{\sqrt{R_\kappa}}{2.30} + \left(\frac{\sqrt{R_\kappa}}{2.30} - \frac{R_\kappa}{8.89}\right)\left[1 - exp\left(-\frac{R_\kappa}{20}\right)\right]^3\right\} \tag{3.12}$$

The turbulent eddy kinematic viscosity scale is κ^2/ε at locations far from the solid wall at high Reynolds number. However, it reduces to $\sqrt{\nu\kappa^2/\varepsilon}$ according to Myong and Kasagi's model [105] due to the effect of turbulent Reynolds number $R_t = \kappa^2/\nu\varepsilon$ in the vicinity of solid walls. Therefore the correct near-wall asymptotic behaviour of turbulent eddy kinematic viscosity is needed by the function f_μ to connect between low-Reynolds-number flows in the vicinity of solid walls and high-Reynolds-number flows away from the wall. The empirical function f_μ is given as

$$f_\mu = 0.4\frac{f_w}{\sqrt{R_t}} + \left(1 - 0.4\frac{f_w}{\sqrt{R_t}}\right)\left[1 - exp\left(-\frac{R_\kappa}{42.63}\right)\right]^3 \tag{3.13}$$

The $f_{\varepsilon 1}$ is equal to unity was suggested by Speziale et al. [77]. The function $f_{\varepsilon 2}$ based on the variation of turbulent Reynolds number was demonstrated to have excellent agreement with experimental data for turbulence energy decay by Hanjalić and Launder [96]. Here $f_{\varepsilon 2}$ is assumed to be a function of the near-wall damping function f_w to ensure reasonable prediction, i.e.

$$f_{\varepsilon 2} = \left\{1 - \frac{0.4}{1.8}exp\left[-\left(\frac{R_t}{6}\right)^2\right]\right\} f_w^2 \tag{3.14}$$

The Dirichlet condition used are $\kappa = 0$ on solid walls. The constants used are given as $c_{\varepsilon 1} = 1.4$ and $c_{\varepsilon 2} = 1.8$.

3.3 The one-equation model: linear $\kappa - l$ formulation

The turbulent eddy kinematic viscosity can be expressed as the product of a lengthscale l^s and a velocity scale u^s:

$$\nu_t = l^s u^s \tag{3.15}$$

By Prandtl's mixing-length hypothesis [70], the lengthscale is replaced with the mixing length l_m and it varies linearly with the distance to the closest wall, the constant of proportionality being the von Kármán number $\sigma_{vk} = 0.41$ in the log-law region of a wall-bounded flow, i.e.

$$l^s = l_m = \sigma_{vk} y \tag{3.16}$$

Also, the velocity scale is based on the turbulent kinetic energy that was suggested by Kolmogorov [71] and Prandtl [72], that is

$$u^s = c_\mu^{1/4} \kappa^{1/2} \tag{3.17}$$

where the turbulent kinetic energy κ is estimated by the transport equation of κ, which is equation (3.3).

Then the turbulent eddy kinematic viscosity becomes

$$\nu_t = c_\mu^{1/4} \kappa^{1/2} l_m \tag{3.18}$$

The dissipation rate ε scale may be written as $U_o^2/\tau_o = U_o^3/l_o$, in which U_o, τ_o and l_o are the characteristic velocity scale, timescale and lengthscale of the largest eddies respectively, at the high Reynolds number being considered, it is reasonable to model ε as

$$\varepsilon = \frac{c_\mu^{3/4} \kappa^{3/2}}{l_m} \tag{3.19}$$

Equations (3.18) and (3.19) can, consequently, eliminate l_m to yield

$$\nu_t = c_\mu \frac{\kappa^2}{\varepsilon} \tag{3.20}$$

Clearly, the above equation is same as Equation (3.7). On the other hand, the mixing length l_m is often related to the lengthscale of the turbulence L as

$$L = l_m \frac{C_D}{c_\mu^{3/4}} \tag{3.21}$$

where the constant $C_D = 1.0$.

However, the dissipation rate ε is taken to be a function of the lengthscale of the turbulence L and hence

$$\varepsilon = C_D \frac{\kappa^{3/2}}{L} \tag{3.22}$$

For the wall damping treatments, Wolfshtein [73] suggested two length scales in the transition region between the laminar sublayer and fully turbulent layer to account for the wall proximity behaviour.
There are two damping functions to account for the wall effect. All in all, ν_t is multiplied by $f_\mu = 1 - e^{-0.160 R_\kappa}$ and ε divided by $f_b = 1 - e^{-0.263 R_\kappa}$.

3.4 The one-equation model: Spalart-Allmaras formulation

Spalart and Allmaras [90] have developed a one-equation turbulence model for the aerodynamic application. This model depends on Galilean invariance, empiricism and dimensional analysis to transport the turbulent eddy kinematic viscosity with modified procedure. The transport equation choose the scalar variable, which follows Baldwin and Barth [106] in choosing the transport quantity $\hat{\nu}$ and much easier to resolve than both turbulent kinetic energy and dissipation rate based on fluctuating velocity components.

In this study, the version of a wall-bounded flow at moderate Reynolds number is selected to model the turbulent eddy kinematic viscosity. The transport equation of the modified turbulent eddy kinematic viscosity $\hat{\nu}$ may be expressed in the form [90]

$$\underbrace{\frac{\partial \hat{\nu}}{\partial t} + \frac{\partial \hat{\nu} \bar{u}_i}{\partial x_i}}_{Convection} = \underbrace{\frac{1}{\sigma_{\hat{\nu}}} \left[\frac{\partial}{\partial x_i} (\nu + \hat{\nu}) \frac{\partial \hat{\nu}}{\partial x_i} + c_{b2} \left(\frac{\partial \hat{\nu}}{\partial x_i} \right)^2 \right]}_{Viscous\ diffusion} - \underbrace{c_{w1} f_w \left(\frac{\hat{\nu}}{y} \right)^2}_{Near-wall\ inviscid\ destruction} + \underbrace{c_{b1} \hat{S} \hat{\nu}}_{Production} \tag{3.23}$$

The turbulent eddy kinematic viscosity ν_t is effective in the log layer of which range is estimated by

$$y^+ \equiv \frac{x_2}{\delta_\nu} = \frac{u_\tau x_2}{\nu} = \sqrt{\frac{\tau_w}{\rho}} \frac{x_2}{\nu} = \frac{x_2}{\sqrt{\nu}} \sqrt{\frac{d\bar{u}_1}{dx_2}\bigg|_{x_2=0}} > 30 \tag{3.24}$$

where y^+ is the non-dimensional distance from the wall normalized by the viscous lengthscale, δ_ν is the viscous lengthscale, u_τ is the friction velocity, τ_w is the wall shear stress. However, $\hat{\nu}$ is calculated as

$$\nu_t = \hat{\nu} f_{\hat{\nu}1}; \qquad f_{\hat{\nu}1} = X^3/(X^3 + c_{\hat{\nu}1}^3); \qquad X \equiv \hat{\nu}/\nu \tag{3.25}$$

where the modified function $f_{\hat{\nu}1}$ is from Mellor and Herring [107]. The constant $c_{\hat{\nu}1}$ is equal to 7.1 from the log law calculation.

According to the free shear flow investigation in two-dimensional mixing layers and wake regimes by Spalart and Allmaras's work, the diffusion Prandtl number of the modified turbulent eddy kinematic viscosity $\sigma_{\hat{\nu}}$ is 2/3, . The constant $c_{b2} = 0.622$ is chosen in the viscous diffusion terms. The value of c_{b1} lies between 0.13 and 0.14 which is taken from experiments of the free shear flow. A value of $c_{b1} = 0.1355$ is used.

The turbulent flow exists only where vorticity is creating from the solid boundaries so the production term is employed by a scalar norm of the vorticity tensor based on the symmetric-deviatoric rate of strain tensor. Also, the magnitude of the vorticity S is replaced with $\hat{S}$, given by

$$\begin{aligned} \hat{S} &\equiv S + (\hat{\nu}/k^2 y^2) f_{\hat{\nu}2}; \qquad f_{\hat{\nu}2} = 1 - X/(1 + X f_{\hat{\nu}1}) \\ S &\equiv \sqrt{\hat{\Omega}_{ij}\hat{\Omega}_{ij}}; \qquad \hat{\Omega}_{ij} \equiv \partial_j \bar{u}_i - \partial_i \bar{u}_j \end{aligned} \tag{3.26}$$

where $\hat{S}$ is determined by the modified function $f_{\hat{\nu}2}$ to maintain its well behaviour of the log-law region all the way to the wall.

The inviscid destruction term is constructed by $-c_{w1}(\hat{\nu}/y)^2$ based on dimensional analysis and the near-wall damping function f_w resulting from algebraic models, that is

$$f_w = g[(1 + c_{w3}^6)/(g^6 + c_{w3}^6)]^{1/6}; \qquad g = r + c_{w2}(r^6 - r); \qquad r \equiv \hat{\nu}/\hat{S}k^2 y^2 \tag{3.27}$$

where the mixing length $l_m = (\hat{\nu}/\hat{S})^{0.5}$ leads to a non-dimensional factor r. The constants are $k = 0.41$, $c_{wl} = c_{b1}/k^2 + (1 + c_{b2})/\sigma_{\hat{\nu}}$, $c_{w2} = 0.3$, $c_{w3} = 2$.

At the solid wall, the Dirichlet boundary condition is $\hat{\nu} = 0$. In other words, the transport equation yields equilibrium all the way to $y = 0$ in the law of the wall. However, this model must be supplied with appropriate initial and boundary conditions.

3.5 Summary

The subject of this chapter is concerned with various turbulence RANS models. Different types of one- and two-equations have been discussed in detail. Near-wall damping treatments are also included in this chapter. It should be noted that all the transport equations discussed in this chapter take a convection-diffusion equation form.

Chapter 4

The Characteristic Based Split (CBS) scheme

In fluid mechanics several difficulties aries when the finite element method is employed. The first and well known difficulty is that no direct variational principle exists for the Navier-Stokes equations to express the extremum of a function, so a weak form of an integral formulation is used. Second, it is important to deal with non-self-adjoint problems of the convective acceleration term which requires specialized procedure. Third is that of dealing with incompressible situations in a manner which satisfies the Ladyshenskaya-Babuška-Brezzi (LBB) restrictions [3, 4, 5].

This chapter addresses the stabilized form of both the matrix free Characteristic Based Split (CBS) scheme based on the artificial compressibility (AC) method and semi-implicit CBS scheme. Also, the dual time-stepping procedure for solving unsteady transient flow is introduced in this chapter.

4.1 Characteristic based schemes

In all areas of fluid dynamics the characteristic based methods are widely employed. A brief background on this method is presented in this section and in the following subsection.

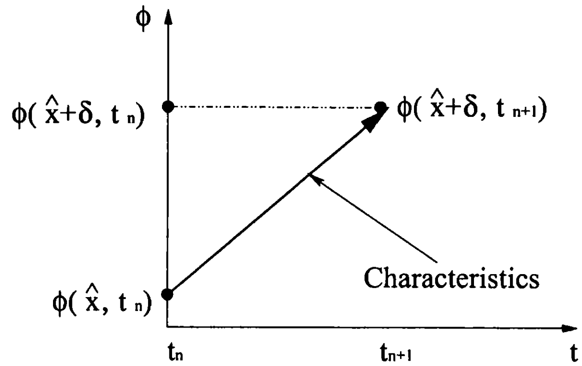

Figure 4.1: A scalar-dependent variable ϕ along characteristics.

4.1.1 Direct characteristic Galerkin procedure

A typical convection-diffusion equation with a scalar-dependent variable ϕ in non-conservation form is [13]

$$\frac{\partial \phi}{\partial t} + u_i \frac{\partial \phi}{\partial x_i} - \frac{\partial}{\partial x_i}\left(\alpha \frac{\partial \phi}{\partial x_i}\right) + Q = 0 \tag{4.1}$$

where u_i is the velocity field to transport quantity ϕ in a convection-diffusion action, α is the diffusion coefficient, Q is any external source or the reaction of ϕ.

In the above equation if only a linear convection term is considered with a constant convection velocity u in one dimension, then the characteristics propagate in $\phi - t$ plane as shown in Figure 4.1. We can thus write

$$\phi\left(\hat{x} + \delta, t_{n+1}\right) - \phi\left(\hat{x}, t_n\right) = 0 \tag{4.2}$$

where δ is the distance travelled by a particle at the speed of the characteristics, which is identical to a constant convection velocity u for scalar problems. $\hat{x} = x - udt$ is the characteristic direction in one dimension.

Also, it is possible to weight Equation (4.2) and integrate over the domain. The weighted residual form at $\hat{x} + \delta$ can be written as

$$\int_{\Omega} w(\hat{x}+\delta)\left[\phi\left(\hat{x}+\delta, t_{n+1}\right)-\phi\left(\hat{x}, t_{n}\right)\right] d\Omega=0 \tag{4.3}$$

By substituting interpolation functions, Equation (4.3) becomes

$$\int_{\Omega} N^{j}(\hat{x}+\delta)\left[N^{i}(\hat{x}+\delta)\phi\left(\hat{x}+\delta, t_{n+1}\right)-N^{i}(\hat{x})\phi\left(\hat{x}, t_{n}\right)\right] d\Omega=0 \tag{4.4}$$

The exact integration of the above equation is not available due to different spatial positions of $N^i(\hat{x})$ and $N^j(\hat{x}+\delta)$. Thus an approximate integration procedure may be used. It is noted that back tracking the position $\hat{x}$ at each time step is not difficult using an approximate integration, apart from complex geometries in multi-dimensional flows [14].

However, in order to overcome the difficulties of the direct method, both the indirect characteristic Galerkin procedure [108, 109] and the explicit characteristic Galerkin procedure [12, 13, 14, 15, 16] have been addressed in the literature. The second one is in the author's view more important to develop a stabilized form.

4.1.2 Explicit characteristic Galerkin procedure

We consider the convection diffusion scalar Equation (4.1) again. Let the trajectory of the reference particle is located at the spatial point $\hat{x}_i$ at time $t = t_{ref}$, so that characteristic direction is given as $\hat{x}_i = x_i - u_i dt$ and therefore

$$\frac{d}{dt}\phi\left(\hat{x}_i(t), t\right)\Big|_{t=t_{ref}} = \left(\frac{\partial\phi\left(\hat{x}_i(t), t\right)}{\partial t}+\frac{\partial\phi\left(\hat{x}_i(t), t\right)}{\partial x_i}\frac{dx_i}{dt}\right)\Big|_{\hat{x}_i=x_i-u_i dt} \tag{4.5}$$

where $dx_i/dt = u_i$

Thus the scalar Equation (4.1) now becomes

$$\frac{d\phi}{dt}-\frac{\partial}{\partial x_i}\left(\alpha\frac{\partial\phi}{\partial x_i}\right)+Q=0 \tag{4.6}$$

It is observed along the characteristics from Equation (4.6) that the convective acceleration term disappears, so the equation is self-adjoint. The temporal discretization is written as

$$
\begin{aligned}
\phi\left(\hat{x}_i(t_{n+1}), t_{n+1}\right) &= \phi\left(\hat{x}_i(t_n), t_n\right) - \\
&- \theta\Delta t\left\{Q\left(\hat{x}_i(t_{n+1}), t_{n+1}\right) - \frac{\partial}{\partial x_i}\left[\alpha\frac{\partial\phi\left(\hat{x}_i(t_{n+1}), t_{n+1}\right)}{\partial x_i}\right]\right\} + \\
&+ (\theta - 1)\Delta t\left\{Q\left(\hat{x}_i(t_n), t_n\right) - \frac{\partial}{\partial x_i}\left[\alpha\frac{\partial\phi\left(\hat{x}_i(t_n), t_n\right)}{\partial x_i}\right]\right\} \qquad (4.7)
\end{aligned}
$$

where $\theta \in [0, 1]$. Crank-Nicolson scheme [110] employs $\theta = 0.5$ to obtain a second order approximation.

Here, $\hat{x}_i$ is expanded by the Taylor series in time that can be approximated up to second order as [13]

$$
\frac{\hat{x}_i(t_{n+1}) - \hat{x}_i(t_n)}{\Delta t} = u_i\left(\hat{x}_i(t_n), t_n\right) + O(\Delta t^2) \qquad (4.8)
$$

Therefore, u_i is expanded by the Taylor series in characteristic direction at $t_{ref} = t_{n+1}$, i.e.

$$
\begin{aligned}
u_i\left(\hat{x}_i(t_n), t_n\right)\Big|_{(x_i-\delta)} &= u_i\left(x_i - \Delta t u_i\left(x_i, t_n\right) + O(\Delta t^2), t_n\right)\Big|_{(x_i-\delta)} \\
&= u_i\left(x_i, t_n\right) - \delta\frac{\partial u_i\left(x_i, t_n\right)}{\partial x_j} + O(\Delta t^2) \qquad (4.9)
\end{aligned}
$$

where δ is the distance travelled by the reference particle in the characteristic direction which is [14, 16]

$$
\delta = \breve{u}_i\Delta t \qquad (4.10)
$$

where

$$
\breve{u}_i = \frac{u_i\left(\hat{x}_i(t_{n+1}), t_{n+1}\right) + u_i\left(\hat{x}_i(t_n), t_n\right)\Big|_{(x_i-\delta)}}{2} \qquad (4.11)
$$

that is an average value of u_i along the characteristics.

Substituting Equations (4.9), (4.10) and (4.11) into Equation (4.8)

$$
\begin{aligned}
x_i &= \hat{x}_i(t_n) + \frac{\Delta t}{2}\left(u_i\left(x_i, t_{n+1}\right) + u_i\left(x_i, t_n\right)\right) - \\
&- \frac{(\Delta t)^2}{2} u_j\left(x_j, t_n\right) \frac{\partial u_i\left(x_i, t_n\right)}{\partial x_j} + O(\Delta t^3) \\
&= \hat{x}_i(t_n) + \Delta t u_i\left(x_i, t_{n+1/2}\right) - \frac{(\Delta t)^2}{2} u_j\left(x_j, t_n\right) \frac{\partial u_i\left(x_i, t_n\right)}{\partial x_j} + O(\Delta t^3) \qquad (4.12)
\end{aligned}
$$

where $u_i(x_i, t_{n+1/2}) = [u_i(x_i, t_{n+1}) + u_i(x_i, t_n)]/2$. From the Taylor series expansion and equation (4.12) we have

$$
\begin{aligned}
&\phi\left(\hat{x}_i(t_n), t_n\right)\Big|_{(x_i-\delta)} \\
&= \phi\left(x_i - \Delta t u_i(x_i, t_{n+1/2}) + \frac{(\Delta t)^2}{2} u_j(x_j, t_n) \frac{\partial u_i(x_i, t_n)}{\partial x_j} + O(\Delta t^3), t_n\right)\Big|_{(x_i-\delta)} \\
&= \phi\left(x_i, t_n\right) - \Delta t u_k(x_k, t_{n+1/2}) \frac{\partial \phi\left(x_k, t_n\right)}{\partial x_k} + \frac{(\Delta t)^2}{2} u_j\left(x_j, t_n\right) \frac{\partial u_i\left(x_i, t_n\right)}{\partial x_j} \frac{\partial \phi\left(x_k, t_n\right)}{\partial x_k} + \\
&+ \frac{(\Delta t)^2}{2} u_j(x_j, t_{n+1/2}) u_k(x_k, t_{n+1/2}) \frac{\partial}{\partial x_j} \frac{\partial \phi\left(x_k, t_n\right)}{\partial x_k} + O(\Delta t^3) \qquad (4.13)
\end{aligned}
$$

For the fully explicit version of the scheme, we write the following approximations

$$
\begin{aligned}
u_i(x_i, t_{n+1/2}) &= u_i(x_i, t_n) + O(\Delta t) \\
\frac{\partial}{\partial x_i} \phi\left(x_i, t_{n+1/2}\right) &= \frac{\partial}{\partial x_i} \phi\left(x_i, t_n\right) + O(\Delta t) \\
Q\left(x_i, t_{n+1/2}\right) &= Q\left(x_i, t_n\right) + O(\Delta t) \qquad (4.14)
\end{aligned}
$$

Thus we have

$$
\begin{aligned}
&\frac{1}{\Delta t}\left[\phi\left(\hat{x}_i(t_{n+1}), t_{n+1}\right) - \phi\left(\hat{x}_i(t_n), t_n\right)\Big|_{(x_i-\delta)}\right] \\
&\quad = \frac{1}{\Delta t}\left[\phi\left(x_i, t_{n+1}\right) - \phi\left(x_i, t_n\right)\right] + u_j(x_j, t_n) \frac{\partial \phi\left(x_j, t_n\right)}{\partial x_j} - \\
&\quad - \frac{\Delta t}{2} u_i(x_i, t_n) \frac{\partial}{\partial x_i}\left(u_j(x_j, t_n) \frac{\partial \phi\left(x_j, t_n\right)}{\partial x_j}\right) + O(\Delta t^3) \qquad (4.15)
\end{aligned}
$$

The diffusion and the source terms are averaged quantities along the characteristics. They are given as

$$\frac{\partial}{\partial x_i}\left(\alpha\frac{\partial\phi\left(\hat{x}_i(t_{n+1}),t_{n+1}\right)}{\partial x_i}\right)+\frac{\partial}{\partial x_i}\left(\alpha\frac{\partial\phi\left(\hat{x}_i(t_n),t_n\right)}{\partial x_i}\right)\Big|_{(\mathbf{x}-\delta)}$$
$$=2\frac{\partial}{\partial x_i}\left(\alpha\frac{\partial\phi\left(x_i,t_n\right)}{\partial x_i}\right)-\Delta t u_j(x_j,t_n)\frac{\partial}{\partial x_j}\left[\frac{\partial}{\partial x_i}\left(\alpha\frac{\partial\phi\left(x_i,t_n\right)}{\partial x_i}\right)\right]+O(\Delta t^2) \tag{4.16}$$

where $\frac{\partial}{\partial x_i}\left(\alpha\frac{\partial\phi(x_i,t_n)}{\partial x_i}\right)=2\frac{\partial}{\partial x_i}\left(\alpha\frac{\partial\phi\left(x_i,t_{n+1/2}\right)}{\partial x_i}\right)-\frac{\partial}{\partial x_i}\left(\alpha\frac{\partial\phi(\hat{x}_i,t_{n+1})}{\partial x_i}\right)$ and

$$Q\left(\hat{x}_i(t_{n+1}),t_{n+1}\right)+Q\left(\hat{x}_i(t_n),t_n\right)\Big|_{(x_i-\delta)}$$
$$=2Q\left(x_i,t_n\right)-\Delta t u_j\left(x_j,t_n\right)\frac{\partial Q\left(x_j,t_n\right)}{\partial x_j}+O(\Delta t^2) \tag{4.17}$$

where $Q\left(x_i,t_n\right)=2Q\left(x_i,t_{n+1/2}\right)-Q\left(\hat{x}_i,t_{n+1}\right)$.

Substituting Equations (4.15), (4.16) and (4.17) into Equation (4.7) with $\theta=0.5$ we finally obtain

$$\begin{aligned}
\Delta\phi &= \phi\left(x_i,t_{n+1}\right)-\phi\left(x_i,t_n\right)\\
&= \Delta t\left[-u_j\left(x_j,t_n\right)\frac{\partial\phi\left(x_j,t_n\right)}{\partial x_j}+\frac{\partial}{\partial x_i}\left(\alpha\frac{\partial\phi\left(x_i,t_n\right)}{\partial x_i}\right)-Q\left(x_i,t_n\right)\right]+\\
&+ \frac{(\Delta t)^2}{2}\left\{u_i\left(x_i,t_n\right)\frac{\partial}{\partial x_i}\left(u_j\left(x_j,t_n\right)\frac{\partial\phi\left(x_j,t_n\right)}{\partial x_j}\right)\right\}+\\
&+ \frac{(\Delta t)^2}{2}\left\{-u_j\left(x_j,t_n\right)\frac{\partial}{\partial x_j}\left[\frac{\partial}{\partial x_i}\left(\alpha\frac{\partial\phi\left(x_i,t_n\right)}{\partial x_i}\right)\right]+u_j\left(x_j,t_n\right)\frac{\partial Q\left(x_j,t_n\right)}{\partial x_j}\right\}
\end{aligned} \tag{4.18}$$

Moreover, if linear elements are used the third and higher order terms in the stabilized formulation may be neglected for the spatial discretization.

4.2 Temporal discretization and splitting procedure

The splitting method follows the process originally introduced by Chorin [111, 112] for incompressible flow in the finite difference analysis. Zienkiewicz and Codina [13] extended the split to solve the governing equations of fluid dynamics for both compressible and incompressible formulations using the characteristic Galerkin procedure. Here, we present the semi-implicit CBS scheme and the matrix free CBS-AC scheme for the Reynolds averaged Navier-Stokes equations.

The non-dimensional form of the governing equations depend on the nature of the flow which can be obtained by employing the following scales

$$\bar{u}_i^* = \frac{\bar{u}_i}{u_\infty}; \quad \rho^* = \frac{\rho}{\rho_\infty}; \quad \mu^* = \frac{\mu}{\mu_\infty}; \quad x_i^* = \frac{x_i}{L}; \quad t^* = \frac{t u_\infty}{L}; \quad \bar{p}^* = \frac{\bar{p}}{\rho_\infty u_\infty^2};$$
$$\kappa^* = \frac{\kappa}{u_\infty^2}; \quad \varepsilon^* = \frac{\varepsilon L}{u_\infty^3}; \quad \hat{\nu}^* = \frac{\hat{\nu}}{\nu_\infty}; \quad \tau_{ij}^* = \frac{\tau_{ij}}{\rho_\infty u_\infty^2}; \quad \tau_{ij}^{R*} = \frac{\tau_{ij}^R}{\rho_\infty u_\infty^2}; \quad \mu_t^* = \frac{\mu_t}{\mu_\infty} \tag{4.19}$$

where an asterisk indicates a non-dimensional quantity and an over-bar indicates a mean value. A subscript ∞ represents a free stream quantity, L is a reference length.

The scheme contains three steps. In the first step, the intermediate momentum is established, in the second step, the pressure (gravitational action neglected) is obtained from a modified continuity equation and finally the intermediate velocity variables are corrected to get the final velocity values. Any turbulent transport equation can be added as a fourth step.

The three steps of time discretization of the scheme may be written in the $semi-discrete\ form$ as (dropping the asterisks from the non-dimensional forms and defining the overline for time-averaged values are dropped as well for simplicity)

Step1: Intermediate momentum

Following Equation (4.18) we get

$$\begin{aligned}\Delta U_j^* &= U_j^* - U_j^n \\ &= \Delta t \left[-\frac{\partial}{\partial x_k}(u_k U_j) + \frac{1}{Re}\frac{\partial \tau_{ij}}{\partial x_i} + \frac{1}{Re}\frac{\partial \tau_{ij}^R}{\partial x_i} \right]^n + \\ &+ \frac{(\Delta t)^2}{2} \left\{ u_m \frac{\partial}{\partial x_m} \left[\frac{\partial}{\partial x_k}(u_k U_j) - \frac{1}{Re}\left(\frac{\partial \tau_{ij}}{\partial x_i} + \frac{\partial \tau_{ij}^R}{\partial x_i} \right) \right] \right\}^n \end{aligned} \tag{4.20}$$

where $U_j^n = U_j(t_n) = \rho u_j^n$ is the momentum of fluid particles per unit volume in which

$\Delta t = t^{n+1} - t^n$ and $\star$ indicates an intermediate quantity. $Re = \rho_\infty u_\infty L/\mu_\infty$ is the Reynolds number.

Step2: Pressure

$$\left(\frac{1}{c^2}\right)^n \Delta p = \left(\frac{1}{c^2}\right)^n (p^{n+1} - p^n)$$
$$= -\Delta t \left[\frac{\partial U_j^n}{\partial x_j} + \theta_1 \frac{\partial \Delta U_j^\star}{\partial x_j} - \Delta t \theta_1 \left(\frac{\partial^2 p^n}{\partial x_j \partial x_j} + \theta_2 \frac{\partial^2 \Delta p}{\partial x_j \partial x_j}\right)\right] \quad (4.21)$$

where c is the speed of sound which assumes density changes are related to pressure changes for small compressibility or elastic deformability and approaches infinity for incompressible flows.

Step3: Momentum correction

$$\Delta U_j = U_j^{n+1} - U_j^n = \Delta U_j^\star - \Delta t \frac{\partial p}{\partial x_j}^{n+\theta_2} \quad (4.22)$$

where $0.5 \leq \theta_1 \leq 1$ and $\theta_2 = 0$ is in the explicit form. $0.5 \leq \theta_1 \leq 1$ and $0.5 \leq \theta_2 \leq 1$ is in the semi-implicit form.

Step4: Turbulence transport equations

<u>Turbulent kinetic energy</u>

$$\Delta K = K^{n+1} - K^n$$
$$= \Delta t \left[-\frac{\partial}{\partial x_j}(u_j K) + \frac{1}{Re}\frac{\partial}{\partial x_j}\left(\mu + \frac{\mu_t}{\sigma_\kappa}\right)\frac{\partial \kappa}{\partial x_j} + \tau_{ij}^R \frac{\partial u_j}{\partial x_i} - E\right]^n +$$
$$+ \frac{(\Delta t)^2}{2}\left\{u_k \frac{\partial}{\partial x_k}\left[\frac{\partial}{\partial x_j}(u_j K) - \frac{1}{Re}\frac{\partial}{\partial x_j}\left(\mu + \frac{\mu_t}{\sigma_\kappa}\right)\frac{\partial \kappa}{\partial x_j} - \tau_{ij}^R \frac{\partial u_j}{\partial x_i} + E\right]\right\}^n \quad (4.23)$$

where $K^n = K(t_n) = \rho\kappa^n$ and $E^n = E(t_n) = \rho\varepsilon^n$.

<u>Dissipation rate of turbulent kinetic energy</u>

$$\Delta E = E^{n+1} - E^n$$
$$= \Delta t \left[-\frac{\partial}{\partial x_j}(u_j E) + \frac{1}{Re}\frac{\partial}{\partial x_j}\left(\mu + \frac{\mu_t}{\sigma_\varepsilon}\right)\frac{\partial \varepsilon}{\partial x_j} + c_{\varepsilon 1}\frac{\varepsilon}{\kappa}\tau_{ij}^R \frac{\partial u_j}{\partial x_i} - c_{\varepsilon 2}\frac{E^2}{K}\right]^n +$$
$$+ \frac{(\Delta t)^2}{2}\left\{u_k \frac{\partial}{\partial x_k}\left[\frac{\partial}{\partial x_j}(u_j E) - \frac{1}{Re}\frac{\partial}{\partial x_j}\left(\mu + \frac{\mu_t}{\sigma_\varepsilon}\right)\frac{\partial \varepsilon}{\partial x_j} - c_{\varepsilon 1}\frac{\varepsilon}{\kappa}\tau_{ij}^R \frac{\partial u_j}{\partial x_i} + c_{\varepsilon 2}\frac{E^2}{K}\right]\right\}^n \quad (4.24)$$

Modified turbulent eddy kinematic viscosity (Spalart-Allmaras model)

$$\begin{aligned}\Delta\hat{\nu} &= \hat{\nu}^{n+1} - \hat{\nu}^{n}\\ &= \Delta t\left[-\frac{\partial}{\partial x_j}(u_j\hat{\nu}) + \frac{1}{\sigma_{\hat{\nu}}Re}\frac{\partial}{\partial x_j}\left(\nu+\hat{\nu}\right)\frac{\partial\hat{\nu}}{\partial x_j} + \frac{c_{b2}}{\sigma_{\hat{\nu}}Re}\left(\frac{\partial\hat{\nu}}{\partial x_j}\right)^2 - \frac{c_{w1}f_w}{Re}\left(\frac{\hat{\nu}}{y}\right)^2\right]^n +\\ &+ \Delta t\left\{c_{b1}\hat{S}\hat{\nu} + \frac{\Delta t}{2}u_i\frac{\partial}{\partial x_i}\left[\frac{\partial}{\partial x_j}(u_j\hat{\nu}) - \frac{1}{\sigma_{\hat{\nu}}Re}\frac{\partial}{\partial x_j}\left(\nu+\hat{\nu}\right)\frac{\partial\hat{\nu}}{\partial x_j}\right]\right\}^n +\\ &+ \frac{(\Delta t)^2}{2}\left\{u_i\frac{\partial}{\partial x_i}\left[-\frac{c_{b2}}{\sigma_{\hat{\nu}}Re}\left(\frac{\partial\hat{\nu}}{\partial x_j}\right)^2 + \frac{c_{w1}f_w}{Re}\left(\frac{\hat{\nu}}{y}\right)^2 - c_{b1}\hat{S}\hat{\nu}\right]\right\}^n\end{aligned} \tag{4.25}$$

The extra second order terms in last part of RHS at step1 and step4 are consistent and reduce oscillations due to the standard Galerkin type discretization of convective terms. The third and higher order terms are generally neglected if linear elements are employed. The boundary conditions for the CBS scheme consist of both Dirichlet and Neumann conditions. The Dirichlet conditions for velocity such as no slip conditions are prescribed at step3. The traction conditions are prescribed at step1. No Dirichlet pressure conditions are essential for the explicit CBS scheme, but at least one pressure boundary condition is essential for the semi-implicit scheme.

4.3 Matrix free CBS-AC scheme

The CBS algorithm based on the artificial compressibility formulation belongs to the class of matrix free methods and this scheme is obtained by substituting $\theta_1 = 1$ and $\theta_2 = 0$. Also, the acoustic wave velocity c needs to be replaced by a finite speed (artificial compressibility) β in Equation (4.21). In general, the artificial compressibility parameter β is calculated from the local velocity scale and the mesh size, as discussed below.

4.3.1 The artificial compressibility (AC) method

The principle of using artificial compressibility for solving incompressible flow equations was first introduced by Chorin [26]. Here, the time derivative of density equation is written as a function of a parameter β and time derivative of pressure. Thus, a matrix free method for solving incompressible viscous flow problems may be constructed using this principle.

The appropriate local time steps to account for the local stability is based on a suitable artificial compressibility parameter β, which is given as [27, 29, 113]

$$\beta = max(e, v_{conv}, v_{diff}) \tag{4.26}$$

where e is small constant, v_{conv} is the convective velocity and v_{diff} is the diffusive velocity, which can be calculated as

$$v_{conv} = \sqrt{u_i u_i} \tag{4.27}$$

$$v_{diff} = \frac{(\nu + \nu_t)}{\sigma_{vn} h Re} \tag{4.28}$$

where $\sigma_{vn} = 0.5$ is the von Neumann number and h is the local element size. In addition, the local time stepping Δt approach with different time steps at nodes are employed to accelerate the solution to steady state. The local time step is calculated as

$$\Delta t = min(\Delta t_{conv}, \Delta t_{diff}) \tag{4.29}$$

where

$$\Delta t_{conv} = \frac{h}{v_{conv} + \beta} \tag{4.30}$$

and

$$\Delta t_{diff} = \frac{\sigma_{vn} h^2 Re}{(\nu + \nu_t)} \tag{4.31}$$

Equation (4.29) is multiplied by a safety factor which is common to both time steps calculated using diffusion and convection velocities. The range of a safety factor varies between 0.1 and 0.8 depending on the problem and mesh used.

As mentioned before the time steps are calculated at nodes. Therefore the local element size, h, at a node ip connected to the number of element ie is defined as

$$h_{ip} = min\left(\frac{3\ Volume}{Area\ of\ the\ opposite\ triangular\ element}\right)_{ie} \tag{4.32}$$

in three-dimensional flows using four noded tetrahedral elements. Similarly

$$h_{ip} = min\left(\frac{2\ Area}{Length\ of\ the\ opposite\ side}\right)_{ie} \tag{4.33}$$

in two-dimensional flows using three noded triangles.

4.3.2 The dual time stepping method

The dual time stepping technique of recovering numerical solutions to transient flow is standard and explained by authors [27, 29]. It requires the addition of a real time term to the correction stage to progress in real time.

This method implies the use of two time steps. The first is a "real" or outer or global or physical time step that corresponds to the temporal discretization of the real physical time variation. Another is an artificial or inner or "local" or pseudo time step which is used to iterate the solution within each real time step. For the inner iterating loop, the local time step is allowed to vary node to node. This means the local time step depends on local element size.

As mentioned before the real transient term is added to the momentum correction and the turbulent transport equations. Thus Equation (4.22) may be re-written as

$$U_j^{n+\theta_1} = \theta_1 \left[U_j^\star - \Delta t \frac{\partial p}{\partial x_j}^{n+\theta_2} \right] + (1-\theta_1)U_j^n - \Delta t \frac{\Delta U_j^\tau}{\Delta \tau} \tag{4.34}$$

where $U_j^{n+\theta_1} \equiv \theta_1 U_j^{n+1} + (1-\theta_1)U_j^n$ in which θ_1 is equal to unity for the matrix free scheme. The real time step is $\Delta\tau$. In order to get a second order real time accuracy, ΔU_j^τ is approximated using

$$\Delta U_j^\tau = \frac{3U_j^{n+1} - 4U_j^m + U_j^{m-1}}{2} \tag{4.35}$$

In the above equation U_j^{n+1} is equal to the nth inner iteration counter within each real time step $\Delta\tau$. The other two values, U_j^m and U_j^{m-1}, need to be appropriately stored at the start of each real time loop. m indicates the real time step counter. The steady state convergence criterion is set within each real time step. The dual time stepping technique leads the transient numerical solution of matrix free CBS-AC algorithm and often referred to as implicit scheme [114].

In a similar fashion, a real time term is added to the turbulence transport equations to recover the real time variation of the turbulent kinetic energy, dissipation rate and turbulent eddy kinematic viscosity.

4.4 Semi-implicit CBS scheme

The only difference between the matrix free CBS-AC scheme and the semi-implicit CBS scheme is that here implicit solution of the pressure Poisson equation is sought. This scheme is obtained by substituting $\theta_1 = 1$ and $\theta_2 = 1$ with the acoustic wave velocity c approaching infinite. Thus, Equation (4.21) can be rewritten as

$$\frac{\partial^2 p^{n+1}}{\partial x_j x_j} = \frac{1}{\Delta t}\frac{\partial U_j^{\star}}{\partial x_j} \tag{4.36}$$

where a critical time step $\Delta t = h/(\|u_j\|)$ is applicable here.

4.4.1 The preconditioned conjugate gradient method

The large storage requirement is the major drawback of semi-implicit CBS scheme, especially in three-dimensional flows, with a sparse system of linear equations [6]. However, one of iterative method, preconditioned conjugate gradient [6], [50]-[53], can reduce the difficulties associated with sparseness of the matrices. This method constructs the residual of conjugate vectors which are the gradient and minimizer of a quadratic functional. The preconditioning matrix leads to rapid convergence depends on the limited condition number, i.e.

$$\Lambda = \frac{\lambda_{max}}{\lambda_{min}} \tag{4.37}$$

where λ_{max} and λ_{min} are the largest and smallest eigenvalues from the solution.

In this study, conjugate gradient algorithm is used to solve the pressure Poisson equation at step2 on the structured and unstructured meshes.

4.5 Spatial discretization and matrix form

The standard Galerkin method is employed for spatial discretization. The following spatial discretization of the variables are employed.

$$U_j = \mathbf{N_u}\tilde{\mathbf{U}}_\mathbf{j};\ \ \Delta U_j = \mathbf{N_u}\Delta\tilde{\mathbf{U}}_\mathbf{j};\ \ \Delta U_j^\star = \mathbf{N_u}\Delta\tilde{\mathbf{U}}_\mathbf{j}^\star;\ \ u_j = \mathbf{N_u}\tilde{\mathbf{u}}_\mathbf{j};\ \ p = \mathbf{N_p}\tilde{\mathbf{p}};$$
$$\Delta p = \mathbf{N_p}\Delta\tilde{\mathbf{p}};\ \ K = \mathbf{N}_\kappa\tilde{\mathbf{K}};\ \ \kappa = \mathbf{N}_\kappa\tilde{\kappa};\ \ E = \mathbf{N}_\varepsilon\tilde{\mathbf{E}};\ \ \varepsilon = \mathbf{N}_\varepsilon\tilde{\varepsilon};\ \ \hat{\nu} = \mathbf{N}_{\hat{\nu}}\tilde{\hat{\nu}} \tag{4.38}$$

In the above equation $\mathbf{N}$ are the shape functions and $\tilde{}$ indicates a nodal quantity, i.e.

$$\tilde{\mathbf{U}}_\mathbf{j} = \begin{bmatrix} U_j^1 & U_j^2 & ... & U_j^k & ... & U_j^l \end{bmatrix}^T$$
$$\mathbf{N} = \begin{bmatrix} N^1 & N^2 & ... & N^k & ... & N^l \end{bmatrix} \tag{4.39}$$

where k is the node identifing number and varies between 1 and l.

Applying the standard Galerkin approximation with the divergence theorem, we get the following weak forms, i.e.

Step1 Weak form of intermediate momentum

$$\begin{aligned}\int_\Omega \mathbf{N_u}^T \Delta U_j^\star d\Omega &= \Delta t \left[-\int_\Omega \mathbf{N_u}^T \frac{\partial}{\partial x_k}(u_k U_j) d\Omega - \frac{1}{Re}\int_\Omega \frac{\partial \mathbf{N_u}^T}{\partial x_i}(\tau_{ij} + \tau_{ij}^R) d\Omega \right]^n + \\ &+ \frac{\Delta t^2}{2}\left[\int_\Omega \frac{\partial}{\partial x_m}(u_m \mathbf{N_u}^T)\left(-\frac{\partial}{\partial x_k}(u_k U_j)\right) d\Omega \right]^n + \\ &+ \Delta t \left[\int_\Gamma \mathbf{N_u}^T \mathbf{t_d} d\Gamma \right]^n \end{aligned} \tag{4.40}$$

In the above equation $\mathbf{t_d} = [(\tau_{ij} + \tau_{ij}^R)/Re]\mathbf{n}$ indicates the part of the traction corresponding to the deviatoric and Reynolds stresses only and $\mathbf{n}$ are the components of the outward normal to the boundaries. As the pressure term is completely removed from the first step, we have only deviatoric and Reynolds stresses part of the traction left in the equation.

Step2 Weak form of pressure equation

Matrix free scheme

$$\int_\Omega \mathbf{N_p}^T \left(\frac{1}{\beta^2}\right)^n \Delta p d\Omega = -\Delta t \int_\Omega \mathbf{N_p}^T \frac{\partial}{\partial x_j} U_j^n d\Omega - \Delta t \int_\Gamma \mathbf{N_p}^T \left(\Delta U_j^\star - \Delta t \frac{\partial p}{\partial x_j}^n\right) n_j d\Gamma + + \Delta t \int_\Omega \frac{\partial \mathbf{N_p}^T}{\partial x_j} \left(\Delta U_j^\star - \Delta t \frac{\partial p}{\partial x_j}^n\right) d\Omega \tag{4.41}$$

In the above equation, pressure and $\Delta U_i^\star$ terms are integrated by parts and n_j are the components of the outward normal to the boundaries.

Semi-implicit scheme

$$\int_\Gamma \mathbf{N_p}^T \frac{\partial p}{\partial x_j}^{n+1} n_j d\Gamma - \int_\Omega \frac{\partial \mathbf{N_p}^T}{\partial x_j} \frac{\partial p}{\partial x_j}^{n+1} d\Omega = \frac{1}{\Delta t} \int_\Omega \mathbf{N_p}^T \frac{\partial U_j^\star}{\partial x_j} d\Omega \tag{4.42}$$

Here, pressure term is integrated by parts.

Step3 Weak form of momentum correction

Matrix free scheme

$$\int_\Omega \mathbf{N_u}^T \Delta U_j d\Omega = \int_\Omega \mathbf{N_u}^T \Delta U_j^\star d\Omega + \Delta t \int_\Omega \frac{\partial \mathbf{N_u}^T}{\partial x_j} p^n d\Omega - \Delta t \int_\Gamma \mathbf{N_u}^T \mathbf{t_p} d\Gamma \tag{4.43}$$

Semi-implicit scheme

$$\int_\Omega \mathbf{N_u}^T \Delta U_j d\Omega = \int_\Omega \mathbf{N_u}^T \Delta U_j^\star d\Omega + \Delta t \int_\Omega \frac{\partial \mathbf{N_u}^T}{\partial x_j} p^{n+1} d\Omega - \Delta t \int_\Gamma \mathbf{N_u}^T \mathbf{t_p} d\Gamma \tag{4.44}$$

In the above two equations $\mathbf{t_p} = (p^n + \theta_2 \Delta p)\mathbf{n}$ only indicates the part of the traction corresponding to the pressure which was removed from step1. It is simply ignored and assumed to be zero as the full traction is prescribed and employed in step1 [115].

Step4: Weak form of turbulence transport equations

Turbulent kinetic energy

$$\begin{aligned}\int_\Omega \mathbf{N}_\kappa{}^T \Delta K d\Omega &= \Delta t \left[-\int_\Omega \mathbf{N}_\kappa{}^T \frac{\partial}{\partial x_j}(u_j K) d\Omega - \frac{1}{Re}\int_\Omega \frac{\partial \mathbf{N}_\kappa{}^T}{\partial x_j}\left(\mu + \frac{\mu_t}{\sigma_\kappa}\right)\frac{\partial \kappa}{\partial x_j} d\Omega\right]^n + \\ &+ \Delta t \left[\int_\Omega \mathbf{N}_\kappa{}^T \tau_{ij}^R \frac{\partial u_j}{\partial x_i} d\Omega - \int_\Omega \mathbf{N}_\kappa{}^T E d\Omega\right]^n + \\ &+ \frac{\Delta t^2}{2}\left[\int_\Omega \frac{\partial}{\partial x_l}(u_l \mathbf{N}_\kappa{}^T)\left(-\frac{\partial}{\partial x_j}(u_j K)\right) d\Omega\right]^n + \\ &+ \Delta t \left[\frac{1}{Re}\int_\Gamma \mathbf{N}_\kappa{}^T \left(\mu + \frac{\mu_t}{\sigma_\kappa}\right)\frac{\partial \kappa}{\partial x_j} n_j d\Gamma\right]^n \end{aligned} \tag{4.45}$$

Dissipation rate of turbulent kinetic energy

$$\begin{aligned}\int_\Omega \mathbf{N}_\varepsilon{}^T \Delta E d\Omega &= \Delta t\left[-\int_\Omega \mathbf{N}_\varepsilon{}^T\frac{\partial}{\partial x_j}(u_jE)d\Omega - \frac{1}{Re}\int_\Omega \frac{\partial \mathbf{N}_\varepsilon{}^T}{\partial x_j}\left(\mu+\frac{\mu_t}{\sigma_\varepsilon}\right)\frac{\partial\varepsilon}{\partial x_j}d\Omega\right]^n + \\ &+ \Delta t\left[\int_\Omega \mathbf{N}_\varepsilon{}^T c_{\varepsilon 1}\frac{\varepsilon}{\kappa}\tau_{ij}^R\frac{\partial u_j}{\partial x_i}d\Omega - \int_\Omega \mathbf{N}_\varepsilon{}^T c_{\varepsilon 2}\frac{E^2}{K}d\Omega\right]^n + \\ &+ \frac{\Delta t^2}{2}\left[\int_\Omega \frac{\partial}{\partial x_l}(u_l\mathbf{N}_\varepsilon{}^T)\left(-\frac{\partial}{\partial x_j}(u_jE)\right)d\Omega\right]^n + \\ &+ \Delta t\left[\frac{1}{Re}\int_\Gamma \mathbf{N}_\varepsilon{}^T\left(\mu+\frac{\mu_t}{\sigma_\varepsilon}\right)\frac{\partial\varepsilon}{\partial x_j}n_jd\Gamma\right]^n \qquad (4.46)\end{aligned}$$

Modified turbulent eddy kinematic viscosity (Spalart-Allmaras model)

$$\begin{aligned}\int_\Omega \mathbf{N}_{\hat\nu}{}^T \Delta\hat\nu d\Omega &= \Delta t\left[-\int_\Omega \mathbf{N}_{\hat\nu}{}^T\frac{\partial}{\partial x_j}(u_j\hat\nu)d\Omega - \frac{1}{\sigma_{\hat\nu}Re}\int_\Omega \frac{\partial \mathbf{N}_{\hat\nu}{}^T}{\partial x_j}(\nu+\hat\nu)\frac{\partial\hat\nu}{\partial x_j}d\Omega\right]^n + \\ &+ \Delta t\left[\int_\Omega \mathbf{N}_{\hat\nu}{}^T\left(c_{b1}\hat S - \frac{c_{w1}f_w}{Re}\frac{\hat\nu}{y^2}\right)\hat\nu d\Omega\right]^n + \\ &+ \Delta t\left[\frac{1}{\sigma_{\hat\nu}Re}\int_\Omega \mathbf{N}_{\hat\nu}{}^T c_{b2}\left(\frac{\partial\hat\nu}{\partial x_j}\right)^2 d\Omega\right]^n + \\ &+ \frac{\Delta t^2}{2}\left[\int_\Omega \frac{\partial}{\partial x_i}(u_i\mathbf{N}_{\hat\nu}{}^T)\left(-\frac{\partial}{\partial x_j}(u_j\hat\nu)\right)d\Omega\right]^n + \\ &+ \Delta t\left[\frac{1}{\sigma_{\hat\nu}Re}\int_\Gamma \mathbf{N}_{\hat\nu}{}^T(\nu+\hat\nu)\frac{\partial\hat\nu}{\partial x_j}n_jd\Gamma\right]^n \qquad (4.47)\end{aligned}$$

The final matrix form of the above weak forms are

Step1: Intermediate momentum

$$\Delta\tilde{\mathbf{U}}^\star = -\mathbf{M_u}^{-1}\Delta t\left[(\mathbf{C_u}\tilde{\mathbf{U}} + \mathbf{K}_\tau\tilde{\mathbf{u}} + \mathbf{C}_{\mathbf{u}\kappa}\tilde{\mathbf{K}} - \mathbf{f_u}) - \Delta t(\mathbf{K_u}\tilde{\mathbf{U}})\right]^n \qquad (4.48)$$

Step2: Pressure

$$(\mathbf{M_p} + \Delta t^2\theta_1\theta_2\mathbf{H})\Delta\tilde{\mathbf{p}} = \Delta t[\mathbf{G}\tilde{\mathbf{U}}^\mathbf{n} + \theta_1\mathbf{G}\Delta\tilde{\mathbf{U}}^\star - \Delta t\theta_1\mathbf{H}\tilde{\mathbf{p}} - \mathbf{f_p}]^n \qquad (4.49)$$

Step3: Momentum correction

$$\Delta\tilde{\mathbf{U}} = \Delta\tilde{\mathbf{U}}^\star - \mathbf{M_u^{-1}}\Delta t\left[\mathbf{G^T}(\tilde{\mathbf{p}}^\mathbf{n} + \theta_2\Delta\tilde{\mathbf{p}})\right] \qquad (4.50)$$

Step4: Turbulence transport equations

Turbulent kinetic energy

$$\Delta\tilde{\mathbf{K}} = -\mathbf{M}_\kappa{}^{-1}\Delta t\left[(\mathbf{C}_\kappa\tilde{\mathbf{K}} + \mathbf{K}_\kappa\tilde{\kappa} - \mathbf{f}_{\kappa\mathbf{\Omega}} - \mathbf{f}_{\kappa\mathbf{\Gamma}}) - \Delta t(\mathbf{K}_{\mathbf{u}\kappa}\tilde{\mathbf{K}})\right]^n \quad (4.51)$$

Dissipation rate of turbulent kinetic energy

$$\Delta\tilde{\mathbf{E}} = -\mathbf{M}_\varepsilon{}^{-1}\Delta t\left[(\mathbf{C}_\varepsilon\tilde{\mathbf{E}} + \mathbf{K}_\varepsilon\tilde{\varepsilon} - \mathbf{f}_{\varepsilon\mathbf{\Omega}} - \mathbf{f}_{\varepsilon\mathbf{\Gamma}}) - \Delta t(\mathbf{K}_{\mathbf{u}\varepsilon}\tilde{\mathbf{E}})\right]^n \quad (4.52)$$

Modified turbulent eddy kinematic viscosity (Spalart-Allmaras model)

$$\Delta\tilde{\hat{\nu}} = -\mathbf{M}_{\hat{\nu}}{}^{-1}\Delta t\left[(\mathbf{C}_{\hat{\nu}}\tilde{\hat{\nu}} + \mathbf{K}_{\hat{\nu}}\tilde{\hat{\nu}} - \mathbf{f}_{\hat{\nu}\mathbf{\Omega}} - \mathbf{f}_{\hat{\nu}\mathbf{\Omega}^*} - \mathbf{f}_{\hat{\nu}\mathbf{\Gamma}}) - \Delta t(\mathbf{K}_{\mathbf{u}\hat{\nu}}\tilde{\hat{\nu}})\right]^n \quad (4.53)$$

where

$$\mathbf{M_u} = \int_\Omega \mathbf{N_u}^T\mathbf{N_u}d\Omega; \quad \mathbf{K}_\tau = \int_\Omega \mathbf{B}^T\frac{[(\nu+\nu_t)\rho]}{Re}\left(\mathbf{I_o} - \frac{2}{3}\mathbf{mm}^T\right)\mathbf{B}d\Omega;$$

$$\mathbf{H} = \int_\Omega (\nabla\mathbf{N_p})^T\nabla\mathbf{N_p}d\Omega; \quad \mathbf{M_p} = \int_\Omega \mathbf{N_p}^T\left(\frac{1}{\beta^2}\right)^n\mathbf{N_p}d\Omega;$$

$$\mathbf{f_p} = \Delta t\int_\Gamma \mathbf{N_p}^T\left[\mathbf{N_u}\tilde{\mathbf{U}}^{\mathbf{n}} + \theta_1\left(\Delta\tilde{\mathbf{U}}^\star - \Delta t\nabla p^{n+\theta_2}\right)\right]\mathbf{n}^T d\Gamma;$$

$$\mathbf{K_u} = -\frac{1}{2}\int_\Omega (\nabla^T(\mathbf{uN_u}))^T(\nabla^T(\mathbf{uN_u}))d\Omega; \quad \mathbf{G} = \int_\Omega (\nabla\mathbf{N_p})^T\mathbf{N_u}d\Omega;$$

$$\mathbf{f_u} = \int_\Gamma \mathbf{N_u}^T\mathbf{t_d}d\Gamma; \quad \mathbf{C_u} = \int_\Omega \mathbf{N_u}^T(\nabla^T(\mathbf{uN_u}))d\Omega; \quad \mathbf{C}_{\mathbf{u}\kappa} = \frac{2}{3}\int_\Omega \mathbf{N_u}^T\nabla\mathbf{N}_\kappa d\Omega;$$

$$\mathbf{M}_\kappa = \int_\Omega \mathbf{N}_\kappa{}^T\mathbf{N}_\kappa d\Omega; \quad \mathbf{K}_\kappa = \int_\Omega (\nabla\mathbf{N}_\kappa)^T\left(\frac{\mu_t + \sigma_\kappa\mu}{\sigma_\kappa Re}\right)\nabla\mathbf{N}_\kappa d\Omega;$$

$$\mathbf{C}_\kappa = \int_\Omega \mathbf{N}_\kappa{}^T(\nabla^T(\mathbf{uN}_\kappa))d\Omega; \quad \mathbf{f}_{\kappa\mathbf{\Omega}} = \int_\Omega \mathbf{N}_\kappa{}^T\left[\tau_{ij}^R\partial_j u_i - \mathbf{N}_\varepsilon\tilde{\mathbf{E}}\right]d\Omega;$$

$$\mathbf{f}_{\kappa\mathbf{\Gamma}} = \int_\Gamma \mathbf{N}_\kappa{}^T t_\kappa d\Gamma; \quad \mathbf{K}_{\mathbf{u}\kappa} = -\frac{1}{2}\int_\Omega (\nabla^T(\mathbf{uN}_\kappa))^T(\nabla^T(\mathbf{uN}_\kappa))d\Omega;$$

$$\mathbf{M}_\varepsilon = \int_\Omega \mathbf{N}_\varepsilon{}^T\mathbf{N}_\varepsilon d\Omega; \quad \mathbf{K}_\varepsilon = \int_\Omega (\nabla\mathbf{N}_\varepsilon)^T\left(\frac{\mu_t + \sigma_\varepsilon\mu}{\sigma_\varepsilon Re}\right)\nabla\mathbf{N}_\varepsilon d\Omega;$$

$$
\begin{aligned}
\mathbf{C}_\varepsilon = \int_\Omega \mathbf{N}_\varepsilon{}^T(\nabla^T(\mathbf{u}\mathbf{N}_\varepsilon))d\Omega; \quad \mathbf{f}_{\varepsilon\boldsymbol{\Omega}} = \frac{E}{K}\int_\Omega \mathbf{N}_\varepsilon{}^T\left[c_{\varepsilon 1}\tau_{ij}^R\partial_j u_i - c_{\varepsilon 2}\mathbf{N}_\varepsilon\tilde{\mathbf{E}}\right]d\Omega; \\
\mathbf{f}_{\varepsilon\boldsymbol{\Gamma}} = \int_\Gamma \mathbf{N}_\varepsilon{}^T t_\varepsilon d\Gamma; \quad \mathbf{K}_{\mathbf{u}\varepsilon} = -\frac{1}{2}\int_\Omega (\nabla^T(\mathbf{u}\mathbf{N}_\varepsilon))^T(\nabla^T(\mathbf{u}\mathbf{N}_\varepsilon))d\Omega; \\
\mathbf{M}_{\hat{\nu}} = \int_\Omega \mathbf{N}_{\hat{\nu}}{}^T\mathbf{N}_{\hat{\nu}}d\Omega; \quad \mathbf{K}_{\hat{\nu}} = \int_\Omega (\nabla\mathbf{N}_{\hat{\nu}})^T\left(\frac{\nu+\hat{\nu}}{\sigma_{\hat{\nu}}Re}\right)\nabla\mathbf{N}_{\hat{\nu}}d\Omega; \\
\mathbf{C}_{\hat{\nu}} = \int_\Omega \mathbf{N}_{\hat{\nu}}{}^T(\nabla^T(\mathbf{u}\mathbf{N}_{\hat{\nu}}))d\Omega; \quad \mathbf{f}_{\hat{\nu}\boldsymbol{\Omega}^*} = \int_\Omega \mathbf{N}_{\hat{\nu}}{}^T\left(c_{b1}\hat{S} - \frac{c_{w1}f_w}{Re}\frac{\hat{\nu}}{y^2}\right)\mathbf{N}_{\hat{\nu}}\tilde{\hat{\nu}}d\Omega; \\
\mathbf{f}_{\hat{\nu}\boldsymbol{\Omega}} = \int_\Omega \mathbf{N}_{\hat{\nu}}{}^T\left(\frac{c_{b2}}{\sigma_{\hat{\nu}}Re}\right)(\partial_i\hat{\nu})^2 d\Omega; \quad \mathbf{f}_{\hat{\nu}\boldsymbol{\Gamma}} = \int_\Gamma \mathbf{N}_{\hat{\nu}}{}^T t_{\hat{\nu}}d\Gamma; \\
\mathbf{K}_{\mathbf{u}\hat{\nu}} = -\frac{1}{2}\int_\Omega (\nabla^T(\mathbf{u}\mathbf{N}_{\hat{\nu}}))^T(\nabla^T(\mathbf{u}\mathbf{N}_{\hat{\nu}}))d\Omega
\end{aligned} \tag{4.54}
$$

In the above the strain shape function matrix $\mathbf{B}$ is given as

$$\mathbf{B} = \mathbf{S}\mathbf{N}_\mathbf{u} \tag{4.55}$$

where $\mathbf{S}$ is an strain matrix operator. For a two dimensional case

$$\mathbf{S} = \left\{\begin{array}{cc} \frac{\partial}{\partial x_1} & 0 \\ 0 & \frac{\partial}{\partial x_2} \\ \frac{\partial}{\partial x_2} & \frac{\partial}{\partial x_1} \end{array}\right\} \tag{4.56}$$

$$\mathbf{m} = [1,1,0]^T \tag{4.57}$$

and

$$\mathbf{I_o} = \begin{bmatrix} 2 & & \\ & 2 & \\ & & 1 \end{bmatrix} \tag{4.58}$$

For a three dimensional case

$$\mathbf{S} = \left\{ \begin{array}{ccc} \frac{\partial}{\partial x_1} & 0 & 0 \\ 0 & \frac{\partial}{\partial x_2} & 0 \\ 0 & 0 & \frac{\partial}{\partial x_3} \\ \frac{\partial}{\partial x_2} & \frac{\partial}{\partial x_1} & 0 \\ 0 & \frac{\partial}{\partial x_3} & \frac{\partial}{\partial x_2} \\ \frac{\partial}{\partial x_3} & 0 & \frac{\partial}{\partial x_1} \end{array} \right\} \tag{4.59}$$

$$\mathbf{m} = [1, 1, 1, 0, 0, 0]^T \tag{4.60}$$

and

$$\mathbf{I_o} = \begin{bmatrix} 2 & & & & & \\ & 2 & & & & \\ & & 2 & & & \\ & & & 1 & & \\ & & & & 1 & \\ & & & & & 1 \end{bmatrix} \tag{4.61}$$

4.6 The restriction of mixed formulations

In many problems of interest the volume remains approximately constant. The behaviour is normally called incompressibility.

Incompressible behaviour is generally defined using both the velocity $\mathbf{u}$ and pressure p parameters. Here often mixed formulations are employed in the finite element literature. Most of such mixed form of the Galerkin method results in discrete equations, which can usually be written in the following standard global matrix form [116]

$$\begin{bmatrix} \mathbf{K} & \mathbf{G}^{\mathrm{T}} \\ \mathbf{G} & \mathbf{M} \end{bmatrix} \begin{bmatrix} \tilde{\mathbf{u}} \\ \tilde{\mathbf{p}} \end{bmatrix} = \begin{bmatrix} \mathbf{f}_1 \\ \mathbf{f}_2 \end{bmatrix} \tag{4.62}$$

where $\tilde{\mathbf{u}}$ is the discrete primary variable and $\tilde{\mathbf{p}}$ is the discrete constraint variable (equivalent to a lagrangian multiplier). The matrix $\mathbf{G}$ is the discrete gradient operator, $\mathbf{K}$ and $\mathbf{M}$ are both $n \times n$ squre symmetric matrices. $\mathbf{K}$ is positive definite and $\mathbf{M}$ is either negative definite or zero, which depends on the property of the type of discretization employed. $\mathbf{f}_1$ and $\mathbf{f}_2$ arise from the force terms.

In this section how to avoid the restriction of LBB stability condition which makes ($\mathbf{M} = \mathbf{0}$) impossible to employ many useful elements is presented [117]. Thus instability generally lead to unphysical pressure oscillation and locking of the velocity field [116].

4.6.1 The CBS form

For Stokes flow, Equation (4.48) in step1 only keeps the viscous diffusion terms and the boundary traction terms [16], i.e.

$$\Delta\tilde{\mathbf{U}}^{\star} = -\mathbf{M}_u{}^{-1}\Delta t_{temp}\left[\mathbf{K}_{\tau}\tilde{\mathbf{u}}^n - \mathbf{f}_u\right]^n \tag{4.63}$$

where a time step Δt_{temp} provides the temporal stability [164].

In step2 the matrix $\mathbf{M}_p$ disappers for incompressibility and $\Delta\tilde{\mathbf{p}}$ equals zero for steady state, so Equation (4.49) can be written as

$$\mathbf{G}\tilde{\mathbf{U}}^n + \theta_1\mathbf{G}\Delta\tilde{\mathbf{U}}^{\star} - \Delta t_{spat}\theta_1\mathbf{H}\tilde{\mathbf{p}}^n = \mathbf{f}_p \tag{4.64}$$

where the spatial stability in the discrete form indicates a time step $\Delta t_{spat} = \iota\Delta t_{temp}$ in which ι is a time step ratio [164].

Then we have $\Delta\tilde{\mathbf{U}} = \mathbf{0}$ in steady state that results in Equation (4.50) in step3 reduce to

$$\Delta\tilde{\mathbf{U}}^{\star} = -\mathbf{M}_u^{-1}\Delta t_{temp}[\mathbf{G}^{\mathrm{T}}\tilde{\mathbf{p}}^n] \tag{4.65}$$

Therefore, the discretization leads to the following matrix form

$$\begin{bmatrix} \mathbf{K}_{\nu} & \mathbf{G}^{\mathrm{T}} \\ \mathbf{G} & \Delta t_{temp}\theta_1\left(\mathbf{G}\mathbf{M}_u^{-1}\mathbf{G}^{\mathrm{T}} - \iota\mathbf{H}\right) \end{bmatrix} \begin{bmatrix} \tilde{\mathbf{U}}^n \\ \tilde{\mathbf{p}}^n \end{bmatrix} = \begin{bmatrix} \mathbf{f}_u \\ \mathbf{f}_p \end{bmatrix} \tag{4.66}$$

where the matrix $\mathbf{K}_{\nu} = \mathbf{K}_{\tau}/\rho$ is the quadratic form. The discrete velocity vector is $\tilde{\mathbf{U}}^n$ and $\tilde{\mathbf{p}}^n$ is the discrete vector of nodal pressures.

If the pressure approximation is assumed to be discontinuous, then

$$\tilde{\mathbf{p}}^n = (\Delta t_{temp}\theta_1)^{-1}\left(\mathbf{G}\mathbf{M}_u^{-1}\mathbf{G}^{\mathrm{T}} - \iota\mathbf{H}\right)^{-1}\mathbf{f}_p - (\Delta t_{temp}\theta_1)^{-1}\left(\mathbf{G}\mathbf{M}_u^{-1}\mathbf{G}^{\mathrm{T}} - \iota\mathbf{H}\right)^{-1}\mathbf{G}\tilde{\mathbf{U}}^n \tag{4.67}$$

and the system for $\tilde{\mathbf{U}}^n$ will be got by eliminating $\tilde{\mathbf{p}}^n$. We can write

$$\left[\mathbf{K}_\nu + \Psi\mathbf{G}^{\mathrm{T}}\mathbf{G}\right]\tilde{\mathbf{U}}^n = \mathbf{f}_u + \Psi\mathbf{G}^{\mathrm{T}}\mathbf{f}_p \tag{4.68}$$

where the penalty function points to $\Psi = -1/(\Delta t_{temp}\theta_1\mathbf{E})$ in which $\mathbf{E} = \mathbf{G}\mathbf{M}_u^{-1}\mathbf{G}^{\mathrm{T}} - \iota\mathbf{H}$ is proportional to Δt_{temp}.

Observe that the bilinear form $\mathbf{K}_\nu$ is symmetric and positive definite from the energy expression of physical considerations. $\mathbf{E}$ is symmetric and negative definite from its quadratic form. The system is, however, always positive definite and leads to a non-singular solution for $\tilde{\mathbf{U}}^n$.

It is noted that the discrete steady state system above do not have a zero diagonal term, so the LBB resrtiction no longer influence the finite element spaces for velocity and pressure. Thus this system theoretically permit arbitrary and convenient interpolation functions to be employed for $\tilde{\mathbf{U}}^n$ and $\tilde{\mathbf{p}}^{\mathbf{n}}$. On the other hand, possibly avoiding difficulties encountered with explicit characteristic-Galerkin procedures, equal interpolation functions are chosen for any variable in this dissertation [13, 14, 118].

4.6.2 The mixed form

If all the pressure gradient terms are retained in the governing equation, the three steps of a stokes flow can be written as

$$\Delta\tilde{\mathbf{U}}^{**} = -\mathbf{M}_u{}^{-1}\Delta t_{temp}\left[\mathbf{K}_\tau\tilde{\mathbf{u}}^n + \mathbf{G}^{\mathrm{T}}\tilde{\mathbf{p}}^n - \bar{\mathbf{f}}_u\right]^n \tag{4.69}$$

where $\bar{\mathbf{f}}_u$ includes the pressure term which is integrated by parts.

$$\Delta\tilde{\mathbf{p}} = \frac{1}{\Delta t_{spat}\theta_1\theta_2}\mathbf{H}^{-1}[\mathbf{G}\tilde{\mathbf{U}}^n + \theta_1\mathbf{G}\Delta\tilde{\mathbf{U}}^{**} - \mathbf{f}_p]^n \tag{4.70}$$

$$\Delta\tilde{\mathbf{U}} = \Delta\tilde{\mathbf{U}}^{\star\star} - \mathbf{M}_u^{-1}\Delta t_{temp}\theta_2\Delta\tilde{\mathbf{p}} \tag{4.71}$$

At steady state $\Delta\tilde{\mathbf{p}} = \Delta\tilde{\mathbf{U}} = \mathbf{0}$ leads to $\Delta\tilde{\mathbf{U}}^{\star\star} = \mathbf{0}$. Finally, a typical algebraic equation set of the form can be obtained

$$\begin{bmatrix} \mathbf{K}_\nu & \mathbf{G}^{\mathrm{T}} \\ \mathbf{G} & \mathbf{0} \end{bmatrix} \begin{bmatrix} \tilde{\mathbf{U}}^n \\ \tilde{\mathbf{p}}^n \end{bmatrix} = \begin{bmatrix} \bar{\mathbf{f}}_u \\ \mathbf{f}_p \end{bmatrix} \tag{4.72}$$

Clearly, the coefficient matrix is not positive definite from its quadratic form, i.e.

$$\begin{bmatrix} 0 \\ 1 \end{bmatrix}^{\mathrm{T}} \begin{bmatrix} \mathbf{K}_\nu & \mathbf{G}^{\mathrm{T}} \\ \mathbf{G} & \mathbf{0} \end{bmatrix} \begin{bmatrix} 0 \\ 1 \end{bmatrix} = 0 \tag{4.73}$$

due to the zero diagonal term results from the mixed formulation for any assembly of elements. Such a system is singular unless the number of degrees of freedom in the $\tilde{\mathbf{U}}^n$ variables is larger than the number of degrees of freedom in the $\tilde{\mathbf{p}}^n$ variables.
Proof: If discontinuous velocities are used and the matrix $\mathbf{K}_\nu$ has unique inverse and is always non-singular and positive definite for standard stokes flows, then we can write from the first equation in Equation (4.72)

$$\tilde{\mathbf{U}}^n = \mathbf{K}_\nu^{-1}\bar{\mathbf{f}}_u - \mathbf{K}_\nu^{-1}\mathbf{G}^{\mathrm{T}}\tilde{\mathbf{p}}^n \tag{4.74}$$

By substituting into the second equation we obtain

$$\mathbf{G}\mathbf{K}_\nu^{-1}\mathbf{G}^{\mathrm{T}}\tilde{\mathbf{p}}^n = -\mathbf{f}_p + \mathbf{G}\mathbf{K}_\nu^{-1}\bar{\mathbf{f}}_u \tag{4.75}$$

which requires that the rank of $\mathbf{K}_\nu$ be greater than or equal to number of pressure degrees of freedom to obtain a unique solution of $\tilde{\mathbf{p}}^n$. Because the rank of $\mathbf{K}_\nu^{-1}$ cannot be greater than the number of velocity degrees of freedom, the number of velocity degrees of freedom over an element must be greater than number of pressure degrees of freedom.

Now let $\mathbf{H} = \mathbf{G}\mathbf{K}_\nu^{-1}\mathbf{G}^{\mathrm{T}}$. And $\mathbf{H}$ is an $n \times n$ square matrix that is non-singular if its rank is equal to n, that is the determinant of $\mathbf{H}$ is not zero. However, the rank of the matrix $\mathbf{H}$ cannot be greater than the rank of matrix $\mathbf{K}_\nu$.

Although the above mentioned requirement is necessary, it is not a sufficient condition to construct a non-singular matrix $\mathbf{H}$. Thus an equivalent condition to the stability criteria of the LBB resrtiction is added, i.e. [16, 117]

$$\mathbf{G}^{\mathrm{T}}\tilde{\mathbf{p}}^{n} \neq \mathbf{0} \quad \text{for all} \quad \tilde{\mathbf{p}}^{n} \neq \mathbf{0} \tag{4.76}$$

In addition, by multiplying $(\tilde{\mathbf{p}}^{n})^{\mathrm{T}}$ in the left hand side of equation (4.75), i.e.

$$(\tilde{\mathbf{p}}^{n})^{\mathrm{T}}\mathbf{G}\mathbf{K}_{\nu}^{-1}\mathbf{G}^{\mathrm{T}}\tilde{\mathbf{p}}^{n} > \mathbf{0} \tag{4.77}$$

if the requirement of (4.76) is satisfied to yield a unique solution. It ,therefore, shows that $\mathbf{K}_{\nu}^{-1}$ is positive definite and the rank of matrix $\mathbf{G}$ equal n. However, we do not use this form to test any cases.

4.7 Steady state convergence

The root mean square (RMS) value of error for the steady state convergence criteria is based on the L_2 norm of the velocity field. It gives the norm of different velocities between time step $n+1$ and n normalized by the Euclidean norm of the velocity at time step $n+1$, which is

$$\|e\|_{L_2} = \frac{\left[\sum_{i=1}^{NN}\left(\|\mathbf{u}\|_i^{n+1} - \|\mathbf{u}\|_i^{n}\right)^2\right]^{1/2}}{\left[\sum_{i=1}^{NN}\left(\|\mathbf{u}\|_i^{n+1}\right)^2\right]^{1/2}} \tag{4.78}$$

where NN are the number of nodes.

4.8 Fundamental aspects of unstructured mesh generation

Any given domain could be systematically decomposed into a set of convex polygons was firstly suggested by Dirichlet [146]. It is known as the Dirichlet tessellation for the geometrical construction of the Voronoi regions [147, 148]. Firstly, let S be a set of sites (i.e. points) in the Euclidean space E^d. Secondly, let d_s be a mapping of E^d to the positive real number for each $s \in S$. Then the Euclidean distance between a site s and a point p is $d_s(p)$.

Thirdly, the Voronoi region $V(s)$ can be defined as the set $\{p \in E^d | d_s(p) < d_t(p), t \in S - s\}$ in the Voronoi cell of s. It is clearly to state a given Voronoi region/convex polygon closer to its central point than to any other. In general, the Voronoi regions which is also called the Voronoi diagrams in the computational geometry are based on a set of non-overlapping convex polygons covering the entire domain.

From this definition, the Voronoi polygon share an edge by connecting a segment of the perpendicular bisector of the line between each pair of sites/points of S has been proved the straight-line dual of Voronoi diagrams is a triangulation by Delaunay [149]. The triangulation can be obtained from an equivalent convex hull for higher dimensions. It is also note that every circumcircle (circumsphere in three dimension) of a triangle contains no other points. Such triangulation is referred to as Delaunay triangulation. The algorithm to construct a Delaunay triangulation from a given set of points follows the early work of Weatherill [150, 151]. Such a method can connect an arbitrary set of points inside a convex hull. An efficient implementation of the Delaunay construction algorithm applies to both two and three dimensions.

In the Delaunay algorithm, automatic point creation can be generated in three ways which ensure a valid boundary conforming assembly of tetrahedra will be produced from an initial surface triangulation in a bounded domain. For each point $\mathbf{r}_o = (x, y, z)$ on the boundary, the point creation distribution function is given as [152]

$$dp_o = \frac{1}{N} \sum_{i=1}^{N} |\mathbf{r}_i - \mathbf{r}_o| \tag{4.79}$$

where $|\ |$ is the Euclidean distance whose point o is surrounded by N points within which no interior point is placed.

Another method to create automatically points is to use a background mesh [153]. It is overlaid over the computational domain with a specified point spacing. However, point creation is controlled by the use of sources, especially point and line sources, to provide grid for unstructured meshes. At position r, local point spacing can be given as [152]

$$dp = A_j e^{B_j |R_j - r|}; \quad j = 1, ..., N \tag{4.80}$$

where the user specified amplification is A_j, the decay parameters of the sources is B_j, and the position of each sources is R_j.

In our work, all meshes are generated using the Parallel simulation user environment II (PSUE-II) code [154]. The boundary of the geometry definition is described in the PSUE-II system in the curve and surface components. The background mesh information includes point, line and planar sources placed in the appropriate area of the computational domain. Once all of the sources have been defined, the simulation process is to generate the surface mesh. Then the eventual aim of the process is to produce a single or a set of several partitions by the parallel volume mesh generator. It should be noted that the FLITE parallel flow solver directly provides all of the necessary information. Also, the mesh refinement is available used by PSUE-II if an initial mesh does not satisfy the need.

4.9 Summary

In this chapter, major part is concerned with explicit characteristic Galerkin procedure to obtain stabilizing terms. Both the matrix free CBS scheme and semi-implicit CBS scheme with various turbulence transport equations are presented. Also, how to circumvent the LBB stability condition is discussed.

Chapter 5

The steady and unsteady laminar flows

5.1 Introduction

The numerical solutions of laminar, incompressible, viscous flow problems, namely flow inside a channel, in a lid-driven cavity, flow over a backward facing step, flow around a circular cylinder and flow past a stationary sphere, are presented in this chapter. The goal is to compare several meshes. The matrix free CBS-AC scheme and the semi-implicit CBS scheme are employed in this chapter.

5.2 Two-dimensional laminar Poiseuille flow inside a channel

A 1×1 square computational domain with no slip condition on top and bottom walls at a Reynolds number of 100 is assumed to test mesh convergence using the CBS-AC scheme. The exact, non-dimensional velocity from inlet is given as [114, 165]

$$\begin{aligned} u_1 &= 4x_2(1-x_2) \\ u_2 &= 0 \end{aligned} \tag{5.1}$$

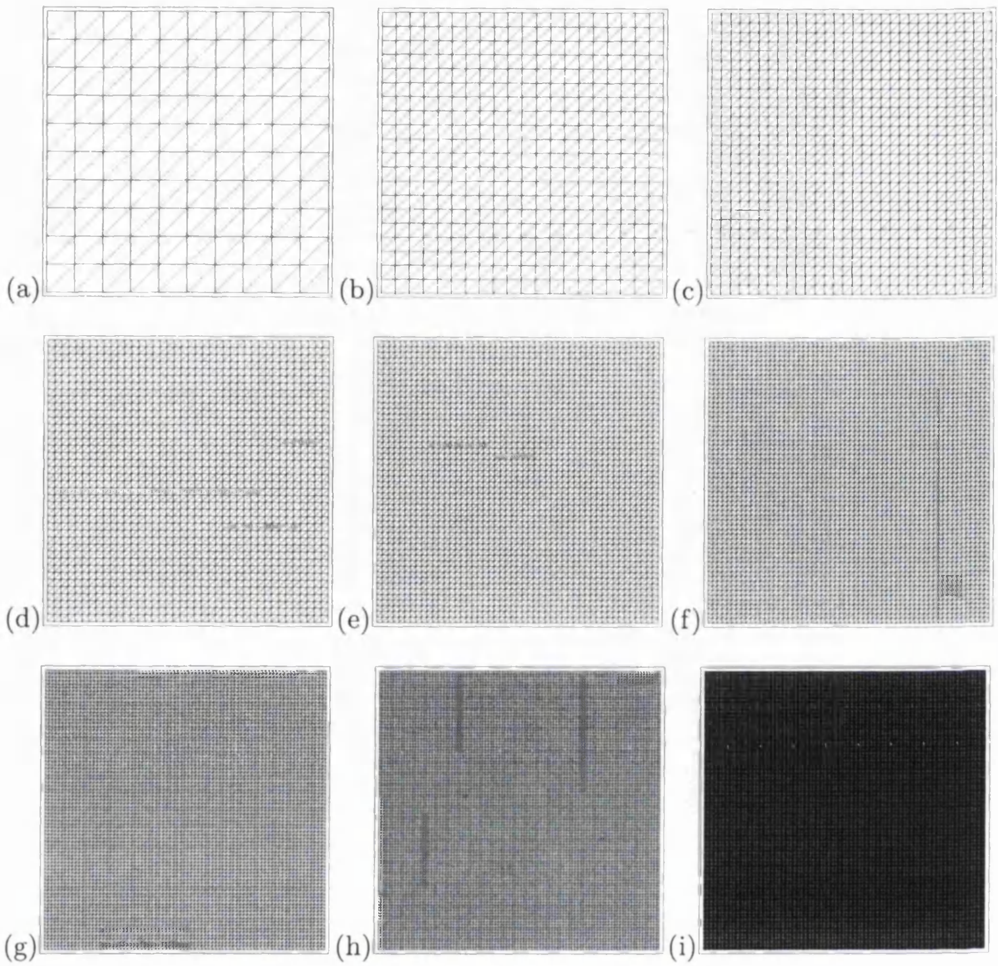

Figure 5.1: Poiseuille flow. (a) Mesh1 (10 ×10); (b) Mesh2 (20 × 20); (c) Mesh3 (30 × 30); (d) Mesh4 (40 × 40); (e) Mesh5 (50 × 50); (f) Mesh6 (60 × 60); (g) Mesh7 (80 × 80); (h) Mesh8 (100 × 100); (i) Mesh9 (200 × 200).

A pressure variation solution is $p = (8/Re)(1 - x_1)$ for this problem. Nine different uniform structured meshes were used as shown in Figure 5.1. Figure 5.2 shows the convergence history to steady state (see Equation (4.78)). It appears certain that the CPU time calculated depends on the element size and total nodes.

The error magnitude of velocity and pressure are expressed as

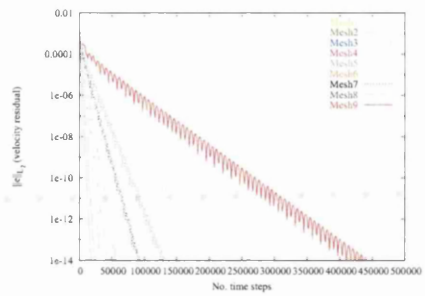

Figure 5.2: Convergence to the steady state for Poiseuille flow using the matrix free CBS-AC scheme.

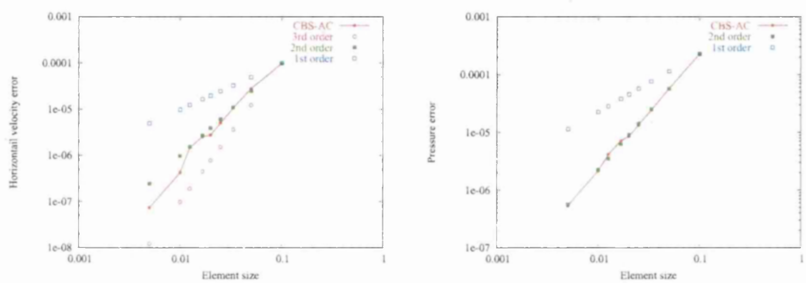

(a) (b)

Figure 5.3: Poiseuille flow using the matrix free CBS-AC scheme at Re=100. (a) Velocity error; (b) Pressure error.

$$E_{u_i} = \left| \sum_{i=1}^{elm} (u_i - u_{exact}) \frac{A_i}{3} \right| \tag{5.2}$$

$$E_p = \left| \sum_{i=1}^{elm} (p - p_{exact}) \frac{A_i}{3} \right| \tag{5.3}$$

where elm is the number of elements.

The errors of horizontal velocity and pressure with mesh convergence using CBS-AC scheme are shown as Figure 5.3(a)-(b). As seen the spatial accuracy of both velocity and pressure are second order.

In Figure 5.4 and Figure 5.5 horizontal velocity component and pressure contours

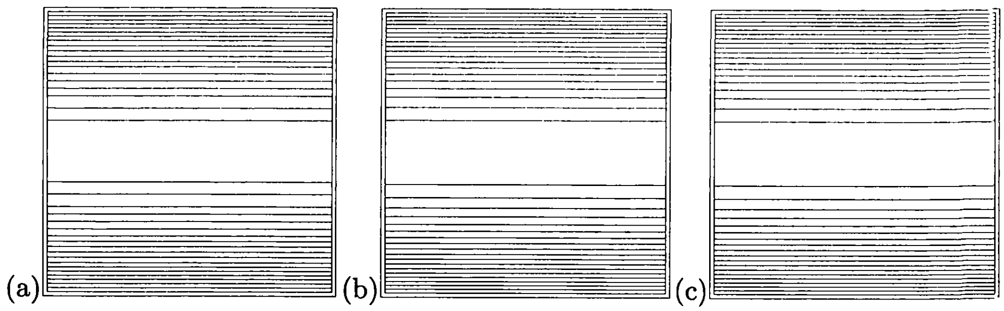

Figure 5.4: Poiseuille flow. Velocity contours for Re=100 (a) Mesh1 (10 ×10); (b) Mesh7 (80 ×80); (c) Mesh9 (200 ×200).

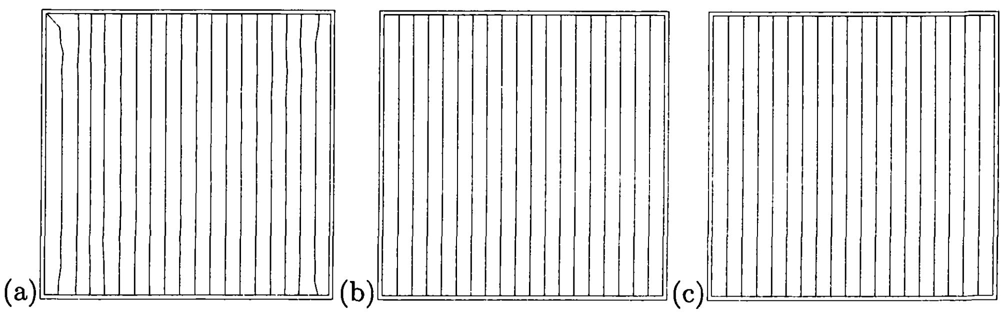

Figure 5.5: Poiseuille flow. Pressure contours for Re=100 (a) Mesh1 (10 ×10); (b) Mesh7 (80 ×80); (c) Mesh9 (200 ×200).

are ploted for three different meshes. The first mesh consists of 11 nodes on the sides. The second and third meshes consist of 81 and 201 nodes on the sides. As seen even the coarsest mesh used gives an excellent accuracy.

5.3 Two-dimensional laminar flow in a lid-driven cavity

This benchmark problem consists of a square geometry along with a moving lid. A non-dimensional horizontal velocity of unity was prescribed on the top-lid. A zero-velocity condition was prescribed on the bottom and side walls. Three different Reynolds numbers, 400, 1000 and 5000, have been investigated. Figure 5.6 shows the three meshes used to solve this problem. The structured mesh1 and unstructured mesh2 are refined close to solid wall. However, the unstructured mesh3 is uniform everywhere.

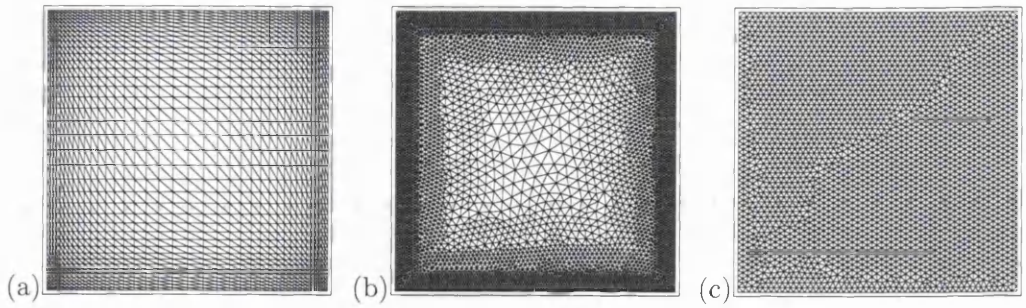

Figure 5.6: Flow inside a lid driven cavity. (a) Structured mesh1 (2888 elements; 1521 nodes); (b) Unstructured mesh2 (10596 elements; 5515 nodes); (c) Unstructured mesh3 (5656 elements; 2929 nodes).

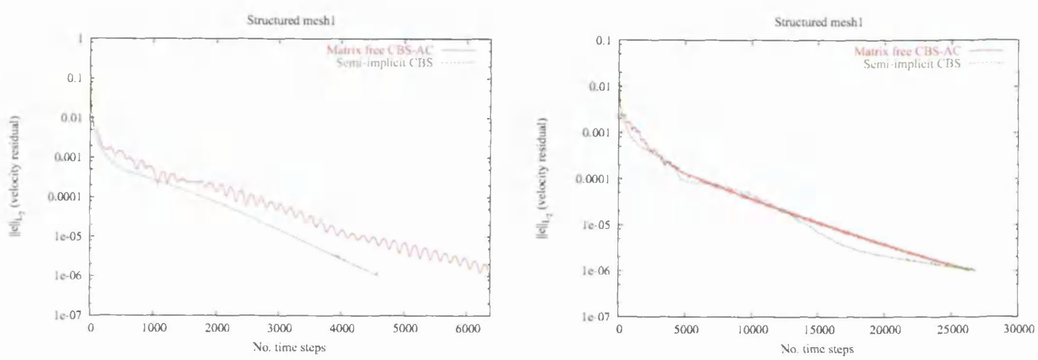

(a) Re=400 (b) Re=5000

Figure 5.7: Convergence to the steady state for the flow inside a lid driven cavity using the matrix free CBS-AC scheme and the semi-implicit CBS scheme on the structured mesh1.

As shown in Figure 5.7, the semi-implicit CBS scheme took less number of time steps to reach steady state than the matrix free CBS-AC scheme at a low Reynolds number, but the difference between the two schemes at a high Reynolds number is very small.

Figure 5.8 provides the comparison of steady state of convergence histories between three different meshes at various Reynolds numbers. All meshes resulted in similar convergence rates except the coarse unstructured mesh (mesh3), which fails to meet the prescribed steady state convergence tolerance at Re = 5000. The steady state tolerance prescribed in these problems is $\|e\|_{L_2} \leq 10^{-6}$ (see Equation (4.78)).

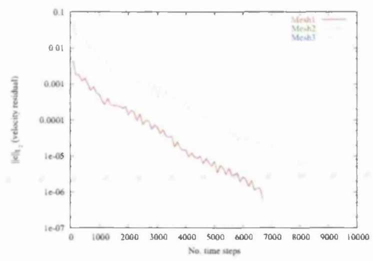

(a)

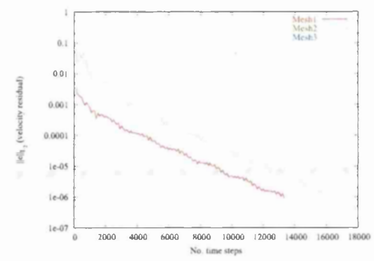

(b)

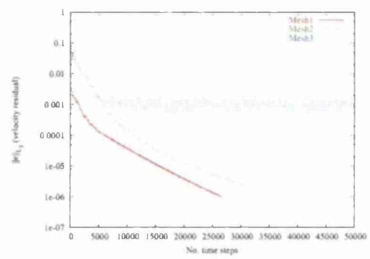

(c)

Figure 5.8: Convergence to the steady state for the flow inside a lid driven cavity using the matrix free CBS-AC scheme on the three different meshes. (a) Re = 400; (b) Re = 1000; (c) Re = 5000.

The horizontal velocity component and pressure pattern for Reynolds number 5000 obtained with the unstructured mesh2 is shown in Figure 5.9. For the contour plots, 24 contour lines are used.

In order to determine the accuracy of the numerical experiment, the velocity distributions at various Reynolds numbers are compared with the benchmark solution by Ghia et al. [119], which were obtained using a very fine grid, and numerical results of Codina et al. [120]. The comparison of the horizontal and vertical velocity profiles along the mid-sections of the cavity are shown in Figures 5.10, 5.11 and 5.12. It is observed that all meshes lead to good results at Re = 400 in Figure 5.10. Some small deviations near to peaks are noticed while the Reynolds number is increased. Major differences are noticed for the case when Re = 5000. Figure 5.12 shows that the structured mesh perform better than the others.

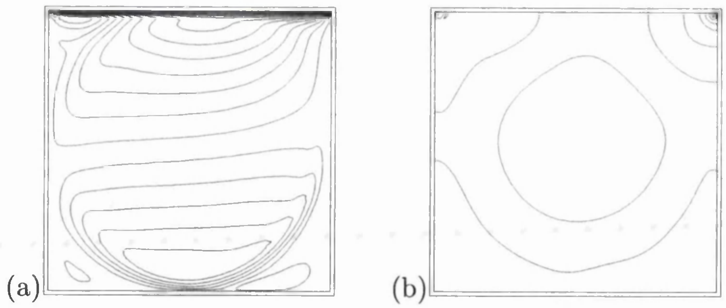

Figure 5.9: Flow inside a lid driven cavity at Re = 5000 using the matrix free CBS-AC scheme on the structured mesh1. (a) Horizontal velocity u_1 contours; (b) Pressure contours.

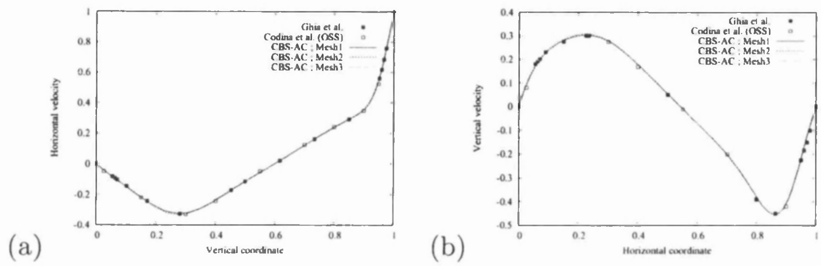

Figure 5.10: Flow inside a lid driven cavity at Re = 400 using the matrix free CBS-AC scheme. (a) u_1 along vertical centre line; (b) u_2 along horizontal centre line.

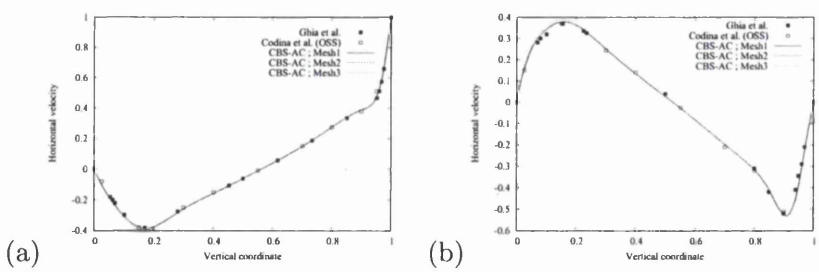

Figure 5.11: Flow inside a lid driven cavity at Re = 1000 using the matrix free CBS-AC scheme. (a) u_1 along vertical centre line; (b) u_2 along horizontal centre line.

5.4 Two-dimensional laminar flow past a backward facing step

For this classical benchmark problem, experimental data are provided by Denham et al. [121]. The entry to the channel is situated at a distance of 4 step lengths upstream. The

(a) (b)

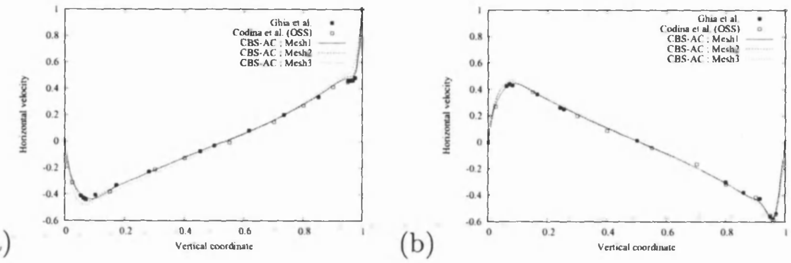

Figure 5.12: Flow inside a lid driven cavity at Re = 5000 using the matrix free CBS-AC scheme. (a) u_1 along vertical centre line; (b) u_2 along horizontal centre line.

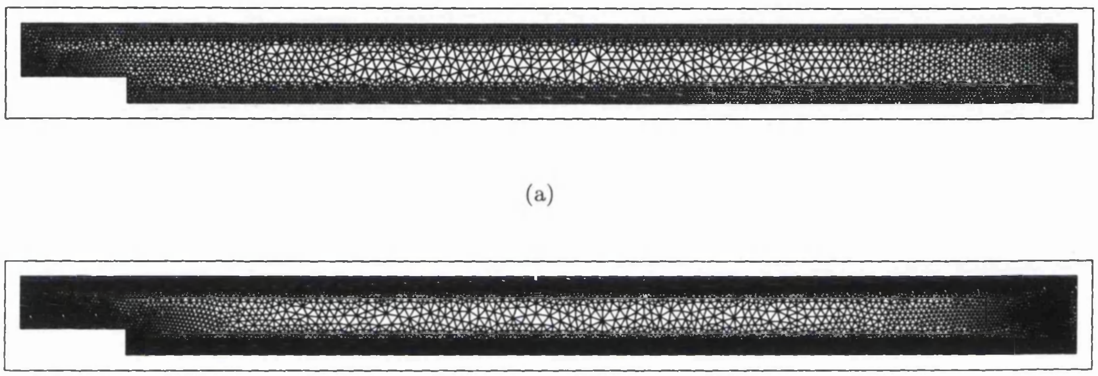

(a)

(b)

Figure 5.13: laminar flow past a backward facing step at Re = 229. (a) Unstructured mesh1 (8662 elements; 4656 nodes); (b) Unstructured mesh2 (22257 elements; 11659 nodes).

total length of domain is 40 step heights and the width is three times step height. The experimental velocity profile [121] is used on the inlet flow. The no-slip condition is prescribed on all solid walls. At the outlet, no Dirichlet boundary condition is employed. Figure 5.13 shows two different unstructured meshes used in the calculations. Both have high resolution near the solid walls. The Reynolds number is 229 which is based on the average velocity of the inflow and the height of the step.

Figure 5.14 shows the steady state convergence histories of the two meshes toward the steady state. As seen, mesh1 is quite fast to reach steady state compared to mesh2 that is more refined near the boundaries.

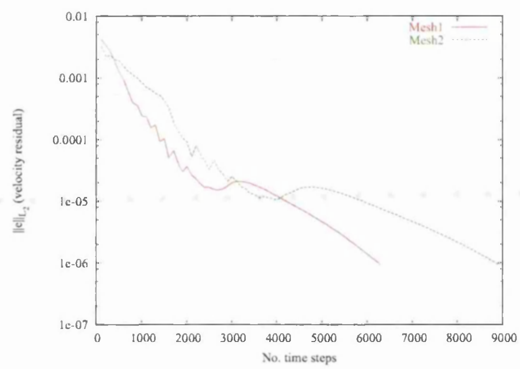

Figure 5.14: Convergence histories for the laminar flow past a backward facing step at Re=229 using the matrix free CBS-AC scheme on the two different unstructured meshes.

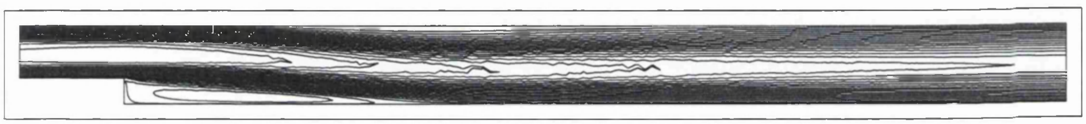

Figure 5.15: Horizontal velocity contours for the laminar flow past a backward facing step at Re = 229 using the matrix free CBS-AC scheme on the unstructured mesh2. ($u_{1_{min}} = -0.14$, $u_{1_{max}} = 1.84$)

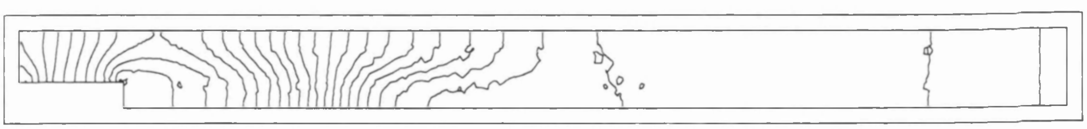

Figure 5.16: Pressure contours for the laminar flow past a backward facing step at Re = 229 using the matrix free CBS-AC scheme on the unstructured mesh2. ($p_{min} = -0.19$, $p_{max} = 0.03$)

Figures 5.15 and 5.16 show horizontal velocity and pressure contours using mesh2. No appreciable non-physical oscillations obtained in the distribution of the variables. Although Dirichlet boundary conditions are not prescribed at the exit, the pressure contours are still smooth.

The comparison of horizontal velocity profiles at several vertical sections on both meshes with experimental values [121] are shown in Figure 5.17. The numerical solutions resulted from using mesh2 are very similar to those obtained by mesh1 except for small

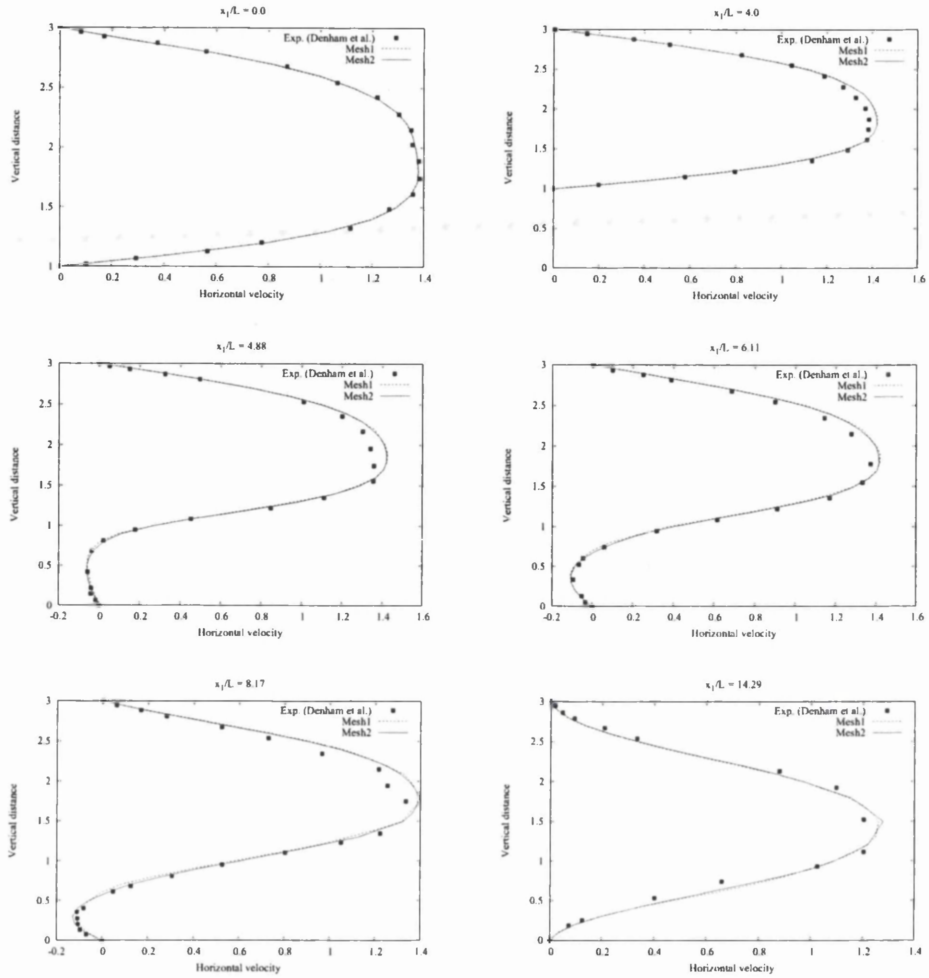

Figure 5.17: Comparison of horizontal velocity profiles different sections with experimental results for the laminar flow past a backward facing step at Re = 229 using the matrix free CBS-AC scheme.

deviations far downstream.

5.5 Two-dimensional laminar flow around a circular cylinder

The domain consists of a circular cylinder placed at a distance of $4D$ from the inlet, where D is the diameter of the cylinder. The distance from the centre of the cylinder to the top and bottom sides is also equal to $4D$. The exit of the domain is placed at a distance of $12D$

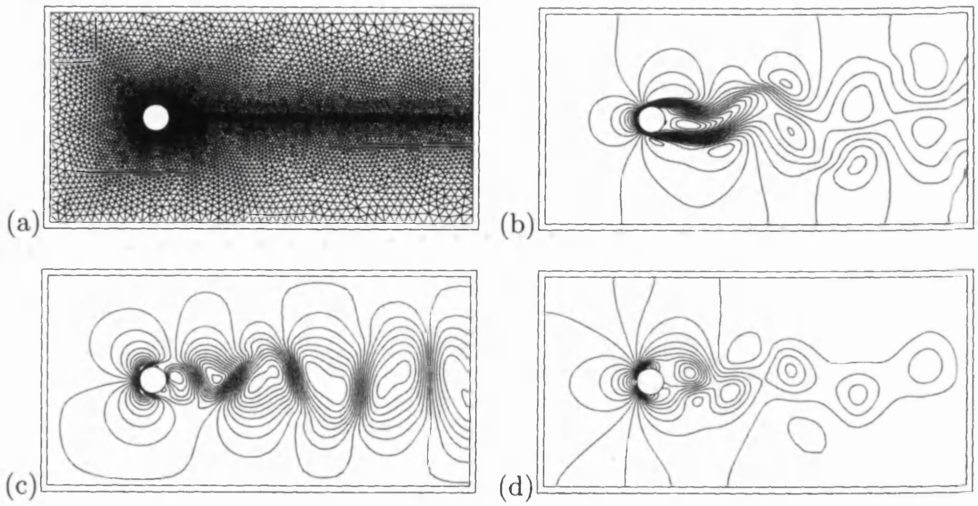

Figure 5.18: Unsteady laminar flow around a circular cylinder at Re = 100 using the matrix free CBS-AC scheme. (a) Unstructured mesh. (Nodes: 9988, Elements: 19650); (b) Horizontal velocity contours. $u_{1_{min}} = -0.26$, $u_{1_{max}} = 1.84$; (c) Vertical velocity contours. $u_{2_{min}} = -0.68$, $u_{2_{max}} = 0.78$; (d) Pressure contours. $p_{min} = -0.66$, $p_{max} = 0.73$.

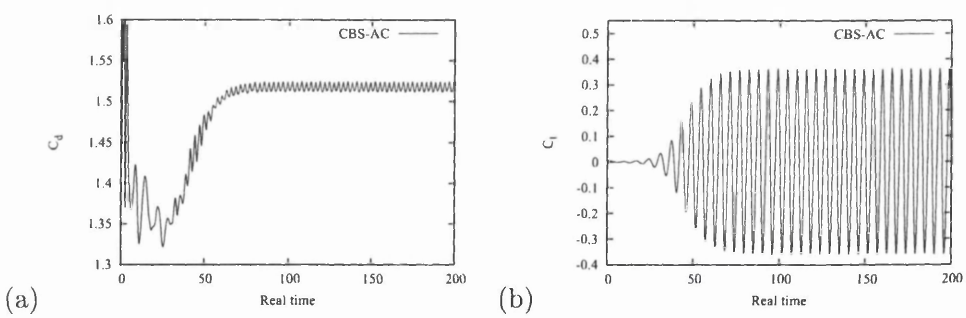

Figure 5.19: Unsteady laminar flow around a circular cylinder at Re = 100 using the matrix free CBS-AC scheme. (a) Drag coefficient variation with respect to real time; (b) Lift coefficient variation with respect to real time.

from the centre of the cylinder. A constant inflow velocity is prescribed. The Reynolds number 100 for the two-dimensional unsteady flow problem is based on the diameter of the cylinder and inlet velocity. The initial conditions are horizontal velocity of unity, vertical velocity of zero and zero pressure.

For each physical real-time step the Euclidean norm of the interface residual of velocity is reduced to 10^{-6} (see Equation (4.78)). It requires from 200 to 300 pseudo-time

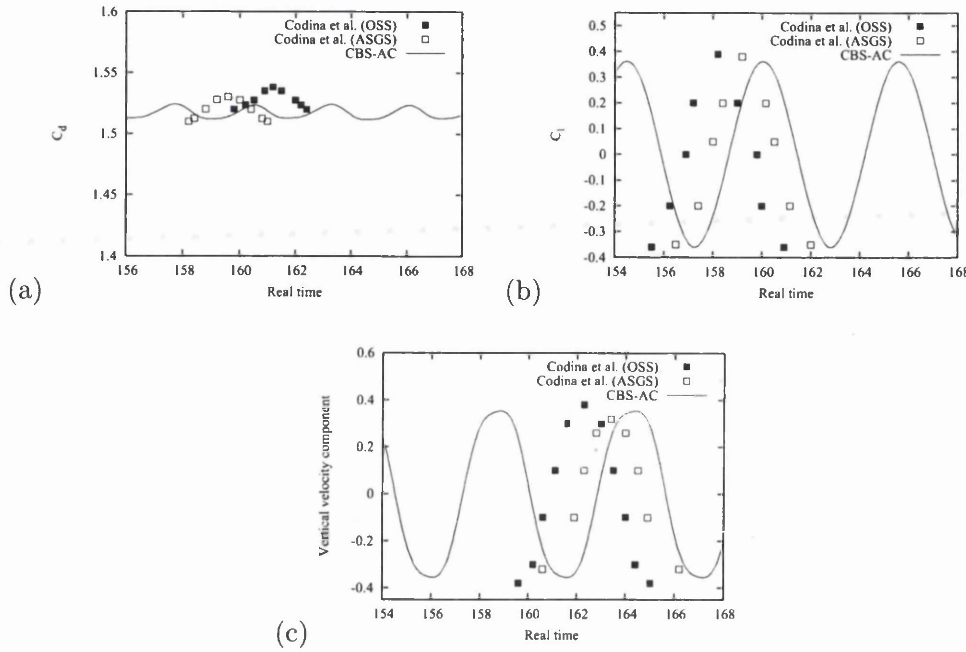

Figure 5.20: Unsteady laminar flow around a circular cylinder at Re = 100 using the matrix free CBS-AC scheme. (a) Drag coefficient; (b) Lift coefficient; (c) Vertical velocity at the central exit point.

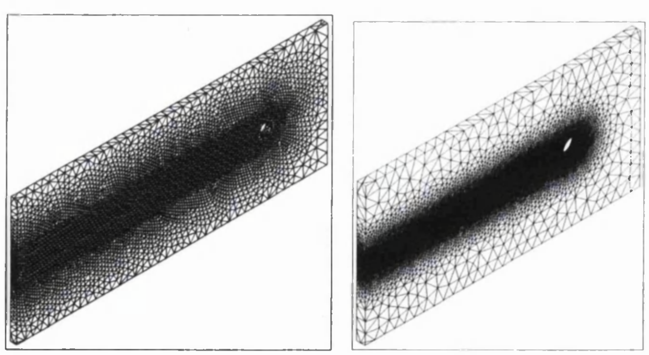

(a) (b)

Figure 5.21: Three-dimensional laminar flow around a circular cylinder. (a) Unstructured mesh1 (Elements: 69948, Nodes: 17382); (b) Unstructured mesh2 (Elements: 606769, Nodes: 115035).

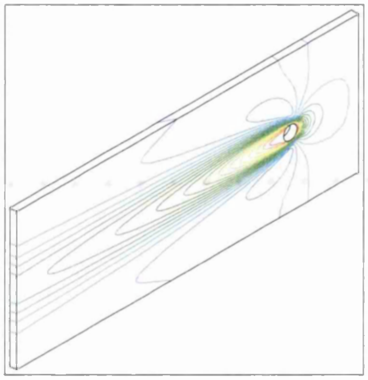

(a) u_1 velocity contours

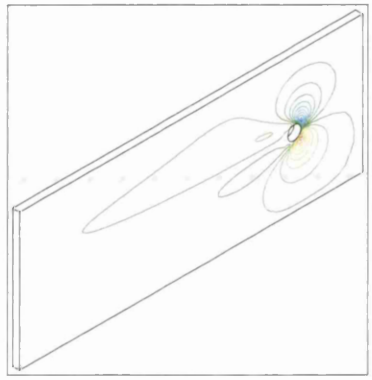

(b) u_3 velocity contours

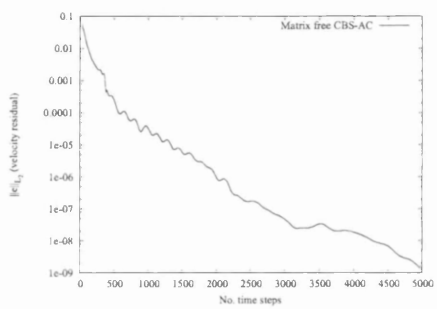

(c)

Figure 5.22: Steady laminar flow around a circular cylinder at Re=20 on unstructured mesh1 using the matrix free CBS-AC scheme. (a) u_1 velocity contours. $u_{1_{min}}$(red) = -0.022, $u_{1_{max}}$(blue) = 1.336; (b) u_3 velocity contours. $u_{3_{min}}$(red) = -0.535, $u_{3_{max}}$(blue) = 0.626; (c) Convergence to the steady state.

iterations to reach the prescribed tolerance with real-time step size of 0.05.

Figure 5.18 shows the computational mesh used for the simulation and all qualitative results. The contours of the horizontal and vertical velocity components and pressure contours at the non-dimensional real time of 200 are shown in Figure 5.18(b)–(d).

Figure 5.19 shows the drag C_d and lift C_l coefficient histories from 0 to 200 real times. The Strouhal number is around 0.121. The time variation of the drag C_d and lift C_l coefficients as well as the vertical velocity at the middle point of the exit section

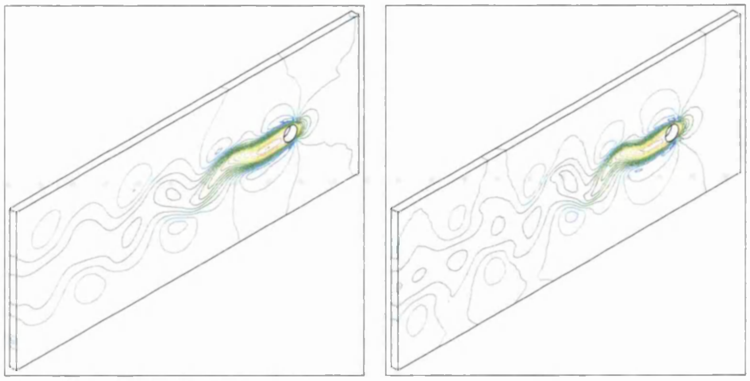

(a) u_1 velocity contours (b) u_1 velocity contours

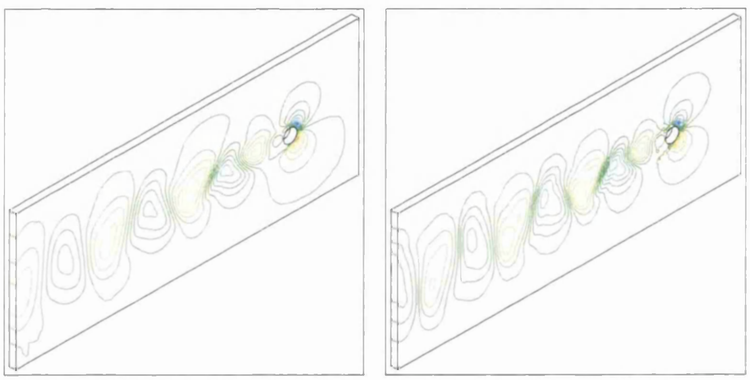

(c) u_3 velocity contours (d) u_3 velocity contours

Figure 5.23: Unsteady laminar flow around a circular cylinder at Re=100 on unstructured mesh1 using the matrix free CBS-AC scheme (left) and the semi-implicit CBS scheme (right). (a) u_1 velocity contours. $u_{1_{min}}$(red) = -0.186, $u_{1_{max}}$(blue) = 1.510; (b) u_1 velocity contours. $u_{1_{min}}$(red) = -0.159, $u_{1_{max}}$(blue) = 1.428; (c) u_3 velocity contours. $u_{3_{min}}$(red) = -0.696, $u_{3_{max}}$(blue) = 0.814; (d) u_3 velocity contours. $u_{3_{min}}$(red) = -0.863, $u_{3_{max}}$(blue) = 0.974.

as compared with the results of Codina et al. [120] are shown in Figure 5.20. As seen, the difference is quite small. The reason for the small difference could be due to the first order splitting error in pressure introduced by CBS algorithm. It leads to more dissipative influence encountered with smaller amplitude and frequency [114, 120, 122]. Note that

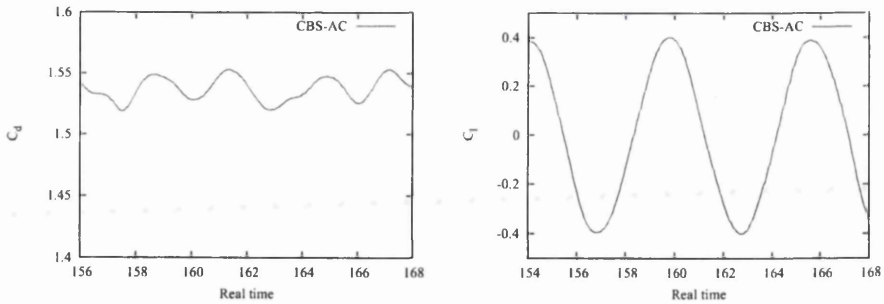

(a) (b)

Figure 5.24: Three-dimensional laminar flow around a circular cylinder at Re=100 on unstructured mesh2 using the matrix free CBS-AC scheme. (a) Drag coefficient; (b) Lift coefficient.

both results of CBS-AC scheme and Codina et al. are produced on the same mesh shown in Figure 5.18(a). The averaged drag coefficient is around 1.528 using the second order accurate Orthogonal Subgrid Scale (OSS) method and 1.521 using the Algebraic Subgrid Scale (ASGS) method while the matrix free CBS-AC scheme gives 1.512 [114].

5.6 Three-dimensional laminar flow around a circular cylinder

The primary objective of the low-Reynolds-number (LRN) flow past a stationary circular cylinder studied here is to compare prediction of quantitative and qualitative results from numerical solutions of the matrix free CBS-AC scheme and the semi-implicit CBS scheme. A constant horizontal-velocity was specified at the inflow and a no-slip condition was prescribed on the cylinder surface. All sides treated as slip walls.

In Figure 5.21 shows two different unstructured finite element meshes used in the flow past a circular cylinder problem.

The convergence history to steady state of the CBS-AC scheme is shown in Figure 5.22(c). The patterns of the horizontal and vertical velocity components based on 20

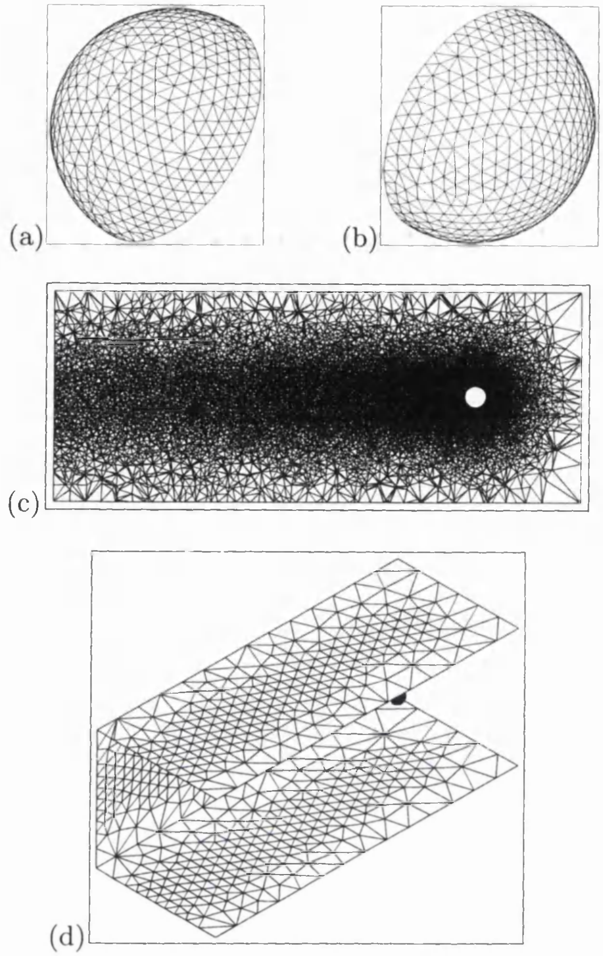

Figure 5.25: Steady laminar flow over a stationary sphere. (a) Concave surface of the sphere mesh; (b) Convex surface of the sphere mesh; (c) Mesh of the central section; (d) Sphere inside a rectangular channel.

contours using the matrix free CBS-AC scheme at Re = 20 are shown in Figure 5.22(a)-(b).

To evaluate the three-dimensional transient capabilities of the matrix free CBS-AC scheme using the dual time stepping procedure and semi-implicit CBS scheme the vortex shedding behind a stationary circular cylinder in cross-flow is studied. The flow has a stagnation point at the front of the cylinder, a unsteady separation region adjacent to the cylinder and periodic vortex shedding in the wake. Figure 5.23 shows the alternating vortex shedding from the upper and lower surface of the cylinder on unstructured mesh1 using both

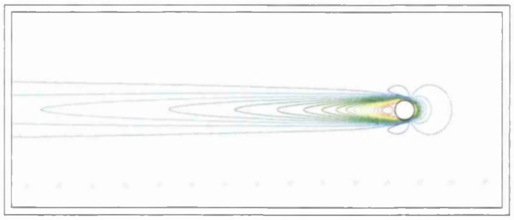

(a) Re=100

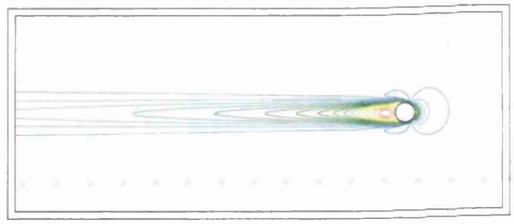

(b) Re=200

Figure 5.26: Steady laminar flow over a stationary sphere using the marix free CBS-AC scheme. Contours of u_1 horizontal velocity component. (a) Re=100. $u_{1_{min}}$(red) = -0.138, $u_{1_{max}}$(blue) = 1.183; (b) Re=200. $u_{1_{min}}$(red) = -0.321, $u_{1_{max}}$(blue) = 1.213.

(a)

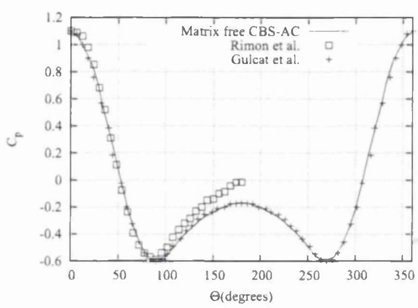

(b)

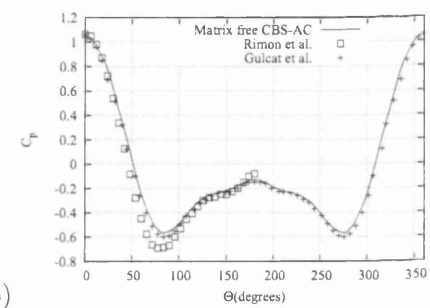

Figure 5.27: Steady laminar flow over a stationary sphere using the marix free CBS-AC scheme. (a) Pressure coefficient at Re = 100; (b) Pressure coefficient at Re = 200.

CBS schemes at Re = 100.

The drag and lift coefficient variations with respect to time using mesh2 are shown in Figure 5.24. As seen, the drag coefficient and lift coefficient from three-dimensional matrix free CBS-AC scheme are almost identical with two-dimensional results (see Figure 5.20). The averaged drag coefficient is around 1.537. The Strouhal number is 0.115.

5.7 Three-dimensional laminar flow past a stationary sphere

The sphere of diameter D is considered inside a rectangular channel of length $25D$ with the inlet boundary located at $5D$ from the centre of the sphere. No slip condition was applied on the surface of the sphere. Inflow velocity was assumed unity. Steady flow around a sphere was introduced into the laminar simulation at the Reynolds numbers of 100 and 200.

The three-dimensional unstructured mesh shown in Figure 5.25 consists of 987958 elements and 164139 nodes. Figure 5.26(a) shows the horizontal velocity component with 20 contours using 0.066 interval at Re = 100 whilst 0.077 interval is used at Re = 200 (see Figure 5.26(b)).

The distribution of pressure on the surface of sphere is compared with two different numerical results [123, 124] in Figure 5.27. The pressure coefficient were calculated by using 102 interpolation points. The averaged pressure quantities at a free stream are 0.0056 and 0.0047 for Re = 100 and 200 respectively. As seen the present predictions agrees well with numerical data of Gülcat et al. [124]. There is a small discrepancy with Rimon et al. [123] results at the back of the sphere surface at Re = 100 and top surface at Re = 200.

5.8 Summary

In this chapter, the matrix free CBS scheme based on the artificial compressibility method has been used to test four classical laminar incompressible flow problems. The problems considered are Poiseuille flow, lid-driven cavity flow, flow over a backward facing step, vertex shedding behind a circular cylinder and steady flow past a stationary sphere. For unsteady, incompressible, circular cylinder flow calculations, a dual-time stepping approach is employed. In general the results presented are accurate and the CBS-AC scheme is proved to be robust in dealing with laminar incompressible flows.

Chapter 6

The double driven cavity flows

6.1 Introduction

The numerical solutions to the incompressible Navier-Stokes equations for steady and unsteady driven cavity problems have been the subject of research for the last four decades [119],[125]-[131]. The cavity flows cover several flow regimes we normally encounter in incompressible fluid dynamics including recirculation, singularity and transient behavior. Flow instability in cavities has been one of the favourite topics of theoretical and numerical fluid dynamics researchers [132]-[134]. However, many of the reported cavity problems are either rectangular shaped or single driven cavities.

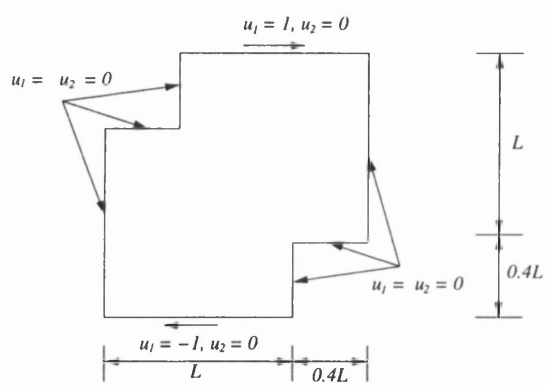

Figure 6.1: A double driven cavity. Problem definition and boundary conditions.

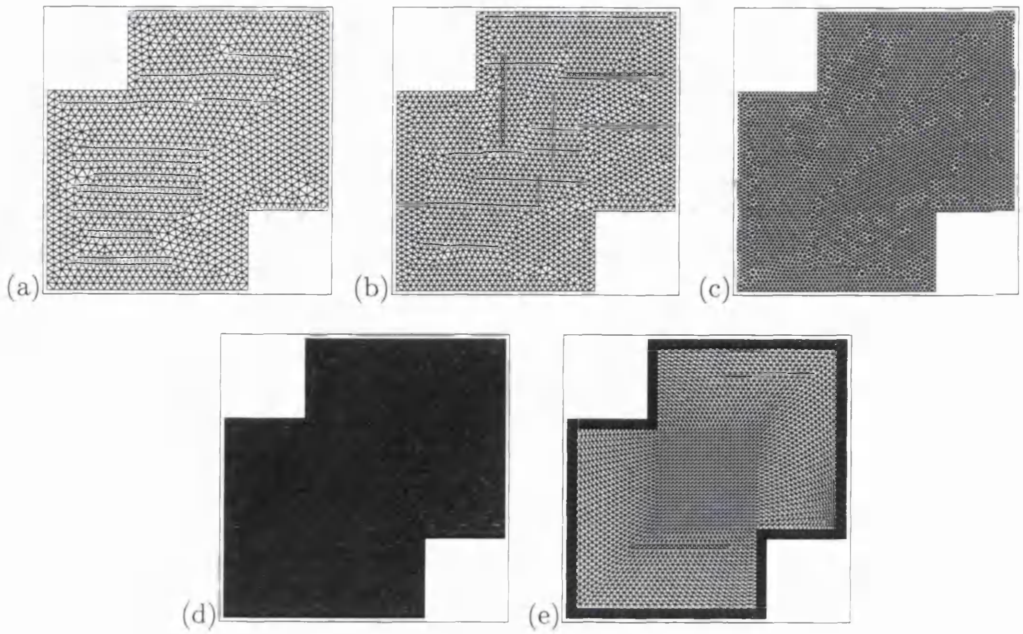

Figure 6.2: Finite element meshes. (a) Unstructured mesh1. (Nodes: 1414, Elements: 2670); (b) Unstructured mesh2. (Nodes: 2106, Elements: 4018); (c) Unstructured mesh3. (Nodes: 4727, Elements: 9164); (d) Unstructured mesh4. (Nodes: 18717, Elements: 36864); (e) Structured mesh5. (Nodes: 5057, Elements:9928).

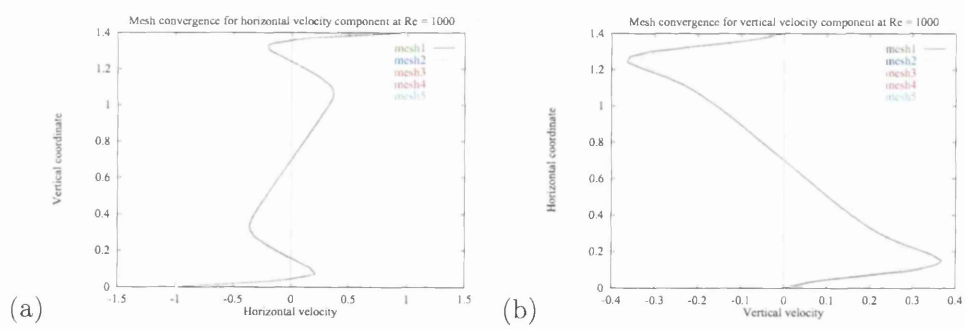

Figure 6.3: Flow inside a double driven cavity using the matrix free CBS-AC scheme. (a) u_1 velocity distribution along $x_1 = 0.7$; (b) u_2 velocity distribution along $x_2 = 0.7$.

It appears that only recently non-rectangular double driven cavities are receiving attention among the researchers and one such problem was discussed by Zhou et al. [135]

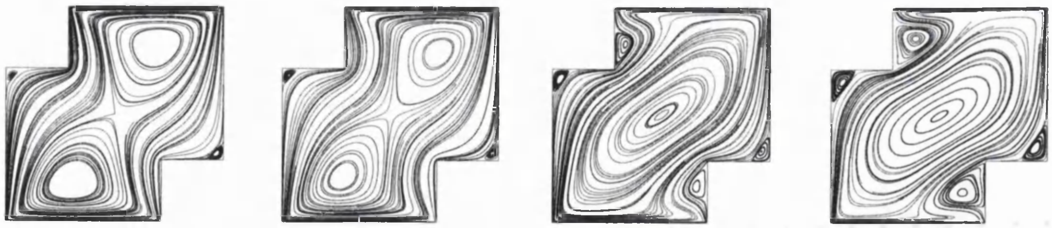

Figure 6.4: Streamlines patterns at steady state for Re = (a) 50; (b) 100; (c) 400; (d) 1000.

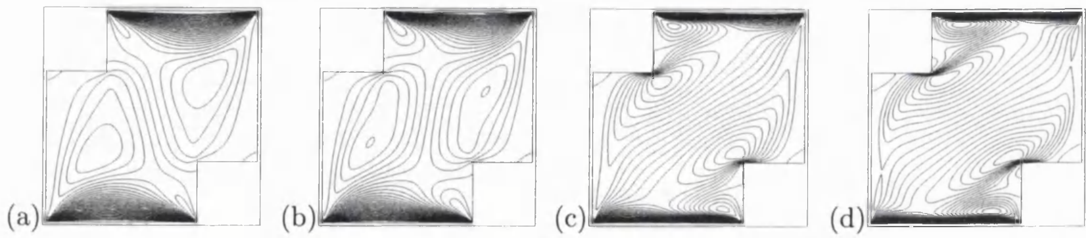

Figure 6.5: u_1 velocity contours at steady state for Re = (a) 50; (b) 100; (c) 400; (d) 1000.

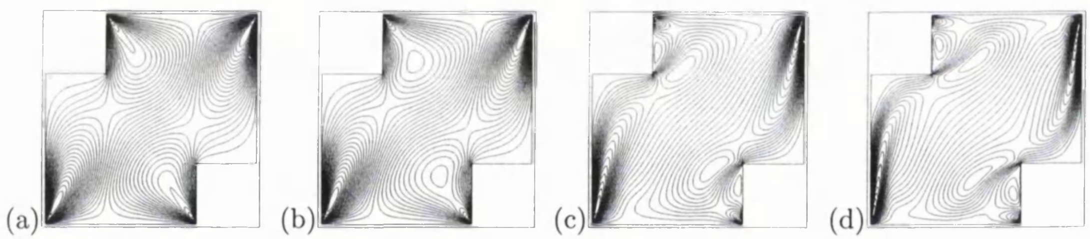

Figure 6.6: u_2 velocity contours at steady state for Re = (a) 50; (b) 100; (c) 400; (d) 1000.

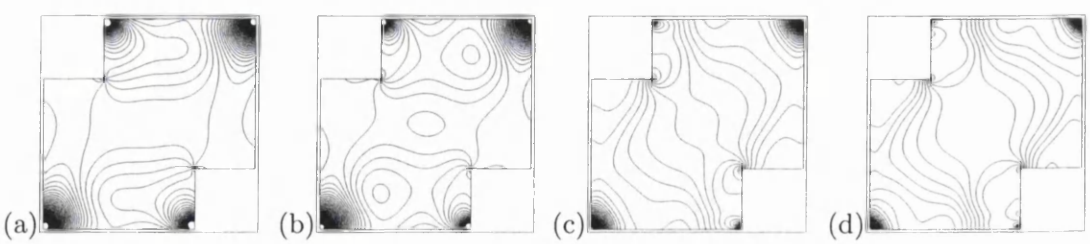

Figure 6.7: Pressure contours at steady state for Re = (a) 50; (b) 100; (c) 400; (d) 1000.

as a potential benchmark problem for testing numerical schemes. They have presented the numerical results for a Reynolds number range of 50-3200. However, the detailed analysis

Table 6.1: Locations and values of the primary vortex.

	Zhou et al.		CBS-AC	
Re	(x, y)	$\omega(x, y)$	(x, y)	$\omega(x, y)$
50	(0.9781, 1.1600)	-3.05843	(0.9776, 1.1478)	-3.07633
	(0.4219, 0.2518)	-3.05670	(0.4263, 0.2473)	-3.10055
100	(1.0172, 1.1091)	-2.72390	(1.0114, 1.1035)	-2.69993
	(0.3828, 0.2889)	-2.72310	(0.3865, 0.2894)	-2.73231
400	(0.7000, 0.7000)	-1.54842	(0.6995, 0.6966)	-1.60552
1000	(0.7000, 0.7000)	-1.41562	(0.6895, 0.6969)	-1.52363

Table 6.2: Locations and values of the first secondary vortex.

	Zhou et al.		CBS-AC	
Re	(x, y)	$\omega(x, y)$	(x, y)	$\omega(x, y)$
50	(1.3556, 0.4405)	0.02395	(1.3566, 0.4446)	0.02786
	(0.0444, 0.9595)	0.02394	(0.0424, 0.9569)	0.02587
100	(1.3556, 0.4486)	0.04399	(1.3566, 0.4446)	0.03975
	(0.0444, 0.9514)	0.04401	(0.0424, 0.9569)	0.03695
400	(1.3500, 0.4656)	0.15569	(1.3483, 0.4688)	0.19767
	(0.0500, 0.9344)	0.15777	(0.0569, 0.9400)	0.19385
1000	(1.3250, 0.4844)	0.53846	(1.3221, 0.4836)	0.65005
	(0.0750, 0.9063)	0.53813	(0.0753, 0.9142)	0.63326

was presented by Zhou et al. only for a steady state Reynolds number range between 50 and 1000.

A double driven cavity is different from the single lid-driven cavity, discussed in many previous papers due to the way the double lids are used as the name suggests. In a double driven cavity the lids are moved on both the top and bottom sides of the cavity. In this study, the flow in a non-rectangular cavity as shown in Figure 6.1 is examined. As mentioned before, this problem was suggested as a benchmark by Zhou et al. [135], and is

Table 6.3: Locations and values of the second secondary vortex.

	Zhou et al.		CBS-AC	
Re	(x, y)	$\omega(x, y)$	(x, y)	$\omega(x, y)$
50				
100				
400	(0.4703, 1.1625) (0.9219, 0.2375)	1.38495 1.38140	(0.4772, 1.1610) (0.9232, 0.2385)	1.70971 1.69442
1000	(0.5484, 1.2000) (0.7256, 0.2000)	2.38557 2.38559	(0.5505, 1.2071) (0.8523, 0.2015)	2.73409 2.60588

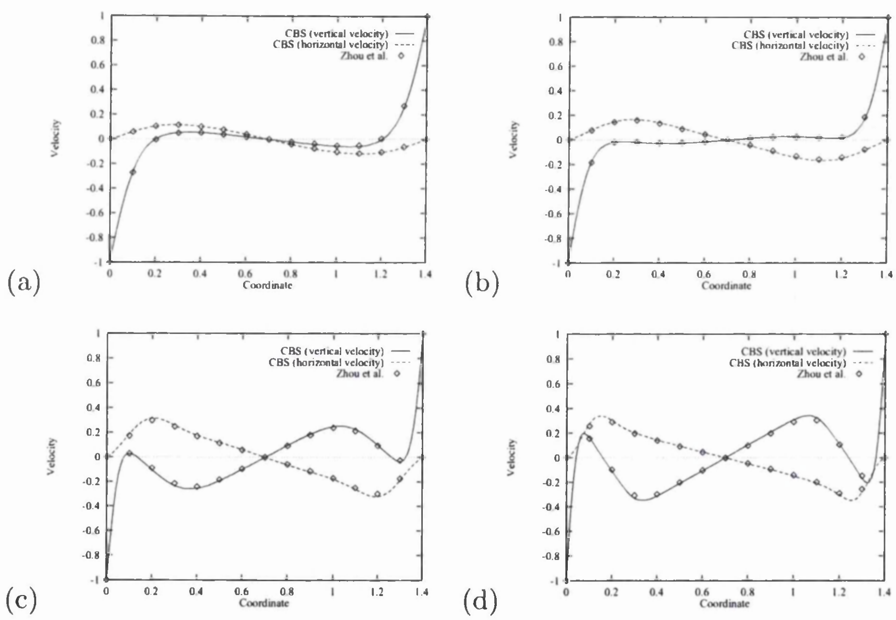

Figure 6.8: The u_1 and u_2 velocity distribution along the middle line of the domain using the matrix free CBS-AC scheme on the unstructured mesh4 at different Reynolds number (a) 50; (b) 100; (c) 400; (d) 1000.

a diagonally symmetrical enclosure with a longer side of size L and a smaller side of size $0.4L$. The top lid is assumed to move at a prescribed positive horizontal velocity value and

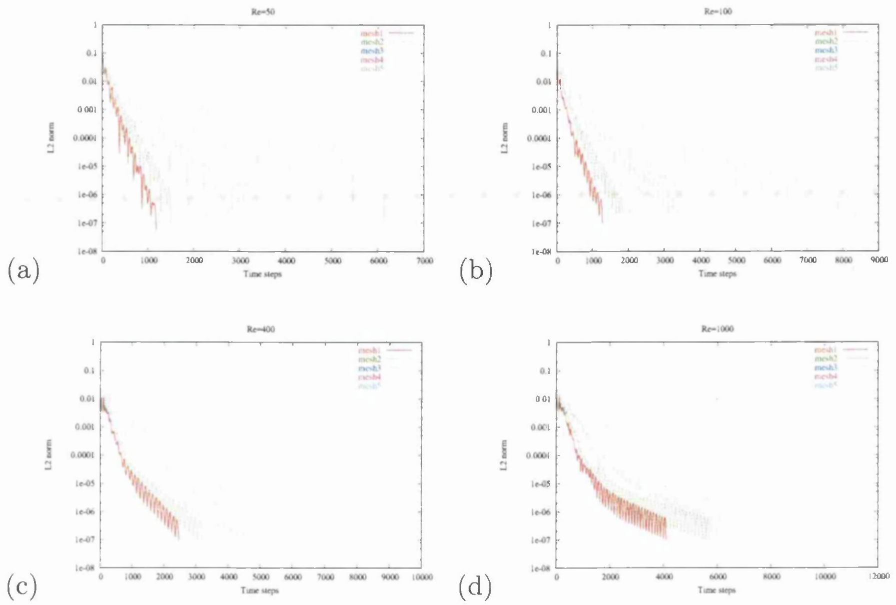

Figure 6.9: Convergence to the steady state for the flow inside a double driven cavity using the matrix free CBS-AC scheme on the several meshes at different Reynolds numbers (a) 50; (b) 100; (c) 400; (d) 1000.

the bottom lid moves with a negative velocity with a magnitude equal to the velocity of the top lid. The Reynolds number is defined based on the magnitude of the prescribed velocity value of the lids and the length L. The velocity components on all other sides are assumed to be equal to zero.

Several meshes have been used in the analysis to assess the convergence properties of the matrix free CBS-AC scheme and also to minimize the error due to the coarseness of the mesh. Five different meshes were employed in the study are shown in Figure 6.2. Although, the fifth mesh used contains structured layers close to the cavity walls, the emphasize of the present work is to use unstructured meshes. All the first four meshes are unstructured meshes starting with a reasonably fine uniform mesh 1 as shown in Figure 6.2(a). Second, third and fourth meshes are generated by consistently refining the mesh by increasing the number of nodes. The fourth mesh includes finer grid close to the walls.

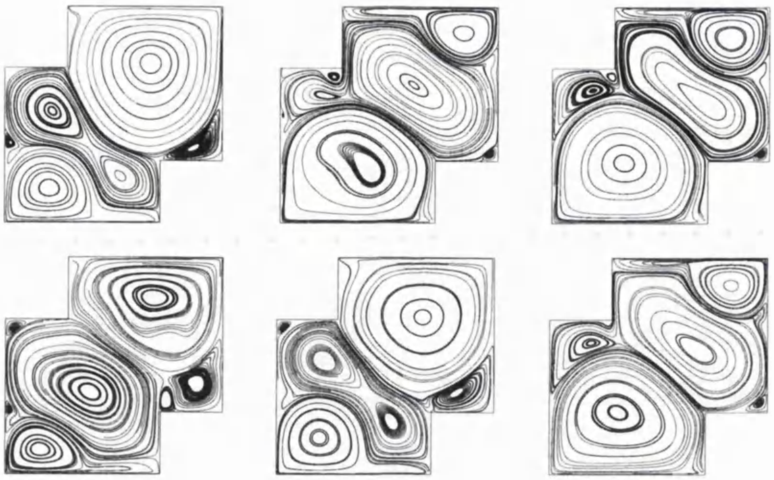

Figure 6.10: The instantaneous transient state for streamlines at Re = 3200 using the matrix free CBS-AC scheme on the unstructured mesh4. (a) Real time = 150; (b) Real time = 200; (c) Real time = 250; (d) Real time = 300; (e) Real time = 350; (f) Real time = 400.

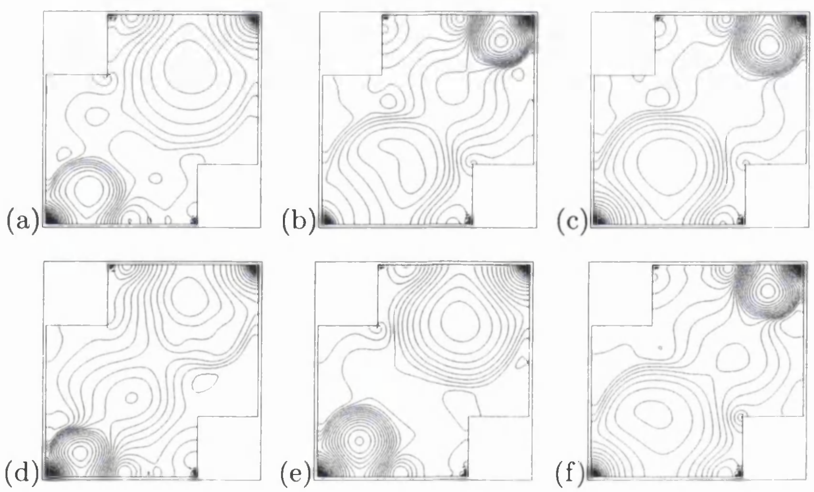

Figure 6.11: The instantaneous transient state contours for pressure distribution at Re = 3200 using the matrix free CBS-AC scheme on the unstructured mesh4. (a) Real time = 150; (b) Real time = 200; (c) Real time = 250; (d) Real time = 300; (e) Real time = 350; (f) Real time = 400.

6.2 Two-dimensional steady flow in a double driven cavity

From Figure 6.3(a), it is easily seen that the differences between the meshes 3, 4 and 5 are negligibly small. However, Figure 6.3(b) shows a small difference in the peak values

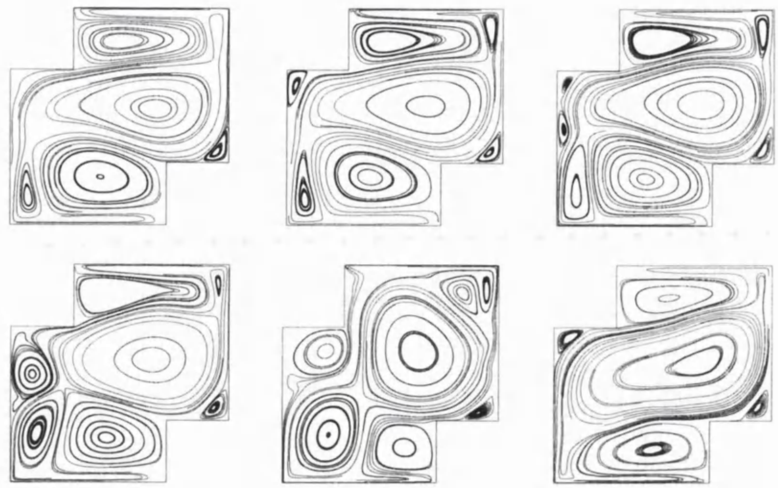

Figure 6.12: The instantaneous transient state for streamlines at Re = 5000 using the matrix free CBS-AC scheme on the unstructured mesh4. (a) Real time = 150; (b) Real time = 160; (c) Real time = 170; (d) Real time = 180; (e) Real time = 190; (f) Real time = 200.

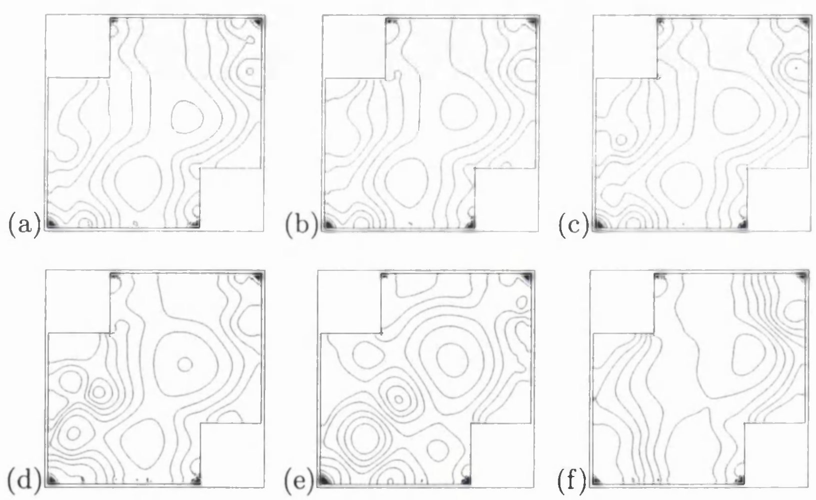

Figure 6.13: The instantaneous transient state contours for pressure distribution at Re = 5000 using the matrix free CBS-AC scheme on the unstructured mesh4. (a) Real time = 150; (b) Real time = 160; (c) Real time = 170; (d) Real time = 180; (e) Real time = 190; (f) Real time = 200.

between the meshes. It is seen that the solution is converging and the difference between the meshes 4 and 5 are less than 2%. It is therefore obvious to use either mesh 4 or 5. In

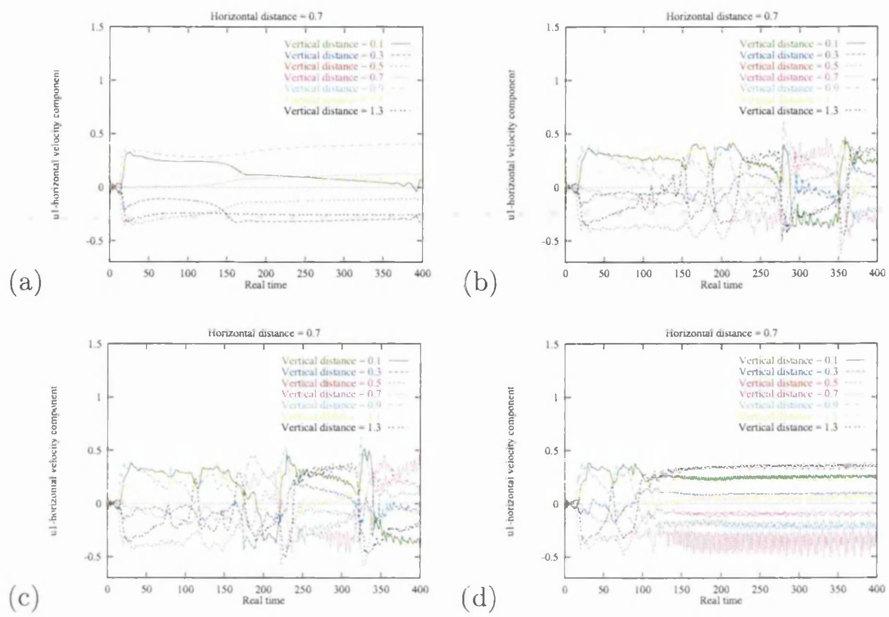

Figure 6.14: u_1 velocity component variation with respect to real time using the matrix free CBS-AC scheme on the unstructured mesh4 at various Reynolds numbers (a) 2000; (b) 3000; (c) 3200; (d) 4000.

the present work mesh 4 is selected in order to show that the present scheme is flexible to use on unstructured meshes at all Reynolds numbers. Whenever if it was found necessary, the solution obtained has been double checked using at least two meshes and the accuracy was verified.

The stream traces in Figure 6.4 show two primary vortices at Re = 50 and 100 and one primary vortex at Re = 400 and 1000. Also, it is observed that there are four secondary vortices atRe = 400 and 1000 and only two vortices at smaller Reynolds number.

Figures 6.5, 6.6 and 6.7 show the contours of all the three variables, u_1, u_2 and p, for different Reynolds numbers. From these contours it is clear that the solution obtained is symmetric with respect to the shorter and longer diagonals of the cavity.

The u_1 velocity contours in Figure 6.5 show the existence of strong u_1 gradients close to the top and bottom lids. As the Reynolds number increases this gradient increases in strength as indicated by the closely packed contours near the top and bottom lids at Re = 400 and 1000. Also at higher Reynolds numbers, stronger u_1 gradients develop close to

(c) 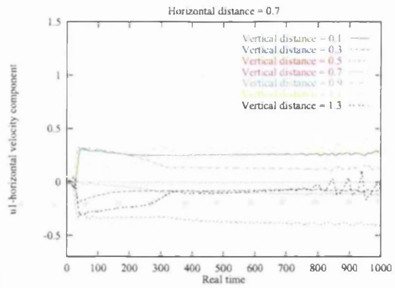

(d) 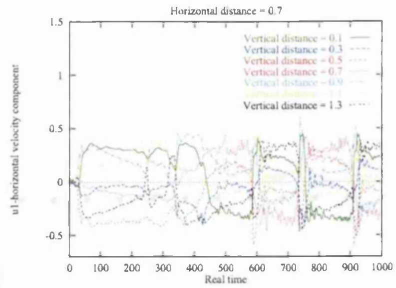

Figure 6.15: u_1 velocity component variation with respect to a longer non-dimensional real time of 1000 using the matrix free CBS-AC scheme on the unstructured mesh4 at two Reynolds numbers. (a) $Re = 2000$; (b) $Re = 3200$.

the inward corners of the enclosure.

The u_2 velocity contours in Figure 6.6 show steeper gradients close to the corners along the vertical walls. The pressure contours shown in Figure 6.7 are marked with very high gradients close to the top and bottom corners of the cavity. This was expected due to the singularity introduced by the sudden change in the velocity at the top and bottom corners.

A comparison of the present unstructured mesh solution with the structured fine mesh solution [135] is shown in Figure 6.8. It is clear that both the finite element solution on unstructured meshes and the fine structured mesh solution are identical.

The vorticity values and locations of the centres of primary, first secondary and second secondary vorticities are listed for different Reynolds numbers along with numerical results of Zhou et al. in Tables 6.1, 6.2 and 6.3. As seen the predictions agree well and differ less than 4% from the reference values.

Figure 6.9 shows the temporal history of convergence for different Reynolds numbers and meshes. To ensure a steady state solution, the convergence criterion is fixed at 10^{-7} for all the variables involved and satisfied in all simulations. Clearly, all the convergence histories of the solution discussed here in general show that the convergence curve is a function of element size.

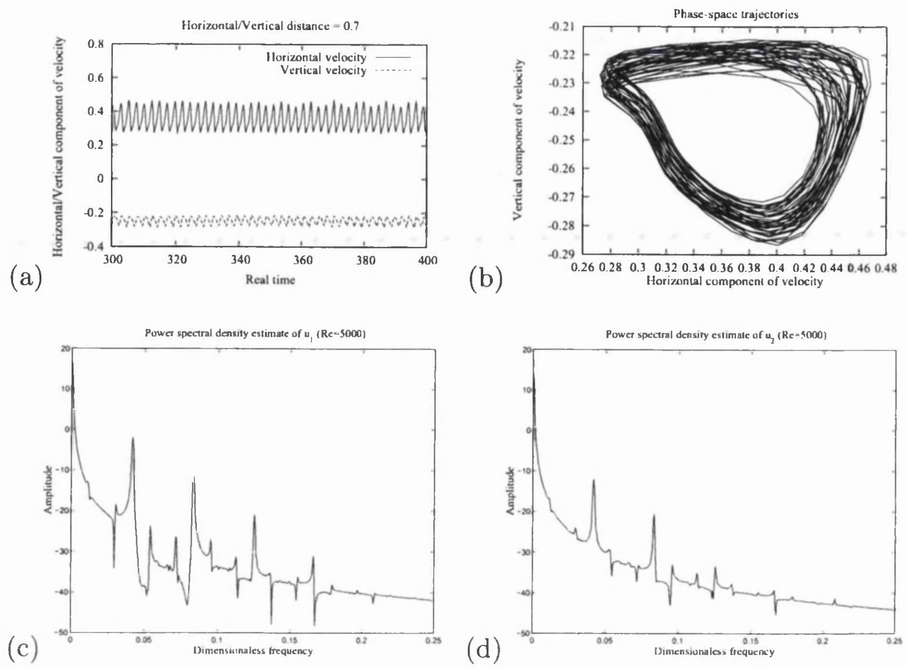

Figure 6.16: Unsteady cavity flow at $Re = 5000$ using the matrix free CBS-AC scheme on the unstructured mesh4. (a) u_1 and u_2 velocities as a function of real time from 300 to 400; (b) Phase-space trajectories of u_1 vs. u_2; (c) Power spectral density of the u_1 velocity; (d) Power spectral density of the u_2 velocity.

6.3 Two-dimensional unsteady flow in a double driven cavity

The steady state solutions were obtained up to a Reynolds number of 1000. Beyond Re = 1000, the steady state criterion discussed in the previous section was not met. It is therefore essential to continue the study to search for transient solution patterns. The unsteady state, beyond Re = 1000, was also observed by Zhou et al. [135] at Re = 3200. They concluded that a multiple steady state exists at Re= 3200 and speculated that this may be caused by the elliptic instability. It was also observed by Zhou et al. that the symmetry of the patterns with respect to the diagonals is lost at Re = 3200.

In order to further enhance the understanding of the transient state, which exists beyond certain Reynolds number, we monitor the velocity distribution at certain points within the domain with respect to the real time. As mentioned before we use the dual time stepping approach and a second order discretization of the real time term. In order

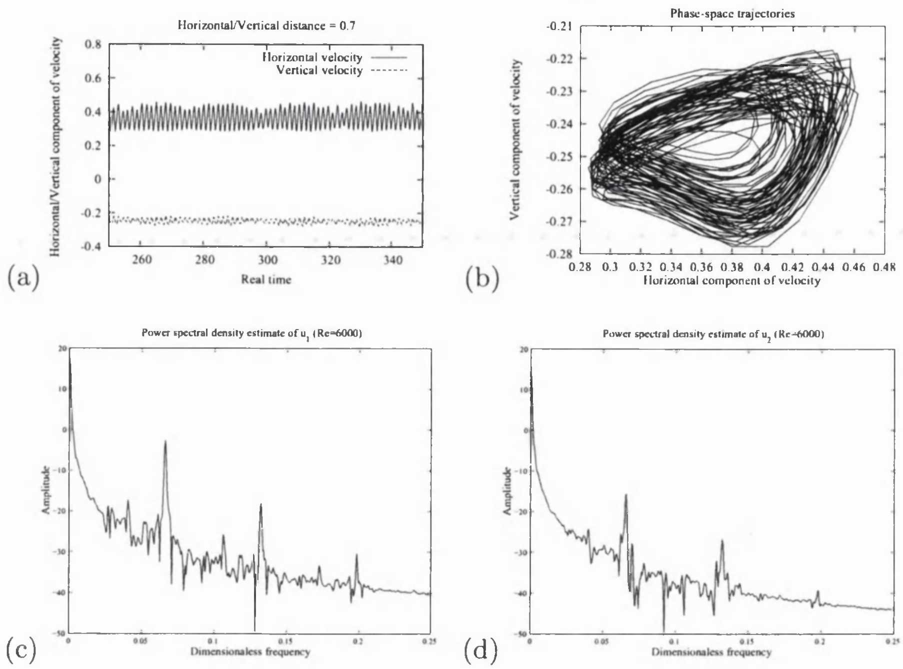

Figure 6.17: Unsteady cavity flow at $Re = 6000$ using the matrix free CBS-AC scheme on the unstructured mesh4. (a) u_1 and u_2 velocities as a function of real time from 250 to 350; (b) Phase-space trajectories of u_1 vs. u_2; (c) Power spectral density of the u_1 velocity; (d) Power spectral density of the u_2 velocity.

to obtain an accurate time description of the variable, we set an instantaneous steady state convergence criterion of 10^{-7} for all the variables within every real time step.

In addition to monitoring velocity distribution at certain points we also observe the overall pattern of the variable distributions within the geometry for different real time steps.

Figures 6.10 to 6.19 show various transient solutions for the Reynolds number range between 2000 and 10000. In general the overall conclusion is that transient state exists from Re = 2000 onwards. Between Re = 2000 and Re = 4000, the flow is unstable but no familiar pattern exists. The flow is chaotic and increases in complexity as the Reynolds number is increased. From Re = 4000 until Re = 5000, the flow enters into a quasi-periodic flow pattern and finally at Re = 10000, no solid conclusion on the type of flow pattern was reached.

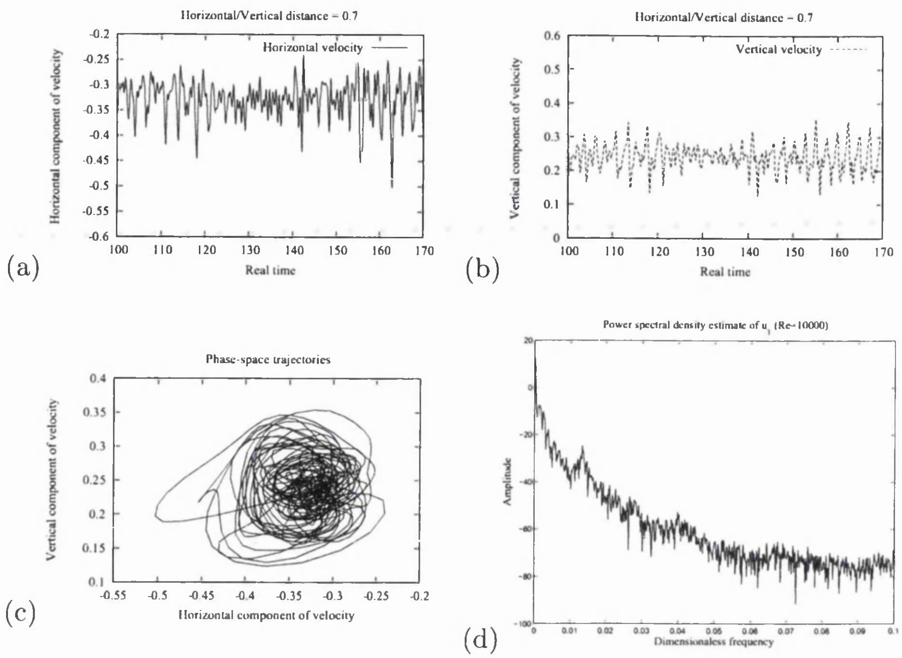

Figure 6.18: Unsteady cavity flow at Re = 10000 using the matrix free CBS-AC scheme on the unstructured mesh4. (a) u_1 velocity as a function of real time from 100 to 170; (b) u_2 velocity as a function of real time; (c) Phase-space trajectories of u_1 vs. u_2; (d) Power spectral density of the u_1 velocity.

Sample solutions of contours at various real times for Re = 3200 and Re = 5000 are shown in Figures 6.10 to 6.13. In Figure 6.10, stream traces with respect to real non-dimensional time is plotted and in Figure 6.11, the corresponding pressure contours are plotted. Figure 6.14(c) shows the corresponding observation of u_1 velocity values at seven different points within the domain. Although the pattern shows some periodic nature of the flow at certain time levels, overall the pattern obtained is non-periodic but transient.

It is observed from Figure 6.10 that the flow is dominated by three major vortices. In addition, there are several secondary vortices developed within the cavity. The major vortices are placed along the longer diagonal of the cavity. The vortices close to the top right corner and bottom left corner grows in strength and reduces in strength with respect to time. When the bottom one grows, top one shrinks and vice versa. When the top main vortex grows to its maximum strength, it creates two eyes in the vortex which lies

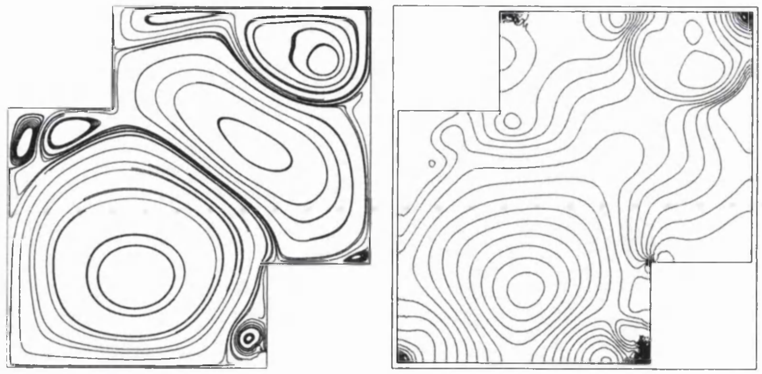

(a) Streamlines (b) Pressure distribution

Figure 6.19: The instantaneous transient state at Re = 10000 for a real time of 200 using the matrix free CBS-AC scheme on the unstructured mesh4.

between the top and bottom vortices. The intermediate vortex generated between the top and bottom vortices is always created at the top portion of the cavity. This vortex is created by a split in the top vortex as it grows in strength. When the bottom one grows in strength, the intermediate one disappear from the bottom portion of the cavity and a new intermediate one is created at the top portion.

Although the pattern of stream traces and pressure contours follow a qualitative cyclic pattern, the quantities in Figure 6.14(c) follow no regular periodic pattern. In order to further confirm the existence of the non-periodic pattern at moderate Reynolds numbers, observation of u_1 is continued for a longer non-dimensional time of 1000 as shown in Figure 6.15. It is evident that no periodic flow state exists at moderate Reynolds numbers.

Figures 6.12 and 6.13 show stream traces and pressure contours at various non-dimensional real times for Re = 5000. These contours are plotted between the non-dimensional time of 150 and 200. The striking difference between the patterns of Re = 3200 and Re = 5000 is that at Re = 5000, the eyes of the vortices are predominantly aligned along the vertical line. However, at Re = 3200, the eyes of the vortices were aligned along the major diagonal of the cavity. Although the quasi-periodic pattern is not very clear from the contours, it is clear from Figure 6.16.

Figure 6.16 depicts the velocity distribution at a fixed point $(x_1, x_2) = (0.7, 0.7)$ of the cavity with respect to real time, phase-space trajectories of u_1 vs. u_2 and the power spectra of velocity at a Reynolds number of 5000. The time evolution of velocity from real time 300 to 400 is shown in Figures 6.16(a). The appearance of a quasi-periodic behaviour at Re=5000 is illustrated. As seen one fundamental frequency around 0.0415 is obtained from the analysis of Fourier power spectral density shown in Figures 6.16(c) and 6.16(d).

For clear visualization of the quasi-periodic flow the Reynolds number is increased to 6000. The time evolution of horizontal/vertical component of velocity, the phase trajectory on $u_1 - u_2$ plane and the power spectra to identify the fundamental frequency are all given in Figure 6.17. As we further increase Reynolds number to 10000, the chaotic pattern is established as demonstrated in Figure 6.18.

Figures 6.18 and 6.19 show the pattern developed at a Reynolds number of 10000. The pattern obtained was not periodic but transient. The turbulent nature of flow is reasonably clear from the arbitrary variation of u_1 and u_2 component of velocity, the phase trajectory on $u_1 - u_2$ plane and Fourier power spectra of velocity observed as shown in Figure 6.18. Figure 6.19 shows the complex nature of flow pattern at a real time of 200. We suspect that the mesh resolution is not good enough to resolve this Reynolds number flow correctly. Therefore the results at Re = 10000 may not be completely independent of the mesh size.

6.4 Summary

In this chapter, the matrix free CBS-AC scheme was employed to study both steady and transient double driven cavity flow. The steady flow regime was observed between the Reynolds numbers of 50 and 1000. Beyond this range the flow is marked with non-periodic and quasi-periodic transient states. At Re = 10000, the flow already started showing the signs of highly arbitrary state indicating a transition to turbulent flow. The objective of this chapter was to give a general and accurate picture of steady and unsteady flows at different Reynolds numbers.

Chapter 7

The steady and unsteady two-dimensional turbulent flows

7.1 Introduction

In this chapter, the matrix free CBS-AC method is used to obtain a stable solution for turbulent incompressible flows. Both explicit solution procedure for steady state problems and the dual time stepping technique for transient problems are discussed. The presented matrix solution free method is efficient compared to other standard explicit schemes, due to the inherent stabilization properties and local time stepping employed. A recent study concluded that for steady state laminar incompressible flow problems, the fully explicit method consumes less CPU time than a semi-implicit scheme with conjugate gradient solution to the pressure equation [136]. Another study indicates that for a time step based on the stability limit of an explicit scheme, the CBS-AC scheme is faster than standard implicit schemes for steady state problems [137]. For unsteady problems, the study is inconclusive. It is therefore sensible to extend the matrix free CBS-AC scheme to solve turbulent incompressible flows and exploit the advantages of such a scheme. For the comparison sake, the semi-implicit CBS scheme is also implemented to solve turbulent flows.

Three different RANS models have been implemented in the matrix free CBS-AC scheme in this study to model turbulence. The first one is the one-equation model with low

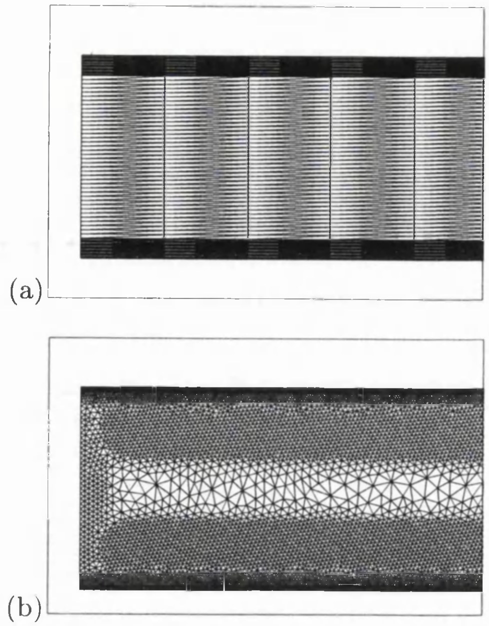

Figure 7.1: Turbulent incompressible flow in a rectangular channel using the matrix free CBS-AC scheme at Re=12300. (a) Structured mesh (7546 elements; 3900 nodes); (b) Unstructured mesh (160756 elements; 83762 nodes).

Reynolds number parameters proposed by Wolfshtein [73]. This model needs discretization and solution of one transport equation for turbulent kinetic energy κ. The second model employed is that of Spalart-Allmaras [90], which again a one equation model and widely employed in aerodynamic flow calculations. The third and fourth models employed are respectively the $\kappa - \varepsilon$ (two-equation) model of Lam et al. [88] and Fan et al. [89] which impose the wall damping procedures on the dissipation rate equation. Full details of the turbulence models and their discretization are discussed in Chapter 3 and 4.

Three different numerical examples are studied using the presented approach. The first benchmark problem is the incompressible turbulent flow through a rectangular channel at a Reynolds number of 12300. The second benchmark problem studied is the turbulent flow past a backward facing step at a Reynolds number of 3025. Finally, the application of unsteady RANS is investigated by solving the vortex shedding behind a circular cylinder at a Reynolds number of 10000. The present numerical results are compared against the experimental and numerical data wherever possible.

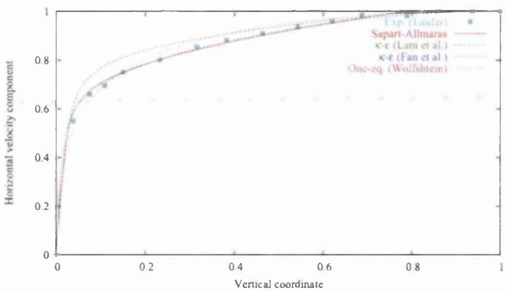

(a)

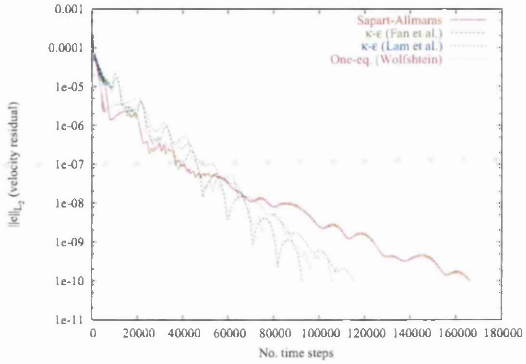

(b)

Figure 7.2: Turbulent incompressible flow in a rectangular channel using the matrix free CBS-AC scheme at Re=12300 on the structured mesh. (a) Comparison of fully developed velocity profiles; (b) Convergence to the steady state

7.2 Two-dimensional turbulent flow in a rectangular channel

The channel is assumed to be two units wide and forty units long. The Reynolds number is defined based on the half width of the channel. A non-dimensional horizontal velocity of unity is assumed at the inlet and the vertical component of velocity is zero. No slip conditions are applied on both walls of the channel. Both structured and unstructured meshes were refined close to the solid wall (see Figure 7.1). The first node from the wall is placed at a non-dimensional distance of 0.005.

For the one equation turbulence model a fixed value of κ=0.05 is assumed at the inlet. On the walls zero value is given for the turbulent kinetic energy.

For the Spalart-Allmaras model the scalar variable $\hat{\nu}$ is prescribed equal to 0.05 at the inlet and zero on the solid walls.

The boundary conditions for the two equation turbulence model are: inlet values of both κ and ε are prescribed (κ=0.05 and ε=0.05) based on the idea proposed in [138]. On the walls κ=0 and $\varepsilon = (2/Re)(d\kappa^{1/2}/dx_2)^2$ is prescribed as proposed in [139].

The comparison of fully developed profile obtained from all the three turbulence models with the experimental data of Laufer [140] using the structured mesh is shown in

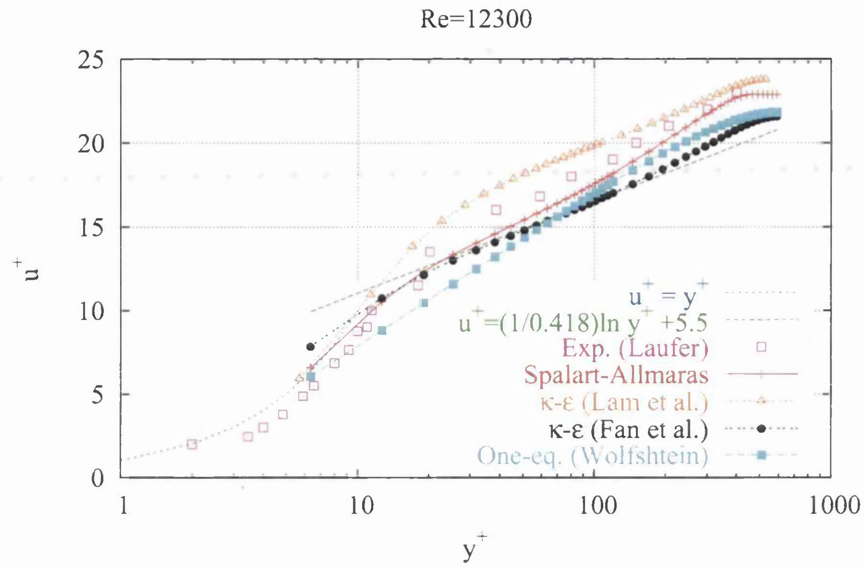

Figure 7.3: Turbulent incompressible flow in a rectangular channel using the matrix free CBS-AC scheme at Re=12300 on the structured mesh. Logarithmic representation of time-averaged velocity profile at several RANS turbulence models.

Figure 7.2(a). Figure 7.2(b) shows the steady state convergence to a tolerance value below 10^{-10}. As seen, the convergence to steady state was rapid when the linear $\kappa - \varepsilon$ model of the Fan-Lakshminarayana-Barnett wall functions [89] were employed. The Spalart-Allmaras model gives results closer to the experimental data than other models as shown in Figure 7.2(a).

Figure 7.3 shows variation of $u^+ \equiv \bar{u}_1/u_\tau = \sqrt{\bar{\rho}}\bar{u}_1/\sqrt{\tau_w}$ with respect to $y^+ \equiv u_\tau x_2/\nu = \sqrt{\tau_w} x_2/\sqrt{\bar{\rho}}\nu$ in fully developed turbulent channel flow using the structured mesh. The distribution from the $\kappa - \varepsilon$ model of Fan-Lakshminarayana-Barnett damping functions closely follow the von Kármán's logarithmic law, except near the solid wall and at the center of the channel. The best fit of the experimental data of Laufer [140] is given by the Spalart-Allmaras model. The one-equation $\kappa - l$ model of Wolfshtein [73] gives a very small logarithmic region. Clearly, the overshoot in the law of the wall in the $\kappa - \varepsilon$ model of the Lam-Bremhorst low Reynolds number formulation [88] results in the over-prediction of the velocity profile in the fully developed flow (see Figure 7.2(a)).

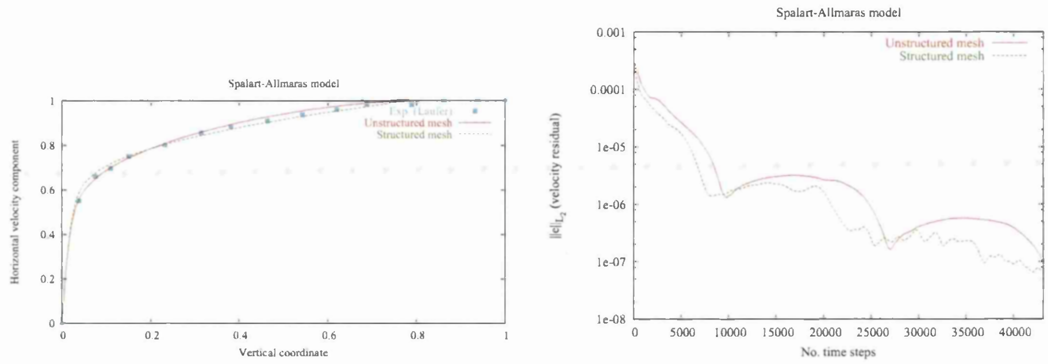

(a) (b)

Figure 7.4: Turbulent incompressible flow in a rectangular channel using the matrix free CBS-AC scheme with the Spalart-Allmaras model at Re=12300. (a) Comparison of fully developed velocity profiles; (b) Convergence to the steady state.

In Figure 7.4(a) the fully developed velocity profile resulted from using the Spalart-Allmaras model on the structured and unstructured meshes is shown. Both numerical results agree with the experimental data. The convergence criterion to steady state used was below 10^{-7} for both meshes (see Figure 7.4(b)). Figure 7.5 shows non-dimensional time-averaged velocity with respect to non-dimensional distance from the solid wall. By comparison with experimental data, the Spalart-Allmaras model using the structured mesh is closer than using the unstructured mesh.

7.3 Two-dimensional turbulent flow past a backward facing step

Another standard test case commonly employed for testing turbulent incompressible flow models at a moderate Reynolds number is the recirculating flow over a backward facing step. Unlike the channel flow, the model has to handle the recirculation region immediately downstream of the step. The definition of the problem is shown in Figure 7.6. The characteristic dimension of the problem is the step height. All other dimensions are defined with

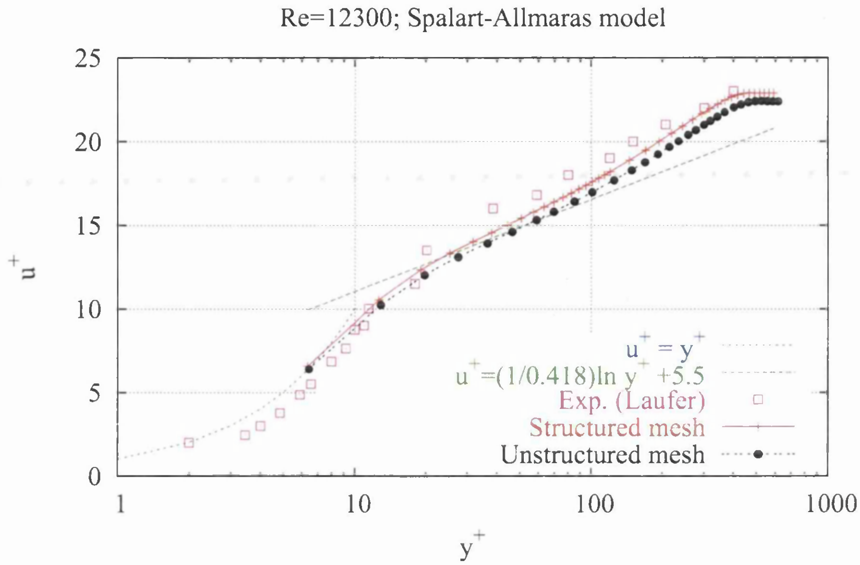

Figure 7.5: Turbulent incompressible flow in a rectangular channel using the matrix free CBS-AC scheme with the Spalart-Allmaras model at Re=12300. Logarithmic representation of time-averaged velocity profile.

respect to the characteristic dimension. The inlet is located at a distance of 4 times the step height from it. The inlet channel height is two times the step height. The total length of the channel is 40 times the step height.

The inlet velocity profile is obtained from the experimental data reported by Denham et al. [141]. No slip conditions apply on the solid walls. For the one-equation and the standard $\kappa-\varepsilon$ model (two-equation) models, the inlet κ and ε profiles are obtained by solving a channel flow problem. For the Spalart-Allmaras model, a fixed value of 0.05 for the modified turbulent eddy viscosity (scalar variable) at the inlet is prescribed. On the walls κ is assumed to be equal to zero. No flux conditions are assumed for ε on the walls. The scalar variable of the Spalart-Allmaras model is also assumed to be zero on the walls.

Figure 7.7 shows the convergence histories to steady state for all the three turbulent models using the matrix free CBS-AC scheme. As seen in Figure 7.7(a) both the two-equation $\kappa-\varepsilon$ model of Fan et al. and the Spalart-Allmaras model reach prescribed residual tolerance 10^{-10} faster than both the one-equation $\kappa-l$ model and the $\kappa-\varepsilon$ of Lam et al.

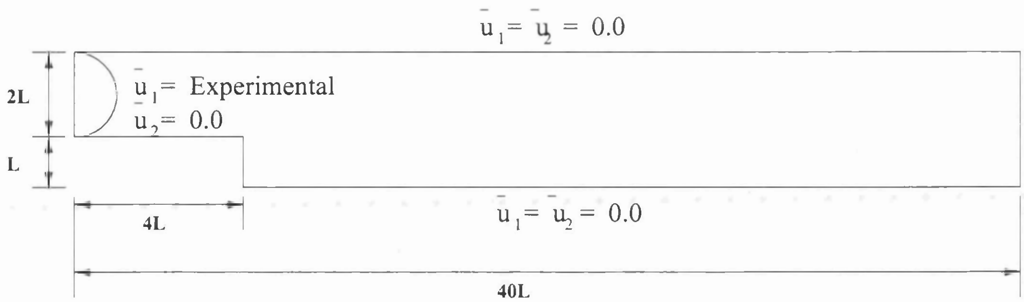

Figure 7.6: Turbulent incompressible flow past a backward facing step. Geometry and boundary conditions.

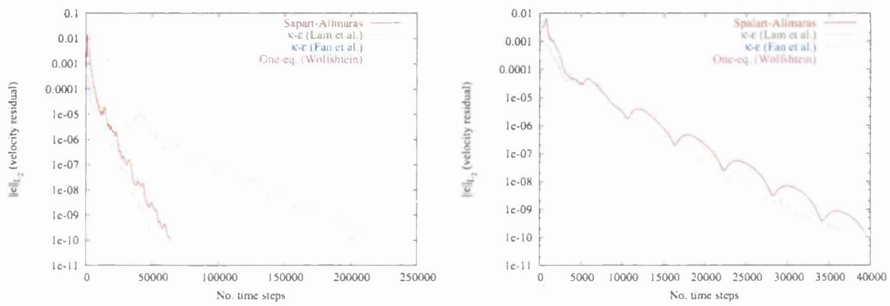

(a) Structured mesh

(b) Unstructured mesh

Figure 7.7: Turbulent incompressible flow past a backward facing step. Steady state convergence histories at Re=3025.

It is expected that the convergence to steady state will not be always monotonic for an explicit time discretization.

Both structured and unstructured meshes are employed in the calculation. Figure 7.8 and 7.9 show the Spalart-Allmaras model solutions on structured and unstructured meshes respectively. The qualitative difference between the two results is almost nil. The quantitative difference between the two solutions are also found to be negligibly small.

The comparison of velocity profiles against the experimental data of Denham et al. [141] is shown in Figure 7.10. It is obvious that the one-equation model failed to predict the recirculation region accurately. The Spalart-Allmaras model and the two-equation models

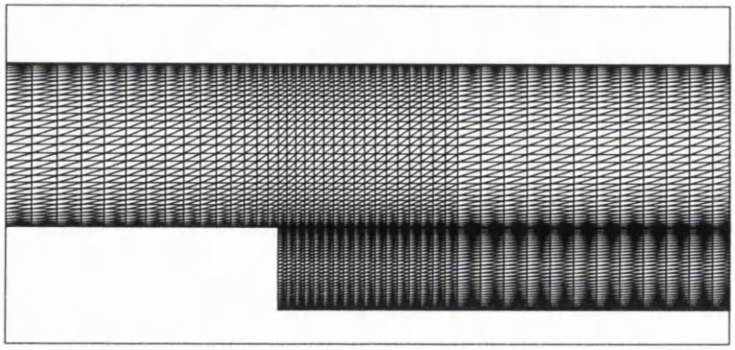

(a) Mesh

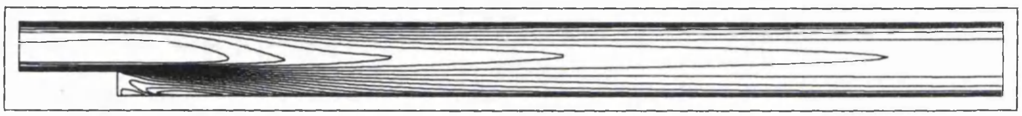

(b) $\bar{u}_1$ contours

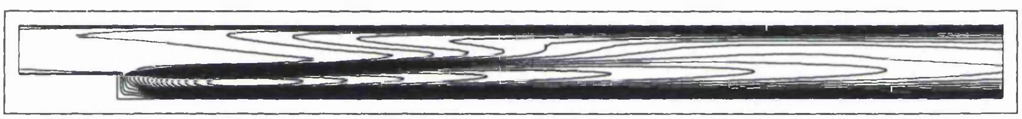

(c) $\hat{\nu}$ contours

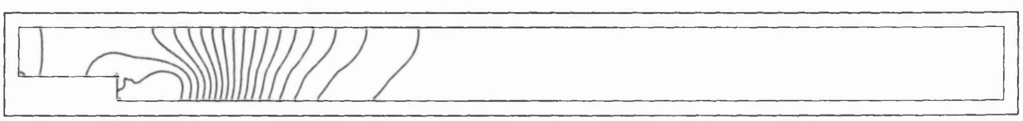

(d) Pressure contours

Figure 7.8: Turbulent incompressible flow past a backward facing step. Structured mesh (Elements: 8092, Nodes: 4183), velocity contours, $\hat{\nu}$ contours and pressure contours at Re=3025 using the matrix free CBS-AC scheme with the Spalart-Allmaras model.

on the other hand predict the recirculation better than the one-equation model. Among the latter models, the Spalart-Allmaras model seems to predict the recirculation more accurately. However, some differences between the experiment and the present predictions of

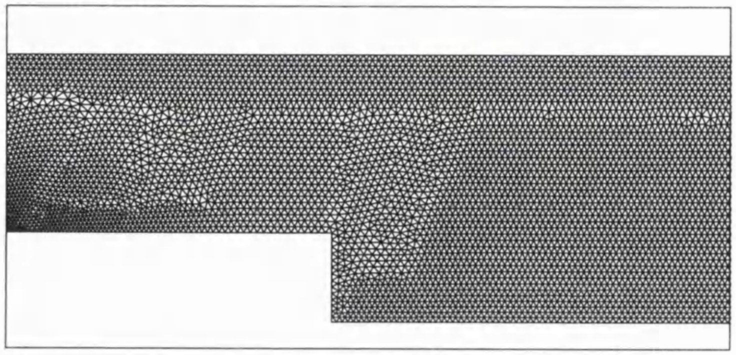

(a) Mesh

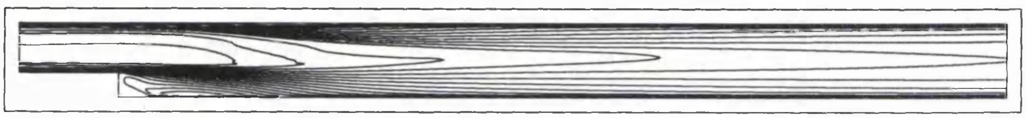

(b) $\bar{u}_1$ contours

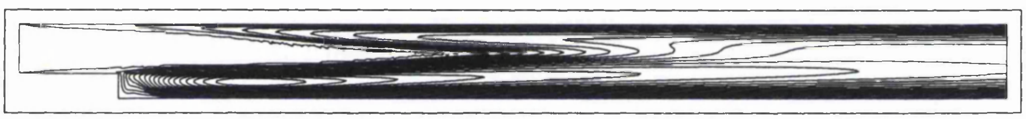

(c) $\hat{\nu}$ contours

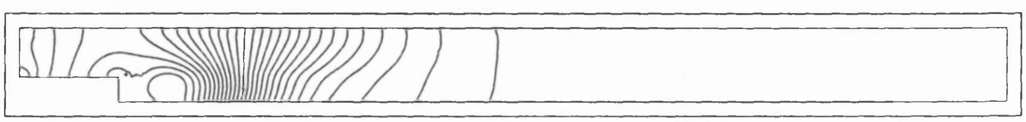

(d) Pressure contours

Figure 7.9: Turbulent incompressible flow past a backward facing step. Unstructured mesh (Elements: 47359, Nodes: 24336), velocity contours, $\hat{\nu}$ contours and pressure contours at Re=3025 using the matrix free CBS-AC scheme with the Spalart-Allmaras model.

the Spalart-Allmaras model are noticed along the top wall.

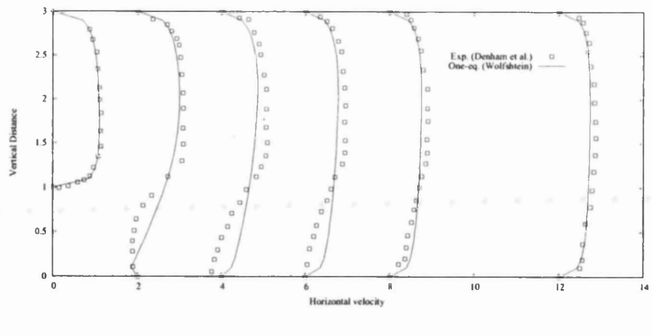

(a) One-equation model

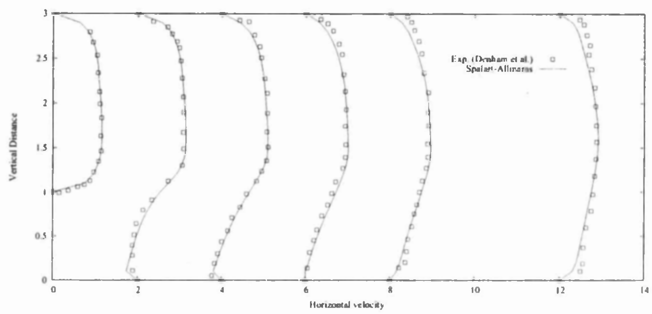

(b) Spalart-Allmaras model

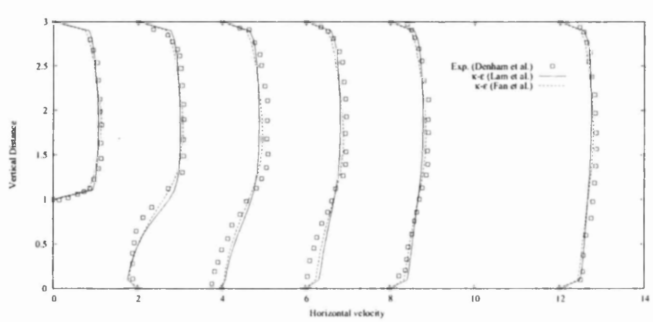

(c) Two-equation models

Figure 7.10: Turbulent incompressible flow past a backward facing step. Velocity profiles at various downstream sections at Re=3025 using the matrix free CBS-AC scheme with several RANS turbulence models.

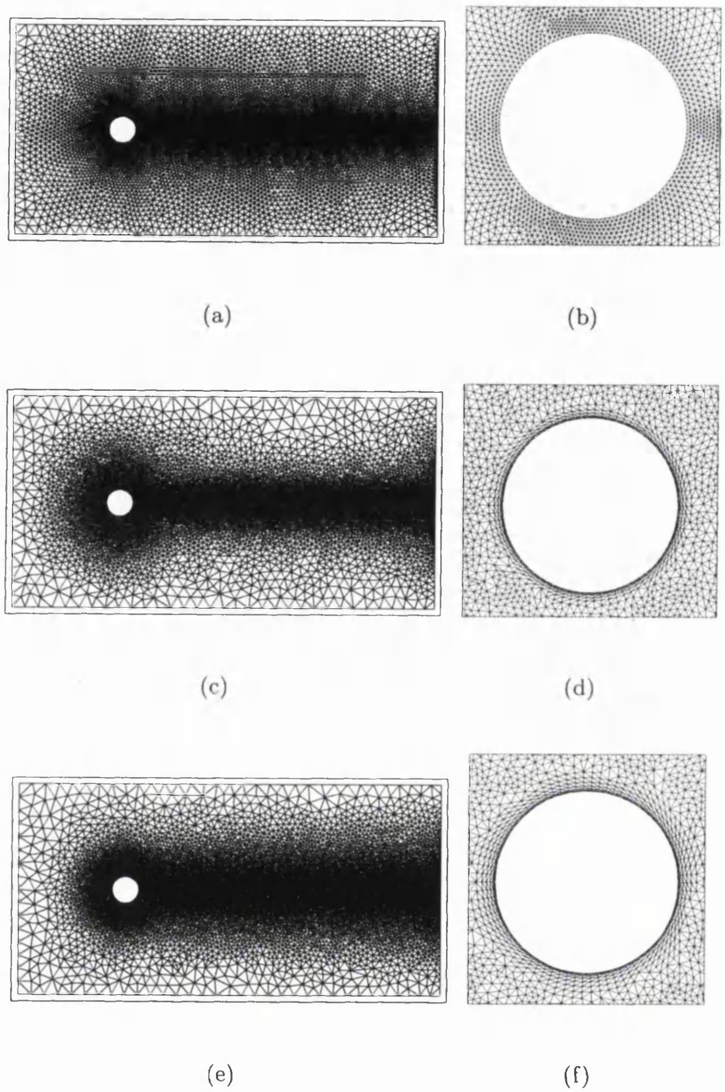

Figure 7.11: Turbulent incompressible flow over a circular cylinder. (a) Unstructured mesh (Elements: 46433, Nodes: 23452); (b) Unstructured mesh of close to solid wall (0.0097 distance); (c) Hybrid mesh1 (Elements: 30299, Nodes: 15277); (d) Hybrid mesh1 of close to solid wall (0.005 distance); (e) Hybrid mesh2 (Elements: 37571, Nodes: 18913); (f) Hybrid mesh2 of close to solid wall (0.001 distance).

7.4 Two-dimensional turbulent flow over a circular cylinder

The dual time stepping technique is used to predict time dependent turbulent flows here. The example considered is the standard test case of transient turbulent incompressible flow

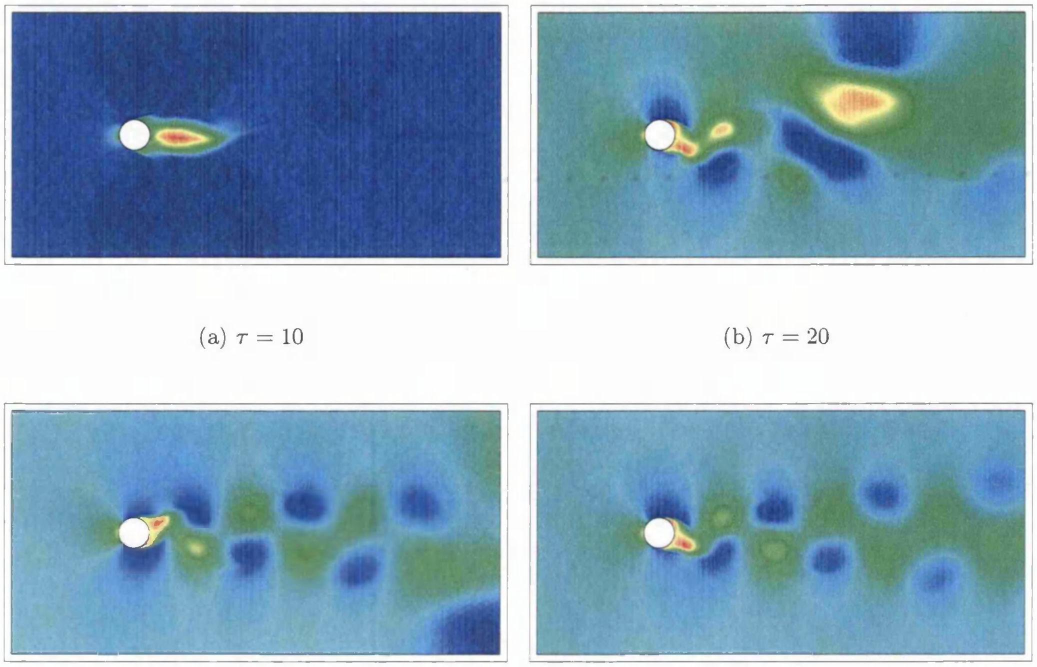

(a) $\tau = 10$

(b) $\tau = 20$

(c) $\tau = 30$

(d) $\tau = 40$

Figure 7.12: Turbulent incompressible flow over a circular cylinder. $\bar{u}_1$ velocity contours at different real time at Re=10000 using the matrix free CBS-AC scheme with the Spalart-Allmaras model.

past a circular cylinder.

Three different finite element meshes used are shown in Figure 7.11. The unstructured mesh was tested by all presented RANS turbulence models. The hybrid mesh was only investigated with circular cylinder wall-bounded flows based on mixing-length hypothesis inside the log-law region while the $\kappa - l$ model of Wolfshtein was employed. However, all the meshes in the vicinity of the cylinder and along the wake region are refined to capture the transient feature of the problem.

Uniform velocity conditions are assumed at the inlet. The Reynolds number is 10000, based on the cylinder diameter and the uniform inflow in the x_1 direction. The real time step size is taken equal to 0.05. The turbulent scalar variable is assumed to be 0.05 at

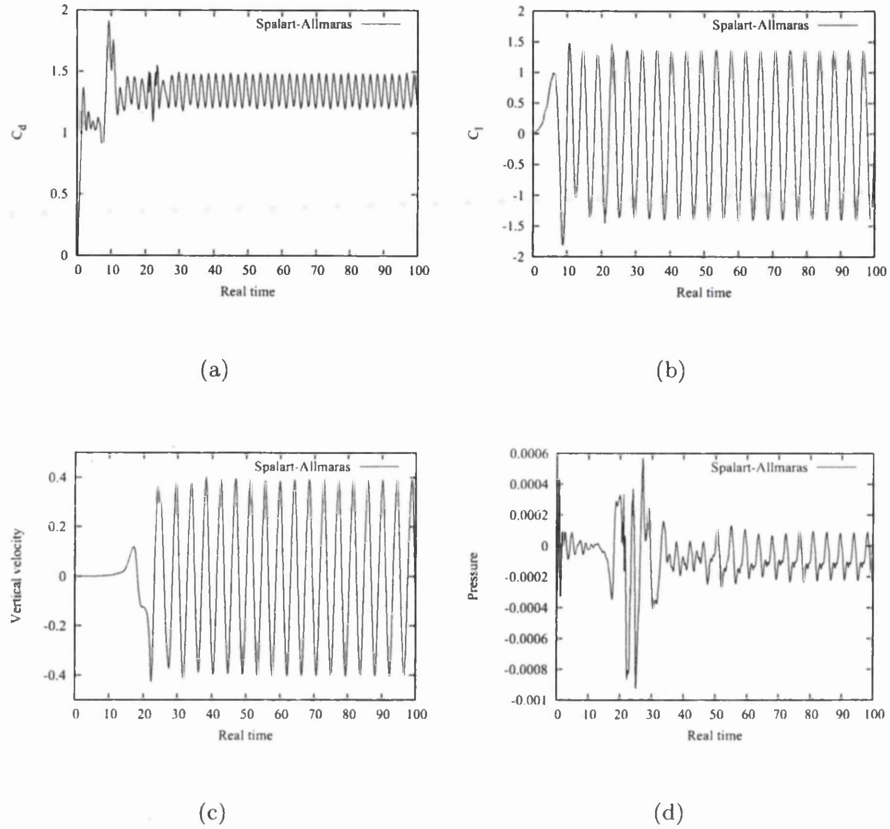

Figure 7.13: Turbulent incompressible flow over a circular cylinder at Re=10000 using the matrix free CBS-AC scheme with the Spalart-Allmaras model. (a) Drag coefficient distribution with respect to real time; (b) Lift coefficient distribution with respect to real time; (c) $\bar{u}_2$ distribution at the central exit point with respect to real time; (d) Pressure distribution at the central exit point with respect to real time.

the inlet for the Spalart-Allmaras model. On the top and bottom sides slip conditions are assumed and no turbulence quantity is prescribed. On the cylinder walls no slip conditions are assumed and the turbulent scalar variable of the Spalart-Allmaras model is assumed to be zero. For the two-equation model, κ and ε values at the inlet are assumed to be 0.0025 and on the solid walls κ is assumed to be zero and ε condition is the same one used for the steady state problems. The Wolfshtein model based on mixing-length hypothesis is modified to give a constant lengthscale if the nearest wall distance is more than 0.05.

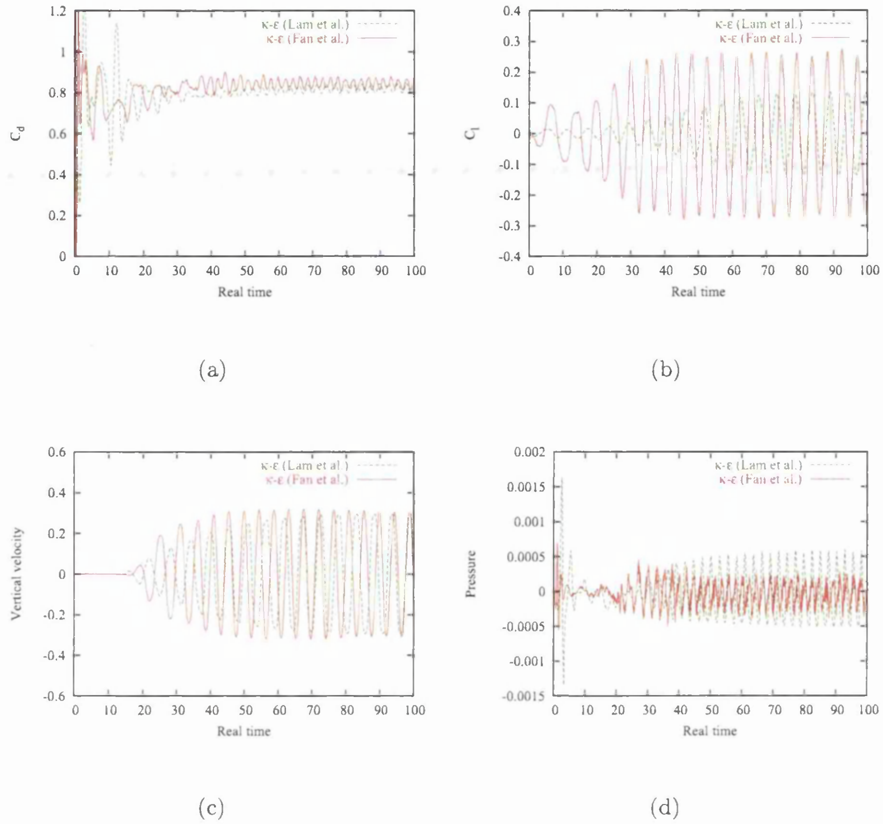

Figure 7.14: Turbulent incompressible flow over a circular cylinder at Re=10000 using the matrix free CBS-AC scheme with the linear $\kappa-\varepsilon$ (two-equation) model. (a) Drag coefficient distribution with respect to real time; (b) Lift coefficient distribution with respect to real time; (c) $\bar{u}_2$ distribution at the central exit point with respect to real time; (d) Pressure distribution at the central exit point with respect to real time.

In the matrix free CBS-AC scheme, the pseudo time step used within each real time step is local and varies between the nodes depending on the local flow field and mesh size. As mentioned before, the L_2 norm of velocity residual is reduced to 10^{-6} within every real time step in order to make sure that local steady state is achieved within each real time step.

The time dependent patterns of horizontal velocity component are shown in Figure 7.12 for different real times to show that the vortex shedding is present. At τ = 10, the

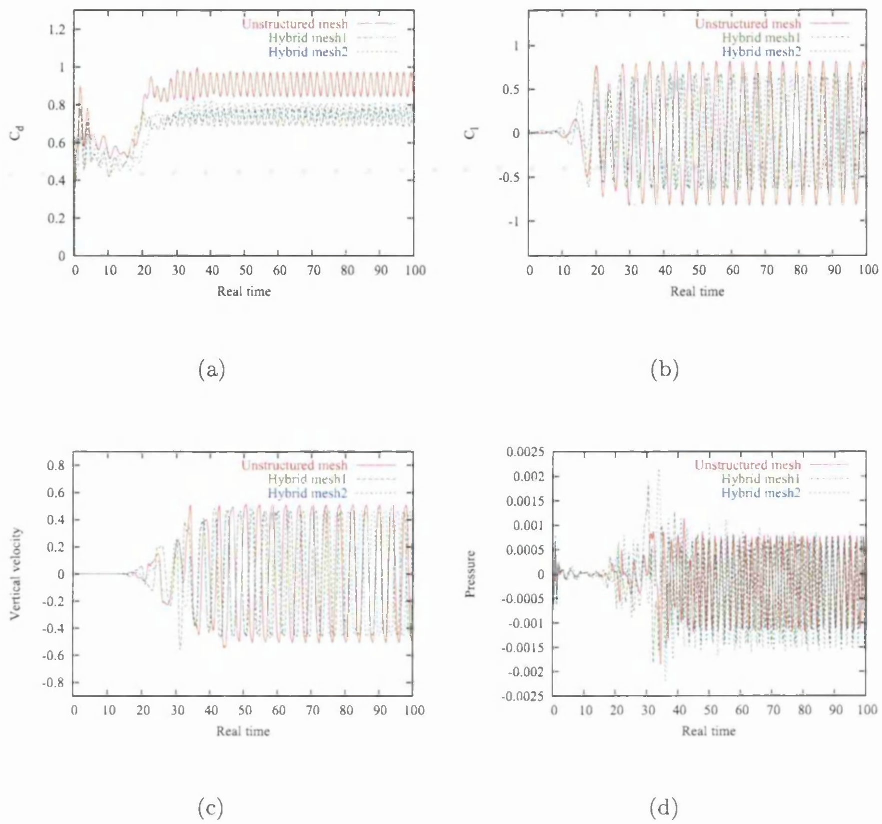

Figure 7.15: Turbulent incompressible flow over a circular cylinder at Re=10000 using the matrix free CBS-AC scheme with the $\kappa - l$ one-equation (Wolfshtein) model. (a) Drag coefficient distribution with respect to real time; (b) Lift coefficient distribution with respect to real time; (c) $\bar{u}_2$ distribution at the central exit point with respect to real time; (d) Pressure distribution at the central exit point with respect to real time.

initial velocity field immediately behind the cylinder looks symmetric but the velocity field at $\tau = 20$ and beyond shows un-symmetric shedding behaviour. From Figure 7.12(b), (c) and (d) it is obvious that the origin of the vortex street shifts between the areas above and below the central axis. The behaviour qualitatively confirms the periodic vortex shedding phenomenon.

Figures 7.13(a) and (b) show respectively the drag and lift coefficients with respect to real time using the matrix free CBS-AC scheme and the Spalart-Allmaras model. As seen

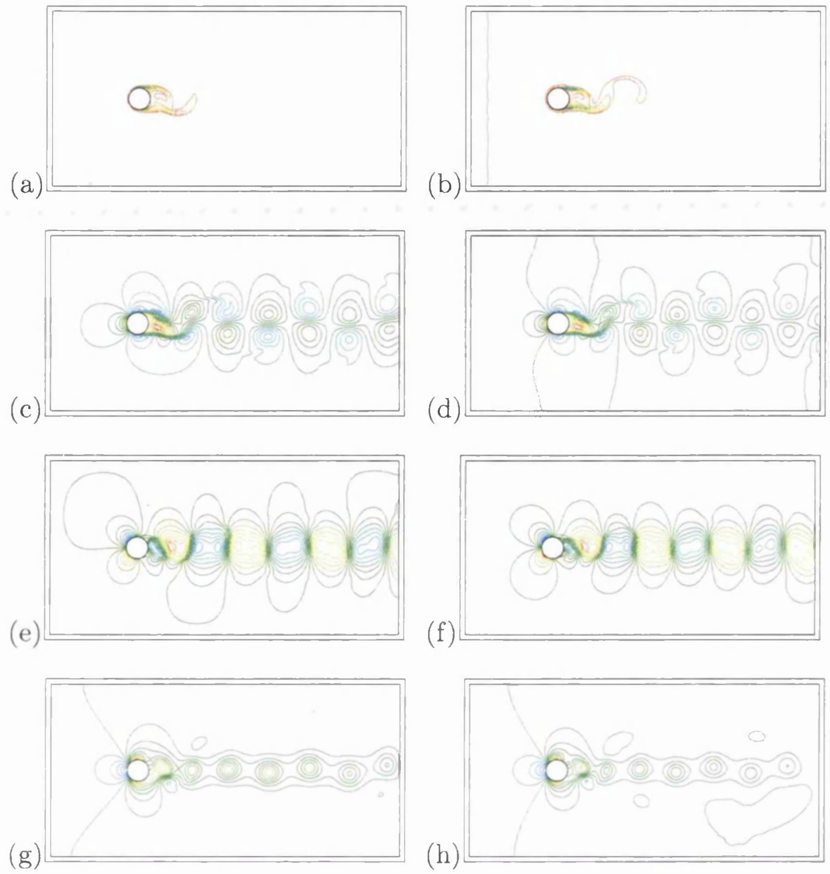

Figure 7.16: Turbulent incompressible flow over a circular cylinder at Re=10000 using the matrix free CBS-AC scheme with the $\kappa - l$ one-equation (Wolfshtein) model on the unstructured mesh (left) and hybrid mesh2 (right). (a) Turbulent kinetic energy κ contours. κ_{min}(red) = 0.0, κ_{max}(blue) = 0.219; (b) Turbulent kinetic energy κ contours. κ_{min}(red) = 0.0, κ_{max}(blue) = 0.119; (c) Horizontal velocity component $\bar{u}_1$ contours. $\bar{u}_{1_{min}}$(red) = -0.517, $\bar{u}_{1_{max}}$(blue) = 1.789; (d) Horizontal velocity component $\bar{u}_1$ contours. $\bar{u}_{1_{min}}$(red) = -0.498, $\bar{u}_{1_{max}}$(blue) = 1.861; (e) Vertical velocity component $\bar{u}_2$ contours. $\bar{u}_{2_{min}}$(red) = -1.0, $\bar{u}_{2_{max}}$(blue) = 1.023; (f) Vertical velocity component $\bar{u}_2$ contours. $\bar{u}_{2_{min}}$(red) = -0.992, $\bar{u}_{2_{max}}$(blue) = 1.037; (g) Pressure contours. p_{min}(red) = -1.118, p_{max}(blue) = 0.714; (h) Pressure contours. p_{min}(red) = -1.163, p_{max}(blue) = 0.691.

the periodic flow and vortex shedding are clearly evident from the graphs. The averaged experimental value of drag coefficient is around 1.12 and the Strouhal number is around 0.2 [142]. Present prediction shows that the averaged value of drag coefficient is around 1.34 and the Strouhal number is 0.154. The large difference in predicted drag coefficient is not

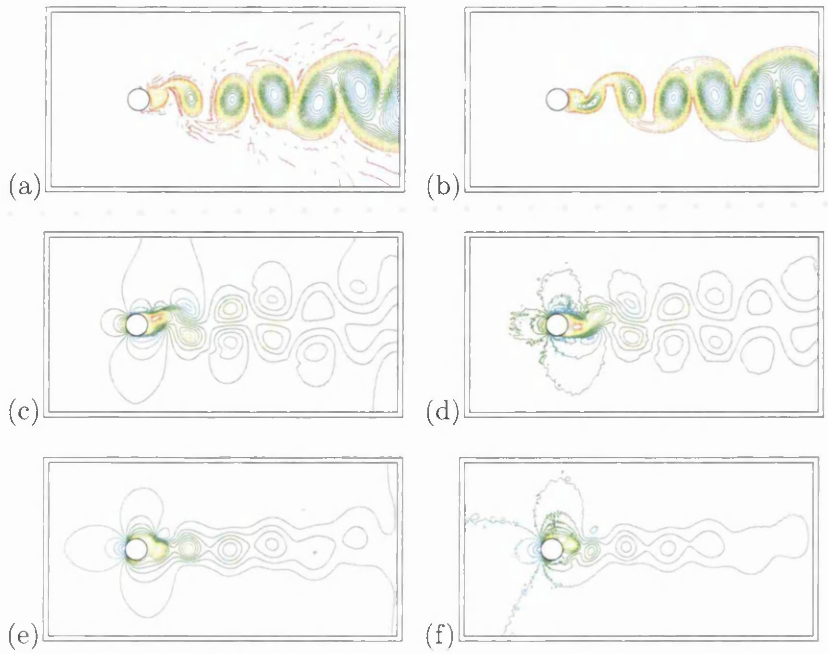

Figure 7.17: Turbulent incompressible flow over a circular cylinder at Re=10000 using the matrix free CBS-AC scheme (left) and the semi-implicit CBS scheme (right) with the Spalart-Allmaras model. (a) Modified turbulent eddy kinematic viscosity $\hat{\nu}$ contours. $\hat{\nu}_{min}$(red) = 0.0, $\hat{\nu}_{max}$(blue) = 460.887; (b) Modified turbulent eddy kinematic viscosity $\hat{\nu}$ contours. $\hat{\nu}_{min}$(red) = 0.0, $\hat{\nu}_{max}$(blue) = 409.792; (c) Horizontal velocity component $\bar{u}_1$ contours. $\bar{u}_{1_{min}}$(red) = -0.533, $\bar{u}_{1_{max}}$(blue) = 2.112; (d) Horizontal velocity component $\bar{u}_1$ contours. $\bar{u}_{1_{min}}$(red) = -0.483, $\bar{u}_{1_{max}}$(blue) = 2.123; (e) Pressure contours. p_{min}(red) = -1.276, p_{max}(blue) = 0.699; (f) Pressure contours. p_{min}(red) = -1.417, p_{max}(blue) = 0.717.

surprising as all the URANS models have accuracy limitations. The two-dimensional LES model reported in reference [143] significantly over predicts the averaged drag coefficient. It appears that some of the non-linear URANS models give results better than the standard URANS models [144]. However, investing in the Spalart-Allmaras model leads to further development towards Detached Eddy Simulation (DES) [86].

The lift coefficient distribution with respect to real time using the Spalart-Allmaras model is shown in Figure 7.13(b). The pattern is periodic and the magnitude of the lift coefficient produced by the Spalart-Allmaras model is in qualitative agreement with other reported results [143]. However, it should be noted that the turbulent flow over a circular cylinder at a Reynolds number of 10000 is essentially three dimensional as shown in reference

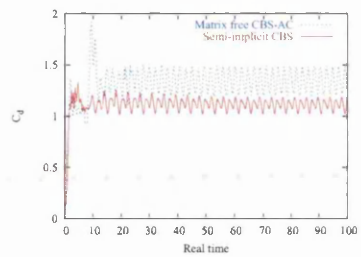

(a)

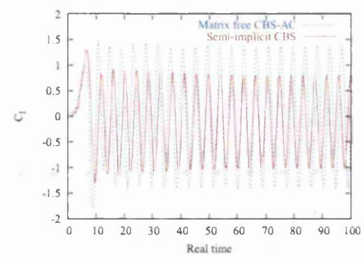

(b)

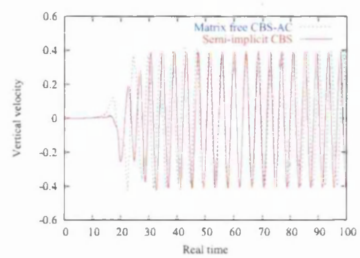

(c)

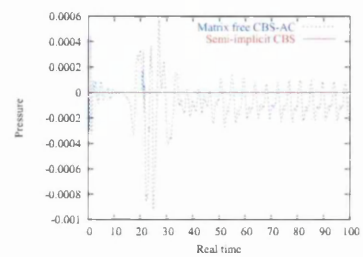

(d)

Figure 7.18: Turbulent incompressible flow over a circular cylinder at Re=10000 using both the matrix free CBS-AC scheme and the semi-implicit CBS scheme with the Spalart-Allmaras model. (a) Drag coefficient distribution with respect to real time; (b) Lift coefficient distribution with respect to real time; (c) $\bar{u}_2$ distribution at the central exit point with respect to real time; (d) Pressure distribution at the central exit point with respect to real time.

[145]. Figure 7.13(c) and (d) show the variation of vertical velocity component and pressure at an exit point at the horizontal centreline of the domain. This is consistent with the drag and lift data.

Figure 7.14 show the drag coefficient, lift coefficient, vertical velocity and pressure variation at an exit point using the matrix free CBS-AC scheme with the two-equation model. Although the velocity distribution at an exit point is similar between the two-equation and the Spalart-Allmaras models, the drag and lift coefficient distribution are quite different. Figure 7.14(a) shows the averaged drag coefficient value obtained is around 0.843 by Fan et al. and 0.811 by Lam et al., which are much smaller than that of the one predicted by the Spalart-Allmaras model. The two-equation models results, however, are very similar to the one reported by [144] for a higher Reynolds number. The averaged lift coefficient obtained by different wall damping functions of the two-equation models are zero (Figure 7.14(b)), which are consistent with reference [144]. For the two-equation models, the Strouhal number based on the lift coefficient was predicted by Fan-Lakshminarayana-Barnett wall functions and Lam-Bremhorst wall functions are 0.155 and 0.127 respectively.

Several numerical solutions using the Wolfshtein $\kappa - l$ model by limiting the mixing length were obtained and shown in Figure 7.15 and 7.16. Three different meshes, one unstructured mesh and two hybrid meshes, were used in the calculation. Figure 7.15 shows the variation of quantitative results with respect to real time. The average drag coefficient obtained are 0.905, 0.728 and 0.765, respectively on unstructured mesh, first and second hybrid meshes. By using the hybrid mesh2, the Strouhal number of 0.185 was obtained which is quite close to experimental solution. Figure 7.16 shows the qualitative results that are almost identical between the meshes used.

In Figure 7.17 there are 20 contours on time dependent patterns at real time $\tau = 100$ using both the matrix free CBS-AC scheme and semi-implicit CBS scheme and the Spalart-Allmaras model. The turbulent eddy kinematic viscosity has influence only along the central region as shown in Figure 7.17(a) and (b). The horizontal velocity component $\bar{u}_1$ contours resulted from the matrix free scheme has less spatial oscillations than using the semi-implicit scheme. (see Figure 7.17(c) and (d)). From Figure 7.17(e) and (f), the Dirichlet condition at the outflow boundary is taken as pressure equal to zero for the semi-implicit scheme, but in the matrix free scheme no pressure at the exit was prescribed. However, both schemes show vertex shedding and periodic turbulent flow behind the cylinder.

Figures 7.18(a) shows the drag coefficient with respect to real time from both the matrix free CBS-AC scheme and semi-implicit CBS scheme and the Spalart-Allmaras model. The semi-implicit CBS scheme gives an averaged drag coefficient of around 1.117 which is quite close to the averaged drag coefficient 1.12 from Schlichting's experiment [142]. The Strouhal number is 0.158. The semi-implicit scheme, however, gives un-symmetric, periodic lift coefficient.

Last but not least, the most important point here is that the explicit scheme along with an implicit dual time stepping approach can satisfactorily model unsteady turbulent incompressible flows.

7.5 Summary

In this chapter, three benchmark problems, a rectangular channel, a backward facing step and a stationary circular cylinder, have been tested using the matrix free CBS-AC scheme. Numerical solutions presented have demonstrated the robustness of using the CBS-AC method to both steady and unsteady two-dimensional incompressible turbulent flows. It appears that the matrix free CBS-AC scheme is well suited for turbulent flow calculations as it was for laminar flow. The semi-implicit CBS scheme was also implemented with the Spalart-Allmaras model to test unsteady turbulent flow around a circular cylinder.

Chapter 8

The steady and unsteady three-dimensional turbulent flows

8.1 Three-dimensional turbulent flow past a backward facing step

The three-dimensional backward facing step flow has been the subject of detailed experimental study by Denham et al. [141]. The geometry and boundary conditions are same as the two-dimensional backward facing step flow except that the pressure at the outflow cross-section was assumed to be zero for using the semi-implicit CBS scheme. The matrix free CBS-AC scheme and the semi-implicit CBS scheme were tested using the Spalart-Allmaras turbulence model.

The unstructured mesh used is shown in Figure 8.1. The mesh is refined in the recirculation zone to capture vortical flows and the reattachment point. Figure 8.2 shows modified turbulent eddy kinematic viscosity contours and velocity component contours from the matrix free CBS-AC scheme and semi-implicit CBS scheme respectively. As seen, the qualitative difference between the two results is almost nil.

Figure 8.3 shows profiles of the comparison of horizontal velocity component at six vertical sections with the experimental data of Denham et al. [141]. The Spalart-Allmaras model predicts the recirculation satisfactorily. The quantitative difference between the

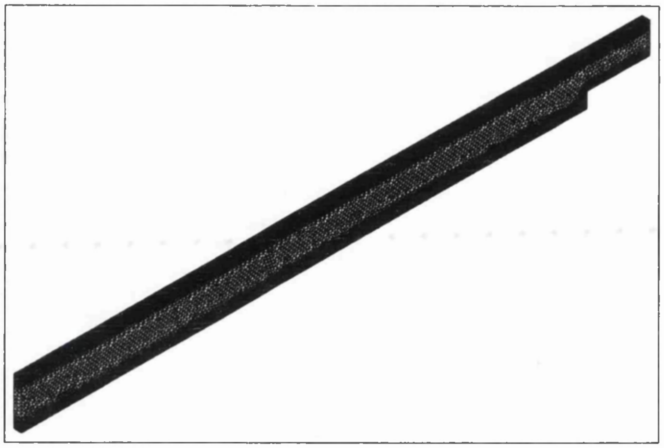

Figure 8.1: Turbulent incompressible flow past a backward facing step at Re=3025. Unstructured mesh of 4 nodes tetrahedral elements (Elements: 297054, Nodes: 65372).

numerical RANS solutions of two schemes are found to be negligibly small. Some differences between the experiment and the present predictions of the Spalart-Allmaras model are noticed along the top wall. However, comparison between two- and three-dimensional flow solutions shows that the results are identical.

The steady state convergence criteria is based on the L_2 norm of the velocity field. It is reduced to a value below 10^{-4}. Figure 8.4 shows the convergence histories to steady state.

8.2 Three-dimensional turbulent flow over a circular cylinder

The Spalart-Allmaras model with the matrix free CBS-AC scheme is tested on three-dimensional turbulent flow past a stationary circular cylinder problem at Re=10000. Uniform velocity conditions in the x_1 direction are assumed at the inlet. The size of real time step was set at 0.05. The turbulent scalar variable (modified turbulent eddy kinematic viscosity) is assumed to be 10^{-8} at the inlet for the Spalart-Allmaras model. On the top and bottom sides slip conditions are assumed and no turbulence quantity is prescribed. On the cylinder walls no slip conditions are assumed and the turbulent scalar variable of the Spalart-Allmaras model is assumed to be zero.

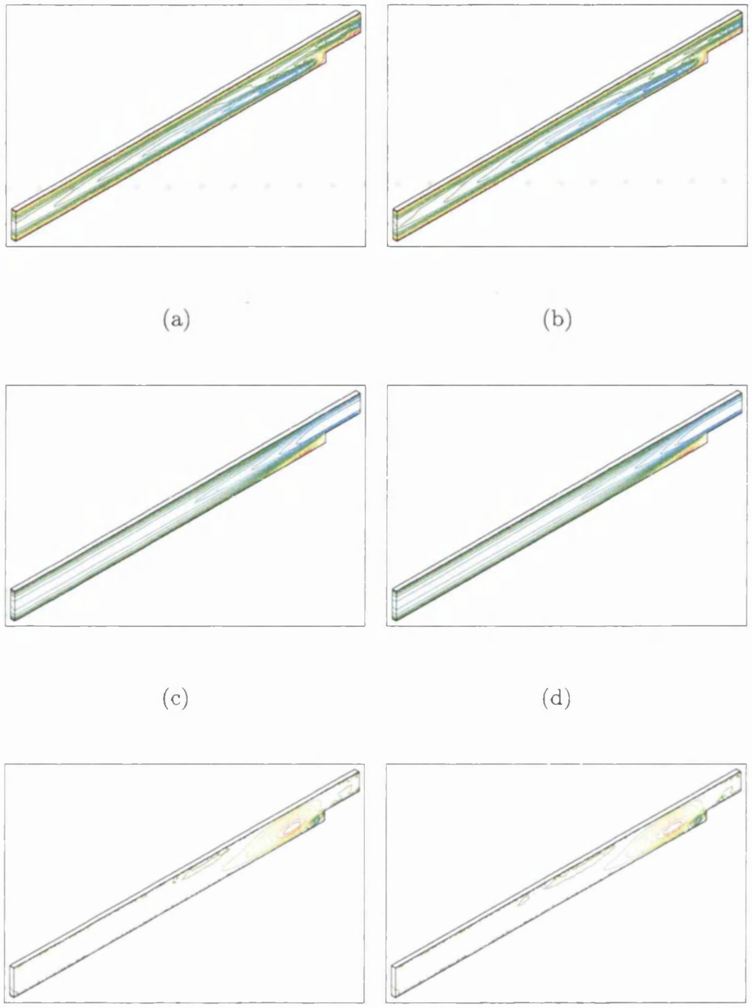

(a) (b) (c) (d) (e) (f)

Figure 8.2: Turbulent incompressible flow past a backward facing step at Re=3025 using both the matrix free CBS-AC scheme (left) and the semi-implicit CBS scheme (right) with the Spalart-Allmaras model. (a) Modified turbulent eddy kinematic viscosity contours. $\hat{\nu}_{min}$(red) = 0.0, $\hat{\nu}_{max}$(blue) = 54.354; (b) Modified turbulent eddy kinematic viscosity contours. $\hat{\nu}_{min}$(red) = 0.0, $\hat{\nu}_{max}$(blue) = 51.873; (c) $\bar{u}_1$ velocity contours. $\bar{u}_{1_{min}}$(red) = -0.345, $\bar{u}_{1_{max}}$(blue) = 1.213; (d) $\bar{u}_1$ velocity contours. $\bar{u}_{1_{min}}$(red) = -0.338, $\bar{u}_{1_{max}}$(blue) = 1.213; (e) $\bar{u}_3$ velocity contours. $\bar{u}_{3_{min}}$(red) = -0.098, $\bar{u}_{3_{max}}$(blue) = 0.150; (f) $\bar{u}_3$ velocity contours. $\bar{u}_{3_{min}}$(red) = -0.097, $\bar{u}_{3_{max}}$(blue) = 0.148.

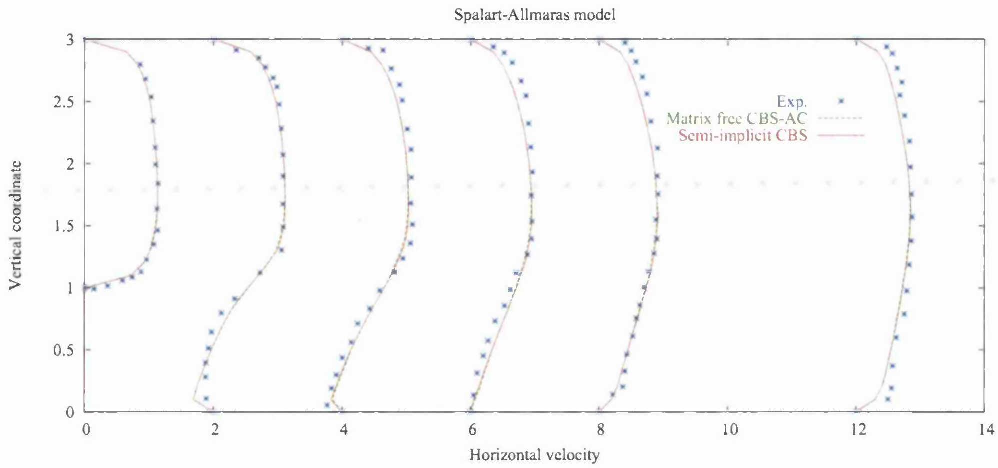

Figure 8.3: Turbulent incompressible flow past a backward facing step. Velocity profiles at various downstream sections at Re=3025 using two different CBS schemes with the Spalart-Allmaras model.

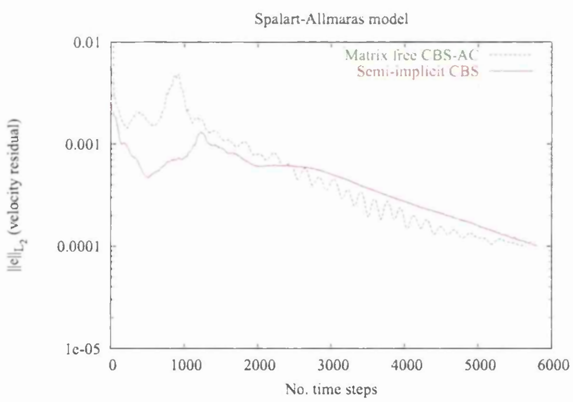

Figure 8.4: Turbulent incompressible flow past a backward facing step. Steady state convergence histories at Re=3025.

The dual time-stepping method was employed with the matrix free CBS-AC scheme. The local time step depends on each element size within every real time step. The convergence criterion of both velocity and pressure residuals is reduced to 10^{-4} per real time step.

Two different meshes used to test the flow past a three-dimensional circular cylin-

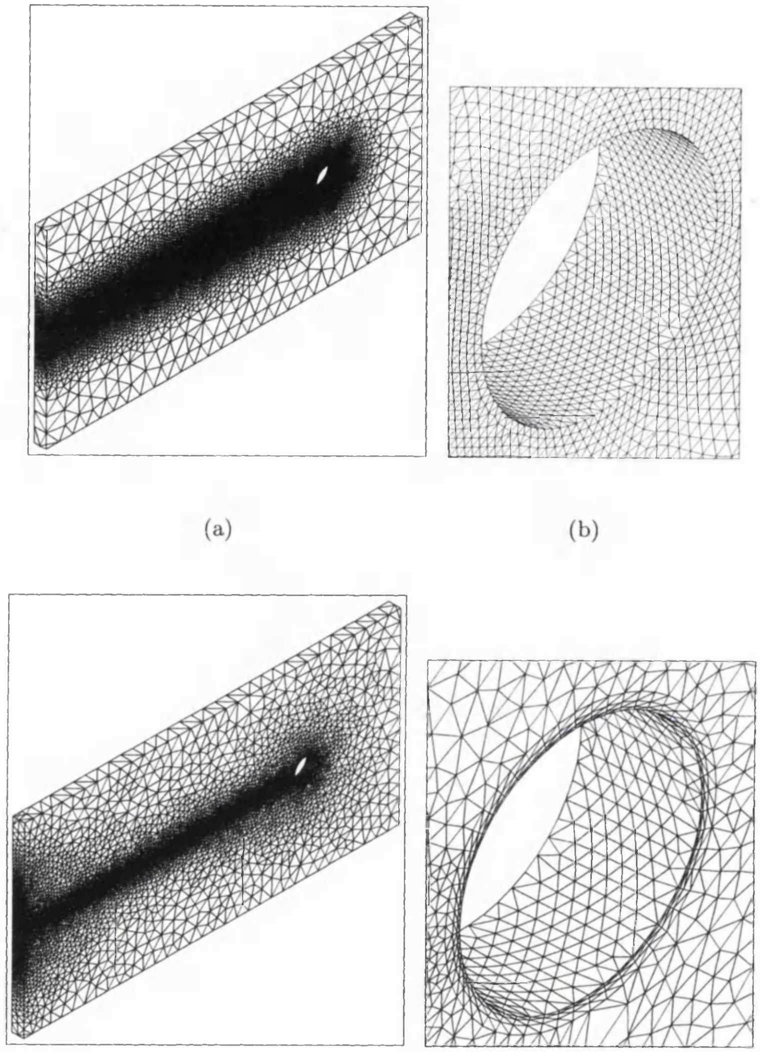

(a) (b)

(c) (d)

Figure 8.5: Turbulent incompressible flow over a circular cylinder at Re=10000 using the matrix free CBS-AC scheme with the Spalart-Allmaras model. (a) Unstructured mesh1 (Elements: 606769, Nodes: 115035); (b) Unstructured mesh1 of close to solid wall (0.038 distance); (c) Hybrid mesh2 (Elements: 489463, Nodes: 88964); (d) Hybrid mesh2 of close to solid wall (0.01 distance).

der problem in this study are shown in Figure 8.5. The fully unstructured mesh (mesh1) used comprises of 606769 tetrahedral elements and 115035 nodes. The hybrid mesh (mesh2)

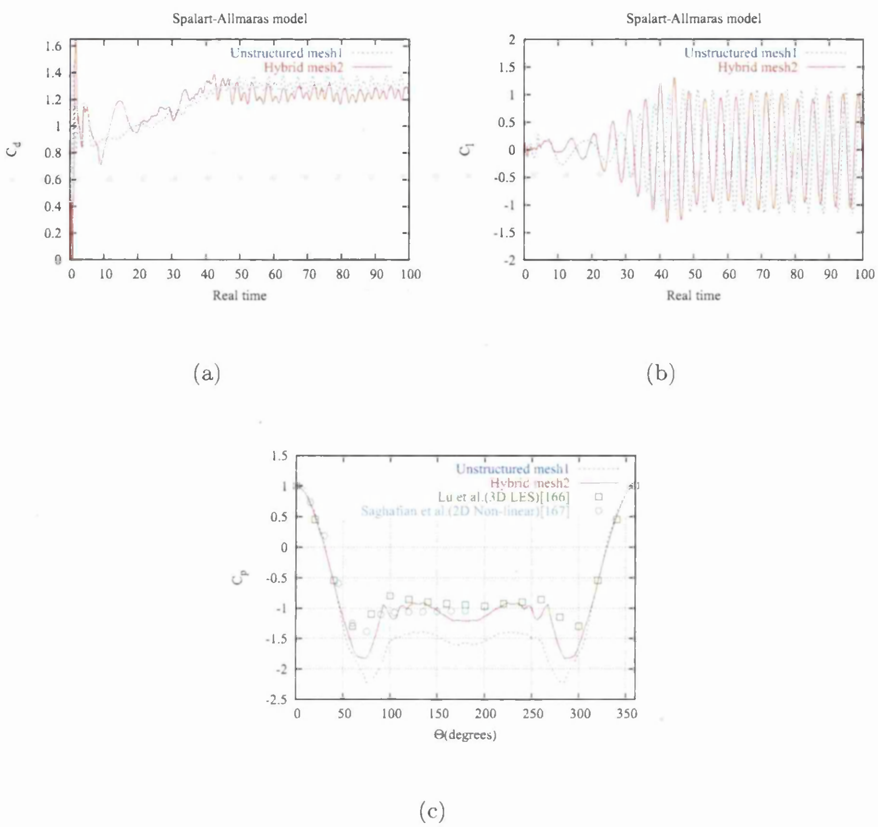

Figure 8.6: Turbulent incompressible flow over a circular cylinder at Re=10000 using the matrix free CBS-AC scheme with the Spalart-Allmaras model. (a) Drag coefficient variation with respect to real time; (b) Lift coefficient variation with respect to real time; (c) Pressure coefficient distribution along the cylinder surface at real time = 100.

consists of three structured layers close to the cylinder surface and unstructured grid away from the wall. Figure 8.5(d) shows the mesh in the vicinity of the cylinder. Both meshes are refined close to the wall and in the wake region to predict the vortex shedding.

Figure 8.6 shows the time variation of drag coefficient, lift coefficient and pressure coefficient using the unstructured and hybrid meshes. The average drag coefficient obtained 1.311 from the unstructured mesh1. The strouhal number is 0.152. The amplitude of lift coefficient is between 1 and -1. The averaged drag coefficient obtained by the hybrid mesh2 is 1.239, which is more accurate than the result of mesh1 in comparison with experimental

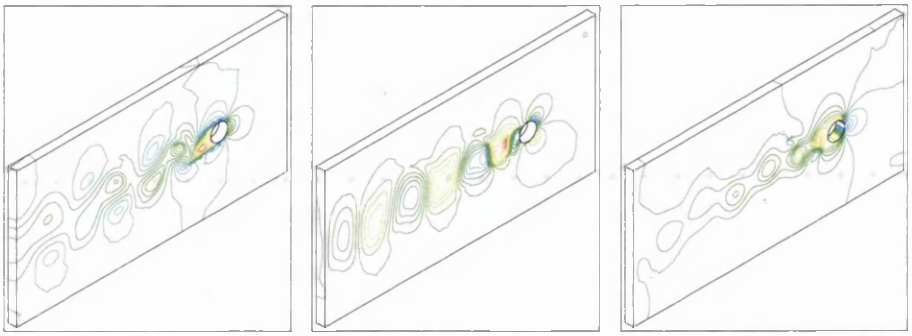

(a) $\bar{u}_1$ contours (b) $\bar{u}_3$ contours (c) Pressure contours

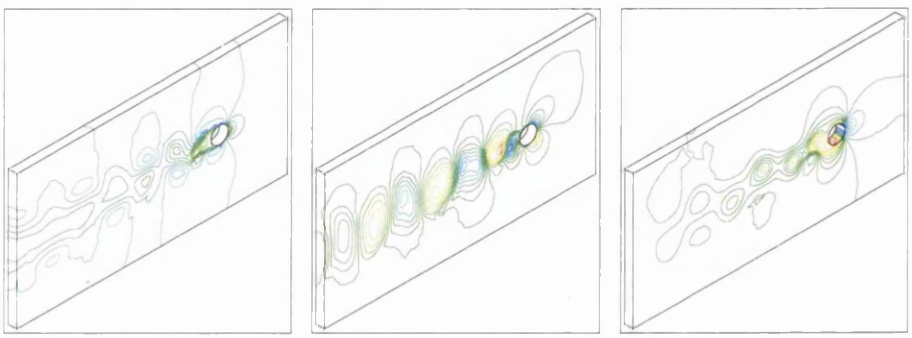

(d) $\bar{u}_1$ contours (e) $\bar{u}_3$ contours (f) Pressure contours

Figure 8.7: Turbulent incompressible flow over a circular cylinder at Re=10000 using the matrix free CBS-AC scheme with the Spalart-Allmaras model on unstructured mesh1 (up) and hybrid mesh2 (down). (a) $\bar{u}_{1_{min}}$(red) = -0.526, $\bar{u}_{1_{max}}$(blue) = 1.928; (b) $\bar{u}_{3_{min}}$(red) = -1.223, $\bar{u}_{3_{max}}$(blue) = 1.437; (c) p_{min}(red) = -1.090, p_{max}(blue) = 0.743; (d) $\bar{u}_{1_{min}}$(red) = -1.135, $\bar{u}_{1_{max}}$(blue) = 1.973; (e) $\bar{u}_{3_{min}}$(red) = -1.074, $\bar{u}_{3_{max}}$(blue) = 1.136; (f) p_{min}(red) = -0.967, p_{max}(blue) = 0.704.

data. The strouhal number here is around 0.144.

In Figure 8.6(c) the pressure coefficient values at Re=10000 are compared with two different turbulence procedures, one is available LES modelling [166] and another numerical data is from non-linear eddy viscosity modelling [167]. As seen the time-averaged pressure distribution on the hybrid mesh2 is in good agreement with LES and non-linear model, except close to stagnation. This may be attributed to turbulence modelling accuracy [144].

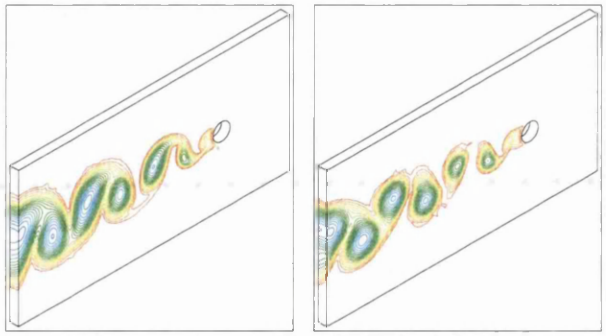

(a) $\hat{\nu}$ contours (b) $\hat{\nu}$ contours

Figure 8.8: Turbulent incompressible flow over a circular cylinder at Re=10000 using the matrix free CBS-AC scheme with the Spalart-Allmaras model on unstructured mesh1 (left) and hybrid mesh2 (right). (a) $\hat{\nu}_{min}$(red) = 0.0, $\hat{\nu}_{max}$(blue) = 368.329; (b) $\hat{\nu}_{min}$(red) = 0.0, $\hat{\nu}_{max}$(blue) = 349.945.

In Figure 8.7 and Figure 8.8 the contours of horizontal velocity component, vertical velocity component, pressure and modified turbulent eddy kinematic viscosity obtained from mesh1 and mesh2 respectively. Both results are almost identical. As seen the origin of the vortex street shifts between the areas above and below the central axis. The behaviour qualitatively confirms the periodic vortex shedding phenomenon.

8.3 Three-dimensional turbulent flow around a stationary sphere

In this section, numerical solutions of turbulent flow over a sphere placed inside a channel at a Reynolds number of 10000 are presented. The computational geometry domain is same as the laminar flow problem in Chapter 5. A uniform flow at the inlet is prescribed and no slip conditions are assumed on the sphere surface. The turbulent scalar variable of the Spalart-Allmaras model at inlet is 10^{-6}. The pressure residual was reduced to 10^{-4} within each real time step.

All sides of the channel are assumed to have slip conditions. Three structured

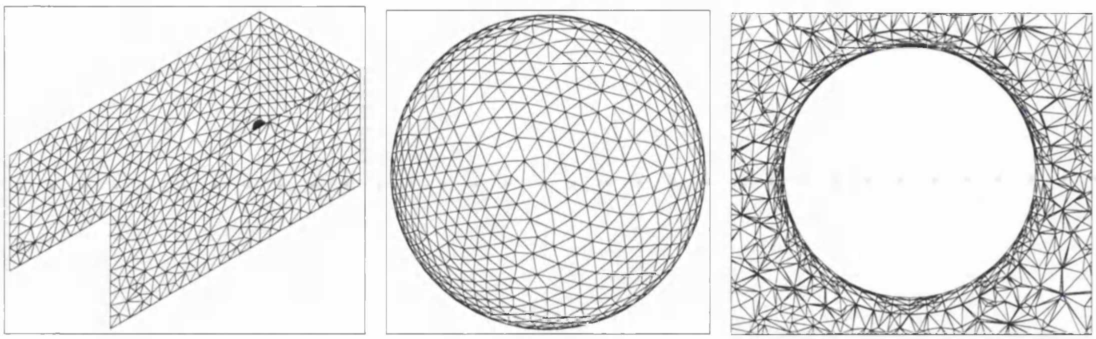

(a) (b) (c)

Figure 8.9: Turbulent incompressible flow over a stationary sphere at Re=10000 using the matrix free CBS-AC scheme with the Spalart-Allmaras model. (a) Sphere inside a rectangular channel; (b) Unstructured mesh on the surface of sphere; (c) Hybrid mesh close to sphere surface.

mesh layers at distances of 0.01, 0.021 and 0.035 close to sphere surface as shown in Figure 8.9.

Figure 8.10(a)-(b) depict drag and lift coefficient variation with respect to real time. As seen the averaged drag coefficient gives 0.31. The experimental measurements for the subcritical flow at Re=10000 [142] gives the averaged drag coefficient was around 0.4. The large difference is due to URANS modelling of the transition. The comparison of the pressure coefficient around the sphere surface is shown in Figure 8.10(c) at real time = 100.

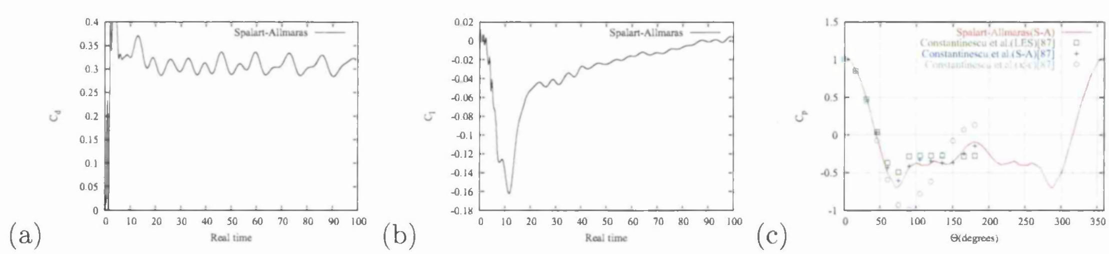

Figure 8.10: Turbulent incompressible flow over a stationary sphere at Re=10000 using the matrix free CBS-AC scheme with the Spalart-Allmaras model. (a) Time variation of Drag coefficient; (b) Time variation of Lift coefficient; (c) Pressure coefficient distribution on the sphere surface at real time = 100.

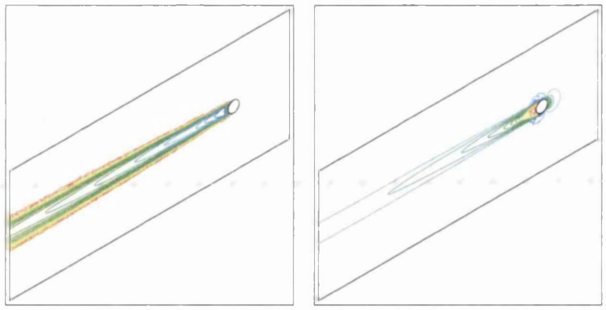

(a) (b)

Figure 8.11: Turbulent incompressible flow over a stationary sphere at Re=10000 using the matrix free CBS-AC scheme with the Spalart-Allmaras model. (a) $\hat{\nu}_{min}$(red) = 0.0, $\hat{\nu}_{max}$(blue) = 116.176; (c) $\bar{u}_{1_{min}}$(red) = -0.413, $\bar{u}_{1_{max}}$(blue) = 1.425.

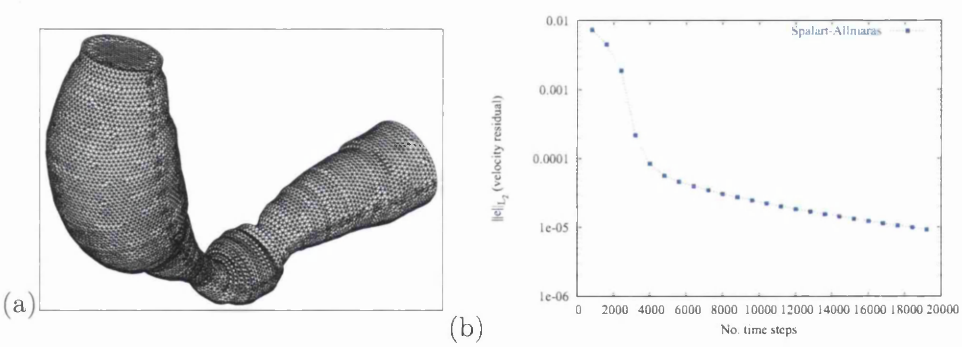

Figure 8.12: Turbulent incompressible flow over a stationary sphere at Re=10000 using the matrix free CBS-AC scheme with the Spalart-Allmaras model. (a) Unstructured finite element mesh (Elements: 185692, Nodes: 35931); (b) Convergence to steady state.

The results presented are almost identical Constantinescu et al.'s work [87].

Figure 8.11 shows modified turbulent eddy kinematic viscosity and horizontal velocity patterns at real time = 100. Each figure contains 20 contour increments.

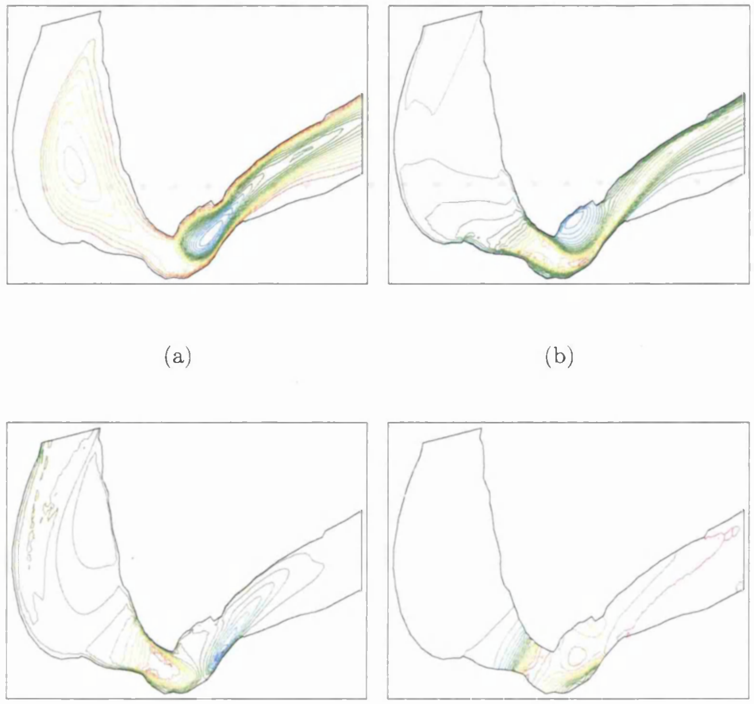

(a) (b) (c) (d)

Figure 8.13: Turbulent incompressible flow through a upper human airway at Re=1000 using the matrix free CBS-AC scheme with the Spalart-Allmaras model. (a) $\hat{\nu}_{min}$(red) = 0.0, $\hat{\nu}_{max}$(blue) = 72.113; (b) $\bar{u}_{1_{min}}$(red) = -1.775, $\bar{u}_{1_{max}}$(blue) = 0.706; (c) $\bar{u}_{3_{min}}$(red) = -1.665, $\bar{u}_{3_{max}}$(blue) = 1.439; (d) p_{min}(red) = 0.0, p_{max}(blue) = 2.302.

8.4 Three-dimensional turbulent flow through a upper human airway

One of the spray dynamics problems, steady flow inside a upper human airway, have been performed with the matrix free CBS-AC scheme and Spalart-Allmaras model. The geometry defined are same as a human throat studied by Gemci et al. [155]. Apparently, most of the literatures on the particle movement in the upper human airway related to sleep apnoea and vocal cord problems [156]-[158]. It is of interest to understand and investigate the respiratory mechanism through fluid dynamics. In the present research the unstructured

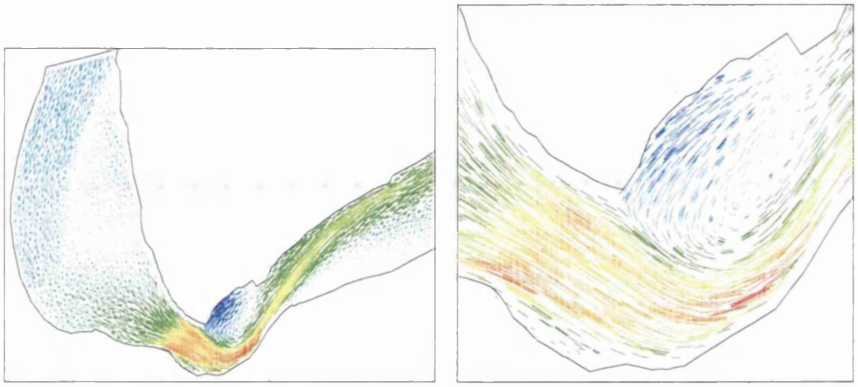

(a) (b)

Figure 8.14: Turbulent incompressible flow through a upper human airway at Re=1000 using the matrix free CBS-AC scheme with the Spalart-Allmaras model. (a) vector pattern of $\bar{u}_1$; (b) vector pattern of $\bar{u}_1$ near to the epiglottis.

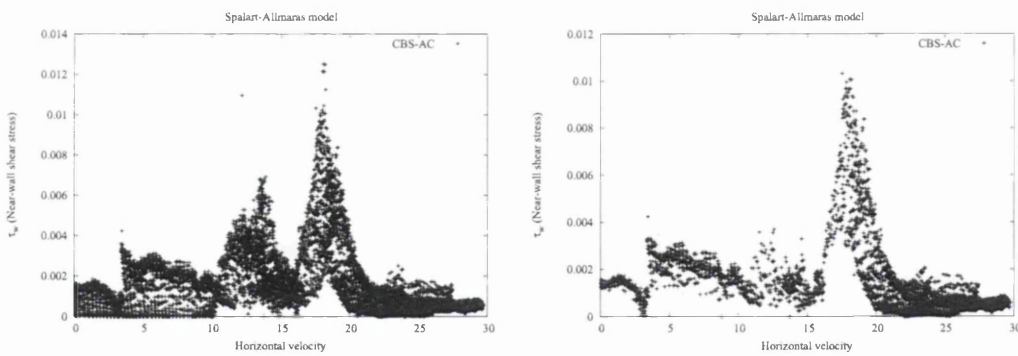

(a) (b)

Figure 8.15: Turbulent incompressible flow through a upper human airway at Re=1000. Distribution of the near-wall shear stress (a) All surfaces; (b) On the superior surfaces.

mesh was employed and shown in Figure 8.12(a). It is generated using PSUE-II code [154]. The computational domain includes 29.68 length, 23.05 height and the diameter of 4.91 at the inlet boundary. The moderate Reynolds number is 1000 based upon the diameter of the narrow profile near to the epiglottis.

Uniform velocity perpendicular to the inlet surface in the downward direction is assumed at the top boundary. No slip conditions are used on the solid walls. At the walls, the modified turbulent eddy kinematic viscosity is equal to zero. Figure 8.12(b) shows the tolerance value was reduced to 10^{-5} to reach steady state.

The contours of modified turbulent eddy kinematic viscosity, $\bar{u}_1$ velocity component, $\bar{u}_3$ velocity component and pressure along the longitudinal central section are shown in Figure 8.13. As seen the narrow portion near to the epiglottis triggers recirculation zone downstream. A very high gradient area is noticed at the narrow portion.

Figure 8.14 shows horizontal velocity vector plots. It is apparent that the recirculation zone is located close to the epiglottis.

Figure 8.15 shows the distribution of near-wall shear stresses around the surface of upper human airway. It is apparent that the maximum near-wall shear stress occurs in the distance 18.082 length of x_1 direction.

8.5 Summary

We have presented numerical solutions of turbulent incompressible flow past a backward facing step using the matrix free CBS-AC scheme and semi-implicit CBS scheme with the Spalart-Allmaras turbulence model. Both schemes give excellent accuracy. For the unsteady flow problem, the averaged drag coefficient and lift coefficient from three-dimensional turbulent incompressible flow over a circular cylinder that agrees with the result of two-dimensional flows. A model of upper human airway flow has also been demonstrated to show that CBS scheme is able to handle more complex geometry.

Chapter 9

Conclusions and future work

9.1 Conclusions

A robust matrix free procedure based on the Characteristic Based Split (CBS) algorithm as well as the artificial compressibility (AC) method has been presented in this thesis. Several numerical problems of laminar and turbulent incompressible flows at a wide range of Reynolds numbers were simulated by the CBS-AC scheme. A dual time stepping approach has been implemented in this scheme, which enabled it to deal with unsteady flows with transient features. The advantages of the proposed scheme include excellent computational efficiency and better accuracy.

An explicit characteristic based procedure with optimal Galerkin spatial approximation plays an essential role in the stability and convergence of the matrix free CBS-AC scheme. The higher order time terms of the discrete form arises due to the Characteristic Galerkin (CG) approximation which leads to a stabilized form and reduce spatial oscillations due to the discretization of the convective acceleration term. Such scheme also circumvents Ladyshenskaya-Babuška-Brezzi (LBB) restriction. The removal of the pressure gradients from the momentum or Reynolds equations allows any order of shape functions used for velocity and pressure. In other words, the temporal discretization were divided into three steps to construct non-singular matrices which guarantee a consistent system. The concept of the employed fractional step method lead to the first order splitting error in pressure.

This can be eliminated by introducing a pressure stabilizing scheme.

Consideration of the standard AC method selected in this thesis without the pre-conditioning matrix. The reason is to simplify the method which gives an accuracy as good as a pre-conditioned scheme. Thus an appropriate AC parameter selection is quite important to calculate local time steps based on the convective and diffusive velocities in conjunction with the element size. The presented results clearly show that the standard method gives results as good as pre-conditioned methods. Further, there are reasons to believe that an explicit and matrix free fractional step method combined with a standard AC method through characteristic time-stepping can give robust and accurate results. Due to these merits, CBS-AC is suitable for solving complex 3D incompressible flow problems.

In order to handle turbulent features, various Reynolds averaged Navier-Stokes (RANS) models were implemented with CBS-AC code. Four turbulence models for near-wall treatments, one equation $\kappa - l$ model of Wolfshtein, one equation Spalart-Allmaras model, two equation linear $\kappa - \varepsilon$ models of Lam-Bremhorst and Fan-Lakshminarayana-Barnett, have been chosen for evaluating moderate Reynolds numbers to compare with available experimental data. The Wolfshtein's model fails to provide the effect of turbulent recirculation and periodic shedding in the wake. On the other hand, the choice of Lam-Bremhorst's wall damping functions was good for the reasonable prediction of turbulent kinetic energy. It should be noted that the damping functions suggested by Fan-Lakshminarayana-Barnett's model might be inappropriate for complex three-dimensional turbulent flows even though the wall-bounded behaviour has been resolved and validated for two-dimensional unsteady turbulent boundary layers. Indeed, the two scalar variables, κ and ε, by which the transport equations have been established are more expensive with CPU time than a one-equation model. A modified turbulent eddy kinematic viscosity was therefore derived by Spalart and Allmaras which was used to solve both 2D and 3D problems in this thesis. It yields better agreement with experimental results and gives rapid convergence to steady state using unstructured or hybrid meshes.

The main objective of this thesis was to develop a matrix free CBS-AC scheme for laminar and turbulent incompressible flows. The major conclusions derived from this study are listed below:

- The explicit characteristic Galerkin procedure is a stabilized form of the matrix free CBS scheme based on the artificial compressibility (AC) method. This method is suitable to carry out both laminar and turbulent incompressible flows on unstructured meshes.
- The Ladyshenskaya-Babuška-Brezzi (LBB) conditions has been satisfied and violent oscillations of pressure from the discretization of governing equations have been eliminated when equal order interpolations for velocity and pressure are used.
- The matrix free CBS-AC scheme via a dual time stepping technique is efficient in saving memory and easy to implement in parallel environment.
- Various RANS models can be employed along with the CBS scheme to accurately predict turbulent incompressible flows.

9.2 Future research

In order to improve the computing costs as well as accuracy of the CBS scheme in the incompressible turbulent regimes, further research can be carried out in the following areas

- To further reduce the computational time, a single-step, explicit multistage Runge-Kutta scheme could be employed to resolve the discrete equations in time-stepping calculations.
- Extension of the proposed scheme to build appropriate preconditioning matrix to compare with the present standard AC method.
- The detached eddy simulation (DES) approach could be implemented and tested on unstructured meshes.
- A better approach for anisotropic and inhomogeneous turbulent characteristics may be employed with the monotone integrated large eddy simulation (MILES). It would be interesting to test CBS-AC scheme to deal with such high-resolution computational fluid dynamics.

- Alternative acceleration techniques such as the multigrid procedure to enhance the rate of convergence is possible.
- An edge-based data structure would be useful in reducing memory and increasing the speed of calculation.
- The better matrix free schemes such as Generalized Minimal Residual (GMRES) method could be employed to accelerate solution procedure.

Bibliography

[1] Bubnov IG. The comments of referee on the reviewing the paper by Professor Timoshenko, S.P. "On the stability of elastic systems" was awarded by the DI Zhuravskii prize. *Sbornik St Petersburg Inta Inzhenerov Putei Soobshch (Symposium of the Institute of Communication Engineers)* 1913; **81**(7):33–36, also see Mikhlin SG. *Variational methods in mathematical physics* translated from the Russian by T.Boddington; editorial introduction by translation editor L.I.G.Chambers. Pergamon, 1964.

[2] Galerkin BG. Sterzhni i plastiny. Ryady v nekotorykh voprosakh uprogogo ravnovesiya sterzhnei i plastin (Rods and plates. Series occurring in various questions concerning the elastic equilibrium of rods and plates). *Vestnik Inzhenerov (Engineers Bulletin)* 1915; **19**:897–908.

[3] Ladyshenskaya OA. *The Mathematical Theory of Viscous Incompressible Flow*, 2nd edition. Gordon and Breach, New York, 1969.

[4] Babuška I. The finite element method with Lagrangian multipliers. *Numerische Mathematik* 1973; **20**:179–192.

[5] Brezzi F. On the existence, uniqueness and approximation of saddle-point problems arising from Lagrange multipliers. *RAIRO-Analyse Numerique-Numerical Analysis* 1974; **8**(R2):129–151.

[6] Zienkiewicz OC, Taylor RL. *The Finite Element Method vol. 1 The Basis*, 5th edition. Butterworth and Heinemann, Oxford, 2000.

[7] Brooks AN, Hughes TJR. Streamline upwind/Petrov-Galerkin formulation for convection dominated flows with particular emphasis on the incompressible Navier-Stokes equation. *Computer Methods in Applied Mechanics and Engineering* 1982; **32**(1-3):199–259.

[8] Hughes TJR, Mallet M. A new finite element method for computational fluid dynamics: III. the generalized streamline operator for multidimensional advective-diffusive systems. *Computer Methods in Applied Mechanics and Engineering* 1986; **58**(3):305–328.

[9] Hughes TJR, Franca LP, Hulbert GM. A new finite element formulation for computational fluid dynamics: VIII. the Galerkin least-squares method for advective-diffusive equations. *Computer Methods in Applied Mechanics and Engineering* 1989; **73**(2):173–189.

[10] Õnate E. Derivation of stabilized equations for numerical solution of advective-diffusive transport and fluid flow problems. *Computer Methods in Applied Mechanics and Engineering* 1998; **151**(1-2):233–265.

[11] Hughes TJR. Multiscale phenomena: Green's functions, the Dirichlet-to-Neumann formulation, subgrid scale models, bubbles and the origins of stabilized methods. *Computer Methods in Applied Mechanics and Engineering* 1995; **127**(1-4):387–401.

[12] Löhner R, Morgan K, Zienkiewicz OC. The solution of non-linear hyperbolic equation systems by the finite element method. *International Journal for Numerical Methods in Fluids* 1984; **4**(11):1043–1063.

[13] Zienkiewicz OC, Codina R. A general algorithm for compressible and incompressible flow –part I. the split, characteristic-based scheme. *International Journal for Numerical Methods in Fluids* 1995; **20**(8-9):869–885.

[14] Nithiarasu P, Codina R, Zienkiewicz OC. The Characteristic Based Split (CBS) Scheme – a unified approach to fluid dynamics. *International Journal for Numerical Methods in Engineering*; (In press 2005); Special issue.

[15] Zienkiewicz OC, Nithiarasu P, Codina R, Vázquez M, Ortiz P. The characteristic-based-split procedure: an efficient and accurate algorithm for fluid problems. *International Journal for Numerical Methods in Fluids* 1999; **31**(1):359–396.

[16] Zienkiewicz OC, Taylor RL. *The Finite Element Method vol. 3 Fluid Dynamics*, 5th edition. Butterworth and Heinemann, Oxford, 2000.

[17] Donea J. A Taylor Galerkin method for convective transport problems. *International Journal for Numerical Methods in Engineering* 1984; **20**(1):101–119.

[18] Donea J, Huerta A. *Finite Element Methods for Flow Problems.* John Wiley & Sons, Chichester, 2003.

[19] Lax PD, Wendroff B. Systems of conservative laws. *Communications on Pure and Applied Mathematics* 1960; **13**:217–237.

[20] Rojek J, Õnate E, Taylor RL. CBS stabilization in dynamics of solids using explicit time integration. *Proceedings of the 4th European Congress on Computational Methods in Applied Sciences and Engineering*, ECCOMAS 2004, Jyväskylä, Finland, 24-28 July 2004.

[21] Ortiz P, Zienkiewicz OC, Szmelter J. CBS finite element modelling of shallow water and transport problems. *Proceedings of the 4th European Congress on Computational Methods in Applied Sciences and Engineering*, ECCOMAS 2004, Jyväskylä, Finland, 24-28 July 2004.

[22] Massarotti N, Nithiarasu P, Zienkiewicz OC. Natural convection in porous medium-fluid interface problems - A finite element analysis by using the CBS procedure. *International Journal of Numerical Methods for Heat & Fluid Flow* 2001; **11**(5-6):473–490.

[23] Massarotti N, Nithiarasu P, Carotenuto A. Microscopic and macroscopic approach for natural convection in enclosures filled with fluid saturated porous medium. *International Journal of Numerical Methods for Heat & Fluid Flow* 2003; **13**(7):862–886.

[24] Lewis RW, Nithiarasu P, Seetharamu KN. *Fundamentals of the finite element method for heat and fluid flow.* John Wiley & Sons, Chichester, 2004.

[25] Nithiarasu P, Massarotti N, Mathur JS. Forced convection heat transfer from solder balls on a printed circuit board using the characteristic based split (CBS) scheme. *International Journal of Numerical Methods for Heat & Fluid Flow* 2005; **15**(1):73–95.

[26] Chorin AJ. A numerical method for solving incompressible viscous flow problem. *Journal of Computational Physics* 1967; **2**(1):12–26.

[27] Nithiarasu P. An efficient artificial compressibility (AC) scheme based on the characteristic based split (CBS) method for incompressible flows. *International Journal for Numerical Methods in Engineering* 2003; **56**(13):1815–1845.

[28] Nithiarasu P, Mathur JS, Weatherill NP, Morgan K. Three dimensional incompressible flow calculations using the Characteristic Based Split (CBS) Scheme. *International Journal for Numerical Methods in Fluids* 2004; **44**(11):1207–1229.

[29] Malan AG, Lewis RW, Nithiarasu P. An improved unsteady, unstructured, artificial compressibility, finite volume scheme for viscous incompressible flows: Part I. Theory and implementation. *International Journal for Numerical Methods in Engineering* 2002; **54**(5):695–714.

[30] Martelli F, Michelassi V. Viscous flow calculations in turbomachninery channels. *Journal De Physique III* 1993; **3**(2):237–253.

[31] Zhang CX. Numerical predictions of turbulent recirculating-flows with a Kappa-Epsilon model. *Journal of Wind Engineering and Industrial Aerodynamics* 1994; **51**(2):177–201.

[32] Pentaris A, Nikolados K, Tsangaris S. Development of projection and artificial compressibility methodologies using the approximate factorization technique. *International Journal for Numerical Methods in Fluids* 1994; **19**(11):1013–1038.

[33] Sheng CH, Taylor LK, Whitefield DL. Multigrid algorithm for 3-dimensional incompressible high-Reynolds number turbulent flows. *AIAA Journal* 1995; **33**(11):2073–2079.

[34] Daclesmariani J, Zilliac CG, Chow JS, Bradshaw P. Numerical experimental-study of a wingtip vortex in the near-field. *AIAA Journal* 1995; **33**(9):1561–1568.

[35] Kuffer J, Muller B, Fannelop TK. Implicit solution method for incompressible Navier-Stokes equations including two-layer $\kappa - \tau$ turbulence model. *AIAA Journal* 1996; **34**(12):2501–2508.

[36] Michelassi V, Migliorini F, Martelli F. Preconditioned scalar approximate factorization method for incompressible fluid flows. *International Journal for Computational Fluid Dynamics* 1996; **7**(4):311–325.

[37] Lin FB, Sotiropoulos F. Strongly-coupled multigrid method for 3-D incompressible flows using near-wall turbulence closures. *Transactions of the ASME Journal of Fluids Engineering* 1997; **119**(2):314–324.

[38] Beddhu M, Jiang MY, Taylor LK, Whitfield DL. Computation of steady and unsteady flows with a free surface around the Wigley hull. *Applied Mathematics and Computation* 1998; **89**(1-3):67–84.

[39] Ekaterinaris JA. Numerical simulation of incompressible two-blade rotor flowfields. *Journal of Propulsion and Power* 1998; **14**(3):367–374.

[40] Neel RE, Walters RW, Simpson RL. Computations of steady and unsteady low-speed turbulent separated flows. *AIAA Journal* 1998; **36**(7):1208–1215.

[41] Dacles-Mariani J, Kwak D, Zilliac G. On numerical errors and turbulence modelling in tip vortex flow prediction. *International Journal for Numerical Methods in Fluids* 1999; **30**(1):65–82.

[42] Sheng CH, Whitfield DL, Anderson WK. Multiblock approach for calculating incompressible fluid flows on unstructured grids. *AIAA Journal* 1999; **37**(2):169–176.

[43] Kim W-W, Menon S. An unsteady incompressible Navier-Stokes solver for large eddy simulation of turbulent flows. *International Journal for Numerical Methods in Fluids* 1999; **31**(6):983–1017.

[44] Govatsos PA, Papantonis DE. A characteristic based method for the calculation of three-dimensional incompressible, turbulent and steady flows in hydraulic turbomachines and installations. *International Journal for Numerical Methods in Fluids* 2000; **34**(1):1–30.

[45] Li TQ, Matusiak J, Lehtimaki R. Numerical simulation of viscous flows with free surface around realistic hull forms with tansom. *International Journal for Numerical Methods in Fluids* 2001; **37**(5):601–624.

[46] Rhee SH, Hino T. Numerical simulation of unsteady turbulent flow around maneuvering prolate spheroid. *AIAA Journal* 2002; **40**(10):2017–2026.

[47] Kataoka H, Mizuno M. Numerical flow computation around aeroelastic 3D square cylinder using inflow turbulence. *Wind and Structures* 2002; **5**(2-4):379–392.

[48] Wen GB, Chen ZB. Unsteady/steady numerical simulation of three-dimensional incompressible Navier-Stokes equations on artificial compressibility. *Applied Mathematics and Mechanics-English Edition* 2004; **25**(1):59–72.

[49] Dourado WMC, Bruel P, Azevedo JLF. A time-accurate pseudo-compressibility approach based on an unstructured hybrid finite volume technique applied to unsteady turbulent premixed flame propagation. *International Journal for Numerical Methods in Fluids* 2004; **44**(10):1063–1091.

[50] Axelsson O, Barker A. *Finite Element Solution of Boundary Value Problems: Theory and Computation.* Academic Press, Orlando, Florida, 1984.

[51] Chandrupatla TR, Belegundu AD. *Introduction to finite elements in engineering*, 3rd edition. Prentice Hall, Upper Saddle River, N.J., 2002.

[52] Shewchuk JR. *An introduction to the conjugate gradient method without the agonizing pain* 1st edition. Carnegie Mellon University, Pittsburgh, 1994.

[53] Hughes TJR, Ferencz RM. Large-scale vectorized implicit calculations in solid mechanics on a cray X-MP/48 utilizing EBE preconditioned conjugate gradients. *Computer Methods in Applied Mechanics and Engineering* 1987; **61**(2):215–248.

[54] Smagorinsky J. General circulation experiments with the primitive equations. *Monthly Weather Review* 1963; **91**(3):99–152.

[55] Smagorinsky J, Manabe S, Holloway JL. Numerical results from a nine-level general circulation model of the atmosphere. *Monthly Weather Review* 1965; **93**(12):727–768.

[56] Germano M, Piomelli U, Moin P, Cabot WH. A dynamic subgrid-scale eddy viscosity model. *Physics of Fluids A. Fluid Dynamics* 1991; **3**(7):1760–1765.

[57] Germano M. Turbulence: the filtering approach. *Journal of Fluid Mechanics* 1992; **238**:325–336.

[58] Lilly DK. A proposed modification of the Germano subgrid-scale closure method. *Physics of Fluids A. Fluid Dynamics* 1992; **4**(3):633–635.

[59] Lesieur M, Métais O. New trends in large-eddy simulations of turbulence. *Annual Review of Fluid Mechanics* 1996; **28**:45–82.

[60] Boris JP, Grinstein FF, Oran ES, Kolbe RL. New insights into large eddy simulation. *Fluid Dynamics Research* 1992; **10**(4-6):199–228.

[61] Tucker PG. Novel MILES computations for jet flows and noise. *International Journal of Heat and Fluid Flow* 2004; **25**(4):625–635.

[62] Grinstein FF, Fureby C. Recent progress on MILES for high Reynolds number flows. *Transactions of the ASME Journal of Fluids Engineering* 2002; **124**(4):848–861.

[63] Fureby C, Grinstein FF. Large eddy simulation of high-Reynolds-number free and wall-bounded flows. *Journal of Computational Physics* 2002; **181**(1):68–97.

[64] Hughes TJR, Mazzei L, Jansen KE. Large eddy simulation and the variational multiscale method. *Computing and Visualization in Science* 2000; **3**(1-2):47–59.

[65] Hughes TJR, Mazzei L, Oberai AA, Wray AA. The multiscale formulation of large eddy simulation: Decay of homogeneous isotropic turbulence. *Physics of Fluids* 2001; **13**(2):505–512.

[66] Hughes TJR, Oberai AA, Mazzei L. Large eddy simulation of turbulent channel flows by the variational multiscale method. *Physics of Fluids* 2001; **13**(6):1784–1799.

[67] Boris JP, Book DL. Flux-Corrected Transport I, SHASTA, a fluid transport algorithm that works. *Journal of Computational Physics* 1973; **11**(1):38–69.

[68] Colella P, Woodward PR. The piecewise parabolic method (PPM) for gas dynamic simulations. *Journal of Computational Physics* 1984; **54**(1):174–201.

[69] Reynolds O. On the dynamical theory of incompressible viscous flows and the determination of the criterion. *Philosophical Transactions of the Royal Society of London. A* 1895; **186**:123–161.

[70] Prandtl L. Bericht über Untersuchungen zur ausgebildeten Turbulenz. *Zeitschrift für Angewandte Mathematik und Mechanik* 1925; **5**(2):136–139, also found published in *Proceedings of the 2rd International Congress for Applied Mechanics*, E. Meissner, eds. Orell Füssli Verlag, Zürich, Switzerland, 12-17 September 1926, pp. 62–75.

[71] Kolmogorov AN. The equations of turbulent motion in an incompressible fluid (in Russian). *Izvestia Akademiia Nauk SSSR, seria Geofizika* 1942; **6**(1-2):56–58.

[72] Prandtl L. Über ein neues Formelsystem für die ausgebildete Turbulenz. *Nachrichten der Gesellschaft für Wissenschaft Göttingen* 1945; *Math.-Physikalische Klasse*:6–19.

[73] Wolfshtein M. The velocity and temperature distribution in one-dimensional flow with turbulence augmentation and pressure gradient. *International Journal of Heat and Mass Transfer* 1969; **12**(3):301–318.

[74] Jones WP, Launder BE. The prediction of laminarization with a two-equation model of turbulence. *International Journal of Heat and Mass Transfer* 1972; **15**(2):301–314.

[75] Launder BE, Spalding DB. The numerical computation of turbulent flows. *Computer Methods in Applied Mechanics and Engineering* 1974; **3**(2):269–289.

[76] Wilcox DC. Reassessment of the scale-determining equation for advanced turbulence models. *AIAA Journal* 1988; **26**(11):1299–1310.

[77] Speziale CG, Abid R, Anderson EC. Critical evaluation of two-equation models for near-wall turbulence. *AIAA Journal* 1992; **30**(2):324–331.

[78] Speziale CG. On nonlinear $\kappa - l$ and $\kappa - \varepsilon$ models of turbulence. *Journal of Fluid Mechanics* 1987; **178**:459–475.

[79] Rubinstein R, Barton JM. Nonlinear Reynolds stress models and the renormalization group. *Physics of Fluids A. Fluid Dynamics* 1990; **2**(8):1472–1476.

[80] Lien FS, Chen WL, Leschziner MA. Low-Reynolds-number eddy-viscosity modelling based on nonlinear stress-strain/vorticity relations. *Proceedings of the 3rd Symposium on Engineering Turbulence Modelling and Measurements*, Crete, Greece, 27-29 May 1996. pp. 91–100.

[81] Apsley D, Chen WL, Leschziner MA, Lien FS. Non-linear eddy-viscosity modelling of separated flows. *Journal of Hydraulic Research* 1997; **35**(6):723–748.

[82] Craft TJ, Launder BE, Suga K. Prediction of turbulent transitional phenomena with a nonlinear eddy-viscosity model. *International Journal of Heat and Fluid Flow* 1997; **18**(1):15–28.

[83] Apsley DD, Leschziner MA. A new low-Reynolds-number nonlinear two-equation turbulence model for complex flows. *International Journal of Heat and Fluid Flow* 1999; **19**(3):209–222.

[84] Kimura I, Hosoda T. A non-linear $\kappa - \varepsilon$ model with realizability for prediction of flows around bluff bodies. *International Journal for Numerical Methods in Fluids* 2003; **42**(8):817–837.

[85] Spalart PR, Jou WH, Strelets M, Allmaras SR. Comments on the feasibility of LES for wings, and on a hybrid RANS/LES approach. *First AFOSR International Conference on DNS/LES*, C.Liu, Z.Liu eds., Ruston, LA, 4-8 August 1997, Advances in DNS/LES, Greyden Press, Columbus, OH.

[86] Spalart PR. Strategies for turbulence modelling and simulations. *International Journal of Heat and Fluid Flow* 2000; **21**(3):252–263.

[87] Constantinescu G, Chapelet M, Squires K. Turbulence modeling applied to flow over a sphere. *AIAA Journal* 2003; **41**(9):1733–1742.

[88] Lam CKG, Bremhorst K. A modified form of the $\kappa-\varepsilon$ model for predicting wall turbulence. *Transactions of the ASME Journal of Fluids Engineering* 1981; **103**(4):456–460.

[89] Fan S, Lakshminarayana B, Barnett M. Low-Reynolds-number $\kappa-\varepsilon$ model for unsteady turbulent boundary-layer flows. *AIAA Journal* 1993; **31**(10):1777–1784.

[90] Spalart PR, Allmaras SR. A one-equation turbulence model for aerodynamic flows. *AIAA paper 92-0439* 1992.

[91] Bernard LM. *An introduction to hydrodynamics and water waves.* Springer-Verlag, New York, 1976.

[92] Pope SB. *Turbulent Flows*, 1st edition. Cambridge University Press, Cambridge, 2000.

[93] Boussinesq VJ. Théorie de l'écoulement tourbillant. *Mémoires présents par divers savants á l'Academic des Sciences de l'Institut National de France* 1877; **23**(1):46–50.

[94] Currie IG. *Fundamental Mechanics of Fluids*, 2nd edition. McGraw-Hill, New York, 1993.

[95] Hanjalić K, Launder BE. A Reynolds stress model of turbulence and its application to thin shear flows. *Journal of Fluid Mechanics* 1972; **52**(4):609–638.

[96] Hanjalić K, Launder BE. Contribution towards a Reynolds-stress closure for low-Reynolds -number turbulence. *Journal of Fluid Mechanics* 1976; **74**(4):593–610.

[97] Hinze JO. *Turbulence* An Introduction to Its Mechanism and Theory. McGraw-Hill, New York, 1959.

[98] Gatski TB, Speziale CG. On explicit algebraic stress models for complex turbulent flows. *Journal of Fluid Mechanics* 1993; **254**:59–78.

[99] Craft TJ, Launder BE, Suga K. Development and applications of a cubic eddy-viscosity model of turbulence. *International Journal of Heat and Fluid flow* 1996; **17**(2):108–115.

[100] Daly BJ, Harlow FH. Transport equations in Turbulence. *The Physics of Fluids* 1970; **13**(11):2634–2649.

[101] Launder BE, Sharma BI. Application of the energy-dissipation model of turbulence to the calculation of flow near a spinning disc. *Letters in Heat and Mass Transfer* 1974; **1**(2):131–138.

[102] Gibson MM, Spalding DB, Zinser W. Boundary-layer calculations using Hassid-Poreh one-equation energy model. *Letters in Heat and Mass Transfer* 1978; **5**(2):73–80.

[103] Jones WP, Launder BE. The calculation of low-Reynolds-number phenomena with a two-equation model of turbulence. *International Journal of Heat and Mass Transfer* 1973; **16**(6):1119–1130.

[104] Patel VC, Rodi W, Scheuerer G. Turbulence models for near-wall and low Reynolds number flows: a review. *AIAA Journal* 1985; **23**(9):1308–1319.

[105] Myong HK, Kasagi N. Prediction of anisotropy of the near-wall turbulence with an anisotropic low-Reynolds number $\kappa - \varepsilon$ model. *Transactions of the ASME Journal of Fluids Engineering* 1990; **112**(4):521–524.

[106] Baldwin BS, Barth TJ. A one-equation turbulence transport model for high Reynolds number wall-bounded flows. *AIAA paper 91-0610* 1991.

[107] Mellor GL, Herring HJ. Two methods of calculating turbulent boundary layer behavior based on numerical solution of the equations of motion. *Proceedings of Conference on Turbulent Boundary Layer Prediction*, Stanford University, 1968.

[108] Morton KW. Generalised Galerkin methods for hyperbolic problems. *Computer Methods in Applied Mechanics and Engineering* 1985; **52**(1-3):847–871.

[109] Donea J, Quartapelle L. An introduction to finite element methods for transient advection problems. *Computer Methods in Applied Mechanics and Engineering* 1992; **95**(2):169–203.

[110] Crank J, Nicolson, P. A practical method for numerical evaluation of solutions of partial differential equations of the heat-conduction type. *Proceedings of the Cambridge Philosophical Society. Mathematical and Physical Sciences* 1947; **43**:50–67, also found re-published in : John Crank 80th birthday special issue *Advances in Computational Mathematics* 1996; **6**(3-4):207–226 .

[111] Chorin AJ. Numerical solution of Navier-Stokes equations. *Mathematics of Computation* 1968; **22**(101-104):745–762.

[112] Chorin AJ. On the convergence of discrete approximation to the Navier-Stokes equations. *Mathematics of Computation* 1969; **23**(105-108):341–353.

[113] Choi YH, Merkle CL. The application of preconditioning in viscous flows. *Journal of Computational Physics* 1993; **105**(2):207–223.

[114] Nithiarasu P, Zienkiewicz OC. Analysis of an explicit and matrix free fractional step method for incompressible flows. *International Journal for Numerical Methods in Engineering*; (In press 2005).

[115] Nithiarasu P. On boundary conditions of the characteristic based split (CBS) algorithm for fluid dynamics. *International Journal for Numerical Methods in Engineering* 2002; **54**(4):523–536.

[116] Hughes TJR. *The Finite Element Method. Linear Static and Dynamic Finite Element Analysis.* Prentice-Hall, New Jersey, 1987.

[117] Zienkiewicz OC, Qu S, Taylor RL, Nakazawa S. The patch test for mixed formulations. *International Journal for Numerical Methods in Engineering* 1986; **23**(10):1873–1883.

[118] Zienkiewicz OC, Wu J. Incompressibility without tears–how to avoid restrictions of mixed formulation. *International Journal for Numerical Methods in Engineering* 1991; **32**(6):1189–1203.

[119] Ghia U, Ghia KN, Shin CT. High-Re solutions for incompressible flow using the Navier-Stokes equations and a multigrid method. *Journal of Computational Physics* 1982; **48**(3):387–411.

[120] Codina R, Coppola-Owem H, Nithiarasu P, Liu CB. Numerical comparison of CBS and SGS as stabilisation techniques for the incompressible Navier-Stokes equations. *International Journal for Numerical Methods in Engineering* 2005; Special issue.

[121] Denham MK, Patrick MA. Laminar flow over a downstream-facing step in a two-dimensional flow channel. *Transactions of the Institution of Chemical Engineers* 1974; **52**:361–367.

[122] Codina R. Stabilized finite element approximation of transient incompressible flows using orthogonal subscales. *Computer Methods in Applied Mechanics and Engineering* 2002; **191**(39-40):4295–4321.

[123] Rimon Y, Cheng SI. Numerical solution of a uniform flow over a sphere at intermediate Reynolds numbers. *The Physics of Fluids* 1969; **12**(5):949–959.

[124] Gülcat Ü, Aslan AR. Accurate 3D viscous incompressible flow calculations with the FEM. *International Journal for Numerical Methods in Fluids* 1997; **25**(9):985–1001.

[125] Burggraf OR. Analytical and numerical studies of the structure of steady separated flows. *Journal of Fluid Mechanics* 1966; **24**(1):113–151.

[126] Benjamin AS, Denny VE. On the convergence of numerical solutions for 2-D flows in a cavity at large Re. *Journal of Computational Physics* 1979; **33**(3):340–358.

[127] Koseff JR, Street RL. The lid-driven cavity: a synthesis of qualitative and quantitative observations. *Transactions of the ASME Journal of Fluids Engineering* 1984; **106**(4):390–398.

[128] Gustafson K, Halasi K. Vortex dynamics of cavity flows. *Journal of Computational Physics* 1986; **64**(2):279–319.

[129] Goodrich JW, Gustafson K, Halasi K. Hopf bifurcation in the driven cavity. *Journal of Computational Physics* 1990; **90**(1):219–261.

[130] Kuhlmann HC, Wanschura M, Rath HJ. Flow in two-sided lid-driven cavities: non-uniqueness, instabilities, and cellular structures. *Journal of Fluid Mechanics* 1997; **336**:267–299.

[131] Albensoeder S, Kuhlmann HC, Rath HJ. Multiplicity of steady two-dimensional flows in two-sided lid-driven cavities. *Theoretical and Computational Fluid Dynamics* 2001; **14**(4):223–241.

[132] Pierrehumbert RT. Universal short-wave instability of two-dimensional eddies in an inviscid fluid. *Physical Review Letters* 1986; **57**(17):2157–2159.

[133] Bayly BJ. Three-dimensional instability of elliptical flow. *Physical Review Letters* 1986; **57**(17):2160–2163.

[134] Kuhlmann HC, Wanschura M, Rath HJ. Elliptic instability in two-sided lid-driven cavity flow. *European Journal of Mechanics B/Fluids* 1998; **17**(4):561–569.

[135] Zhou YC, Patnaik BSV, Wan DC, Wei GW. DSC solution for flow in a staggered double lid driven cavity. *International Journal for Numerical Methods in Engineering* 2003; **57**(2):211–234.

[136] Masarotti N, Arpino F, Nithiarasu P. Fully explicit and semi-implicit CBS procedures for incompressible flows. *Proceedings of the 4th European Congress on Computational Methods in Applied Sciences and Engineering*, ECCOMAS 2004, Jyväskylä, Finland, 24-28 July 2004.

[137] Codina R, Coppola-Owem H, Nithiarasu P, Liu CB. Numerical comparison of CBS and SGS as stabilisation techniques for the incompressible Navier-Stokes equations. *Proceedings of the 4th European Congress on Computational Methods in Applied Sciences and Engineering*, ECCOMAS 2004, Jyväskylä, Finland, 24-28 July 2004.

[138] Johansson SH, Davidson L, Olsson E. Numerical simulation of vortex shedding past triangular cylinders at high Reynolds number using a $\kappa-\varepsilon$ model. *International Journal for Numerical Methods in Fluids* 1993; **16**(10):859–878.

[139] Yang Z, Shih TH. New time scale based $\kappa - \varepsilon$ model for near-wall turbulence. *AIAA Journal* 1993; **31**(7):1191–1198.

[140] Laufer J. Investigation of turbulent flow in a two-dimensional channel. *NACA Report* 1951; **1053**:1247–1266.

[141] Denham MK, Briard P, Patrick MA. A directionally-sensitive laser anemometer for velocity measurements in highly turbulent flows. *Journal of Physics E: Scientific Instruments* 1975; **8**(8):681–683.

[142] Schlichting H. *Boundary-Layer Theory.* New York: McGraw-Hill, 1979.

[143] Selvam RP. Finite element modelling of flow around a circular cylinder using LES. *Journal of Wind Engineering and Industrial Aerodynamics* 1997; **67-68**:129–139.

[144] Tutar M, HoldøAE. Computational modelling of flow around a circular cylinder in sub-critical flow regime with various turbulence models. *International Journal for Numerical Methods in Fluid* 2001; **35**(7):763–784.

[145] Kalro V, Tezduyar T. Parallel 3D computation of unsteady flows around circular cylinder *Parallel Computing* 1997; **23**(9):1235–1248.

[146] Dirichlet GL. Über die Reduction der positivien Quadratischen formen mit drei Undestimmten ganzen Zahlen. *Journal für die reine und angewandte Mathematik* 1850; **40**:209-227.

[147] Voronoi G. Nouvelles applications des paramétres continus à la théorie des formes quadratiques. premier Mémoire: Sur quelques propriétés des formes quadratiques positives parfaites. *Journal für die reine und angewandte Mathematik* 1907; **133**:97-178.

[148] Voronoi G. Nouvelles applications des paramétres continus à la théorie des formes quadratiques. premier Mémoire: Recherches sur les parallélloédres primitifs. *Journal für die reine und angewandte Mathematik* 1908; **134**:198-287.

[149] Delaunay B. Sur la sphére vide. *Izvestia Akademii Nauk SSSR, Otdelenie Matematicheskikh i Estestvennykh Nauk* 1934; **7**(6):793-800.

[150] Weatherill NP. The generation of unstructured grids using Dirichlet tessellations. *Princeton University, MAE Report* 1985; **1715**.

[151] Weatherill NP. Delaunay triangulation in computational fluid dynamics. *Computers & Mathematics with Applications* 1992; **24**(5-6):129–150.

[152] Weatherill NP, Hassan O. Efficient three-dimensional delaunay triangulation with automatic point creation and imposed boundary constraints. *International Journal for Numerical Methods in Engineering* 1994; **37**(12):2005–2039.

[153] Peraire J, Vahdati M, Morgan K, Zienkiewicz OC. Adaptive remeshing for compressible flow computations. *Journal of Computational Physics* 1987; **72**(2):449–466.

[154] Weatherill NP, Hassan O, Morgan K, Jones JW, Larwood B. Towards fully parallel aerospace simulations on unstructured meshes. *Engineering Computations* 2001; **18**(3-4):347–375.

[155] Gemci T, Corcoran TE, Yakut K, Shortall B, Chigier N. Spray dynamics and deposition of inhaled medications in the throat. *ILASS-Europe 2001*, Zuirch 2-6, September 2001.

[156] Li WI, Edwards DA. Aerosol particle transport and deaggregation phenomena in the mouth and throat. *Advanced Drug Delivery Reviews* 1997; **26**(1):41–49.

[157] Li WI, Perzl M, Heyder J, Langer R, Brain JD, Englmeier KH, Niven RW, Edwards DA. Aerodynamics and aerosol particle deaggregation phenomena in model oral-pharyngeal cavities. *Journal of Aerosol Science* 1996; **27**(8):1269–1286.

[158] Martonen TB, Zhang Z, Yue G, Musante CJ. 3-D particle transport within the human upper respiratory tract. *Journal of Aerosol Science* 2002; **33**(8):1095–1110.

[159] Pacheco PS. *Parallel programming with MPI.* Morgan Kaufmann, San Francisco, 1997.

[160] Grama A, Gupta A, Karypis G, Kumar V. *Introduction to Parallel Computing*, 2nd edition. Addison-Wesley, Harlow, 2003.

[161] Reddy JN. *An Introduction to the Finite Element Method*, 2nd edition. McGraw-Hill, New York, 1993.

[162] Speziale CG, Sarkar S, Gatski TB. Modelling the pressure-strain correlation of turbulence: an invariant dynamical systems approach. *Journal of Fluid Mechanics* 1991; **227**:245–272.

[163] Pope SB. A more general effective viscosity hypothesis. *Journal of Fluid Mechanics* 1975; **72**:331–340.

[164] Nithiarasu P, Zienkiewicz OC. On stabilization of the CBS algorithm: Internal and external time steps. *International Journal for Numerical Methods in Engineering* 2000; **48**(6):875–880.

[165] Abanto J, Pelletier D, Garon A, Trépanier JY. Verification of some commerical CFD codes on atypical CFD problems. *AIAA paper 2005-0682* 2005.

[166] Lu X, Dalton C, Zhang J. Application of large eddy simulation to an oscillating flow past a circular cylinder. *Transactions of the ASME Journal of Fluids Engineering* 1997; **119**(3):519–525.

[167] Lu X, Dalton C, Zhang J. Application of large eddy simulation to an oscillating flow past a circular cylinder. *Journal of Fluids and Structures* 2003; **17**(8):1213–1236.

Appendix A

Two-dimensional matrix coefficients of the CBS algorithm with RANS turbulence models

The two-dimensional matrix coefficients of a linear triangular element based on the Galerkin spatial approximation indicate nodal values and all the discretized matrices and vectors. The standard finite element shape functions $\mathbf{N}_\varphi$ depended on any variable φ, i.e.

$$\varphi\mathbf{N} = \begin{bmatrix} \varphi^1 N_\varphi^1 & N\varphi^2 & \ldots & N\varphi^k & \ldots & N\varphi^l \end{bmatrix} \tag{A.1}$$

where k is the node identifying number and $l = 3$ for a 3-nodes triangular element.

The 6×6 symmetric, lumped mass matrix for the intermediate momentum is given as

$$\mathbf{M_u} = \int_\Omega \left[M_u^{i,j}\right] d\Omega = \int_\Omega \mathbf{N_u}^T \mathbf{N_u} d\Omega \tag{A.2}$$

where the matrix coefficients $\left[M_u^{i,j}\right]$ are (i row; j column)

$$M_u^{1,2} = M_u^{2,1} = M_u^{1,4} = M_u^{4,1} = M_u^{1,6} = M_u^{6,1} = M_u^{2,3} = M_u^{3,2} = M_u^{2,5} =$$
$$= M_u^{5,2} = M_u^{3,4} = M_u^{4,3} = M_u^{3,6} = M_u^{6,3} = M_u^{4,5} = M_u^{5,4} = M_u^{5,6} =$$

$$= M_u^{6,5} = 0$$

$$M_u^{1,1} = M_u^{2,2} = N_u^1 N_u^1$$

$$M_u^{3,3} = M_u^{4,4} = N_u^2 N_u^2$$

$$M_u^{5,5} = M_u^{6,6} = N_u^3 N_u^3$$

$$M_u^{1,3} = M_u^{3,1} = M_u^{2,4} = M_u^{4,2} = N_u^1 N_u^2$$

$$M_u^{1,5} = M_u^{5,1} = M_u^{2,6} = M_u^{6,2} = N_u^1 N_u^3$$

$$M_u^{3,5} = M_u^{5,3} = M_u^{4,6} = M_u^{6,4} = N_u^2 N_u^3 \tag{A.3}$$

The 6×6 convection matrix of the velocities for the intermediate momentum is given as

$$\mathbf{C_u} = \int_\Omega \left[C_u^{i,j}\right] d\Omega = \int_\Omega \mathbf{N_u}^T (\nabla^T(\mathbf{uN_u})) d\Omega \tag{A.4}$$

where the divergence operator of discretized velocities is

$$\nabla^T(\mathbf{uN_u}) = \left\{ \begin{array}{cc} \frac{\partial}{\partial x_1} & \frac{\partial}{\partial x_2} \\ \frac{\partial}{\partial x_2} & \frac{\partial}{\partial x_1} \end{array} \right\} \begin{bmatrix} u_1 & u_2 \\ u_2 & u_1 \end{bmatrix} \begin{bmatrix} N_u^1 & 0 & N_u^2 & 0 & N_u^3 & 0 \\ 0 & N_u^1 & 0 & N_u^2 & 0 & N_u^3 \end{bmatrix} \tag{A.5}$$

and the matrix coefficients $\left[C_u^{i,j}\right]$ are

$$C_u^{1,2} = C_u^{2,1} = C_u^{1,4} = C_u^{4,1} = C_u^{1,6} = C_u^{6,1} = C_u^{2,3} = C_u^{3,2} = C_u^{2,5} = C_u^{5,2} =$$

$$= C_u^{3,4} = C_u^{4,3} = C_u^{3,6} = C_u^{6,3} = C_u^{4,5} = C_u^{5,4} = C_u^{5,6} = C_u^{6,5} = 0$$

$$C_u^{1,1} = C_u^{2,2} = N_u^1 \left(\frac{\partial u_1 N_u^1}{\partial x_1} + \frac{\partial u_2 N_u^1}{\partial x_2} \right)$$

$$C_u^{3,3} = C_u^{4,4} = N_u^2 \left(\frac{\partial u_1 N_u^2}{\partial x_1} + \frac{\partial u_2 N_u^2}{\partial x_2} \right)$$

$$C_u^{5,5} = C_u^{6,6} = N_u^3 \left(\frac{\partial u_1 N_u^3}{\partial x_1} + \frac{\partial u_2 N_u^3}{\partial x_2} \right)$$

$$C_u^{3,1} = C_u^{4,2} = N_u^2 \left(\frac{\partial u_1 N_u^1}{\partial x_1} + \frac{\partial u_2 N_u^1}{\partial x_2} \right)$$

$$C_u^{5,1} = C_u^{6,2} = N_u^3\left(\frac{\partial u_1 N_u^1}{\partial x_1} + \frac{\partial u_2 N_u^1}{\partial x_2}\right)$$
$$C_u^{1,3} = C_u^{2,4} = N_u^1\left(\frac{\partial u_1 N_u^2}{\partial x_1} + \frac{\partial u_2 N_u^2}{\partial x_2}\right)$$
$$C_u^{5,3} = C_u^{6,4} = N_u^3\left(\frac{\partial u_1 N_u^2}{\partial x_1} + \frac{\partial u_2 N_u^2}{\partial x_2}\right)$$
$$C_u^{1,5} = C_u^{2,6} = N_u^1\left(\frac{\partial u_1 N_u^3}{\partial x_1} + \frac{\partial u_2 N_u^3}{\partial x_2}\right)$$
$$C_u^{3,5} = C_u^{4,6} = N_u^2\left(\frac{\partial u_1 N_u^3}{\partial x_1} + \frac{\partial u_2 N_u^3}{\partial x_2}\right) \tag{A.6}$$

The 6×6 symmetric diffusion matrix for the intermediate momentum is given as

$$\mathbf{K}_\tau = \frac{(\mu + \mu_t)}{Re}\int_\Omega \left[K_\tau^{i,j}\right] d\Omega = \int_\Omega \mathbf{B^T}\frac{(\mu+\mu_t)}{Re}\left(\mathbf{I_o} - \frac{2}{3}\mathbf{mm^T}\right)\mathbf{B}d\Omega \tag{A.7}$$

where the matrix coefficients $\left[K_\tau^{i,j}\right]$ are

$$K_\tau^{1,1} = \frac{4}{3}\left(\frac{\partial N_u^1}{\partial x_1}\right)^2 + \left(\frac{\partial N_u^1}{\partial x_2}\right)^2; \quad K_\tau^{2,2} = \frac{4}{3}\left(\frac{\partial N_u^1}{\partial x_2}\right)^2 + \left(\frac{\partial N_u^1}{\partial x_1}\right)^2$$
$$K_\tau^{3,3} = \frac{4}{3}\left(\frac{\partial N_u^2}{\partial x_1}\right)^2 + \left(\frac{\partial N_u^2}{\partial x_2}\right)^2; \quad K_\tau^{4,4} = \frac{4}{3}\left(\frac{\partial N_u^2}{\partial x_2}\right)^2 + \left(\frac{\partial N_u^2}{\partial x_1}\right)^2$$
$$K_\tau^{5,5} = \frac{4}{3}\left(\frac{\partial N_u^3}{\partial x_1}\right)^2 + \left(\frac{\partial N_u^3}{\partial x_2}\right)^2; \quad K_\tau^{6,6} = \frac{4}{3}\left(\frac{\partial N_u^3}{\partial x_2}\right)^2 + \left(\frac{\partial N_u^3}{\partial x_1}\right)^2$$
$$K_\tau^{1,2} = K_\tau^{2,1} = -\frac{2}{3}\frac{\partial N_u^1}{\partial x_1}\frac{\partial N_u^1}{\partial x_2} + \frac{\partial N_u^1}{\partial x_2}\frac{\partial N_u^1}{\partial x_1}$$
$$K_\tau^{1,3} = K_\tau^{3,1} = \frac{4}{3}\frac{\partial N_u^1}{\partial x_1}\frac{\partial N_u^2}{\partial x_1} + \frac{\partial N_u^1}{\partial x_2}\frac{\partial N_u^2}{\partial x_2}$$
$$K_\tau^{1,4} = K_\tau^{4,1} = -\frac{2}{3}\frac{\partial N_u^1}{\partial x_1}\frac{\partial N_u^2}{\partial x_2} + \frac{\partial N_u^1}{\partial x_2}\frac{\partial N_u^2}{\partial x_1}$$
$$K_\tau^{1,5} = K_\tau^{5,1} = \frac{4}{3}\frac{\partial N_u^1}{\partial x_1}\frac{\partial N_u^3}{\partial x_1} + \frac{\partial N_u^1}{\partial x_2}\frac{\partial N_u^3}{\partial x_2}$$
$$K_\tau^{1,6} = K_\tau^{6,1} = -\frac{2}{3}\frac{\partial N_u^1}{\partial x_1}\frac{\partial N_u^3}{\partial x_2} + \frac{\partial N_u^1}{\partial x_2}\frac{\partial N_u^3}{\partial x_1}$$
$$K_\tau^{2,3} = K_\tau^{3,2} = -\frac{2}{3}\frac{\partial N_u^1}{\partial x_2}\frac{\partial N_u^2}{\partial x_1} + \frac{\partial N_u^1}{\partial x_1}\frac{\partial N_u^2}{\partial x_2}$$
$$K_\tau^{2,4} = K_\tau^{4,2} = \frac{4}{3}\frac{\partial N_u^1}{\partial x_2}\frac{\partial N_u^2}{\partial x_2} + \frac{\partial N_u^1}{\partial x_1}\frac{\partial N_u^2}{\partial x_1}$$

$$K_\tau^{2,5} = K_\tau^{5,2} = -\frac{2}{3}\frac{\partial N_u^1}{\partial x_2}\frac{\partial N_u^3}{\partial x_1} + \frac{\partial N_u^1}{\partial x_1}\frac{\partial N_u^3}{\partial x_2}$$
$$K_\tau^{2,6} = K_\tau^{6,2} = \frac{4}{3}\frac{\partial N_u^1}{\partial x_2}\frac{\partial N_u^3}{\partial x_2} + \frac{\partial N_u^1}{\partial x_1}\frac{\partial N_u^3}{\partial x_1}$$
$$K_\tau^{3,4} = K_\tau^{4,3} = -\frac{2}{3}\frac{\partial N_u^2}{\partial x_1}\frac{\partial N_u^2}{\partial x_2} + \frac{\partial N_u^2}{\partial x_2}\frac{\partial N_u^2}{\partial x_1}$$
$$K_\tau^{3,5} = K_\tau^{5,3} = \frac{4}{3}\frac{\partial N_u^2}{\partial x_1}\frac{\partial N_u^3}{\partial x_1} + \frac{\partial N_u^2}{\partial x_2}\frac{\partial N_u^3}{\partial x_2}$$
$$K_\tau^{3,6} = K_\tau^{6,3} = -\frac{2}{3}\frac{\partial N_u^2}{\partial x_1}\frac{\partial N_u^3}{\partial x_2} + \frac{\partial N_u^2}{\partial x_2}\frac{\partial N_u^3}{\partial x_1}$$
$$K_\tau^{4,5} = K_\tau^{5,4} = -\frac{2}{3}\frac{\partial N_u^2}{\partial x_2}\frac{\partial N_u^3}{\partial x_1} + \frac{\partial N_u^2}{\partial x_1}\frac{\partial N_u^3}{\partial x_2}$$
$$K_\tau^{4,6} = K_\tau^{6,4} = \frac{4}{3}\frac{\partial N_u^2}{\partial x_2}\frac{\partial N_u^3}{\partial x_2} + \frac{\partial N_u^2}{\partial x_1}\frac{\partial N_u^3}{\partial x_1}$$
$$K_\tau^{5,6} = K_\tau^{6,5} = -\frac{2}{3}\frac{\partial N_u^3}{\partial x_1}\frac{\partial N_u^3}{\partial x_2} + \frac{\partial N_u^3}{\partial x_2}\frac{\partial N_u^3}{\partial x_1} \tag{A.8}$$

The 6×6 matrix of the isotropic turbulence for the intermediate momentum is given as

$$\mathbf{C_{u\kappa}} = \frac{2}{3}\int_\Omega \left[C_{u\kappa}^{i,j}\right] d\Omega = \frac{2}{3}\int_\Omega \mathbf{N_u}^T \nabla \mathbf{N}_\kappa d\Omega \tag{A.9}$$

where the matrix coefficients $\left[C_{u\kappa}^{i,j}\right]$ are

$$C_{u\kappa}^{1,2} = C_{u\kappa}^{2,1} = C_{u\kappa}^{1,4} = C_{u\kappa}^{4,1} = C_{u\kappa}^{1,6} = C_{u\kappa}^{6,1} = C_{u\kappa}^{2,3} = C_{u\kappa}^{3,2} = C_{u\kappa}^{2,5} = C_{u\kappa}^{5,2} =$$
$$= C_{u\kappa}^{3,4} = C_{u\kappa}^{4,3} = C_{u\kappa}^{3,6} = C_{u\kappa}^{6,3} = C_{u\kappa}^{4,5} = C_{u\kappa}^{5,4} = C_{u\kappa}^{5,6} = C_{u\kappa}^{6,5} = 0$$
$$C_{u\kappa}^{1,1} = N_u^1\frac{\partial N_\kappa^1}{\partial x_1}; \quad C_{u\kappa}^{1,3} = N_u^1\frac{\partial N_\kappa^2}{\partial x_1}; \quad C_{u\kappa}^{1,5} = N_u^1\frac{\partial N_\kappa^3}{\partial x_1}; \quad C_{u\kappa}^{2,2} = N_u^1\frac{\partial N_\kappa^1}{\partial x_2};$$
$$C_{u\kappa}^{2,4} = N_u^1\frac{\partial N_\kappa^2}{\partial x_2}; \quad C_{u\kappa}^{2,6} = N_u^1\frac{\partial N_\kappa^3}{\partial x_2}; \quad C_{u\kappa}^{3,1} = N_u^2\frac{\partial N_\kappa^1}{\partial x_1}; \quad C_{u\kappa}^{3,3} = N_u^2\frac{\partial N_\kappa^2}{\partial x_1};$$
$$C_{u\kappa}^{3,5} = N_u^2\frac{\partial N_\kappa^3}{\partial x_1}; \quad C_{u\kappa}^{4,2} = N_u^2\frac{\partial N_\kappa^1}{\partial x_2}; \quad C_{u\kappa}^{4,4} = N_u^2\frac{\partial N_\kappa^2}{\partial x_2}; \quad C_{u\kappa}^{4,6} = N_u^2\frac{\partial N_\kappa^3}{\partial x_2};$$
$$C_{u\kappa}^{5,1} = N_u^3\frac{\partial N_\kappa^1}{\partial x_1}; \quad C_{u\kappa}^{5,3} = N_u^3\frac{\partial N_\kappa^2}{\partial x_1}; \quad C_{u\kappa}^{5,5} = N_u^3\frac{\partial N_\kappa^3}{\partial x_1}; \quad C_{u\kappa}^{6,2} = N_u^3\frac{\partial N_\kappa^1}{\partial x_2};$$
$$C_{u\kappa}^{6,4} = N_u^3\frac{\partial N_\kappa^2}{\partial x_2}; \quad C_{u\kappa}^{6,6} = N_u^3\frac{\partial N_\kappa^3}{\partial x_2} \tag{A.10}$$

The 6×1 traction vector for the intermediate momentum is given as

$$\mathbf{f_u} = \frac{(\mu+\mu_t)}{Re}\int_\Gamma \left[f_u^{i,j}\right] d\Gamma = \int_\Gamma \mathbf{N_u}^T \mathbf{t_d} d\Gamma \tag{A.11}$$

In the above equation of the vector coefficients $\left[f_u^{i,j}\right]$ are

$$\begin{aligned}
f_u^{1,1} &= N_u^1\left[\frac{4}{3}\left(u_1^1\frac{\partial N_u^1}{\partial x_1}+u_1^2\frac{\partial N_u^2}{\partial x_1}+u_1^3\frac{\partial N_u^3}{\partial x_1}\right)-\frac{2}{3}\left(u_2^1\frac{\partial N_u^1}{\partial x_2}+u_2^2\frac{\partial N_u^2}{\partial x_2}+u_2^3\frac{\partial N_u^3}{\partial x_2}\right)\right]\hat{n}_{x_1}+\\
&+ N_u^1\left[\left(u_2^1\frac{\partial N_u^1}{\partial x_1}+u_2^2\frac{\partial N_u^2}{\partial x_1}+u_2^3\frac{\partial N_u^3}{\partial x_1}+u_1^1\frac{\partial N_u^1}{\partial x_2}+u_1^2\frac{\partial N_u^2}{\partial x_2}+u_1^3\frac{\partial N_u^3}{\partial x_2}\right)\right]\hat{n}_{x_2}\\
f_u^{2,1} &= N_u^1\left[\frac{4}{3}\left(u_2^1\frac{\partial N_u^1}{\partial x_2}+u_2^2\frac{\partial N_u^2}{\partial x_2}+u_2^3\frac{\partial N_u^3}{\partial x_2}\right)-\frac{2}{3}\left(u_1^1\frac{\partial N_u^1}{\partial x_1}+u_1^2\frac{\partial N_u^2}{\partial x_1}+u_1^3\frac{\partial N_u^3}{\partial x_1}\right)\right]\hat{n}_{x_2}+\\
&+ N_u^1\left[\left(u_1^1\frac{\partial N_u^1}{\partial x_2}+u_1^2\frac{\partial N_u^2}{\partial x_2}+u_1^3\frac{\partial N_u^3}{\partial x_2}+u_2^1\frac{\partial N_u^1}{\partial x_1}+u_2^2\frac{\partial N_u^2}{\partial x_1}+u_2^3\frac{\partial N_u^3}{\partial x_1}\right)\right]\hat{n}_{x_1}\\
f_u^{3,1} &= N_u^2\left[\frac{4}{3}\left(u_1^1\frac{\partial N_u^1}{\partial x_1}+u_1^2\frac{\partial N_u^2}{\partial x_1}+u_1^3\frac{\partial N_u^3}{\partial x_1}\right)-\frac{2}{3}\left(u_2^1\frac{\partial N_u^1}{\partial x_2}+u_2^2\frac{\partial N_u^2}{\partial x_2}+u_2^3\frac{\partial N_u^3}{\partial x_2}\right)\right]\hat{n}_{x_1}+\\
&+ N_u^2\left[\left(u_2^1\frac{\partial N_u^1}{\partial x_1}+u_2^2\frac{\partial N_u^2}{\partial x_1}+u_2^3\frac{\partial N_u^3}{\partial x_1}+u_1^1\frac{\partial N_u^1}{\partial x_2}+u_1^2\frac{\partial N_u^2}{\partial x_2}+u_1^3\frac{\partial N_u^3}{\partial x_2}\right)\right]\hat{n}_{x_2}\\
f_u^{4,1} &= N_u^2\left[\frac{4}{3}\left(u_2^1\frac{\partial N_u^1}{\partial x_2}+u_2^2\frac{\partial N_u^2}{\partial x_2}+u_2^3\frac{\partial N_u^3}{\partial x_2}\right)-\frac{2}{3}\left(u_1^1\frac{\partial N_u^1}{\partial x_1}+u_1^2\frac{\partial N_u^2}{\partial x_1}+u_1^3\frac{\partial N_u^3}{\partial x_1}\right)\right]\hat{n}_{x_2}+\\
&+ N_u^2\left[\left(u_1^1\frac{\partial N_u^1}{\partial x_2}+u_1^2\frac{\partial N_u^2}{\partial x_2}+u_1^3\frac{\partial N_u^3}{\partial x_2}+u_2^1\frac{\partial N_u^1}{\partial x_1}+u_2^2\frac{\partial N_u^2}{\partial x_1}+u_2^3\frac{\partial N_u^3}{\partial x_1}\right)\right]\hat{n}_{x_1}\\
f_u^{5,1} &= N_u^3\left[\frac{4}{3}\left(u_1^1\frac{\partial N_u^1}{\partial x_1}+u_1^2\frac{\partial N_u^2}{\partial x_1}+u_1^3\frac{\partial N_u^3}{\partial x_1}\right)-\frac{2}{3}\left(u_2^1\frac{\partial N_u^1}{\partial x_2}+u_2^2\frac{\partial N_u^2}{\partial x_2}+u_2^3\frac{\partial N_u^3}{\partial x_2}\right)\right]\hat{n}_{x_1}+\\
&+ N_u^3\left[\left(u_2^1\frac{\partial N_u^1}{\partial x_1}+u_2^2\frac{\partial N_u^2}{\partial x_1}+u_2^3\frac{\partial N_u^3}{\partial x_1}+u_1^1\frac{\partial N_u^1}{\partial x_2}+u_1^2\frac{\partial N_u^2}{\partial x_2}+u_1^3\frac{\partial N_u^3}{\partial x_2}\right)\right]\hat{n}_{x_2}\\
f_u^{6,1} &= N_u^3\left[\frac{4}{3}\left(u_2^1\frac{\partial N_u^1}{\partial x_2}+u_2^2\frac{\partial N_u^2}{\partial x_2}+u_2^3\frac{\partial N_u^3}{\partial x_2}\right)-\frac{2}{3}\left(u_1^1\frac{\partial N_u^1}{\partial x_1}+u_1^2\frac{\partial N_u^2}{\partial x_1}+u_1^3\frac{\partial N_u^3}{\partial x_1}\right)\right]\hat{n}_{x_2}+\\
&+ N_u^3\left[\left(u_1^1\frac{\partial N_u^1}{\partial x_2}+u_1^2\frac{\partial N_u^2}{\partial x_2}+u_1^3\frac{\partial N_u^3}{\partial x_2}+u_2^1\frac{\partial N_u^1}{\partial x_1}+u_2^2\frac{\partial N_u^2}{\partial x_1}+u_2^3\frac{\partial N_u^3}{\partial x_1}\right)\right]\hat{n}_{x_1}
\end{aligned}\tag{A.12}$$

where both $\hat{n}_{x_1}$ and $\hat{n}_{x_2}$ are normal vectors.

The 6×6 symmetric convection matrix of the stabilization for the intermediate momentum is given as

$$\mathbf{K_u} = -\frac{1}{2}\int_\Omega \left[K_u^{i,j}\right] d\Omega = -\frac{1}{2}\int_\Omega (\nabla^T(\mathbf{uN_u}))^T(\nabla^T(\mathbf{uN_u}))d\Omega \tag{A.13}$$

where the matrix coefficients $\left[K_u^{i,j}\right]$ are

$$K_u^{1,2} = K_u^{2,1} = K_u^{1,4} = K_u^{4,1} = K_u^{1,6} = K_u^{6,1} = K_u^{2,3} = K_u^{3,2} = K_u^{2,5} = K_u^{5,2} =$$
$$= K_u^{3,4} = K_u^{4,3} = K_u^{3,6} = K_u^{6,3} = K_u^{4,5} = K_u^{5,4} = K_u^{5,6} = K_u^{6,5} = 0$$
$$K_u^{1,1} = K_u^{2,2} = \left(\frac{\partial u_1 N_u^1}{\partial x_1} + \frac{\partial u_2 N_u^1}{\partial x_2}\right)^2$$
$$K_u^{3,3} = K_u^{4,4} = \left(\frac{\partial u_1 N_u^2}{\partial x_1} + \frac{\partial u_2 N_u^2}{\partial x_2}\right)^2$$
$$K_u^{5,5} = K_u^{6,6} = \left(\frac{\partial u_1 N_u^3}{\partial x_1} + \frac{\partial u_2 N_u^3}{\partial x_2}\right)^2$$
$$K_u^{1,3} = K_u^{3,1} = K_u^{2,4} = K_u^{4,2} = \left(\frac{\partial u_1 N_u^1}{\partial x_1} + \frac{\partial u_2 N_u^1}{\partial x_2}\right)\left(\frac{\partial u_1 N_u^2}{\partial x_1} + \frac{\partial u_2 N_u^2}{\partial x_2}\right)$$
$$K_u^{1,5} = K_u^{5,1} = K_u^{2,6} = K_u^{6,2} = \left(\frac{\partial u_1 N_u^1}{\partial x_1} + \frac{\partial u_2 N_u^1}{\partial x_2}\right)\left(\frac{\partial u_1 N_u^3}{\partial x_1} + \frac{\partial u_2 N_u^3}{\partial x_2}\right)$$
$$K_u^{3,5} = K_u^{5,3} = K_u^{4,6} = K_u^{6,4} = \left(\frac{\partial u_1 N_u^2}{\partial x_1} + \frac{\partial u_2 N_u^2}{\partial x_2}\right)\left(\frac{\partial u_1 N_u^3}{\partial x_1} + \frac{\partial u_2 N_u^3}{\partial x_2}\right) \tag{A.14}$$

The 3×3 symmetric, lumped mass matrix for the pressure is given as

$$\mathbf{M_p} = \left(\frac{1}{\beta^2}\right)^n \int_\Omega \left[M_p^{i,j}\right] d\Omega = \int_\Omega \mathbf{N_p^T} \left(\frac{1}{\beta^2}\right)^n \mathbf{N_p} d\Omega \tag{A.15}$$

where the matrix coefficients $\left[M_p^{i,j}\right]$ are

$$M_p^{1,1} = N_p^1 N_p^1; \quad M_p^{2,2} = N_p^2 N_p^2; \quad M_p^{3,3} = N_p^3 N_p^3$$
$$M_p^{1,2} = M_p^{2,1} = N_p^1 N_p^2; \quad M_p^{1,3} = M_p^{3,1} = N_p^1 N_p^3$$
$$M_p^{2,3} = M_p^{3,2} = N_p^2 N_p^3 \tag{A.16}$$

The 3×3 symmetric, second lumped mass matrix for the pressure is given as

$$\mathbf{H} = \int_\Omega \left[H^{i,j}\right] d\Omega = \int_\Omega (\nabla \mathbf{N_p})^T \nabla \mathbf{N_p} d\Omega \tag{A.17}$$

where the matrix coefficients $\left[H^{i,j}\right]$ are

$$H^{1,1} = \left(\frac{\partial N_p^1}{\partial x_1}\right)^2 + \left(\frac{\partial N_p^1}{\partial x_2}\right)^2$$

$$H^{2,2} = \left(\frac{\partial N_p^2}{\partial x_1}\right)^2 + \left(\frac{\partial N_p^2}{\partial x_2}\right)^2$$

$$H^{3,3} = \left(\frac{\partial N_p^3}{\partial x_1}\right)^2 + \left(\frac{\partial N_p^3}{\partial x_2}\right)^2$$

$$H^{1,2} = H^{2,1} = \left(\frac{\partial N_p^1}{\partial x_1}\right)\left(\frac{\partial N_p^2}{\partial x_1}\right) + \left(\frac{\partial N_p^1}{\partial x_2}\right)\left(\frac{\partial N_p^2}{\partial x_2}\right)$$

$$H^{1,3} = H^{3,1} = \left(\frac{\partial N_p^1}{\partial x_1}\right)\left(\frac{\partial N_p^3}{\partial x_1}\right) + \left(\frac{\partial N_p^1}{\partial x_2}\right)\left(\frac{\partial N_p^3}{\partial x_2}\right)$$

$$H^{2,3} = H^{3,2} = \left(\frac{\partial N_p^2}{\partial x_1}\right)\left(\frac{\partial N_p^3}{\partial x_1}\right) + \left(\frac{\partial N_p^2}{\partial x_2}\right)\left(\frac{\partial N_p^3}{\partial x_2}\right) \tag{A.18}$$

The 3×6 gradient (operator) matrix is given as

$$\mathbf{G} = \int_\Omega \left[G^{i,j}\right] d\Omega = \int_\Omega (\nabla \mathbf{N_p})^T \mathbf{N_u} d\Omega \tag{A.19}$$

where the matrix coefficients $\left[G^{i,j}\right]$ are

$$G^{1,1} = N_u^1 \left(\frac{\partial N_p^1}{\partial x_1}\right); \quad G^{1,2} = N_u^1 \left(\frac{\partial N_p^1}{\partial x_2}\right); \quad G^{1,3} = N_u^2 \left(\frac{\partial N_p^1}{\partial x_1}\right)$$

$$G^{1,4} = N_u^2 \left(\frac{\partial N_p^1}{\partial x_2}\right); \quad G^{1,5} = N_u^3 \left(\frac{\partial N_p^1}{\partial x_1}\right); \quad G^{1,6} = N_u^3 \left(\frac{\partial N_p^1}{\partial x_2}\right)$$

$$G^{2,1} = N_u^1 \left(\frac{\partial N_p^2}{\partial x_1}\right); \quad G^{2,2} = N_u^1 \left(\frac{\partial N_p^2}{\partial x_2}\right); \quad G^{2,3} = N_u^2 \left(\frac{\partial N_p^2}{\partial x_1}\right)$$

$$G^{2,4} = N_u^2 \left(\frac{\partial N_p^2}{\partial x_2}\right); \quad G^{2,5} = N_u^3 \left(\frac{\partial N_p^2}{\partial x_1}\right); \quad G^{2,6} = N_u^3 \left(\frac{\partial N_p^2}{\partial x_2}\right)$$

$$G^{3,1} = N_u^1 \left(\frac{\partial N_p^3}{\partial x_1}\right); \quad G^{3,2} = N_u^1 \left(\frac{\partial N_p^3}{\partial x_2}\right); \quad G^{3,3} = N_u^2 \left(\frac{\partial N_p^3}{\partial x_1}\right)$$

$$G^{3,4} = N_u^2 \left(\frac{\partial N_p^3}{\partial x_2}\right); \quad G^{3,5} = N_u^3 \left(\frac{\partial N_p^3}{\partial x_1}\right); \quad G^{3,6} = N_u^3 \left(\frac{\partial N_p^3}{\partial x_2}\right) \tag{A.20}$$

The 3×1 forcing vector for the pressure is given as

$$\mathbf{f_p} = \Delta t \int_\Gamma \left[f_p^{i,j}\right] d\Gamma = \Delta t \int_\Gamma \mathbf{N_p^T} \left[\mathbf{N_u}\tilde{\mathbf{U}}^{\mathbf{n}} + \theta_1 \left(\Delta\tilde{\mathbf{U}}^* - \Delta t \nabla p^{n+\theta_2}\right)\right] \mathbf{n^T} d\Gamma \tag{A.21}$$

where the vector coefficients $\left[f_p^{i,j}\right]$ are

$$
\begin{aligned}
f_p^{1,1} &= N_p^1 \left[\left(N_u^1\tilde{U}_1^1 + N_u^2\tilde{U}_1^2 + N_u^3\tilde{U}_1^3\right)\hat{n}_{x_1} + \left(N_u^1\tilde{U}_2^1 + N_u^2\tilde{U}_2^2 + N_u^3\tilde{U}_2^3\right)\hat{n}_{x_2}\right] \\
f_p^{2,1} &= N_p^2 \left[\left(N_u^1\tilde{U}_1^1 + N_u^2\tilde{U}_1^2 + N_u^3\tilde{U}_1^3\right)\hat{n}_{x_1} + \left(N_u^1\tilde{U}_2^1 + N_u^2\tilde{U}_2^2 + N_u^3\tilde{U}_2^3\right)\hat{n}_{x_2}\right] \\
f_p^{3,1} &= N_p^3 \left[\left(N_u^1\tilde{U}_1^1 + N_u^2\tilde{U}_1^2 + N_u^3\tilde{U}_1^3\right)\hat{n}_{x_1} + \left(N_u^1\tilde{U}_2^1 + N_u^2\tilde{U}_2^2 + N_u^3\tilde{U}_2^3\right)\hat{n}_{x_2}\right]
\end{aligned} \tag{A.22}
$$

The 3×3 symmetric, lumped mass matrix for the turbulent kinetic energy is given as

$$
\mathbf{M}_\kappa = \int_\Omega \left[M_\kappa^{i,j}\right] d\Omega = \int_\Omega \mathbf{N}_\kappa{}^T \mathbf{N}_\kappa d\Omega \tag{A.23}
$$

where the matrix coefficients $\left[M_\kappa^{i,j}\right]$ are

$$
\begin{aligned}
&M_\kappa^{1,1} = N_\kappa^1 N_\kappa^1; \quad M_\kappa^{2,2} = N_\kappa^2 N_\kappa^2; \quad M_\kappa^{3,3} = N_\kappa^3 N_\kappa^3 \\
&M_\kappa^{1,2} = M_\kappa^{2,1} = N_\kappa^1 N_\kappa^2; \quad M_\kappa^{1,3} = M_\kappa^{3,1} = N_\kappa^1 N_\kappa^3 \\
&M_\kappa^{2,3} = M_\kappa^{3,2} = N_\kappa^2 N_\kappa^3
\end{aligned} \tag{A.24}
$$

The 3×3 convection matrix for the turbulent kinetic energy is given as

$$
\mathbf{C}_\kappa = \int_\Omega \left[C_\kappa^{i,j}\right] d\Omega = \int_\Omega \mathbf{N}_\kappa{}^T (\nabla^T (\mathbf{u}\mathbf{N}_\kappa)) d\Omega \tag{A.25}
$$

where the matrix coefficients $\left[C_\kappa^{i,j}\right]$ are

$$
\begin{aligned}
&C_\kappa^{1,1} = N_\kappa^1 \left(\frac{\partial u_1 N_\kappa^1}{\partial x_1} + \frac{\partial u_2 N_\kappa^1}{\partial x_2}\right); \quad C_\kappa^{2,2} = N_\kappa^2 \left(\frac{\partial u_1 N_\kappa^2}{\partial x_1} + \frac{\partial u_2 N_\kappa^2}{\partial x_2}\right) \\
&C_\kappa^{3,3} = N_\kappa^3 \left(\frac{\partial u_1 N_\kappa^3}{\partial x_1} + \frac{\partial u_2 N_\kappa^3}{\partial x_2}\right); \quad C_\kappa^{1,2} = N_\kappa^1 \left(\frac{\partial u_1 N_\kappa^2}{\partial x_1} + \frac{\partial u_2 N_\kappa^2}{\partial x_2}\right) \\
&C_\kappa^{2,1} = N_\kappa^2 \left(\frac{\partial u_1 N_\kappa^1}{\partial x_1} + \frac{\partial u_2 N_\kappa^1}{\partial x_2}\right); \quad C_\kappa^{1,3} = N_\kappa^1 \left(\frac{\partial u_1 N_\kappa^3}{\partial x_1} + \frac{\partial u_2 N_\kappa^3}{\partial x_2}\right) \\
&C_\kappa^{3,1} = N_\kappa^3 \left(\frac{\partial u_1 N_\kappa^1}{\partial x_1} + \frac{\partial u_2 N_\kappa^1}{\partial x_2}\right); \quad C_\kappa^{2,3} = N_\kappa^2 \left(\frac{\partial u_1 N_\kappa^3}{\partial x_1} + \frac{\partial u_2 N_\kappa^3}{\partial x_2}\right) \\
&C_\kappa^{3,2} = N_\kappa^3 \left(\frac{\partial u_1 N_\kappa^2}{\partial x_1} + \frac{\partial u_2 N_\kappa^2}{\partial x_2}\right)
\end{aligned} \tag{A.26}
$$

The 3×3 symmetric diffusion matrix for the turbulent kinetic energy is given as

$$\mathbf{K}_\kappa = \frac{1}{Re}\left(\mu + \frac{\mu_t}{\sigma_\kappa}\right)\int_\Omega \left[K_\kappa^{i,j}\right] d\Omega = \int_\Omega (\nabla \mathbf{N}_\kappa)^T \left(\frac{\mu_t + \sigma_\kappa \mu}{\sigma_\kappa Re}\right) \nabla \mathbf{N}_\kappa d\Omega \tag{A.27}$$

where the matrix coefficients $\left[K_\kappa^{i,j}\right]$ are

$$\begin{aligned}
K_\kappa^{1,1} &= \left(\frac{\partial N_\kappa^1}{\partial x_1}\right)^2 + \left(\frac{\partial N_\kappa^1}{\partial x_2}\right)^2; \quad K_\kappa^{2,2} = \left(\frac{\partial N_\kappa^2}{\partial x_1}\right)^2 + \left(\frac{\partial N_\kappa^2}{\partial x_2}\right)^2 \\
K_\kappa^{3,3} &= \left(\frac{\partial N_\kappa^3}{\partial x_1}\right)^2 + \left(\frac{\partial N_\kappa^3}{\partial x_2}\right)^2; \quad K_\kappa^{1,2} = K_\kappa^{2,1} = \frac{\partial N_\kappa^1}{\partial x_1}\frac{\partial N_\kappa^2}{\partial x_1} + \frac{\partial N_\kappa^1}{\partial x_2}\frac{\partial N_\kappa^2}{\partial x_2} \\
K_\kappa^{1,3} = K_\kappa^{3,1} &= \frac{\partial N_\kappa^1}{\partial x_1}\frac{\partial N_\kappa^3}{\partial x_1} + \frac{\partial N_\kappa^1}{\partial x_2}\frac{\partial N_\kappa^3}{\partial x_2}; \quad K_\kappa^{2,3} = K_\kappa^{3,2} = \frac{\partial N_\kappa^2}{\partial x_1}\frac{\partial N_\kappa^3}{\partial x_1} + \frac{\partial N_\kappa^2}{\partial x_2}\frac{\partial N_\kappa^3}{\partial x_2}
\end{aligned} \tag{A.28}$$

The 3×1 vector based on both the generation and source terms of the turbulent kinetic energy equation is given as

$$\mathbf{f}_{\kappa\Omega} = \int_\Omega \left[f_{\kappa\Omega}^{i,j}\right] d\Omega = \int_\Omega {\mathbf{N}_\kappa}^T \Upsilon_\kappa^{II} d\Omega = \int_\Omega {\mathbf{N}_\kappa}^T \left[\tau_{ij}^R \partial_j u_i - \mathbf{N}_\epsilon \tilde{\mathbf{E}}\right] d\Omega \tag{A.29}$$

where $\Upsilon_\kappa^{II} = r_{1\kappa} + r_{2\kappa} + r_{3\kappa} + r_{4\kappa} + r_{5\kappa} + r_{6\kappa}$ may be respectively expressed

$$\begin{aligned}
r_{1\kappa} &= \frac{4\mu_t}{3Re}\left(u_1^1\frac{\partial N_u^1}{\partial x_1} + u_1^2\frac{\partial N_u^2}{\partial x_1} + u_1^3\frac{\partial N_u^3}{\partial x_1}\right)^2 - \\
&- \frac{2\mu_t}{3Re}\left(u_2^1\frac{\partial N_u^1}{\partial x_2} + u_2^2\frac{\partial N_u^2}{\partial x_2} + u_2^3\frac{\partial N_u^3}{\partial x_2}\right)\left(u_1^1\frac{\partial N_u^1}{\partial x_1} + u_1^2\frac{\partial N_u^2}{\partial x_1} + u_1^3\frac{\partial N_u^3}{\partial x_1}\right) \\
r_{2\kappa} &= \frac{4\mu_t}{3Re}\left(u_2^1\frac{\partial N_u^1}{\partial x_2} + u_2^2\frac{\partial N_u^2}{\partial x_2} + u_2^3\frac{\partial N_u^3}{\partial x_2}\right)^2 - \\
&- \frac{2\mu_t}{3Re}\left(u_1^1\frac{\partial N_u^1}{\partial x_1} + u_1^2\frac{\partial N_u^2}{\partial x_1} + u_1^3\frac{\partial N_u^3}{\partial x_1}\right)\left(u_2^1\frac{\partial N_u^1}{\partial x_2} + u_2^2\frac{\partial N_u^2}{\partial x_2} + u_2^3\frac{\partial N_u^3}{\partial x_2}\right) \\
r_{3\kappa} &= \frac{\mu_t}{Re}\left(u_1^1\frac{\partial N_u^1}{\partial x_2} + u_1^2\frac{\partial N_u^2}{\partial x_2} + u_1^3\frac{\partial N_u^3}{\partial x_2}\right)^2 + \\
&+ \frac{\mu_t}{Re}\left(u_2^1\frac{\partial N_u^1}{\partial x_1} + u_2^2\frac{\partial N_u^2}{\partial x_1} + u_2^3\frac{\partial N_u^3}{\partial x_1}\right)\left(u_1^1\frac{\partial N_u^1}{\partial x_2} + u_1^2\frac{\partial N_u^2}{\partial x_2} + u_1^3\frac{\partial N_u^3}{\partial x_2}\right)
\end{aligned}$$

$$
\begin{aligned}
r_{4\kappa} &= \frac{\mu_t}{Re}\left(u_2^1\frac{\partial N_u^1}{\partial x_1}+u_2^2\frac{\partial N_u^2}{\partial x_1}+u_2^3\frac{\partial N_u^3}{\partial x_1}\right)^2+ \\
&+ \frac{\mu_t}{Re}\left(u_1^1\frac{\partial N_u^1}{\partial x_2}+u_1^2\frac{\partial N_u^2}{\partial x_2}+u_1^3\frac{\partial N_u^3}{\partial x_2}\right)\left(u_2^1\frac{\partial N_u^1}{\partial x_1}+u_2^2\frac{\partial N_u^2}{\partial x_1}+u_2^3\frac{\partial N_u^3}{\partial x_1}\right) \\
r_{5\kappa} &= -\frac{2}{3}\left(K^1N_\kappa^1+K^2N_\kappa^2+K^3N_\kappa^3\right) \\
&\left(u_1^1\frac{\partial N_u^1}{\partial x_1}+u_1^2\frac{\partial N_u^2}{\partial x_1}+u_1^3\frac{\partial N_u^3}{\partial x_1}+u_2^1\frac{\partial N_u^1}{\partial x_2}+u_2^2\frac{\partial N_u^2}{\partial x_2}+u_2^3\frac{\partial N_u^3}{\partial x_2}\right) \\
r_{6\kappa} &= -\left(E^1N_\varepsilon^1+E^2N_\varepsilon^2+E^3N_\varepsilon^3\right)
\end{aligned} \tag{A.30}
$$

Thus the vector coefficients $\left[f_{\kappa\Omega}^{i,j}\right]$ are

$$
f_{\kappa\Omega}^{1,1}=N_\kappa^1\Upsilon_\kappa^{II};\quad f_{\kappa\Omega}^{2,1}=N_\kappa^2\Upsilon_\kappa^{II};\quad f_{\kappa\Omega}^{3,1}=N_\kappa^3\Upsilon_\kappa^{II} \tag{A.31}
$$

The 3×1 forcing vector for the turbulent kinetic energy is given as

$$
\mathbf{f}_{\kappa\Gamma}=\frac{1}{Re}\left(\mu+\frac{\mu_t}{\sigma_\kappa}\right)\int_\Gamma\left[f_{\kappa\Gamma}^{i,j}\right]d\Gamma=\int_\Gamma \mathbf{N}_\kappa{}^T t_\kappa d\Gamma \tag{A.32}
$$

where the vector coefficients $\left[f_{\kappa\Gamma}^{i,j}\right]$ are

$$
\begin{aligned}
f_{\kappa\Gamma}^{1,1} &= N_\kappa^1\left[\left(\kappa^1\frac{\partial N_\kappa^1}{\partial x_1}+\kappa^2\frac{\partial N_\kappa^2}{\partial x_1}+\kappa^3\frac{\partial N_\kappa^3}{\partial x_1}\right)\hat{n}_{x_1}+\left(\kappa^1\frac{\partial N_\kappa^1}{\partial x_2}+\kappa^2\frac{\partial N_\kappa^2}{\partial x_2}+\kappa^3\frac{\partial N_\kappa^3}{\partial x_2}\right)\hat{n}_{x_2}\right] \\
f_{\kappa\Gamma}^{2,1} &= N_\kappa^2\left[\left(\kappa^1\frac{\partial N_\kappa^1}{\partial x_1}+\kappa^2\frac{\partial N_\kappa^2}{\partial x_1}+\kappa^3\frac{\partial N_\kappa^3}{\partial x_1}\right)\hat{n}_{x_1}+\left(\kappa^1\frac{\partial N_\kappa^1}{\partial x_2}+\kappa^2\frac{\partial N_\kappa^2}{\partial x_2}+\kappa^3\frac{\partial N_\kappa^3}{\partial x_2}\right)\hat{n}_{x_2}\right] \\
f_{\kappa\Gamma}^{3,1} &= N_\kappa^3\left[\left(\kappa^1\frac{\partial N_\kappa^1}{\partial x_1}+\kappa^2\frac{\partial N_\kappa^2}{\partial x_1}+\kappa^3\frac{\partial N_\kappa^3}{\partial x_1}\right)\hat{n}_{x_1}+\left(\kappa^1\frac{\partial N_\kappa^1}{\partial x_2}+\kappa^2\frac{\partial N_\kappa^2}{\partial x_2}+\kappa^3\frac{\partial N_\kappa^3}{\partial x_2}\right)\hat{n}_{x_2}\right]
\end{aligned} \tag{A.33}
$$

The 3×3 symmetric convection matrix of the stabilization for the turbulent kinetic energy is given as

$$
\mathbf{K}_{\mathbf{u}\kappa}=-\frac{1}{2}\int_\Omega\left[K_{u\kappa}^{i,j}\right]d\Omega=-\frac{1}{2}\int_\Omega(\nabla^T(\mathbf{u}\mathbf{N}_\kappa))^T(\nabla^T(\mathbf{u}\mathbf{N}_\kappa))d\Omega \tag{A.34}
$$

where the matrix coefficients $\left[K_{u\kappa}^{i,j}\right]$ are

$$K_{u\kappa}^{1,1} = \left(\frac{\partial u_1 N_\kappa^1}{\partial x_1} + \frac{\partial u_2 N_\kappa^1}{\partial x_2}\right)^2; \quad K_{u\kappa}^{2,2} = \left(\frac{\partial u_1 N_\kappa^2}{\partial x_1} + \frac{\partial u_2 N_\kappa^2}{\partial x_2}\right)^2$$

$$K_{u\kappa}^{3,3} = \left(\frac{\partial u_1 N_\kappa^3}{\partial x_1} + \frac{\partial u_2 N_\kappa^3}{\partial x_2}\right)^2$$

$$K_{u\kappa}^{1,2} = K_{u\kappa}^{2,1} = \left(\frac{\partial u_1 N_\kappa^1}{\partial x_1} + \frac{\partial u_2 N_\kappa^1}{\partial x_2}\right)\left(\frac{\partial u_1 N_\kappa^2}{\partial x_1} + \frac{\partial u_2 N_\kappa^2}{\partial x_2}\right)$$

$$K_{u\kappa}^{1,3} = K_{u\kappa}^{3,1} = \left(\frac{\partial u_1 N_\kappa^1}{\partial x_1} + \frac{\partial u_2 N_\kappa^1}{\partial x_2}\right)\left(\frac{\partial u_1 N_\kappa^3}{\partial x_1} + \frac{\partial u_2 N_\kappa^3}{\partial x_2}\right)$$

$$K_{u\kappa}^{2,3} = K_{u\kappa}^{3,2} = \left(\frac{\partial u_1 N_\kappa^2}{\partial x_1} + \frac{\partial u_2 N_\kappa^2}{\partial x_2}\right)\left(\frac{\partial u_1 N_\kappa^3}{\partial x_1} + \frac{\partial u_2 N_\kappa^3}{\partial x_2}\right) \tag{A.35}$$

The 3×3 symmetric, lumped mass matrix for the dissipation rate is given as

$$\mathbf{M}_\varepsilon = \int_\Omega \left[M_\varepsilon^{i,j}\right] d\Omega = \int_\Omega \mathbf{N}_\varepsilon{}^T \mathbf{N}_\varepsilon d\Omega \tag{A.36}$$

where the matrix coefficients $\left[M_\varepsilon^{i,j}\right]$ are

$$M_\varepsilon^{1,1} = N_\varepsilon^1 N_\varepsilon^1; \quad M_\varepsilon^{2,2} = N_\varepsilon^2 N_\varepsilon^2; \quad M_\varepsilon^{3,3} = N_\varepsilon^3 N_\varepsilon^3$$

$$M_\varepsilon^{1,2} = M_\varepsilon^{2,1} = N_\varepsilon^1 N_\varepsilon^2; \quad M_\varepsilon^{1,3} = M_\varepsilon^{3,1} = N_\varepsilon^1 N_\varepsilon^3$$

$$M_\varepsilon^{2,3} = M_\varepsilon^{3,2} = N_\varepsilon^2 N_\varepsilon^3 \tag{A.37}$$

The 3×3 convection matrix for the dissipation rate is given as

$$\mathbf{C}_\varepsilon = \int_\Omega \left[C_\varepsilon^{i,j}\right] d\Omega = \int_\Omega \mathbf{N}_\varepsilon{}^T (\nabla^T (\mathbf{u}\mathbf{N}_\varepsilon)) d\Omega \tag{A.38}$$

where the matrix coefficients $\left[C_\varepsilon^{i,j}\right]$ are

$$C_\varepsilon^{1,1} = N_\varepsilon^1 \left(\frac{\partial u_1 N_\varepsilon^1}{\partial x_1} + \frac{\partial u_2 N_\varepsilon^1}{\partial x_2}\right); \quad C_\varepsilon^{2,2} = N_\varepsilon^2 \left(\frac{\partial u_1 N_\varepsilon^2}{\partial x_1} + \frac{\partial u_2 N_\varepsilon^2}{\partial x_2}\right)$$

$$C_\varepsilon^{3,3} = N_\varepsilon^3 \left(\frac{\partial u_1 N_\varepsilon^3}{\partial x_1} + \frac{\partial u_2 N_\varepsilon^3}{\partial x_2}\right); \quad C_\varepsilon^{1,2} = N_\varepsilon^1 \left(\frac{\partial u_1 N_\varepsilon^2}{\partial x_1} + \frac{\partial u_2 N_\varepsilon^2}{\partial x_2}\right)$$

$$C_\varepsilon^{2,1} = N_\varepsilon^2 \left(\frac{\partial u_1 N_\varepsilon^1}{\partial x_1} + \frac{\partial u_2 N_\varepsilon^1}{\partial x_2}\right); \quad C_\varepsilon^{1,3} = N_\varepsilon^1 \left(\frac{\partial u_1 N_\varepsilon^3}{\partial x_1} + \frac{\partial u_2 N_\varepsilon^3}{\partial x_2}\right)$$

$$C_\varepsilon^{3,1} = N_\varepsilon^3\left(\frac{\partial u_1 N_\varepsilon^1}{\partial x_1} + \frac{\partial u_2 N_\varepsilon^1}{\partial x_2}\right); \quad C_\varepsilon^{2,3} = N_\varepsilon^2\left(\frac{\partial u_1 N_\varepsilon^3}{\partial x_1} + \frac{\partial u_2 N_\varepsilon^3}{\partial x_2}\right)$$
$$C_\varepsilon^{3,2} = N_\varepsilon^3\left(\frac{\partial u_1 N_\varepsilon^2}{\partial x_1} + \frac{\partial u_2 N_\varepsilon^2}{\partial x_2}\right) \tag{A.39}$$

The 3×3 symmetric diffusion matrix for the dissipation rate is given as

$$\mathbf{K}_\varepsilon = \frac{1}{Re}\left(\mu + \frac{\mu_t}{\sigma_\varepsilon}\right)\int_\Omega \left[K_\varepsilon^{i,j}\right] d\Omega = \int_\Omega (\nabla \mathbf{N}_\varepsilon)^T\left(\frac{\mu_t + \sigma_\varepsilon \mu}{\sigma_\varepsilon Re}\right)\nabla \mathbf{N}_\varepsilon d\Omega \tag{A.40}$$

where the matrix coefficients $\left[K_\varepsilon^{i,j}\right]$ are

$$K_\varepsilon^{1,1} = \left(\frac{\partial N_\varepsilon^1}{\partial x_1}\right)^2 + \left(\frac{\partial N_\varepsilon^1}{\partial x_2}\right)^2; \quad K_\varepsilon^{2,2} = \left(\frac{\partial N_\varepsilon^2}{\partial x_1}\right)^2 + \left(\frac{\partial N_\varepsilon^2}{\partial x_2}\right)^2$$
$$K_\varepsilon^{3,3} = \left(\frac{\partial N_\varepsilon^3}{\partial x_1}\right)^2 + \left(\frac{\partial N_\varepsilon^3}{\partial x_2}\right)^2; \quad K_\varepsilon^{1,2} = K_\varepsilon^{2,1} = \frac{\partial N_\varepsilon^1}{\partial x_1}\frac{\partial N_\varepsilon^2}{\partial x_1} + \frac{\partial N_\varepsilon^1}{\partial x_2}\frac{\partial N_\varepsilon^2}{\partial x_2}$$
$$K_\varepsilon^{1,3} = K_\varepsilon^{3,1} = \frac{\partial N_\varepsilon^1}{\partial x_1}\frac{\partial N_\varepsilon^3}{\partial x_1} + \frac{\partial N_\varepsilon^1}{\partial x_2}\frac{\partial N_\varepsilon^3}{\partial x_2}; \quad K_\varepsilon^{2,3} = K_\varepsilon^{3,2} = \frac{\partial N_\varepsilon^2}{\partial x_1}\frac{\partial N_\varepsilon^3}{\partial x_1} + \frac{\partial N_\varepsilon^2}{\partial x_2}\frac{\partial N_\varepsilon^3}{\partial x_2} \tag{A.41}$$

The 3×1 vector based on both the generation and source terms of the dissipation rate equation is given as

$$\mathbf{f}_{\varepsilon\Omega} = \frac{E}{K}\int_\Omega \left[f_{\varepsilon\Omega}^{i,j}\right] d\Omega = \int_\Omega \mathbf{N}_\varepsilon{}^T \frac{E}{K}\Upsilon_\varepsilon^{II} d\Omega = \int_\Omega \mathbf{N}_\varepsilon{}^T \frac{E}{K}\left[c_{\varepsilon 1}\tau_{ij}^R \partial_j u_i - c_{\varepsilon 2}\mathbf{N}_\varepsilon \tilde{\mathbf{E}}\right] d\Omega \tag{A.42}$$

where $\Upsilon_\varepsilon^{II} = r_{1\varepsilon} + r_{2\varepsilon} + r_{3\varepsilon} + r_{4\varepsilon} + r_{5\varepsilon} + r_{6\varepsilon}$ may be respectively expressed

$$\begin{aligned}
r_{1\varepsilon} &= \frac{4c_{\varepsilon 1}\mu_t}{3Re}\left(u_1^1\frac{\partial N_u^1}{\partial x_1} + u_1^2\frac{\partial N_u^2}{\partial x_1} + u_1^3\frac{\partial N_u^3}{\partial x_1}\right)^2 - \\
&- \frac{2c_{\varepsilon 1}\mu_t}{3Re}\left(u_2^1\frac{\partial N_u^1}{\partial x_2} + u_2^2\frac{\partial N_u^2}{\partial x_2} + u_2^3\frac{\partial N_u^3}{\partial x_2}\right)\left(u_1^1\frac{\partial N_u^1}{\partial x_1} + u_1^2\frac{\partial N_u^2}{\partial x_1} + u_1^3\frac{\partial N_u^3}{\partial x_1}\right) \\
r_{2\varepsilon} &= \frac{4c_{\varepsilon 1}\mu_t}{3Re}\left(u_2^1\frac{\partial N_u^1}{\partial x_2} + u_2^2\frac{\partial N_u^2}{\partial x_2} + u_2^3\frac{\partial N_u^3}{\partial x_2}\right)^2 - \\
&- \frac{2c_{\varepsilon 1}\mu_t}{3Re}\left(u_1^1\frac{\partial N_u^1}{\partial x_1} + u_1^2\frac{\partial N_u^2}{\partial x_1} + u_1^3\frac{\partial N_u^3}{\partial x_1}\right)\left(u_2^1\frac{\partial N_u^1}{\partial x_2} + u_2^2\frac{\partial N_u^2}{\partial x_2} + u_2^3\frac{\partial N_u^3}{\partial x_2}\right)
\end{aligned}$$

$$
\begin{aligned}
r_{3\varepsilon} &= \frac{c_{\varepsilon 1}\mu_t}{Re}\left(u_1^1\frac{\partial N_u^1}{\partial x_2}+u_1^2\frac{\partial N_u^2}{\partial x_2}+u_1^3\frac{\partial N_u^3}{\partial x_2}\right)^2+\\
&+ \frac{c_{\varepsilon 1}\mu_t}{Re}\left(u_2^1\frac{\partial N_u^1}{\partial x_1}+u_2^2\frac{\partial N_u^2}{\partial x_1}+u_2^3\frac{\partial N_u^3}{\partial x_1}\right)\left(u_1^1\frac{\partial N_u^1}{\partial x_2}+u_1^2\frac{\partial N_u^2}{\partial x_2}+u_1^3\frac{\partial N_u^3}{\partial x_2}\right)\\
r_{4\varepsilon} &= \frac{c_{\varepsilon 1}\mu_t}{Re}\left(u_2^1\frac{\partial N_u^1}{\partial x_1}+u_2^2\frac{\partial N_u^2}{\partial x_1}+u_2^3\frac{\partial N_u^3}{\partial x_1}\right)^2+\\
&+ \frac{c_{\varepsilon 1}\mu_t}{Re}\left(u_1^1\frac{\partial N_u^1}{\partial x_2}+u_1^2\frac{\partial N_u^2}{\partial x_2}+u_1^3\frac{\partial N_u^3}{\partial x_2}\right)\left(u_2^1\frac{\partial N_u^1}{\partial x_1}+u_2^2\frac{\partial N_u^2}{\partial x_1}+u_2^3\frac{\partial N_u^3}{\partial x_1}\right)\\
r_{5\varepsilon} &= -\frac{2c_{\varepsilon 1}}{3}\left(K^1N_\varepsilon^1+K^2N_\varepsilon^2+K^3N_\varepsilon^3\right)\\
&\quad \left(u_1^1\frac{\partial N_u^1}{\partial x_1}+u_1^2\frac{\partial N_u^2}{\partial x_1}+u_1^3\frac{\partial N_u^3}{\partial x_1}+u_2^1\frac{\partial N_u^1}{\partial x_2}+u_2^2\frac{\partial N_u^2}{\partial x_2}+u_2^3\frac{\partial N_u^3}{\partial x_2}\right)\\
r_{6\varepsilon} &= -c_{\varepsilon 2}\left(E^1N_\varepsilon^1+E^2N_\varepsilon^2+E^3N_\varepsilon^3\right) \qquad \text{(A.43)}
\end{aligned}
$$

Thus the vector coefficients $\left[f_{\varepsilon\Omega}^{i,j}\right]$ are

$$
f_{\varepsilon\Omega}^{1,1}=N_\varepsilon^1\Upsilon_\varepsilon^{II};\qquad f_{\varepsilon\Omega}^{2,1}=N_\varepsilon^2\Upsilon_\varepsilon^{II};\qquad f_{\varepsilon\Omega}^{3,1}=N_\varepsilon^3\Upsilon_\varepsilon^{II} \qquad \text{(A.44)}
$$

The 3×1 forcing vector for the dissipation rate is given as

$$
\mathbf{f}_{\varepsilon\Gamma}=\frac{1}{Re}\left(\mu+\frac{\mu_t}{\sigma_\varepsilon}\right)\int_\Gamma\left[f_{\varepsilon\Gamma}^{i,j}\right]d\Gamma=\int_\Gamma \mathbf{N}_\varepsilon{}^T t_\varepsilon d\Gamma \qquad \text{(A.45)}
$$

where the vector coefficients $\left[f_{\varepsilon\Gamma}^{i,j}\right]$ are

$$
\begin{aligned}
f_{\varepsilon\Gamma}^{1,1} &= N_\varepsilon^1\left[\left(\varepsilon^1\frac{\partial N_\varepsilon^1}{\partial x_1}+\varepsilon^2\frac{\partial N_\varepsilon^2}{\partial x_1}+\varepsilon^3\frac{\partial N_\varepsilon^3}{\partial x_1}\right)\hat{n}_{x_1}+\left(\varepsilon^1\frac{\partial N_\varepsilon^1}{\partial x_2}+\varepsilon^2\frac{\partial N_\varepsilon^2}{\partial x_2}+\varepsilon^3\frac{\partial N_\varepsilon^3}{\partial x_2}\right)\hat{n}_{x_2}\right]\\
f_{\varepsilon\Gamma}^{2,1} &= N_\varepsilon^2\left[\left(\varepsilon^1\frac{\partial N_\varepsilon^1}{\partial x_1}+\varepsilon^2\frac{\partial N_\varepsilon^2}{\partial x_1}+\varepsilon^3\frac{\partial N_\varepsilon^3}{\partial x_1}\right)\hat{n}_{x_1}+\left(\varepsilon^1\frac{\partial N_\varepsilon^1}{\partial x_2}+\varepsilon^2\frac{\partial N_\varepsilon^2}{\partial x_2}+\varepsilon^3\frac{\partial N_\varepsilon^3}{\partial x_2}\right)\hat{n}_{x_2}\right]\\
f_{\varepsilon\Gamma}^{3,1} &= N_\varepsilon^3\left[\left(\varepsilon^1\frac{\partial N_\varepsilon^1}{\partial x_1}+\varepsilon^2\frac{\partial N_\varepsilon^2}{\partial x_1}+\varepsilon^3\frac{\partial N_\varepsilon^3}{\partial x_1}\right)\hat{n}_{x_1}+\left(\varepsilon^1\frac{\partial N_\varepsilon^1}{\partial x_2}+\varepsilon^2\frac{\partial N_\varepsilon^2}{\partial x_2}+\varepsilon^3\frac{\partial N_\varepsilon^3}{\partial x_2}\right)\hat{n}_{x_2}\right]
\end{aligned}
\qquad \text{(A.46)}
$$

The 3×3 symmetric convection matrix of the stabilization for the dissipation rate is given as

$$
\mathbf{K}_{\mathbf{u}\varepsilon}=-\frac{1}{2}\int_\Omega\left[K_{u\varepsilon}^{i,j}\right]d\Omega=-\frac{1}{2}\int_\Omega(\nabla^T(\mathbf{u}\mathbf{N}_\varepsilon))^T(\nabla^T(\mathbf{u}\mathbf{N}_\varepsilon))d\Omega \qquad \text{(A.47)}
$$

where the matrix coefficients $\left[K_{u\varepsilon}^{i,j}\right]$ are

$$K_{u\varepsilon}^{1,1} = \left(\frac{\partial u_1 N_\varepsilon^1}{\partial x_1} + \frac{\partial u_2 N_\varepsilon^1}{\partial x_2}\right)^2; \quad K_{u\varepsilon}^{2,2} = \left(\frac{\partial u_1 N_\varepsilon^2}{\partial x_1} + \frac{\partial u_2 N_\varepsilon^2}{\partial x_2}\right)^2$$
$$K_{u\varepsilon}^{3,3} = \left(\frac{\partial u_1 N_\varepsilon^3}{\partial x_1} + \frac{\partial u_2 N_\varepsilon^3}{\partial x_2}\right)^2$$
$$K_{u\varepsilon}^{1,2} = K_{u\varepsilon}^{2,1} = \left(\frac{\partial u_1 N_\varepsilon^1}{\partial x_1} + \frac{\partial u_2 N_\varepsilon^1}{\partial x_2}\right)\left(\frac{\partial u_1 N_\varepsilon^2}{\partial x_1} + \frac{\partial u_2 N_\varepsilon^2}{\partial x_2}\right)$$
$$K_{u\varepsilon}^{1,3} = K_{u\varepsilon}^{3,1} = \left(\frac{\partial u_1 N_\varepsilon^1}{\partial x_1} + \frac{\partial u_2 N_\varepsilon^1}{\partial x_2}\right)\left(\frac{\partial u_1 N_\varepsilon^3}{\partial x_1} + \frac{\partial u_2 N_\varepsilon^3}{\partial x_2}\right)$$
$$K_{u\varepsilon}^{2,3} = K_{u\varepsilon}^{3,2} = \left(\frac{\partial u_1 N_\varepsilon^2}{\partial x_1} + \frac{\partial u_2 N_\varepsilon^2}{\partial x_2}\right)\left(\frac{\partial u_1 N_\varepsilon^3}{\partial x_1} + \frac{\partial u_2 N_\varepsilon^3}{\partial x_2}\right) \tag{A.48}$$

The 3 × 3 symmetric, lumped mass matrix for the modified turbulent eddy kinematic viscosity is given as

$$\mathbf{M}_{\hat{\nu}} = \int_\Omega \left[M_{\hat{\nu}}^{i,j}\right] d\Omega = \int_\Omega \mathbf{N}_{\hat{\nu}}{}^T \mathbf{N}_{\hat{\nu}} d\Omega \tag{A.49}$$

where the matrix coefficients $\left[M_{\hat{\nu}}^{i,j}\right]$ are

$$M_{\hat{\nu}}^{1,1} = N_{\hat{\nu}}^1 N_{\hat{\nu}}^1; \quad M_{\hat{\nu}}^{2,2} = N_{\hat{\nu}}^2 N_{\hat{\nu}}^2; \quad M_{\hat{\nu}}^{3,3} = N_{\hat{\nu}}^3 N_{\hat{\nu}}^3$$
$$M_{\hat{\nu}}^{1,2} = M_{\hat{\nu}}^{2,1} = N_{\hat{\nu}}^1 N_{\hat{\nu}}^2; \quad M_{\hat{\nu}}^{1,3} = M_{\hat{\nu}}^{3,1} = N_{\hat{\nu}}^1 N_{\hat{\nu}}^3$$
$$M_{\hat{\nu}}^{2,3} = M_{\hat{\nu}}^{3,2} = N_{\hat{\nu}}^2 N_{\hat{\nu}}^3 \tag{A.50}$$

The 3 × 3 convection matrix for the modified turbulent eddy kinematic viscosity is given as

$$\mathbf{C}_{\hat{\nu}} = \int_\Omega \left[C_{\hat{\nu}}^{i,j}\right] d\Omega = \int_\Omega \mathbf{N}_{\hat{\nu}}{}^T (\nabla^T (\mathbf{u}\mathbf{N}_{\hat{\nu}})) d\Omega \tag{A.51}$$

where the matrix coefficients $\left[C_{\hat{\nu}}^{i,j}\right]$ are

$$C_{\hat{\nu}}^{1,1} = N_{\hat{\nu}}^1 \left(\frac{\partial u_1 N_{\hat{\nu}}^1}{\partial x_1} + \frac{\partial u_2 N_{\hat{\nu}}^1}{\partial x_2}\right); \quad C_{\hat{\nu}}^{2,2} = N_{\hat{\nu}}^2 \left(\frac{\partial u_1 N_{\hat{\nu}}^2}{\partial x_1} + \frac{\partial u_2 N_{\hat{\nu}}^2}{\partial x_2}\right)$$

$$C_{\hat{\nu}}^{3,3} = N_{\hat{\nu}}^3 \left(\frac{\partial u_1 N_{\hat{\nu}}^3}{\partial x_1} + \frac{\partial u_2 N_{\hat{\nu}}^3}{\partial x_2} \right); \quad C_{\hat{\nu}}^{1,2} = N_{\hat{\nu}}^1 \left(\frac{\partial u_1 N_{\hat{\nu}}^2}{\partial x_1} + \frac{\partial u_2 N_{\hat{\nu}}^2}{\partial x_2} \right)$$

$$C_{\hat{\nu}}^{2,1} = N_{\hat{\nu}}^2 \left(\frac{\partial u_1 N_{\hat{\nu}}^1}{\partial x_1} + \frac{\partial u_2 N_{\hat{\nu}}^1}{\partial x_2} \right); \quad C_{\hat{\nu}}^{1,3} = N_{\hat{\nu}}^1 \left(\frac{\partial u_1 N_{\hat{\nu}}^3}{\partial x_1} + \frac{\partial u_2 N_{\hat{\nu}}^3}{\partial x_2} \right)$$

$$C_{\hat{\nu}}^{3,1} = N_{\hat{\nu}}^3 \left(\frac{\partial u_1 N_{\hat{\nu}}^1}{\partial x_1} + \frac{\partial u_2 N_{\hat{\nu}}^1}{\partial x_2} \right); \quad C_{\hat{\nu}}^{2,3} = N_{\hat{\nu}}^2 \left(\frac{\partial u_1 N_{\hat{\nu}}^3}{\partial x_1} + \frac{\partial u_2 N_{\hat{\nu}}^3}{\partial x_2} \right)$$

$$C_{\hat{\nu}}^{3,2} = N_{\hat{\nu}}^3 \left(\frac{\partial u_1 N_{\hat{\nu}}^2}{\partial x_1} + \frac{\partial u_2 N_{\hat{\nu}}^2}{\partial x_2} \right) \tag{A.52}$$

The 3 × 3 symmetric matrix resulted from first diffusion term in the modified turbulent eddy kinematic viscosity equation is given as

$$\mathbf{K}_{\hat{\nu}} = \frac{\nu + \hat{\nu}}{\sigma_{\hat{\nu}} Re} \int_{\Omega} \left[K_{\hat{\nu}}^{i,j} \right] d\Omega = \int_{\Omega} (\nabla \mathbf{N}_{\hat{\nu}})^T \left(\frac{\nu + \hat{\nu}}{\sigma_{\hat{\nu}} Re} \right) \nabla \mathbf{N}_{\hat{\nu}} d\Omega \tag{A.53}$$

where the matrix coefficients $\left[K_{\hat{\nu}}^{i,j} \right]$ are

$$K_{\hat{\nu}}^{1,1} = \left(\frac{\partial N_{\hat{\nu}}^1}{\partial x_1} \right)^2 + \left(\frac{\partial N_{\hat{\nu}}^1}{\partial x_2} \right)^2; \quad K_{\hat{\nu}}^{2,2} = \left(\frac{\partial N_{\hat{\nu}}^2}{\partial x_1} \right)^2 + \left(\frac{\partial N_{\hat{\nu}}^2}{\partial x_2} \right)^2$$

$$K_{\hat{\nu}}^{3,3} = \left(\frac{\partial N_{\hat{\nu}}^3}{\partial x_1} \right)^2 + \left(\frac{\partial N_{\hat{\nu}}^3}{\partial x_2} \right)^2; \quad K_{\hat{\nu}}^{1,2} = K_{\hat{\nu}}^{2,1} = \frac{\partial N_{\hat{\nu}}^1}{\partial x_1} \frac{\partial N_{\hat{\nu}}^2}{\partial x_1} + \frac{\partial N_{\hat{\nu}}^1}{\partial x_2} \frac{\partial N_{\hat{\nu}}^2}{\partial x_2}$$

$$K_{\hat{\nu}}^{1,3} = K_{\hat{\nu}}^{3,1} = \frac{\partial N_{\hat{\nu}}^1}{\partial x_1} \frac{\partial N_{\hat{\nu}}^3}{\partial x_1} + \frac{\partial N_{\hat{\nu}}^1}{\partial x_2} \frac{\partial N_{\hat{\nu}}^3}{\partial x_2}; \quad K_{\hat{\nu}}^{2,3} = K_{\hat{\nu}}^{3,2} = \frac{\partial N_{\hat{\nu}}^2}{\partial x_1} \frac{\partial N_{\hat{\nu}}^3}{\partial x_1} + \frac{\partial N_{\hat{\nu}}^2}{\partial x_2} \frac{\partial N_{\hat{\nu}}^3}{\partial x_2} \tag{A.54}$$

The 3 × 1 vector resulted from second diffusion term in the modified turbulent eddy kinematic viscosity equation is given as

$$\mathbf{f}_{\hat{\nu}\Omega} = \frac{c_{b2}}{\sigma_{\hat{\nu}} Re} \int_{\Omega} \left[f_{\hat{\nu}\Omega}^{i,j} \right] d\Omega = \int_{\Omega} \mathbf{N}_{\hat{\nu}}{}^T \left(\frac{c_{b2}}{\sigma_{\hat{\nu}} Re} \right) (\partial_i \hat{\nu})^2 d\Omega \tag{A.55}$$

where the vector coefficients $\left[f_{\hat{\nu}\Omega}^{i,j} \right]$ are

$$\begin{aligned}
f_{\hat{\nu}\Omega}^{1,1} &= N_{\hat{\nu}}^1 \left[\left(\hat{\nu}^1 \frac{\partial N_{\hat{\nu}}^1}{\partial x_1} + \hat{\nu}^2 \frac{\partial N_{\hat{\nu}}^2}{\partial x_1} + \hat{\nu}^3 \frac{\partial N_{\hat{\nu}}^3}{\partial x_1} \right)^2 + \left(\hat{\nu}^1 \frac{\partial N_{\hat{\nu}}^1}{\partial x_2} + \hat{\nu}^2 \frac{\partial N_{\hat{\nu}}^2}{\partial x_2} + \hat{\nu}^3 \frac{\partial N_{\hat{\nu}}^3}{\partial x_2} \right)^2 \right] \\
f_{\hat{\nu}\Omega}^{2,1} &= N_{\hat{\nu}}^2 \left[\left(\hat{\nu}^1 \frac{\partial N_{\hat{\nu}}^1}{\partial x_1} + \hat{\nu}^2 \frac{\partial N_{\hat{\nu}}^2}{\partial x_1} + \hat{\nu}^3 \frac{\partial N_{\hat{\nu}}^3}{\partial x_1} \right)^2 + \left(\hat{\nu}^1 \frac{\partial N_{\hat{\nu}}^1}{\partial x_2} + \hat{\nu}^2 \frac{\partial N_{\hat{\nu}}^2}{\partial x_2} + \hat{\nu}^3 \frac{\partial N_{\hat{\nu}}^3}{\partial x_2} \right)^2 \right] \\
f_{\hat{\nu}\Omega}^{3,1} &= N_{\hat{\nu}}^3 \left[\left(\hat{\nu}^1 \frac{\partial N_{\hat{\nu}}^1}{\partial x_1} + \hat{\nu}^2 \frac{\partial N_{\hat{\nu}}^2}{\partial x_1} + \hat{\nu}^3 \frac{\partial N_{\hat{\nu}}^3}{\partial x_1} \right)^2 + \left(\hat{\nu}^1 \frac{\partial N_{\hat{\nu}}^1}{\partial x_2} + \hat{\nu}^2 \frac{\partial N_{\hat{\nu}}^2}{\partial x_2} + \hat{\nu}^3 \frac{\partial N_{\hat{\nu}}^3}{\partial x_2} \right)^2 \right]
\end{aligned} \tag{A.56}$$

The 3 × 1 vector based on both the production and destruction terms of the modified turbulent eddy kinematic viscosity equation is given as

$$\mathbf{f}_{\hat{\nu}\Omega^*} = \left(c_{b1}\hat{S} - \frac{c_{w1}f_w}{Re}\frac{\hat{\nu}}{y^2}\right)\int_\Omega \left[f^{i,j}_{\hat{\nu}\Omega^*}\right] d\Omega = \int_\Omega \mathbf{N}_{\hat{\nu}}{}^T\left(c_{b1}\hat{S} - \frac{c_{w1}f_w}{Re}\frac{\hat{\nu}}{y^2}\right)\mathbf{N}_{\hat{\nu}}\tilde{\nu}d\Omega \quad \text{(A.57)}$$

where the vector coefficients $\left[f^{i,j}_{\hat{\nu}\Omega^*}\right]$ are

$$\begin{aligned} f^{1,1}_{\hat{\nu}\Omega^*} &= N^1_{\hat{\nu}}\left(\hat{\nu}^1N^1_{\hat{\nu}} + \hat{\nu}^2N^2_{\hat{\nu}} + \hat{\nu}^3N^3_{\hat{\nu}}\right) \\ f^{2,1}_{\hat{\nu}\Omega^*} &= N^2_{\hat{\nu}}\left(\hat{\nu}^1N^1_{\hat{\nu}} + \hat{\nu}^2N^2_{\hat{\nu}} + \hat{\nu}^3N^3_{\hat{\nu}}\right) \\ f^{3,1}_{\hat{\nu}\Omega^*} &= N^3_{\hat{\nu}}\left(\hat{\nu}^1N^1_{\hat{\nu}} + \hat{\nu}^2N^2_{\hat{\nu}} + \hat{\nu}^3N^3_{\hat{\nu}}\right) \end{aligned} \quad \text{(A.58)}$$

The 3 × 1 forcing vector for the modified turbulent eddy kinematic viscosity is given as

$$\mathbf{f}_{\hat{\nu}\Gamma} = \frac{\nu + \hat{\nu}}{\sigma_{\hat{\nu}}Re}\int_\Gamma \left[f^{i,j}_{\hat{\nu}\Gamma}\right] d\Gamma = \int_\Gamma \mathbf{N}_{\hat{\nu}}{}^T t_{\hat{\nu}} d\Gamma \quad \text{(A.59)}$$

where the vector coefficients $\left[f^{i,j}_{\hat{\nu}\Gamma}\right]$ are

$$\begin{aligned} f^{1,1}_{\hat{\nu}\Gamma} &= N^1_{\hat{\nu}}\left[\left(\hat{\nu}^1\frac{\partial N^1_{\hat{\nu}}}{\partial x_1} + \hat{\nu}^2\frac{\partial N^2_{\hat{\nu}}}{\partial x_1} + \hat{\nu}^3\frac{\partial N^3_{\hat{\nu}}}{\partial x_1}\right)\hat{n}_{x_1} + \left(\hat{\nu}^1\frac{\partial N^1_{\hat{\nu}}}{\partial x_2} + \hat{\nu}^2\frac{\partial N^2_{\hat{\nu}}}{\partial x_2} + \hat{\nu}^3\frac{\partial N^3_{\hat{\nu}}}{\partial x_2}\right)\hat{n}_{x_2}\right] \\ f^{2,1}_{\hat{\nu}\Gamma} &= N^2_{\hat{\nu}}\left[\left(\hat{\nu}^1\frac{\partial N^1_{\hat{\nu}}}{\partial x_1} + \hat{\nu}^2\frac{\partial N^2_{\hat{\nu}}}{\partial x_1} + \hat{\nu}^3\frac{\partial N^3_{\hat{\nu}}}{\partial x_1}\right)\hat{n}_{x_1} + \left(\hat{\nu}^1\frac{\partial N^1_{\hat{\nu}}}{\partial x_2} + \hat{\nu}^2\frac{\partial N^2_{\hat{\nu}}}{\partial x_2} + \hat{\nu}^3\frac{\partial N^3_{\hat{\nu}}}{\partial x_2}\right)\hat{n}_{x_2}\right] \\ f^{3,1}_{\hat{\nu}\Gamma} &= N^3_{\hat{\nu}}\left[\left(\hat{\nu}^1\frac{\partial N^1_{\hat{\nu}}}{\partial x_1} + \hat{\nu}^2\frac{\partial N^2_{\hat{\nu}}}{\partial x_1} + \hat{\nu}^3\frac{\partial N^3_{\hat{\nu}}}{\partial x_1}\right)\hat{n}_{x_1} + \left(\hat{\nu}^1\frac{\partial N^1_{\hat{\nu}}}{\partial x_2} + \hat{\nu}^2\frac{\partial N^2_{\hat{\nu}}}{\partial x_2} + \hat{\nu}^3\frac{\partial N^3_{\hat{\nu}}}{\partial x_2}\right)\hat{n}_{x_2}\right] \end{aligned} \quad \text{(A.60)}$$

The 3 × 3 symmetric convection matrix of the stabilization for the modified turbulent eddy kinematic viscosity is given as

$$\mathbf{K}_{\mathbf{u}\hat{\nu}} = -\frac{1}{2}\int_\Omega \left[K^{i,j}_{u\hat{\nu}}\right] d\Omega = -\frac{1}{2}\int_\Omega (\nabla^T(\mathbf{u}\mathbf{N}_{\hat{\nu}}))^T(\nabla^T(\mathbf{u}\mathbf{N}_{\hat{\nu}}))d\Omega \quad \text{(A.61)}$$

where the matrix coefficients $\left[K^{i,j}_{u\hat{\nu}}\right]$ are

$$K_{u\hat{\nu}}^{1,1} = \left(\frac{\partial u_1 N_{\hat{\nu}}^1}{\partial x_1} + \frac{\partial u_2 N_{\hat{\nu}}^1}{\partial x_2}\right)^2; \quad K_{u\hat{\nu}}^{2,2} = \left(\frac{\partial u_1 N_{\hat{\nu}}^2}{\partial x_1} + \frac{\partial u_2 N_{\hat{\nu}}^2}{\partial x_2}\right)^2$$

$$K_{u\hat{\nu}}^{3,3} = \left(\frac{\partial u_1 N_{\hat{\nu}}^3}{\partial x_1} + \frac{\partial u_2 N_{\hat{\nu}}^3}{\partial x_2}\right)^2$$

$$K_{u\hat{\nu}}^{1,2} = K_{u\hat{\nu}}^{2,1} = \left(\frac{\partial u_1 N_{\hat{\nu}}^1}{\partial x_1} + \frac{\partial u_2 N_{\hat{\nu}}^1}{\partial x_2}\right)\left(\frac{\partial u_1 N_{\hat{\nu}}^2}{\partial x_1} + \frac{\partial u_2 N_{\hat{\nu}}^2}{\partial x_2}\right)$$

$$K_{u\hat{\nu}}^{1,3} = K_{u\hat{\nu}}^{3,1} = \left(\frac{\partial u_1 N_{\hat{\nu}}^1}{\partial x_1} + \frac{\partial u_2 N_{\hat{\nu}}^1}{\partial x_2}\right)\left(\frac{\partial u_1 N_{\hat{\nu}}^3}{\partial x_1} + \frac{\partial u_2 N_{\hat{\nu}}^3}{\partial x_2}\right)$$

$$K_{u\hat{\nu}}^{2,3} = K_{u\hat{\nu}}^{3,2} = \left(\frac{\partial u_1 N_{\hat{\nu}}^2}{\partial x_1} + \frac{\partial u_2 N_{\hat{\nu}}^2}{\partial x_2}\right)\left(\frac{\partial u_1 N_{\hat{\nu}}^3}{\partial x_1} + \frac{\partial u_2 N_{\hat{\nu}}^3}{\partial x_2}\right) \tag{A.62}$$

Appendix B

Three-dimensional matrix coefficients of the CBS algorithm with RANS turbulence models

Here we display the 3D matrix coefficients of a 4-nodes tetrahedral element.

The 12×12 symmetric, lumped mass matrix for the intermediate momentum is given as

$$\mathbf{M_u} = \int_\Omega \left[M_u^{i,j}\right] d\Omega = \int_\Omega \mathbf{N_u}^T \mathbf{N_u} d\Omega \tag{B.1}$$

where the matrix coefficients $\left[M_u^{i,j}\right]$ are (i row; j column)

$$\begin{aligned}
M_u^{1,2} &= M_u^{2,1} = M_u^{1,3} = M_u^{3,1} = M_u^{1,5} = M_u^{5,1} = M_u^{1,6} = M_u^{6,1} = M_u^{1,8} = \\
&= M_u^{8,1} = M_u^{1,9} = M_u^{9,1} = M_u^{11,1} = M_u^{1,11} = M_u^{12,1} = M_u^{1,12} = M_u^{2,3} = \\
&= M_u^{3,2} = M_u^{2,4} = M_u^{4,2} = M_u^{2,6} = M_u^{6,2} = M_u^{2,7} = M_u^{7,2} = M_u^{2,9} = \\
&= M_u^{9,2} = M_u^{2,10} = M_u^{10,2} = M_u^{2,12} = M_u^{12,2} = M_u^{3,4} = M_u^{4,3} = M_u^{3,5} = \\
&= M_u^{5,3} = M_u^{3,7} = M_u^{7,3} = M_u^{3,8} = M_u^{8,3} = M_u^{3,10} = M_u^{10,3} = M_u^{3,11} = \\
&= M_u^{11,3} = M_u^{4,5} = M_u^{5,4} = M_u^{4,6} = M_u^{6,4} = M_u^{4,8} = M_u^{8,4} = M_u^{4,9} =
\end{aligned}$$

$$= M_u^{9,4} = M_u^{4,11} = M_u^{11,4} = M_u^{4,12} = M_u^{12,4} = M_u^{5,6} = M_u^{6,5} = M_u^{5,7} =$$
$$= M_u^{7,5} = M_u^{5,9} = M_u^{9,5} = M_u^{5,10} = M_u^{10,5} = M_u^{5,12} = M_u^{12,5} = M_u^{6,7} =$$
$$= M_u^{7,6} = M_u^{6,8} = M_u^{8,6} = M_u^{6,10} = M_u^{10,6} = M_u^{6,11} = M_u^{11,6} = M_u^{7,8} =$$
$$= M_u^{8,7} = M_u^{7,9} = M_u^{9,7} = M_u^{7,11} = M_u^{11,7} = M_u^{7,12} = M_u^{12,7} = M_u^{8,9} =$$
$$= M_u^{9,8} = M_u^{8,10} = M_u^{10,8} = M_u^{8,12} = M_u^{12,8} = M_u^{9,10} = M_u^{10,9} =$$
$$= M_u^{9,11} = M_u^{11,9} = M_u^{10,11} = M_u^{11,10} = M_u^{10,12} = M_u^{12,10} = M_u^{11,12} =$$
$$= M_u^{12,11} = 0$$
$$M_u^{1,1} = M_u^{2,2} = M_u^{3,3} = N_u^1 N_u^1$$
$$M_u^{4,4} = M_u^{5,5} = M_u^{6,6} = N_u^2 N_u^2$$
$$M_u^{7,7} = M_u^{8,8} = M_u^{9,9} = N_u^3 N_u^3$$
$$M_u^{10,10} = M_u^{11,11} = M_u^{12,12} = N_u^4 N_u^4$$
$$M_u^{1,4} = M_u^{4,1} = M_u^{2,5} = M_u^{5,2} = M_u^{3,6} = M_u^{6,3} = N_u^1 N_u^2$$
$$M_u^{4,7} = M_u^{7,4} = M_u^{5,8} = M_u^{8,5} = M_u^{6,9} = M_u^{9,6} = N_u^2 N_u^3$$
$$M_u^{7,10} = M_u^{10,7} = M_u^{8,11} = M_u^{11,8} = M_u^{9,12} = M_u^{12,9} = N_u^3 N_u^4$$
$$M_u^{1,7} = M_u^{7,1} = M_u^{2,8} = M_u^{8,2} = M_u^{3,9} = M_u^{9,3} = N_u^1 N_u^3$$
$$M_u^{4,10} = M_u^{10,4} = M_u^{5,11} = M_u^{11,5} = M_u^{6,12} = M_u^{12,6} = N_u^2 N_u^4$$
$$M_u^{1,10} = M_u^{10,1} = M_u^{2,11} = M_u^{11,2} = M_u^{3,12} = M_u^{12,3} = N_u^1 N_u^4 \tag{B.2}$$

The 12×12 convection matrix of the velocities for the intermediate momentum is given as

$$\mathbf{C_u} = \int_\Omega \left[C_u^{i,j}\right] d\Omega = \int_\Omega \mathbf{N_u}^T (\nabla^T (\mathbf{u N_u})) d\Omega \tag{B.3}$$

where the matrix coefficients $\left[C_u^{i,j}\right]$ are

$$C_u^{1,2} = C_u^{2,1} = C_u^{1,3} = C_u^{3,1} = C_u^{1,5} = C_u^{5,1} = C_u^{1,6} = C_u^{6,1} = C_u^{1,8} =$$
$$= C_u^{8,1} = C_u^{1,9} = C_u^{9,1} = C_u^{1,11} = C_u^{11,1} = C_u^{1,12} = C_u^{12,1} = C_u^{2,3} =$$
$$= C_u^{3,2} = C_u^{2,4} = C_u^{4,2} = C_u^{2,6} = C_u^{6,2} = C_u^{2,7} = C_u^{7,2} = C_u^{2,9} =$$

$$= C_u^{9,2} = C_u^{2,10} = C_u^{10,2} = C_u^{2,12} = C_u^{12,2} = C_u^{3,4} = C_u^{4,3} = C_u^{3,5} =$$
$$= C_u^{5,3} = C_u^{3,7} = C_u^{7,3} = C_u^{3,8} = C_u^{8,3} = C_u^{3,10} = C_u^{10,3} = C_u^{3,11} =$$
$$= C_u^{11,3} = C_u^{4,5} = C_u^{5,4} = C_u^{4,6} = C_u^{6,4} = C_u^{4,8} = C_u^{8,4} = C_u^{4,9} =$$
$$= C_u^{9,4} = C_u^{4,11} = C_u^{11,4} = C_u^{4,12} = C_u^{12,4} = C_u^{5,6} = C_u^{6,5} = C_u^{5,7} =$$
$$= C_u^{7,5} = C_u^{5,9} = C_u^{9,5} = C_u^{5,10} = C_u^{10,5} = C_u^{5,12} = C_u^{12,5} = C_u^{6,7} =$$
$$= C_u^{7,6} = C_u^{6,8} = C_u^{8,6} = C_u^{6,10} = C_u^{10,6} = C_u^{6,11} = C_u^{11,6} = C_u^{7,8} =$$
$$= C_u^{8,7} = C_u^{7,9} = C_u^{9,7} = C_u^{7,11} = C_u^{11,7} = C_u^{7,12} = C_u^{12,7} = C_u^{8,9} =$$
$$= C_u^{9,8} = C_u^{8,10} = C_u^{10,8} = C_u^{8,12} = C_u^{12,8} = C_u^{9,10} = C_u^{10,9} = C_u^{9,11} =$$
$$= C_u^{11,9} = C_u^{10,11} = C_u^{11,10} = C_u^{10,12} = C_u^{12,10} = C_u^{11,12} = C_u^{12,11} = 0$$

$$C_u^{1,1} = C_u^{2,2} = C_u^{3,3} = N_u^1 \left(\frac{\partial u_1 N_u^1}{\partial x_1} + \frac{\partial u_2 N_u^1}{\partial x_2} + \frac{\partial u_3 N_u^1}{\partial x_3} \right)$$
$$C_u^{4,1} = C_u^{5,2} = C_u^{6,3} = N_u^2 \left(\frac{\partial u_1 N_u^1}{\partial x_1} + \frac{\partial u_2 N_u^1}{\partial x_2} + \frac{\partial u_3 N_u^1}{\partial x_3} \right)$$
$$C_u^{7,1} = C_u^{8,2} = C_u^{9,3} = N_u^3 \left(\frac{\partial u_1 N_u^1}{\partial x_1} + \frac{\partial u_2 N_u^1}{\partial x_2} + \frac{\partial u_3 N_u^1}{\partial x_3} \right)$$
$$C_u^{10,1} = C_u^{11,2} = C_u^{12,3} = N_u^4 \left(\frac{\partial u_1 N_u^1}{\partial x_1} + \frac{\partial u_2 N_u^1}{\partial x_2} + \frac{\partial u_3 N_u^1}{\partial x_3} \right)$$
$$C_u^{1,4} = C_u^{2,5} = C_u^{3,6} = N_u^1 \left(\frac{\partial u_1 N_u^2}{\partial x_1} + \frac{\partial u_2 N_u^2}{\partial x_2} + \frac{\partial u_3 N_u^2}{\partial x_3} \right)$$
$$C_u^{4,4} = C_u^{5,5} = C_u^{6,6} = N_u^2 \left(\frac{\partial u_1 N_u^2}{\partial x_1} + \frac{\partial u_2 N_u^2}{\partial x_2} + \frac{\partial u_3 N_u^2}{\partial x_3} \right)$$
$$C_u^{7,4} = C_u^{8,5} = C_u^{9,6} = N_u^3 \left(\frac{\partial u_1 N_u^2}{\partial x_1} + \frac{\partial u_2 N_u^2}{\partial x_2} + \frac{\partial u_3 N_u^2}{\partial x_3} \right)$$
$$C_u^{10,4} = C_u^{11,5} = C_u^{12,6} = N_u^4 \left(\frac{\partial u_1 N_u^2}{\partial x_1} + \frac{\partial u_2 N_u^2}{\partial x_2} + \frac{\partial u_3 N_u^2}{\partial x_3} \right)$$
$$C_u^{1,7} = C_u^{2,8} = C_u^{3,9} = N_u^1 \left(\frac{\partial u_1 N_u^3}{\partial x_1} + \frac{\partial u_2 N_u^3}{\partial x_2} + \frac{\partial u_3 N_u^3}{\partial x_3} \right)$$
$$C_u^{4,7} = C_u^{5,8} = C_u^{6,9} = N_u^2 \left(\frac{\partial u_1 N_u^3}{\partial x_1} + \frac{\partial u_2 N_u^3}{\partial x_2} + \frac{\partial u_3 N_u^3}{\partial x_3} \right)$$
$$C_u^{7,7} = C_u^{8,8} = C_u^{9,9} = N_u^3 \left(\frac{\partial u_1 N_u^3}{\partial x_1} + \frac{\partial u_2 N_u^3}{\partial x_2} + \frac{\partial u_3 N_u^3}{\partial x_3} \right)$$
$$C_u^{10,7} = C_u^{11,8} = C_u^{12,9} = N_u^4 \left(\frac{\partial u_1 N_u^3}{\partial x_1} + \frac{\partial u_2 N_u^3}{\partial x_2} + \frac{\partial u_3 N_u^3}{\partial x_3} \right)$$
$$C_u^{1,10} = C_u^{2,11} = C_u^{3,12} = N_u^1 \left(\frac{\partial u_1 N_u^4}{\partial x_1} + \frac{\partial u_2 N_u^4}{\partial x_2} + \frac{\partial u_3 N_u^4}{\partial x_3} \right)$$

$$C_u^{4,10} = C_u^{5,11} = C_u^{6,12} = N_u^2 \left(\frac{\partial u_1 N_u^4}{\partial x_1} + \frac{\partial u_2 N_u^4}{\partial x_2} + \frac{\partial u_3 N_u^4}{\partial x_3} \right)$$
$$C_u^{7,10} = C_u^{8,11} = C_u^{9,12} = N_u^3 \left(\frac{\partial u_1 N_u^4}{\partial x_1} + \frac{\partial u_2 N_u^4}{\partial x_2} + \frac{\partial u_3 N_u^4}{\partial x_3} \right)$$
$$C_u^{10,10} = C_u^{11,11} = C_u^{12,12} = N_u^4 \left(\frac{\partial u_1 N_u^4}{\partial x_1} + \frac{\partial u_2 N_u^4}{\partial x_2} + \frac{\partial u_3 N_u^4}{\partial x_3} \right) \tag{B.4}$$

The 12×12 symmetric diffusion matrix for the intermediate momentum is given as

$$\mathbf{K}_\tau = \frac{[(\nu + \nu_T)\rho]}{Re} \int_\Omega [K_\tau^{i,j}]\, d\Omega = \frac{[(\nu + \nu_T)\rho]}{Re} \int_\Omega \mathbf{B^T} \left(\mathbf{I_o} - \frac{2}{3}\mathbf{m}\mathbf{m^T} \right) \mathbf{B} d\Omega \tag{B.5}$$

where the matrix coefficients $\left[K_\tau^{i,j}\right]$ are

$$K_\tau^{1,1} = \frac{4}{3}\left(\frac{\partial N_u^1}{\partial x_1}\right)^2 + \left(\frac{\partial N_u^1}{\partial x_2}\right)^2 + \left(\frac{\partial N_u^1}{\partial x_3}\right)^2$$
$$K_\tau^{2,2} = \frac{4}{3}\left(\frac{\partial N_u^1}{\partial x_2}\right)^2 + \left(\frac{\partial N_u^1}{\partial x_1}\right)^2 + \left(\frac{\partial N_u^1}{\partial x_3}\right)^2$$
$$K_\tau^{3,3} = \frac{4}{3}\left(\frac{\partial N_u^1}{\partial x_3}\right)^2 + \left(\frac{\partial N_u^1}{\partial x_2}\right)^2 + \left(\frac{\partial N_u^1}{\partial x_1}\right)^2$$
$$K_\tau^{4,4} = \frac{4}{3}\left(\frac{\partial N_u^2}{\partial x_1}\right)^2 + \left(\frac{\partial N_u^2}{\partial x_2}\right)^2 + \left(\frac{\partial N_u^2}{\partial x_3}\right)^2$$
$$K_\tau^{5,5} = \frac{4}{3}\left(\frac{\partial N_u^2}{\partial x_2}\right)^2 + \left(\frac{\partial N_u^2}{\partial x_1}\right)^2 + \left(\frac{\partial N_u^2}{\partial x_3}\right)^2$$
$$K_\tau^{6,6} = \frac{4}{3}\left(\frac{\partial N_u^2}{\partial x_3}\right)^2 + \left(\frac{\partial N_u^2}{\partial x_2}\right)^2 + \left(\frac{\partial N_u^2}{\partial x_1}\right)^2$$
$$K_\tau^{7,7} = \frac{4}{3}\left(\frac{\partial N_u^3}{\partial x_1}\right)^2 + \left(\frac{\partial N_u^3}{\partial x_2}\right)^2 + \left(\frac{\partial N_u^3}{\partial x_3}\right)^2$$
$$K_\tau^{8,8} = \frac{4}{3}\left(\frac{\partial N_u^3}{\partial x_2}\right)^2 + \left(\frac{\partial N_u^3}{\partial x_1}\right)^2 + \left(\frac{\partial N_u^3}{\partial x_3}\right)^2$$
$$K_\tau^{9,9} = \frac{4}{3}\left(\frac{\partial N_u^3}{\partial x_3}\right)^2 + \left(\frac{\partial N_u^3}{\partial x_2}\right)^2 + \left(\frac{\partial N_u^3}{\partial x_1}\right)^2$$
$$K_\tau^{10,10} = \frac{4}{3}\left(\frac{\partial N_u^4}{\partial x_1}\right)^2 + \left(\frac{\partial N_u^4}{\partial x_2}\right)^2 + \left(\frac{\partial N_u^4}{\partial x_3}\right)^2$$
$$K_\tau^{11,11} = \frac{4}{3}\left(\frac{\partial N_u^4}{\partial x_2}\right)^2 + \left(\frac{\partial N_u^4}{\partial x_1}\right)^2 + \left(\frac{\partial N_u^4}{\partial x_3}\right)^2$$

$$K_\tau^{12,12} = \frac{4}{3}\left(\frac{\partial N_u^4}{\partial x_3}\right)^2 + \left(\frac{\partial N_u^4}{\partial x_2}\right)^2 + \left(\frac{\partial N_u^4}{\partial x_1}\right)^2$$

$$K_\tau^{1,2} = K_\tau^{2,1} = -\frac{2}{3}\frac{\partial N_u^1}{\partial x_1}\frac{\partial N_u^1}{\partial x_2} + \frac{\partial N_u^1}{\partial x_2}\frac{\partial N_u^1}{\partial x_1}$$

$$K_\tau^{1,3} = K_\tau^{3,1} = -\frac{2}{3}\frac{\partial N_u^1}{\partial x_1}\frac{\partial N_u^1}{\partial x_3} + \frac{\partial N_u^1}{\partial x_3}\frac{\partial N_u^1}{\partial x_1}$$

$$K_\tau^{1,4} = K_\tau^{4,1} = \frac{4}{3}\frac{\partial N_u^1}{\partial x_1}\frac{\partial N_u^2}{\partial x_1} + \frac{\partial N_u^1}{\partial x_2}\frac{\partial N_u^2}{\partial x_2} + \frac{\partial N_u^1}{\partial x_3}\frac{\partial N_u^2}{\partial x_3}$$

$$K_\tau^{1,5} = K_\tau^{5,1} = -\frac{2}{3}\frac{\partial N_u^1}{\partial x_1}\frac{\partial N_u^2}{\partial x_2} + \frac{\partial N_u^1}{\partial x_2}\frac{\partial N_u^2}{\partial x_1}$$

$$K_\tau^{1,6} = K_\tau^{6,1} = -\frac{2}{3}\frac{\partial N_u^1}{\partial x_1}\frac{\partial N_u^2}{\partial x_3} + \frac{\partial N_u^1}{\partial x_3}\frac{\partial N_u^2}{\partial x_1}$$

$$K_\tau^{1,7} = K_\tau^{7,1} = \frac{4}{3}\frac{\partial N_u^1}{\partial x_1}\frac{\partial N_u^3}{\partial x_1} + \frac{\partial N_u^1}{\partial x_2}\frac{\partial N_u^3}{\partial x_2} + \frac{\partial N_u^1}{\partial x_3}\frac{\partial N_u^3}{\partial x_3}$$

$$K_\tau^{1,8} = K_\tau^{8,1} = -\frac{2}{3}\frac{\partial N_u^1}{\partial x_1}\frac{\partial N_u^3}{\partial x_2} + \frac{\partial N_u^1}{\partial x_2}\frac{\partial N_u^3}{\partial x_1}$$

$$K_\tau^{1,9} = K_\tau^{9,1} = -\frac{2}{3}\frac{\partial N_u^1}{\partial x_1}\frac{\partial N_u^3}{\partial x_3} + \frac{\partial N_u^1}{\partial x_3}\frac{\partial N_u^3}{\partial x_1}$$

$$K_\tau^{1,10} = K_\tau^{10,1} = \frac{4}{3}\frac{\partial N_u^1}{\partial x_1}\frac{\partial N_u^4}{\partial x_1} + \frac{\partial N_u^1}{\partial x_2}\frac{\partial N_u^4}{\partial x_2} + \frac{\partial N_u^1}{\partial x_3}\frac{\partial N_u^4}{\partial x_3}$$

$$K_\tau^{1,11} = K_\tau^{11,1} = -\frac{2}{3}\frac{\partial N_u^1}{\partial x_1}\frac{\partial N_u^4}{\partial x_2} + \frac{\partial N_u^1}{\partial x_2}\frac{\partial N_u^4}{\partial x_1}$$

$$K_\tau^{1,12} = K_\tau^{12,1} = -\frac{2}{3}\frac{\partial N_u^1}{\partial x_1}\frac{\partial N_u^4}{\partial x_3} + \frac{\partial N_u^1}{\partial x_3}\frac{\partial N_u^4}{\partial x_1}$$

$$K_\tau^{2,3} = K_\tau^{3,2} = -\frac{2}{3}\frac{\partial N_u^1}{\partial x_2}\frac{\partial N_u^1}{\partial x_3} + \frac{\partial N_u^1}{\partial x_3}\frac{\partial N_u^1}{\partial x_2}$$

$$K_\tau^{2,4} = K_\tau^{4,2} = -\frac{2}{3}\frac{\partial N_u^1}{\partial x_2}\frac{\partial N_u^2}{\partial x_1} + \frac{\partial N_u^1}{\partial x_1}\frac{\partial N_u^2}{\partial x_2}$$

$$K_\tau^{2,5} = K_\tau^{5,2} = \frac{4}{3}\frac{\partial N_u^1}{\partial x_2}\frac{\partial N_u^2}{\partial x_2} + \frac{\partial N_u^1}{\partial x_1}\frac{\partial N_u^2}{\partial x_1} + \frac{\partial N_u^1}{\partial x_3}\frac{\partial N_u^2}{\partial x_3}$$

$$K_\tau^{2,6} = K_\tau^{6,2} = -\frac{2}{3}\frac{\partial N_u^1}{\partial x_2}\frac{\partial N_u^2}{\partial x_3} + \frac{\partial N_u^1}{\partial x_3}\frac{\partial N_u^2}{\partial x_2}$$

$$K_\tau^{2,7} = K_\tau^{7,2} = -\frac{2}{3}\frac{\partial N_u^1}{\partial x_2}\frac{\partial N_u^3}{\partial x_1} + \frac{\partial N_u^1}{\partial x_1}\frac{\partial N_u^3}{\partial x_2}$$

$$K_\tau^{2,8} = K_\tau^{8,2} = \frac{4}{3}\frac{\partial N_u^1}{\partial x_2}\frac{\partial N_u^3}{\partial x_2} + \frac{\partial N_u^1}{\partial x_1}\frac{\partial N_u^3}{\partial x_1} + \frac{\partial N_u^1}{\partial x_3}\frac{\partial N_u^3}{\partial x_3}$$

$$K_\tau^{2,9} = K_\tau^{9,2} = -\frac{2}{3}\frac{\partial N_u^1}{\partial x_2}\frac{\partial N_u^3}{\partial x_3} + \frac{\partial N_u^1}{\partial x_3}\frac{\partial N_u^3}{\partial x_2}$$

$$K_\tau^{2,10} = K_\tau^{10,2} = -\frac{2}{3}\frac{\partial N_u^1}{\partial x_2}\frac{\partial N_u^4}{\partial x_1} + \frac{\partial N_u^1}{\partial x_1}\frac{\partial N_u^4}{\partial x_2}$$

$$K_\tau^{2,11} = K_\tau^{11,2} = \frac{4}{3}\frac{\partial N_u^1}{\partial x_2}\frac{\partial N_u^4}{\partial x_2} + \frac{\partial N_u^1}{\partial x_1}\frac{\partial N_u^4}{\partial x_1} + \frac{\partial N_u^1}{\partial x_3}\frac{\partial N_u^4}{\partial x_3}$$
$$K_\tau^{2,12} = K_\tau^{12,2} = -\frac{2}{3}\frac{\partial N_u^1}{\partial x_2}\frac{\partial N_u^4}{\partial x_3} + \frac{\partial N_u^1}{\partial x_3}\frac{\partial N_u^4}{\partial x_2}$$
$$K_\tau^{3,4} = K_\tau^{4,3} = -\frac{2}{3}\frac{\partial N_u^1}{\partial x_3}\frac{\partial N_u^2}{\partial x_1} + \frac{\partial N_u^1}{\partial x_1}\frac{\partial N_u^2}{\partial x_3}$$
$$K_\tau^{3,5} = K_\tau^{5,3} = -\frac{2}{3}\frac{\partial N_u^1}{\partial x_3}\frac{\partial N_u^2}{\partial x_2} + \frac{\partial N_u^1}{\partial x_2}\frac{\partial N_u^2}{\partial x_3}$$
$$K_\tau^{3,6} = K_\tau^{6,3} = \frac{4}{3}\frac{\partial N_u^1}{\partial x_3}\frac{\partial N_u^2}{\partial x_3} + \frac{\partial N_u^1}{\partial x_2}\frac{\partial N_u^2}{\partial x_2} + \frac{\partial N_u^1}{\partial x_1}\frac{\partial N_u^2}{\partial x_1}$$
$$K_\tau^{3,7} = K_\tau^{7,3} = -\frac{2}{3}\frac{\partial N_u^1}{\partial x_3}\frac{\partial N_u^3}{\partial x_1} + \frac{\partial N_u^1}{\partial x_1}\frac{\partial N_u^3}{\partial x_3}$$
$$K_\tau^{3,8} = K_\tau^{8,3} = -\frac{2}{3}\frac{\partial N_u^1}{\partial x_3}\frac{\partial N_u^3}{\partial x_2} + \frac{\partial N_u^1}{\partial x_2}\frac{\partial N_u^3}{\partial x_3}$$
$$K_\tau^{3,9} = K_\tau^{9,3} = \frac{4}{3}\frac{\partial N_u^1}{\partial x_3}\frac{\partial N_u^3}{\partial x_3} + \frac{\partial N_u^1}{\partial x_2}\frac{\partial N_u^3}{\partial x_2} + \frac{\partial N_u^1}{\partial x_1}\frac{\partial N_u^3}{\partial x_1}$$
$$K_\tau^{3,10} = K_\tau^{10,3} = -\frac{2}{3}\frac{\partial N_u^1}{\partial x_3}\frac{\partial N_u^4}{\partial x_1} + \frac{\partial N_u^1}{\partial x_1}\frac{\partial N_u^4}{\partial x_3}$$
$$K_\tau^{3,11} = K_\tau^{11,3} = -\frac{2}{3}\frac{\partial N_u^1}{\partial x_3}\frac{\partial N_u^4}{\partial x_2} + \frac{\partial N_u^1}{\partial x_2}\frac{\partial N_u^4}{\partial x_3}$$
$$K_\tau^{3,12} = K_\tau^{12,3} = \frac{4}{3}\frac{\partial N_u^1}{\partial x_3}\frac{\partial N_u^4}{\partial x_3} + \frac{\partial N_u^1}{\partial x_2}\frac{\partial N_u^4}{\partial x_2} + \frac{\partial N_u^1}{\partial x_1}\frac{\partial N_u^4}{\partial x_1}$$
$$K_\tau^{4,5} = K_\tau^{5,4} = -\frac{2}{3}\frac{\partial N_u^2}{\partial x_1}\frac{\partial N_u^2}{\partial x_2} + \frac{\partial N_u^2}{\partial x_2}\frac{\partial N_u^2}{\partial x_1}$$
$$K_\tau^{4,6} = K_\tau^{6,4} = -\frac{2}{3}\frac{\partial N_u^2}{\partial x_1}\frac{\partial N_u^2}{\partial x_3} + \frac{\partial N_u^2}{\partial x_3}\frac{\partial N_u^2}{\partial x_1}$$
$$K_\tau^{4,7} = K_\tau^{7,4} = \frac{4}{3}\frac{\partial N_u^2}{\partial x_1}\frac{\partial N_u^3}{\partial x_1} + \frac{\partial N_u^2}{\partial x_2}\frac{\partial N_u^3}{\partial x_2} + \frac{\partial N_u^2}{\partial x_3}\frac{\partial N_u^3}{\partial x_3}$$
$$K_\tau^{4,8} = K_\tau^{8,4} = -\frac{2}{3}\frac{\partial N_u^2}{\partial x_1}\frac{\partial N_u^3}{\partial x_2} + \frac{\partial N_u^2}{\partial x_2}\frac{\partial N_u^3}{\partial x_1}$$
$$K_\tau^{4,9} = K_\tau^{9,4} = -\frac{2}{3}\frac{\partial N_u^2}{\partial x_1}\frac{\partial N_u^3}{\partial x_3} + \frac{\partial N_u^2}{\partial x_3}\frac{\partial N_u^3}{\partial x_1}$$
$$K_\tau^{4,10} = K_\tau^{10,4} = \frac{4}{3}\frac{\partial N_u^2}{\partial x_1}\frac{\partial N_u^4}{\partial x_1} + \frac{\partial N_u^2}{\partial x_2}\frac{\partial N_u^4}{\partial x_2} + \frac{\partial N_u^2}{\partial x_3}\frac{\partial N_u^4}{\partial x_3}$$
$$K_\tau^{4,11} = K_\tau^{11,4} = -\frac{2}{3}\frac{\partial N_u^2}{\partial x_1}\frac{\partial N_u^4}{\partial x_2} + \frac{\partial N_u^2}{\partial x_2}\frac{\partial N_u^4}{\partial x_1}$$
$$K_\tau^{4,12} = K_\tau^{12,4} = -\frac{2}{3}\frac{\partial N_u^2}{\partial x_1}\frac{\partial N_u^4}{\partial x_3} + \frac{\partial N_u^2}{\partial x_3}\frac{\partial N_u^4}{\partial x_1}$$
$$K_\tau^{5,6} = K_\tau^{6,5} = -\frac{2}{3}\frac{\partial N_u^2}{\partial x_2}\frac{\partial N_u^2}{\partial x_3} + \frac{\partial N_u^2}{\partial x_3}\frac{\partial N_u^2}{\partial x_2}$$

$$K_\tau^{5,7} = K_\tau^{7,5} = -\frac{2}{3}\frac{\partial N_u^2}{\partial x_2}\frac{\partial N_u^3}{\partial x_1} + \frac{\partial N_u^2}{\partial x_1}\frac{\partial N_u^3}{\partial x_2}$$

$$K_\tau^{5,8} = K_\tau^{8,5} = \frac{4}{3}\frac{\partial N_u^2}{\partial x_2}\frac{\partial N_u^3}{\partial x_2} + \frac{\partial N_u^2}{\partial x_1}\frac{\partial N_u^3}{\partial x_1} + \frac{\partial N_u^2}{\partial x_3}\frac{\partial N_u^3}{\partial x_3}$$

$$K_\tau^{5,9} = K_\tau^{9,5} = -\frac{2}{3}\frac{\partial N_u^2}{\partial x_2}\frac{\partial N_u^3}{\partial x_3} + \frac{\partial N_u^2}{\partial x_3}\frac{\partial N_u^3}{\partial x_2}$$

$$K_\tau^{5,10} = K_\tau^{10,5} = -\frac{2}{3}\frac{\partial N_u^2}{\partial x_2}\frac{\partial N_u^4}{\partial x_1} + \frac{\partial N_u^2}{\partial x_1}\frac{\partial N_u^4}{\partial x_2}$$

$$K_\tau^{5,11} = K_\tau^{11,5} = \frac{4}{3}\frac{\partial N_u^2}{\partial x_2}\frac{\partial N_u^4}{\partial x_2} + \frac{\partial N_u^2}{\partial x_1}\frac{\partial N_u^4}{\partial x_1} + \frac{\partial N_u^2}{\partial x_3}\frac{\partial N_u^4}{\partial x_3}$$

$$K_\tau^{5,12} = K_\tau^{12,5} = -\frac{2}{3}\frac{\partial N_u^2}{\partial x_2}\frac{\partial N_u^4}{\partial x_3} + \frac{\partial N_u^2}{\partial x_3}\frac{\partial N_u^4}{\partial x_2}$$

$$K_\tau^{6,7} = K_\tau^{7,6} = -\frac{2}{3}\frac{\partial N_u^2}{\partial x_3}\frac{\partial N_u^3}{\partial x_1} + \frac{\partial N_u^2}{\partial x_1}\frac{\partial N_u^3}{\partial x_3}$$

$$K_\tau^{6,8} = K_\tau^{8,6} = -\frac{2}{3}\frac{\partial N_u^2}{\partial x_3}\frac{\partial N_u^3}{\partial x_2} + \frac{\partial N_u^2}{\partial x_2}\frac{\partial N_u^3}{\partial x_3}$$

$$K_\tau^{6,9} = K_\tau^{9,6} = \frac{4}{3}\frac{\partial N_u^2}{\partial x_3}\frac{\partial N_u^3}{\partial x_3} + \frac{\partial N_u^2}{\partial x_2}\frac{\partial N_u^3}{\partial x_2} + \frac{\partial N_u^2}{\partial x_1}\frac{\partial N_u^3}{\partial x_1}$$

$$K_\tau^{6,10} = K_\tau^{10,6} = -\frac{2}{3}\frac{\partial N_u^2}{\partial x_3}\frac{\partial N_u^4}{\partial x_1} + \frac{\partial N_u^2}{\partial x_1}\frac{\partial N_u^4}{\partial x_3}$$

$$K_\tau^{6,11} = K_\tau^{11,6} = -\frac{2}{3}\frac{\partial N_u^2}{\partial x_3}\frac{\partial N_u^4}{\partial x_2} + \frac{\partial N_u^2}{\partial x_2}\frac{\partial N_u^4}{\partial x_3}$$

$$K_\tau^{6,12} = K_\tau^{12,6} = \frac{4}{3}\frac{\partial N_u^2}{\partial x_3}\frac{\partial N_u^4}{\partial x_3} + \frac{\partial N_u^2}{\partial x_2}\frac{\partial N_u^4}{\partial x_2} + \frac{\partial N_u^2}{\partial x_1}\frac{\partial N_u^4}{\partial x_1}$$

$$K_\tau^{7,8} = K_\tau^{8,7} = -\frac{2}{3}\frac{\partial N_u^3}{\partial x_1}\frac{\partial N_u^3}{\partial x_2} + \frac{\partial N_u^3}{\partial x_2}\frac{\partial N_u^3}{\partial x_1}$$

$$K_\tau^{7,9} = K_\tau^{9,7} = -\frac{2}{3}\frac{\partial N_u^3}{\partial x_1}\frac{\partial N_u^3}{\partial x_3} + \frac{\partial N_u^3}{\partial x_3}\frac{\partial N_u^3}{\partial x_1}$$

$$K_\tau^{7,10} = K_\tau^{10,7} = \frac{4}{3}\frac{\partial N_u^3}{\partial x_1}\frac{\partial N_u^4}{\partial x_1} + \frac{\partial N_u^3}{\partial x_2}\frac{\partial N_u^4}{\partial x_2} + \frac{\partial N_u^3}{\partial x_3}\frac{\partial N_u^4}{\partial x_3}$$

$$K_\tau^{7,11} = K_\tau^{11,7} = -\frac{2}{3}\frac{\partial N_u^3}{\partial x_1}\frac{\partial N_u^4}{\partial x_2} + \frac{\partial N_u^3}{\partial x_2}\frac{\partial N_u^4}{\partial x_1}$$

$$K_\tau^{7,12} = K_\tau^{12,7} = -\frac{2}{3}\frac{\partial N_u^3}{\partial x_1}\frac{\partial N_u^4}{\partial x_3} + \frac{\partial N_u^3}{\partial x_3}\frac{\partial N_u^4}{\partial x_1}$$

$$K_\tau^{8,9} = K_\tau^{9,8} = -\frac{2}{3}\frac{\partial N_u^3}{\partial x_2}\frac{\partial N_u^3}{\partial x_3} + \frac{\partial N_u^3}{\partial x_3}\frac{\partial N_u^3}{\partial x_2}$$

$$K_\tau^{8,10} = K_\tau^{10,8} = -\frac{2}{3}\frac{\partial N_u^3}{\partial x_2}\frac{\partial N_u^4}{\partial x_1} + \frac{\partial N_u^3}{\partial x_1}\frac{\partial N_u^4}{\partial x_2}$$

$$K_\tau^{8,11} = K_\tau^{11,8} = \frac{4}{3}\frac{\partial N_u^3}{\partial x_2}\frac{\partial N_u^4}{\partial x_2} + \frac{\partial N_u^3}{\partial x_1}\frac{\partial N_u^4}{\partial x_1} + \frac{\partial N_u^3}{\partial x_3}\frac{\partial N_u^4}{\partial x_3}$$

$$K_\tau^{8,12} = K_\tau^{12,8} = -\frac{2}{3}\frac{\partial N_u^3}{\partial x_2}\frac{\partial N_u^4}{\partial x_3} + \frac{\partial N_u^3}{\partial x_3}\frac{\partial N_u^4}{\partial x_2}$$
$$K_\tau^{9,10} = K_\tau^{10,9} = -\frac{2}{3}\frac{\partial N_u^3}{\partial x_3}\frac{\partial N_u^4}{\partial x_1} + \frac{\partial N_u^3}{\partial x_1}\frac{\partial N_u^4}{\partial x_3}$$
$$K_\tau^{9,11} = K_\tau^{11,9} = -\frac{2}{3}\frac{\partial N_u^3}{\partial x_3}\frac{\partial N_u^4}{\partial x_2} + \frac{\partial N_u^3}{\partial x_2}\frac{\partial N_u^4}{\partial x_3}$$
$$K_\tau^{9,12} = K_\tau^{12,9} = \frac{4}{3}\frac{\partial N_u^3}{\partial x_3}\frac{\partial N_u^4}{\partial x_3} + \frac{\partial N_u^3}{\partial x_2}\frac{\partial N_u^4}{\partial x_2} + \frac{\partial N_u^3}{\partial x_1}\frac{\partial N_u^4}{\partial x_1}$$
$$K_\tau^{10,11} = K_\tau^{11,10} = -\frac{2}{3}\frac{\partial N_u^4}{\partial x_1}\frac{\partial N_u^4}{\partial x_2} + \frac{\partial N_u^4}{\partial x_2}\frac{\partial N_u^4}{\partial x_1}$$
$$K_\tau^{10,12} = K_\tau^{12,10} = -\frac{2}{3}\frac{\partial N_u^4}{\partial x_1}\frac{\partial N_u^4}{\partial x_3} + \frac{\partial N_u^4}{\partial x_3}\frac{\partial N_u^4}{\partial x_1}$$
$$K_\tau^{11,12} = K_\tau^{12,11} = -\frac{2}{3}\frac{\partial N_u^4}{\partial x_2}\frac{\partial N_u^4}{\partial x_3} + \frac{\partial N_u^4}{\partial x_3}\frac{\partial N_u^4}{\partial x_2} \tag{B.6}$$

The 12 × 12 matrix of the isotropic turbulence for the intermediate momentum is given as

$$\mathbf{C_{u\kappa}} = \frac{2}{3}\int_\Omega \left[C_{u\kappa}^{i,j}\right] d\Omega = \frac{2}{3}\int_\Omega \mathbf{N_u}^T \nabla \mathbf{N}_\kappa d\Omega \tag{B.7}$$

where the matrix coefficients $\left[C_{u\kappa}^{i,j}\right]$ are

$$\begin{aligned}
C_{u\kappa}^{1,2} &= C_{u\kappa}^{2,1} = C_{u\kappa}^{1,3} = C_{u\kappa}^{3,1} = C_{u\kappa}^{1,5} = C_{u\kappa}^{5,1} = C_{u\kappa}^{1,6} = C_{u\kappa}^{6,1} = C_{u\kappa}^{1,8} = \\
&= C_{u\kappa}^{8,1} = C_{u\kappa}^{1,9} = C_{u\kappa}^{9,1} = C_{u\kappa}^{1,11} = C_{u\kappa}^{11,1} = C_{u\kappa}^{1,12} = C_{u\kappa}^{12,1} = C_{u\kappa}^{2,3} = C_{u\kappa}^{3,2} = \\
&= C_{u\kappa}^{2,4} = C_{u\kappa}^{4,2} = C_{u\kappa}^{2,6} = C_{u\kappa}^{6,2} = C_{u\kappa}^{2,7} = C_{u\kappa}^{7,2} = C_{u\kappa}^{2,9} = C_{u\kappa}^{9,2} = C_{u\kappa}^{2,10} = \\
&= C_{u\kappa}^{10,2} = C_{u\kappa}^{2,12} = C_{u\kappa}^{12,2} = C_{u\kappa}^{3,4} = C_{u\kappa}^{4,3} = C_{u\kappa}^{3,5} = C_{u\kappa}^{5,3} = C_{u\kappa}^{3,7} = C_{u\kappa}^{7,3} = \\
&= C_{u\kappa}^{3,8} = C_{u\kappa}^{8,3} = C_{u\kappa}^{3,10} = C_{u\kappa}^{10,3} = C_{u\kappa}^{3,11} = C_{u\kappa}^{11,3} = C_{u\kappa}^{4,5} = C_{u\kappa}^{5,4} = C_{u\kappa}^{4,6} = \\
&= C_{u\kappa}^{6,4} = C_{u\kappa}^{4,8} = C_{u\kappa}^{8,4} = C_{u\kappa}^{4,9} = C_{u\kappa}^{9,4} = C_{u\kappa}^{4,11} = C_{u\kappa}^{11,4} = C_{u\kappa}^{4,12} = C_{u\kappa}^{12,4} = \\
&= C_{u\kappa}^{5,6} = C_{u\kappa}^{6,5} = C_{u\kappa}^{5,7} = C_{u\kappa}^{7,5} = C_{u\kappa}^{5,9} = C_{u\kappa}^{9,5} = C_{u\kappa}^{5,10} = C_{u\kappa}^{10,5} = C_{u\kappa}^{5,12} = \\
&= C_{u\kappa}^{12,5} = C_{u\kappa}^{6,7} = C_{u\kappa}^{7,6} = C_{u\kappa}^{6,8} = C_{u\kappa}^{8,6} = C_{u\kappa}^{6,10} = C_{u\kappa}^{10,6} = C_{u\kappa}^{6,11} = C_{u\kappa}^{11,6} = \\
&= C_{u\kappa}^{7,8} = C_{u\kappa}^{8,7} = C_{u\kappa}^{7,9} = C_{u\kappa}^{9,7} = C_{u\kappa}^{7,11} = C_{u\kappa}^{11,7} = C_{u\kappa}^{7,12} = C_{u\kappa}^{12,7} = C_{u\kappa}^{8,9} = \\
&= C_{u\kappa}^{9,8} = C_{u\kappa}^{8,10} = C_{u\kappa}^{10,8} = C_{u\kappa}^{8,12} = C_{u\kappa}^{12,8} = C_{u\kappa}^{9,10} = C_{u\kappa}^{10,9} = C_{u\kappa}^{9,11} = C_{u\kappa}^{11,9} = \\
&= C_{u\kappa}^{10,11} = C_{u\kappa}^{11,10} = C_{u\kappa}^{10,12} = C_{u\kappa}^{12,10} = C_{u\kappa}^{11,12} = C_{u\kappa}^{12,11} = 0
\end{aligned}$$

$$
\begin{aligned}
&C_{u\kappa}^{1,1} = N_u^1 \frac{\partial N_\kappa^1}{\partial x_1}; \quad C_{u\kappa}^{1,4} = N_u^1 \frac{\partial N_\kappa^2}{\partial x_1}; \quad C_{u\kappa}^{1,7} = N_u^1 \frac{\partial N_\kappa^3}{\partial x_1}; \quad C_{u\kappa}^{1,10} = N_u^1 \frac{\partial N_\kappa^4}{\partial x_1} \\
&C_{u\kappa}^{2,2} = N_u^1 \frac{\partial N_\kappa^1}{\partial x_2}; \quad C_{u\kappa}^{2,5} = N_u^1 \frac{\partial N_\kappa^2}{\partial x_2}; \quad C_{u\kappa}^{2,8} = N_u^1 \frac{\partial N_\kappa^3}{\partial x_2}; \quad C_{u\kappa}^{2,11} = N_u^1 \frac{\partial N_\kappa^4}{\partial x_2} \\
&C_{u\kappa}^{3,3} = N_u^1 \frac{\partial N_\kappa^1}{\partial x_3}; \quad C_{u\kappa}^{3,6} = N_u^1 \frac{\partial N_\kappa^2}{\partial x_3}; \quad C_{u\kappa}^{3,9} = N_u^1 \frac{\partial N_\kappa^3}{\partial x_3}; \quad C_{u\kappa}^{3,12} = N_u^1 \frac{\partial N_\kappa^4}{\partial x_3} \\
&C_{u\kappa}^{4,1} = N_u^2 \frac{\partial N_\kappa^1}{\partial x_1}; \quad C_{u\kappa}^{4,4} = N_u^2 \frac{\partial N_\kappa^2}{\partial x_1}; \quad C_{u\kappa}^{4,7} = N_u^2 \frac{\partial N_\kappa^3}{\partial x_1}; \quad C_{u\kappa}^{4,10} = N_u^2 \frac{\partial N_\kappa^4}{\partial x_1} \\
&C_{u\kappa}^{5,2} = N_u^2 \frac{\partial N_\kappa^1}{\partial x_2}; \quad C_{u\kappa}^{5,5} = N_u^2 \frac{\partial N_\kappa^2}{\partial x_2}; \quad C_{u\kappa}^{5,8} = N_u^2 \frac{\partial N_\kappa^3}{\partial x_2}; \quad C_{u\kappa}^{5,11} = N_u^2 \frac{\partial N_\kappa^4}{\partial x_2} \\
&C_{u\kappa}^{6,3} = N_u^2 \frac{\partial N_\kappa^1}{\partial x_3}; \quad C_{u\kappa}^{6,6} = N_u^2 \frac{\partial N_\kappa^2}{\partial x_3}; \quad C_{u\kappa}^{6,9} = N_u^2 \frac{\partial N_\kappa^3}{\partial x_3}; \quad C_{u\kappa}^{6,12} = N_u^2 \frac{\partial N_\kappa^4}{\partial x_3} \\
&C_{u\kappa}^{7,1} = N_u^3 \frac{\partial N_\kappa^1}{\partial x_1}; \quad C_{u\kappa}^{7,4} = N_u^3 \frac{\partial N_\kappa^2}{\partial x_1}; \quad C_{u\kappa}^{7,7} = N_u^3 \frac{\partial N_\kappa^3}{\partial x_1}; \quad C_{u\kappa}^{7,10} = N_u^3 \frac{\partial N_\kappa^4}{\partial x_1} \\
&C_{u\kappa}^{8,2} = N_u^3 \frac{\partial N_\kappa^1}{\partial x_2}; \quad C_{u\kappa}^{8,5} = N_u^3 \frac{\partial N_\kappa^2}{\partial x_2}; \quad C_{u\kappa}^{8,8} = N_u^3 \frac{\partial N_\kappa^3}{\partial x_2}; \quad C_{u\kappa}^{8,11} = N_u^3 \frac{\partial N_\kappa^4}{\partial x_2} \\
&C_{u\kappa}^{9,3} = N_u^3 \frac{\partial N_\kappa^1}{\partial x_3}; \quad C_{u\kappa}^{9,6} = N_u^3 \frac{\partial N_\kappa^2}{\partial x_3}; \quad C_{u\kappa}^{9,9} = N_u^3 \frac{\partial N_\kappa^3}{\partial x_3}; \quad C_{u\kappa}^{9,12} = N_u^3 \frac{\partial N_\kappa^4}{\partial x_3} \\
&C_{u\kappa}^{10,1} = N_u^4 \frac{\partial N_\kappa^1}{\partial x_1}; \quad C_{u\kappa}^{10,4} = N_u^4 \frac{\partial N_\kappa^2}{\partial x_1}; \quad C_{u\kappa}^{10,7} = N_u^4 \frac{\partial N_\kappa^3}{\partial x_1}; \quad C_{u\kappa}^{10,10} = N_u^4 \frac{\partial N_\kappa^4}{\partial x_1} \\
&C_{u\kappa}^{11,2} = N_u^4 \frac{\partial N_\kappa^1}{\partial x_2}; \quad C_{u\kappa}^{11,5} = N_u^4 \frac{\partial N_\kappa^2}{\partial x_2}; \quad C_{u\kappa}^{11,8} = N_u^4 \frac{\partial N_\kappa^3}{\partial x_2}; \quad C_{u\kappa}^{11,11} = N_u^4 \frac{\partial N_\kappa^4}{\partial x_2} \\
&C_{u\kappa}^{12,3} = N_u^4 \frac{\partial N_\kappa^1}{\partial x_3}; \quad C_{u\kappa}^{12,6} = N_u^4 \frac{\partial N_\kappa^2}{\partial x_3}; \quad C_{u\kappa}^{12,9} = N_u^4 \frac{\partial N_\kappa^3}{\partial x_3}; \quad C_{u\kappa}^{12,12} = N_u^4 \frac{\partial N_\kappa^4}{\partial x_3}
\end{aligned} \tag{B.8}
$$

The 12×1 traction vector for the intermediate momentum is given as

$$
\mathbf{f_u} = \frac{[(\nu + \nu_t)\rho]}{Re} \int_\Gamma \left[f_u^{i,j}\right] d\Gamma = \int_\Gamma \mathbf{N_u}^T \mathbf{t_d} d\Gamma \tag{B.9}
$$

In the above equation a matrix of shape functions defined as

$$
\mathbf{N_u} = \begin{bmatrix} N_u^1 & 0 & 0 & N_u^2 & 0 & 0 & N_u^3 & 0 & 0 & N_u^4 & 0 & 0 \\ 0 & N_u^1 & 0 & 0 & N_u^2 & 0 & 0 & N_u^3 & 0 & 0 & N_u^4 & 0 \\ 0 & 0 & N_u^1 & 0 & 0 & N_u^2 & 0 & 0 & N_u^3 & 0 & 0 & N_u^4 \end{bmatrix} \tag{B.10}
$$

and the traction is

$$\mathbf{t_d} = \frac{(\nu + \nu_T)\,\rho}{Re} \begin{bmatrix} t_d^1 \\ t_d^2 \\ t_d^3 \end{bmatrix} \tag{B.11}$$

where

$$\begin{aligned}
t_d^1 \;=\; & \frac{4}{3}\left(u_1^1\frac{\partial N_u^1}{\partial x_1} + u_1^2\frac{\partial N_u^2}{\partial x_1} + u_1^3\frac{\partial N_u^3}{\partial x_1} + u_1^4\frac{\partial N_u^4}{\partial x_1}\right)\hat{n}_{x_1} - \\
- \; & \frac{2}{3}\left(u_2^1\frac{\partial N_u^1}{\partial x_2} + u_2^2\frac{\partial N_u^2}{\partial x_2} + u_2^3\frac{\partial N_u^3}{\partial x_2} + u_2^4\frac{\partial N_u^4}{\partial x_2}\right)\hat{n}_{x_1} - \\
- \; & \frac{2}{3}\left(u_3^1\frac{\partial N_u^1}{\partial x_3} + u_3^2\frac{\partial N_u^2}{\partial x_3} + u_3^3\frac{\partial N_u^3}{\partial x_3} + u_3^4\frac{\partial N_u^4}{\partial x_3}\right)\hat{n}_{x_1} + \\
+ \; & \left(u_2^1\frac{\partial N_u^1}{\partial x_1} + u_2^2\frac{\partial N_u^2}{\partial x_1} + u_2^3\frac{\partial N_u^3}{\partial x_1} + u_2^4\frac{\partial N_u^4}{\partial x_1}\right)\hat{n}_{x_2} + \\
+ \; & \left(u_1^1\frac{\partial N_u^1}{\partial x_2} + u_1^2\frac{\partial N_u^2}{\partial x_2} + u_1^3\frac{\partial N_u^3}{\partial x_2} + u_1^4\frac{\partial N_u^4}{\partial x_2}\right)\hat{n}_{x_2} + \\
+ \; & \left(u_3^1\frac{\partial N_u^1}{\partial x_1} + u_3^2\frac{\partial N_u^2}{\partial x_1} + u_3^3\frac{\partial N_u^3}{\partial x_1} + u_3^4\frac{\partial N_u^4}{\partial x_1}\right)\hat{n}_{x_3} + \\
+ \; & \left(u_1^1\frac{\partial N_u^1}{\partial x_3} + u_1^2\frac{\partial N_u^2}{\partial x_3} + u_1^3\frac{\partial N_u^3}{\partial x_3} + u_1^4\frac{\partial N_u^4}{\partial x_3}\right)\hat{n}_{x_3} \\
t_d^2 \;=\; & \frac{4}{3}\left(u_2^1\frac{\partial N_u^1}{\partial x_2} + u_2^2\frac{\partial N_u^2}{\partial x_2} + u_2^3\frac{\partial N_u^3}{\partial x_2} + u_2^4\frac{\partial N_u^4}{\partial x_2}\right)\hat{n}_{x_1} - \\
- \; & \frac{2}{3}\left(u_1^1\frac{\partial N_u^1}{\partial x_1} + u_1^2\frac{\partial N_u^2}{\partial x_1} + u_1^3\frac{\partial N_u^3}{\partial x_1} + u_1^4\frac{\partial N_u^4}{\partial x_1}\right)\hat{n}_{x_1} - \\
- \; & \frac{2}{3}\left(u_3^1\frac{\partial N_u^1}{\partial x_3} + u_3^2\frac{\partial N_u^2}{\partial x_3} + u_3^3\frac{\partial N_u^3}{\partial x_3} + u_3^4\frac{\partial N_u^4}{\partial x_3}\right)\hat{n}_{x_1} + \\
+ \; & \left(u_1^1\frac{\partial N_u^1}{\partial x_2} + u_1^2\frac{\partial N_u^2}{\partial x_2} + u_1^3\frac{\partial N_u^3}{\partial x_2} + u_1^4\frac{\partial N_u^4}{\partial x_2}\right)\hat{n}_{x_2} + \\
+ \; & \left(u_2^1\frac{\partial N_u^1}{\partial x_1} + u_2^2\frac{\partial N_u^2}{\partial x_1} + u_2^3\frac{\partial N_u^3}{\partial x_1} + u_2^4\frac{\partial N_u^4}{\partial x_1}\right)\hat{n}_{x_2} + \\
+ \; & \left(u_3^1\frac{\partial N_u^1}{\partial x_2} + u_3^2\frac{\partial N_u^2}{\partial x_2} + u_3^3\frac{\partial N_u^3}{\partial x_2} + u_3^4\frac{\partial N_u^4}{\partial x_2}\right)\hat{n}_{x_3} + \\
+ \; & \left(u_2^1\frac{\partial N_u^1}{\partial x_3} + u_2^2\frac{\partial N_u^2}{\partial x_3} + u_2^3\frac{\partial N_u^3}{\partial x_3} + u_2^4\frac{\partial N_u^4}{\partial x_3}\right)\hat{n}_{x_3}
\end{aligned}$$

$$\begin{aligned}
t_d^3 &= \frac{4}{3}\left(u_3^1\frac{\partial N_u^1}{\partial x_3}+u_3^2\frac{\partial N_u^2}{\partial x_3}+u_3^3\frac{\partial N_u^3}{\partial x_3}+u_3^4\frac{\partial N_u^4}{\partial x_3}\right)\hat{n}_{x_1} - \\
&- \frac{2}{3}\left(u_1^1\frac{\partial N_u^1}{\partial x_1}+u_1^2\frac{\partial N_u^2}{\partial x_1}+u_1^3\frac{\partial N_u^3}{\partial x_1}+u_1^4\frac{\partial N_u^4}{\partial x_1}\right)\hat{n}_{x_1} - \\
&- \frac{2}{3}\left(u_2^1\frac{\partial N_u^1}{\partial x_2}+u_2^2\frac{\partial N_u^2}{\partial x_2}+u_2^3\frac{\partial N_u^3}{\partial x_2}+u_2^4\frac{\partial N_u^4}{\partial x_2}\right)\hat{n}_{x_1} + \\
&+ \left(u_1^1\frac{\partial N_u^1}{\partial x_3}+u_1^2\frac{\partial N_u^2}{\partial x_3}+u_1^3\frac{\partial N_u^3}{\partial x_3}+u_1^4\frac{\partial N_u^4}{\partial x_3}\right)\hat{n}_{x_2} + \\
&+ \left(u_3^1\frac{\partial N_u^1}{\partial x_1}+u_3^2\frac{\partial N_u^2}{\partial x_1}+u_3^3\frac{\partial N_u^3}{\partial x_1}+u_3^4\frac{\partial N_u^4}{\partial x_1}\right)\hat{n}_{x_2} + \\
&+ \left(u_2^1\frac{\partial N_u^1}{\partial x_3}+u_2^2\frac{\partial N_u^2}{\partial x_3}+u_2^3\frac{\partial N_u^3}{\partial x_3}+u_2^4\frac{\partial N_u^4}{\partial x_3}\right)\hat{n}_{x_3} + \\
&+ \left(u_3^1\frac{\partial N_u^1}{\partial x_2}+u_3^2\frac{\partial N_u^2}{\partial x_2}+u_3^3\frac{\partial N_u^3}{\partial x_2}+u_3^4\frac{\partial N_u^4}{\partial x_2}\right)\hat{n}_{x_3} \qquad \text{(B.12)}
\end{aligned}$$

where both $\hat{n}_{x_1}$, $\hat{n}_{x_2}$ and $\hat{n}_{x_3}$ are normal vectors.

The 12×12 symmetric convection matrix of the stabilization for the intermediate momentum is given as

$$\mathbf{K_u} = -\frac{1}{2}\int_\Omega [K_u^{i,j}]\, d\Omega = -\frac{1}{2}\int_\Omega (\nabla^T(\mathbf{uN_u}))^T(\nabla^T(\mathbf{uN_u}))d\Omega \qquad \text{(B.13)}$$

where

$$(\nabla^T(\mathbf{u}\mathbf{N_u}))^T = \begin{bmatrix} \frac{\partial u_1 N_u^1}{\partial x_1} + \frac{\partial u_2 N_u^1}{\partial x_2} + \frac{\partial u_3 N_u^1}{\partial x_3} & 0 & 0 \\ 0 & \frac{\partial u_1 N_u^1}{\partial x_1} + \frac{\partial u_2 N_u^1}{\partial x_2} + \frac{\partial u_3 N_u^1}{\partial x_3} & 0 \\ 0 & 0 & \frac{\partial u_1 N_u^1}{\partial x_1} + \frac{\partial u_2 N_u^1}{\partial x_2} + \frac{\partial u_3 N_u^1}{\partial x_3} \\ \frac{\partial u_1 N_u^2}{\partial x_1} + \frac{\partial u_2 N_u^2}{\partial x_2} + \frac{\partial u_3 N_u^2}{\partial x_3} & 0 & 0 \\ 0 & \frac{\partial u_1 N_u^2}{\partial x_1} + \frac{\partial u_2 N_u^2}{\partial x_2} + \frac{\partial u_3 N_u^2}{\partial x_3} & 0 \\ 0 & 0 & \frac{\partial u_1 N_u^2}{\partial x_1} + \frac{\partial u_2 N_u^2}{\partial x_2} + \frac{\partial u_3 N_u^2}{\partial x_3} \\ \frac{\partial u_1 N_u^3}{\partial x_1} + \frac{\partial u_2 N_u^3}{\partial x_2} + \frac{\partial u_3 N_u^3}{\partial x_3} & 0 & 0 \\ 0 & \frac{\partial u_1 N_u^3}{\partial x_1} + \frac{\partial u_2 N_u^3}{\partial x_2} + \frac{\partial u_3 N_u^3}{\partial x_3} & 0 \\ 0 & 0 & \frac{\partial u_1 N_u^3}{\partial x_1} + \frac{\partial u_2 N_u^3}{\partial x_2} + \frac{\partial u_3 N_u^3}{\partial x_3} \\ \frac{\partial u_1 N_u^4}{\partial x_1} + \frac{\partial u_2 N_u^4}{\partial x_2} + \frac{\partial u_3 N_u^4}{\partial x_3} & 0 & 0 \\ 0 & \frac{\partial u_1 N_u^4}{\partial x_1} + \frac{\partial u_2 N_u^4}{\partial x_2} + \frac{\partial u_3 N_u^4}{\partial x_3} & 0 \\ 0 & 0 & \frac{\partial u_1 N_u^4}{\partial x_1} + \frac{\partial u_2 N_u^4}{\partial x_2} + \frac{\partial u_3 N_u^4}{\partial x_3} \end{bmatrix} \tag{B.14}$$

The 4×4 symmetric, lumped mass matrix for the pressure is given as

$$\mathbf{M_p} = \left(\frac{1}{\beta^2}\right)^n \int_\Omega \left[M_p^{i,j}\right] d\Omega = \int_\Omega \mathbf{N_p^T} \left(\frac{1}{\beta^2}\right)^n \mathbf{N_p} d\Omega \tag{B.15}$$

where

$$\mathbf{N_p} = \begin{bmatrix} N_p^1 & N_p^2 & N_p^3 & N_p^4 \end{bmatrix}^T \tag{B.16}$$

The 4×4 symmetric, second lumped mass matrix for the pressure is given as

$$\mathbf{H} = \int_\Omega \left[H^{i,j}\right] d\Omega = \int_\Omega (\nabla \mathbf{N_p})^T \nabla \mathbf{N_p} d\Omega \tag{B.17}$$

and the 4×12 gradient (operator) matrix is given as

$$\mathbf{G} = \int_\Omega \left[G^{i,j}\right] d\Omega = \int_\Omega (\nabla \mathbf{N_p})^T \mathbf{N_u} d\Omega \tag{B.18}$$

where

$$\nabla \mathbf{N_p} = \left\{ \begin{array}{c} \frac{\partial}{\partial x_1} \\ \frac{\partial}{\partial x_2} \\ \frac{\partial}{\partial x_3} \end{array} \right\} \left[\begin{array}{cccc} N_p^1 & N_p^2 & N_p^3 & N_p^4 \end{array} \right] \tag{B.19}$$

The 4×1 forcing vector for the pressure is given as

$$\mathbf{f_p} = \Delta t \int_\Gamma [f_p^{i,j}]\, d\Gamma = \Delta t \int_\Gamma \mathbf{N_p^T} \left[\mathbf{N_u} \tilde{\mathbf{U}}^\mathbf{n} + \theta_1 \left(\Delta \tilde{\mathbf{U}}^* - \Delta t \nabla p^{n+\theta_2} \right) \right] \mathbf{n^T} d\Gamma \tag{B.20}$$

where the vector coefficients $\left[f_p^{i,j} \right]$ are

$$\begin{aligned}
f_p^{1,1} &= N_p^1 \left(N_u^1 \tilde{U}_1^1 + N_u^2 \tilde{U}_1^2 + N_u^3 \tilde{U}_1^3 + N_u^4 \tilde{U}_1^4 \right) \hat{n}_{x_1} + \\
&+ N_p^1 \left(N_u^1 \tilde{U}_2^1 + N_u^2 \tilde{U}_2^2 + N_u^3 \tilde{U}_2^3 + N_u^4 \tilde{U}_2^4 \right) \hat{n}_{x_2} + \\
&+ N_p^1 \left(N_u^1 \tilde{U}_3^1 + N_u^2 \tilde{U}_3^2 + N_u^3 \tilde{U}_3^3 + N_u^4 \tilde{U}_3^4 \right) \hat{n}_{x_3} \\
f_p^{2,1} &= N_p^2 \left(N_u^1 \tilde{U}_1^1 + N_u^2 \tilde{U}_1^2 + N_u^3 \tilde{U}_1^3 + N_u^4 \tilde{U}_1^4 \right) \hat{n}_{x_1} + \\
&+ N_p^2 \left(N_u^1 \tilde{U}_2^1 + N_u^2 \tilde{U}_2^2 + N_u^3 \tilde{U}_2^3 + N_u^4 \tilde{U}_2^4 \right) \hat{n}_{x_2} + \\
&+ N_p^2 \left(N_u^1 \tilde{U}_3^1 + N_u^2 \tilde{U}_3^2 + N_u^3 \tilde{U}_3^3 + N_u^4 \tilde{U}_3^4 \right) \hat{n}_{x_3} \\
f_p^{3,1} &= N_p^3 \left(N_u^1 \tilde{U}_1^1 + N_u^2 \tilde{U}_1^2 + N_u^3 \tilde{U}_1^3 + N_u^4 \tilde{U}_1^4 \right) \hat{n}_{x_1} + \\
&+ N_p^3 \left(N_u^1 \tilde{U}_2^1 + N_u^2 \tilde{U}_2^2 + N_u^3 \tilde{U}_2^3 + N_u^4 \tilde{U}_2^4 \right) \hat{n}_{x_2} + \\
&+ N_p^3 \left(N_u^1 \tilde{U}_3^1 + N_u^2 \tilde{U}_3^2 + N_u^3 \tilde{U}_3^3 + N_u^4 \tilde{U}_3^4 \right) \hat{n}_{x_3} \\
f_p^{4,1} &= N_p^4 \left(N_u^1 \tilde{U}_1^1 + N_u^2 \tilde{U}_1^2 + N_u^3 \tilde{U}_1^3 + N_u^4 \tilde{U}_1^4 \right) \hat{n}_{x_1} + \\
&+ N_p^4 \left(N_u^1 \tilde{U}_2^1 + N_u^2 \tilde{U}_2^2 + N_u^3 \tilde{U}_2^3 + N_u^4 \tilde{U}_2^4 \right) \hat{n}_{x_2} + \\
&+ N_p^4 \left(N_u^1 \tilde{U}_3^1 + N_u^2 \tilde{U}_3^2 + N_u^3 \tilde{U}_3^3 + N_u^4 \tilde{U}_3^4 \right) \hat{n}_{x_3}
\end{aligned} \tag{B.21}$$

The 4×4 symmetric, lumped mass matrix for the turbulent kinetic energy is given as

$$\mathbf{M}_\kappa = \int_\Omega [M_\kappa^{i,j}]\, d\Omega = \int_\Omega \mathbf{N}_\kappa{}^T \mathbf{N}_\kappa d\Omega \tag{B.22}$$

where the matrix coefficients $\left[M_\kappa^{i,j} \right]$ are

$$
\begin{aligned}
&M_\kappa^{1,1} = N_\kappa^1 N_\kappa^1; \quad M_\kappa^{2,2} = N_\kappa^2 N_\kappa^2; \quad M_\kappa^{3,3} = N_\kappa^3 N_\kappa^3; \quad M_\kappa^{4,4} = N_\kappa^4 N_\kappa^4 \\
&M_\kappa^{1,2} = M_\kappa^{2,1} = N_\kappa^1 N_\kappa^2; \quad M_\kappa^{1,3} = M_\kappa^{3,1} = N_\kappa^1 N_\kappa^3; \quad M_\kappa^{1,4} = M_\kappa^{4,1} = N_\kappa^1 N_\kappa^4 \\
&M_\kappa^{2,3} = M_\kappa^{3,2} = N_\kappa^2 N_\kappa^3; \quad M_\kappa^{2,4} = M_\kappa^{4,2} = N_\kappa^2 N_\kappa^4; \quad M_\kappa^{3,4} = M_\kappa^{4,3} = N_\kappa^3 N_\kappa^4
\end{aligned} \tag{B.23}
$$

The 4×4 convection matrix for the turbulent kinetic energy is given as

$$
\mathbf{C}_\kappa = \int_\Omega \left[C_\kappa^{i,j}\right] d\Omega = \int_\Omega \mathbf{N}_\kappa{}^T (\nabla^T (\mathbf{u}\mathbf{N}_\kappa)) d\Omega \tag{B.24}
$$

where the matrix coefficients $\left[C_\kappa^{i,j}\right]$ are

$$
\begin{aligned}
C_\kappa^{1,1} &= N_\kappa^1 \left(\frac{\partial u_1 N_\kappa^1}{\partial x_1} + \frac{\partial u_2 N_\kappa^1}{\partial x_2} + \frac{\partial u_3 N_\kappa^1}{\partial x_3}\right); \quad C_\kappa^{2,2} = N_\kappa^2 \left(\frac{\partial u_1 N_\kappa^2}{\partial x_1} + \frac{\partial u_2 N_\kappa^2}{\partial x_2} + \frac{\partial u_3 N_\kappa^2}{\partial x_3}\right) \\
C_\kappa^{3,3} &= N_\kappa^3 \left(\frac{\partial u_1 N_\kappa^3}{\partial x_1} + \frac{\partial u_2 N_\kappa^3}{\partial x_2} + \frac{\partial u_3 N_\kappa^3}{\partial x_3}\right); \quad C_\kappa^{4,4} = N_\kappa^4 \left(\frac{\partial u_1 N_\kappa^4}{\partial x_1} + \frac{\partial u_2 N_\kappa^4}{\partial x_2} + \frac{\partial u_3 N_\kappa^4}{\partial x_3}\right) \\
C_\kappa^{1,2} &= N_\kappa^1 \left(\frac{\partial u_1 N_\kappa^2}{\partial x_1} + \frac{\partial u_2 N_\kappa^2}{\partial x_2} + \frac{\partial u_3 N_\kappa^2}{\partial x_3}\right); \quad C_\kappa^{2,1} = N_\kappa^2 \left(\frac{\partial u_1 N_\kappa^1}{\partial x_1} + \frac{\partial u_2 N_\kappa^1}{\partial x_2} + \frac{\partial u_3 N_\kappa^1}{\partial x_3}\right) \\
C_\kappa^{1,3} &= N_\kappa^1 \left(\frac{\partial u_1 N_\kappa^3}{\partial x_1} + \frac{\partial u_2 N_\kappa^3}{\partial x_2} + \frac{\partial u_3 N_\kappa^3}{\partial x_3}\right); \quad C_\kappa^{3,1} = N_\kappa^3 \left(\frac{\partial u_1 N_\kappa^1}{\partial x_1} + \frac{\partial u_2 N_\kappa^1}{\partial x_2} + \frac{\partial u_3 N_\kappa^1}{\partial x_3}\right) \\
C_\kappa^{1,4} &= N_\kappa^1 \left(\frac{\partial u_1 N_\kappa^4}{\partial x_1} + \frac{\partial u_2 N_\kappa^4}{\partial x_2} + \frac{\partial u_3 N_\kappa^4}{\partial x_3}\right); \quad C_\kappa^{4,1} = N_\kappa^4 \left(\frac{\partial u_1 N_\kappa^1}{\partial x_1} + \frac{\partial u_2 N_\kappa^1}{\partial x_2} + \frac{\partial u_3 N_\kappa^1}{\partial x_3}\right) \\
C_\kappa^{2,3} &= N_\kappa^2 \left(\frac{\partial u_1 N_\kappa^3}{\partial x_1} + \frac{\partial u_2 N_\kappa^3}{\partial x_2} + \frac{\partial u_3 N_\kappa^3}{\partial x_3}\right); \quad C_\kappa^{3,2} = N_\kappa^3 \left(\frac{\partial u_1 N_\kappa^2}{\partial x_1} + \frac{\partial u_2 N_\kappa^2}{\partial x_2} + \frac{\partial u_3 N_\kappa^2}{\partial x_3}\right) \\
C_\kappa^{2,4} &= N_\kappa^2 \left(\frac{\partial u_1 N_\kappa^4}{\partial x_1} + \frac{\partial u_2 N_\kappa^4}{\partial x_2} + \frac{\partial u_3 N_\kappa^4}{\partial x_3}\right); \quad C_\kappa^{4,2} = N_\kappa^4 \left(\frac{\partial u_1 N_\kappa^2}{\partial x_1} + \frac{\partial u_2 N_\kappa^2}{\partial x_2} + \frac{\partial u_3 N_\kappa^2}{\partial x_3}\right) \\
C_\kappa^{3,4} &= N_\kappa^3 \left(\frac{\partial u_1 N_\kappa^4}{\partial x_1} + \frac{\partial u_2 N_\kappa^4}{\partial x_2} + \frac{\partial u_3 N_\kappa^4}{\partial x_3}\right); \quad C_\kappa^{4,3} = N_\kappa^4 \left(\frac{\partial u_1 N_\kappa^3}{\partial x_1} + \frac{\partial u_2 N_\kappa^3}{\partial x_2} + \frac{\partial u_3 N_\kappa^3}{\partial x_3}\right)
\end{aligned} \tag{B.25}
$$

The 4×4 symmetric diffusion matrix for the turbulent kinetic energy is given as

$$
\mathbf{K}_\kappa = \frac{1}{Re}\left(\mu + \frac{\mu_t}{\sigma_\kappa}\right) \int_\Omega \left[K_\kappa^{i,j}\right] d\Omega = \int_\Omega (\nabla \mathbf{N}_\kappa)^T \left(\frac{\mu_t + \sigma_\kappa \mu}{\sigma_\kappa Re}\right) \nabla \mathbf{N}_\kappa d\Omega \tag{B.26}
$$

where the matrix coefficients $\left[K_\kappa^{i,j}\right]$ are

$$K_\kappa^{1,1} = \left(\frac{\partial N_\kappa^1}{\partial x_1}\right)^2 + \left(\frac{\partial N_\kappa^1}{\partial x_2}\right)^2 + \left(\frac{\partial N_\kappa^1}{\partial x_3}\right)^2 ; \quad K_\kappa^{2\ 2} = \left(\frac{\partial N_\kappa^2}{\partial x_1}\right)^2 + \left(\frac{\partial N_\kappa^2}{\partial x_2}\right)^2 + \left(\frac{\partial N_\kappa^2}{\partial x_3}\right)^2$$
$$K_\kappa^{3\ 3} = \left(\frac{\partial N_\kappa^3}{\partial x_1}\right)^2 + \left(\frac{\partial N_\kappa^3}{\partial x_2}\right)^2 + \left(\frac{\partial N_\kappa^3}{\partial x_3}\right)^2 ; \quad K_\kappa^{4\ 4} = \left(\frac{\partial N_\kappa^4}{\partial x_1}\right)^2 + \left(\frac{\partial N_\kappa^4}{\partial x_2}\right)^2 + \left(\frac{\partial N_\kappa^4}{\partial x_3}\right)^2$$
$$K_\kappa^{1\ 2} = K_\kappa^{2\ 1} = \frac{\partial N_\kappa^1}{\partial x_1}\frac{\partial N_\kappa^2}{\partial x_1} + \frac{\partial N_\kappa^1}{\partial x_2}\frac{\partial N_\kappa^2}{\partial x_2} + \frac{\partial N_\kappa^1}{\partial x_3}\frac{\partial N_\kappa^2}{\partial x_3}$$
$$K_\kappa^{1\ 3} = K_\kappa^{3\ 1} = \frac{\partial N_\kappa^1}{\partial x_1}\frac{\partial N_\kappa^3}{\partial x_1} + \frac{\partial N_\kappa^1}{\partial x_2}\frac{\partial N_\kappa^3}{\partial x_2} + \frac{\partial N_\kappa^1}{\partial x_3}\frac{\partial N_\kappa^3}{\partial x_3}$$
$$K_\kappa^{1\ 4} = K_\kappa^{4\ 1} = \frac{\partial N_\kappa^1}{\partial x_1}\frac{\partial N_\kappa^4}{\partial x_1} + \frac{\partial N_\kappa^1}{\partial x_2}\frac{\partial N_\kappa^4}{\partial x_2} + \frac{\partial N_\kappa^1}{\partial x_3}\frac{\partial N_\kappa^4}{\partial x_3}$$
$$K_\kappa^{2\ 3} = K_\kappa^{3\ 2} = \frac{\partial N_\kappa^2}{\partial x_1}\frac{\partial N_\kappa^3}{\partial x_1} + \frac{\partial N_\kappa^2}{\partial x_2}\frac{\partial N_\kappa^3}{\partial x_2} + \frac{\partial N_\kappa^2}{\partial x_3}\frac{\partial N_\kappa^3}{\partial x_3}$$
$$K_\kappa^{2\ 4} = K_\kappa^{4\ 2} = \frac{\partial N_\kappa^2}{\partial x_1}\frac{\partial N_\kappa^4}{\partial x_1} + \frac{\partial N_\kappa^2}{\partial x_2}\frac{\partial N_\kappa^4}{\partial x_2} + \frac{\partial N_\kappa^2}{\partial x_3}\frac{\partial N_\kappa^4}{\partial x_3}$$
$$K_\kappa^{3\ 4} = K_\kappa^{4\ 3} = \frac{\partial N_\kappa^3}{\partial x_1}\frac{\partial N_\kappa^4}{\partial x_1} + \frac{\partial N_\kappa^3}{\partial x_2}\frac{\partial N_\kappa^4}{\partial x_2} + \frac{\partial N_\kappa^3}{\partial x_3}\frac{\partial N_\kappa^4}{\partial x_3}$$
(B.27)

The 4×1 vector based on both the generation and source terms of the turbulent kinetic energy equation is given as

$$\mathbf{f}_{\kappa\Omega} = \int_\Omega \left[f_{\kappa\Omega}^{i,j}\right] d\Omega = \int_\Omega \mathbf{N}_\kappa{}^T \Upsilon_\kappa^{III} d\Omega = \int_\Omega \mathbf{N}_\kappa{}^T \left[\tau_{ij}^R \partial_j u_i - \mathbf{N}_\varepsilon \tilde{\mathbf{E}}\right] d\Omega \qquad \text{(B.28)}$$

where $\Upsilon_\kappa^{III} = r_{1\kappa} + r_{2\kappa} + r_{3\kappa} + r_{4\kappa} + r_{5\kappa} + r_{6\kappa} + r_{7\kappa} + r_{8\kappa} + r_{9\kappa} + r_{10\kappa} + r_{11\kappa}$ may be respectively expressed

$$\begin{aligned} r_{1\kappa} &= \frac{4\mu_t}{3Re}\left(u_1^1\frac{\partial N_u^1}{\partial x_1} + u_1^2\frac{\partial N_u^2}{\partial x_1} + u_1^3\frac{\partial N_u^3}{\partial x_1} + u_1^4\frac{\partial N_u^4}{\partial x_1}\right)^2 - \\ &- \frac{2\mu_t}{3Re}\left(u_2^1\frac{\partial N_u^1}{\partial x_2} + u_2^2\frac{\partial N_u^2}{\partial x_2} + u_2^3\frac{\partial N_u^3}{\partial x_2} + u_2^4\frac{\partial N_u^4}{\partial x_2}\right) \\ &\quad \left(u_1^1\frac{\partial N_u^1}{\partial x_1} + u_1^2\frac{\partial N_u^2}{\partial x_1} + u_1^3\frac{\partial N_u^3}{\partial x_1} + u_1^4\frac{\partial N_u^4}{\partial x_1}\right) - \\ &- \frac{2\mu_t}{3Re}\left(u_3^1\frac{\partial N_u^1}{\partial x_3} + u_3^2\frac{\partial N_u^2}{\partial x_3} + u_3^3\frac{\partial N_u^3}{\partial x_3} + u_3^4\frac{\partial N_u^4}{\partial x_3}\right) \end{aligned}$$

$$
\begin{aligned}
& \left(u_1^1\frac{\partial N_u^1}{\partial x_1}+u_1^2\frac{\partial N_u^2}{\partial x_1}+u_1^3\frac{\partial N_u^3}{\partial x_1}+u_1^4\frac{\partial N_u^4}{\partial x_1}\right) \\
r_{2\kappa} \;=\; & \frac{4\mu_t}{3Re}\left(u_2^1\frac{\partial N_u^1}{\partial x_2}+u_2^2\frac{\partial N_u^2}{\partial x_2}+u_2^3\frac{\partial N_u^3}{\partial x_2}+u_2^4\frac{\partial N_u^4}{\partial x_2}\right)^2- \\
- & \frac{2\mu_t}{3Re}\left(u_3^1\frac{\partial N_u^1}{\partial x_3}+u_3^2\frac{\partial N_u^2}{\partial x_3}+u_3^3\frac{\partial N_u^3}{\partial x_3}+u_3^4\frac{\partial N_u^4}{\partial x_3}\right) \\
& \left(u_2^1\frac{\partial N_u^1}{\partial x_2}+u_2^2\frac{\partial N_u^2}{\partial x_2}+u_2^3\frac{\partial N_u^3}{\partial x_2}+u_2^4\frac{\partial N_u^4}{\partial x_2}\right)- \\
- & \frac{2\mu_t}{3Re}\left(u_1^1\frac{\partial N_u^1}{\partial x_1}+u_1^2\frac{\partial N_u^2}{\partial x_1}+u_1^3\frac{\partial N_u^3}{\partial x_1}+u_1^4\frac{\partial N_u^4}{\partial x_1}\right) \\
& \left(u_2^1\frac{\partial N_u^1}{\partial x_2}+u_2^2\frac{\partial N_u^2}{\partial x_2}+u_2^3\frac{\partial N_u^3}{\partial x_2}+u_2^4\frac{\partial N_u^4}{\partial x_2}\right) \\
r_{3\kappa} \;=\; & \frac{4\mu_t}{3Re}\left(u_3^1\frac{\partial N_u^1}{\partial x_3}+u_3^2\frac{\partial N_u^2}{\partial x_3}+u_3^3\frac{\partial N_u^3}{\partial x_3}+u_3^4\frac{\partial N_u^4}{\partial x_3}\right)^2- \\
- & \frac{2\mu_t}{3Re}\left(u_1^1\frac{\partial N_u^1}{\partial x_1}+u_1^2\frac{\partial N_u^2}{\partial x_1}+u_1^3\frac{\partial N_u^3}{\partial x_1}+u_1^4\frac{\partial N_u^4}{\partial x_1}\right) \\
& \left(u_3^1\frac{\partial N_u^1}{\partial x_3}+u_3^2\frac{\partial N_u^2}{\partial x_3}+u_3^3\frac{\partial N_u^3}{\partial x_3}+u_3^4\frac{\partial N_u^4}{\partial x_3}\right)- \\
- & \frac{2\mu_t}{3Re}\left(u_2^1\frac{\partial N_u^1}{\partial x_2}+u_2^2\frac{\partial N_u^2}{\partial x_2}+u_2^3\frac{\partial N_u^3}{\partial x_2}+u_2^4\frac{\partial N_u^4}{\partial x_2}\right) \\
& \left(u_3^1\frac{\partial N_u^1}{\partial x_3}+u_3^2\frac{\partial N_u^2}{\partial x_3}+u_3^3\frac{\partial N_u^3}{\partial x_3}+u_3^4\frac{\partial N_u^4}{\partial x_3}\right) \\
r_{4\kappa} \;=\; & \frac{\mu_t}{Re}\left(u_1^1\frac{\partial N_u^1}{\partial x_2}+u_1^2\frac{\partial N_u^2}{\partial x_2}+u_1^3\frac{\partial N_u^3}{\partial x_2}+u_1^4\frac{\partial N_u^4}{\partial x_2}\right)^2+ \\
+ & \frac{\mu_t}{Re}\left(u_2^1\frac{\partial N_u^1}{\partial x_1}+u_2^2\frac{\partial N_u^2}{\partial x_1}+u_2^3\frac{\partial N_u^3}{\partial x_1}+u_2^4\frac{\partial N_u^4}{\partial x_1}\right) \\
& \left(u_1^1\frac{\partial N_u^1}{\partial x_2}+u_1^2\frac{\partial N_u^2}{\partial x_2}+u_1^3\frac{\partial N_u^3}{\partial x_2}+u_1^4\frac{\partial N_u^4}{\partial x_2}\right) \\
r_{5\kappa} \;=\; & \frac{\mu_t}{Re}\left(u_2^1\frac{\partial N_u^1}{\partial x_1}+u_2^2\frac{\partial N_u^2}{\partial x_1}+u_2^3\frac{\partial N_u^3}{\partial x_1}+u_2^4\frac{\partial N_u^4}{\partial x_1}\right)^2+ \\
+ & \frac{\mu_t}{Re}\left(u_1^1\frac{\partial N_u^1}{\partial x_2}+u_1^2\frac{\partial N_u^2}{\partial x_2}+u_1^3\frac{\partial N_u^3}{\partial x_2}+u_1^4\frac{\partial N_u^4}{\partial x_2}\right) \\
& \left(u_2^1\frac{\partial N_u^1}{\partial x_1}+u_2^2\frac{\partial N_u^2}{\partial x_1}+u_2^3\frac{\partial N_u^3}{\partial x_1}+u_2^4\frac{\partial N_u^4}{\partial x_1}\right) \\
r_{6\kappa} \;=\; & \frac{\mu_t}{Re}\left(u_1^1\frac{\partial N_u^1}{\partial x_3}+u_1^2\frac{\partial N_u^2}{\partial x_3}+u_1^3\frac{\partial N_u^3}{\partial x_3}+u_1^4\frac{\partial N_u^4}{\partial x_3}\right)^2+ \\
+ & \frac{\mu_t}{Re}\left(u_3^1\frac{\partial N_u^1}{\partial x_1}+u_3^2\frac{\partial N_u^2}{\partial x_1}+u_3^3\frac{\partial N_u^3}{\partial x_1}+u_3^4\frac{\partial N_u^4}{\partial x_1}\right)
\end{aligned}
$$

$$
\begin{aligned}
& \left(u_1^1\frac{\partial N_u^1}{\partial x_3}+u_1^2\frac{\partial N_u^2}{\partial x_3}+u_1^3\frac{\partial N_u^3}{\partial x_3}+u_1^4\frac{\partial N_u^4}{\partial x_3}\right) \\
r_{7\kappa} &= \frac{\mu_t}{Re}\left(u_3^1\frac{\partial N_u^1}{\partial x_1}+u_3^2\frac{\partial N_u^2}{\partial x_1}+u_3^3\frac{\partial N_u^3}{\partial x_1}+u_3^4\frac{\partial N_u^4}{\partial x_1}\right)^2+ \\
&+ \frac{\mu_t}{Re}\left(u_1^1\frac{\partial N_u^1}{\partial x_3}+u_1^2\frac{\partial N_u^2}{\partial x_3}+u_1^3\frac{\partial N_u^3}{\partial x_3}+u_1^4\frac{\partial N_u^4}{\partial x_3}\right) \\
& \left(u_3^1\frac{\partial N_u^1}{\partial x_1}+u_3^2\frac{\partial N_u^2}{\partial x_1}+u_3^3\frac{\partial N_u^3}{\partial x_1}+u_3^4\frac{\partial N_u^4}{\partial x_1}\right) \\
r_{8\kappa} &= \frac{\mu_t}{Re}\left(u_2^1\frac{\partial N_u^1}{\partial x_3}+u_2^2\frac{\partial N_u^2}{\partial x_3}+u_2^3\frac{\partial N_u^3}{\partial x_3}+u_2^4\frac{\partial N_u^4}{\partial x_3}\right)^2+ \\
&+ \frac{\mu_t}{Re}\left(u_3^1\frac{\partial N_u^1}{\partial x_2}+u_3^2\frac{\partial N_u^2}{\partial x_2}+u_3^3\frac{\partial N_u^3}{\partial x_2}+u_3^4\frac{\partial N_u^4}{\partial x_2}\right) \\
& \left(u_2^1\frac{\partial N_u^1}{\partial x_3}+u_2^2\frac{\partial N_u^2}{\partial x_3}+u_2^3\frac{\partial N_u^3}{\partial x_3}+u_2^4\frac{\partial N_u^4}{\partial x_3}\right) \\
r_{9\kappa} &= \frac{\mu_t}{Re}\left(u_3^1\frac{\partial N_u^1}{\partial x_2}+u_3^2\frac{\partial N_u^2}{\partial x_2}+u_3^3\frac{\partial N_u^3}{\partial x_2}+u_3^4\frac{\partial N_u^4}{\partial x_2}\right)^2+ \\
&+ \frac{\mu_t}{Re}\left(u_2^1\frac{\partial N_u^1}{\partial x_3}+u_2^2\frac{\partial N_u^2}{\partial x_3}+u_2^3\frac{\partial N_u^3}{\partial x_3}+u_2^4\frac{\partial N_u^4}{\partial x_3}\right) \\
& \left(u_3^1\frac{\partial N_u^1}{\partial x_2}+u_3^2\frac{\partial N_u^2}{\partial x_2}+u_3^3\frac{\partial N_u^3}{\partial x_2}+u_3^4\frac{\partial N_u^4}{\partial x_2}\right) \\
r_{10\kappa} &= -\frac{2}{3}\left(K^1N_\kappa^1+K^2N_\kappa^2+K^3N_\kappa^3+K^4N_\kappa^4\right) \\
& \left(u_1^1\frac{\partial N_u^1}{\partial x_1}+u_1^2\frac{\partial N_u^2}{\partial x_1}+u_1^3\frac{\partial N_u^3}{\partial x_1}+u_1^4\frac{\partial N_u^4}{\partial x_1}\right)- \\
&- \frac{2}{3}\left(K^1N_\kappa^1+K^2N_\kappa^2+K^3N_\kappa^3+K^4N_\kappa^4\right)\left(u_2^1\frac{\partial N_u^1}{\partial x_2}+u_2^2\frac{\partial N_u^2}{\partial x_2}+u_2^3\frac{\partial N_u^3}{\partial x_2}+u_2^4\frac{\partial N_u^4}{\partial x_2}\right)- \\
&- \frac{2}{3}\left(K^1N_\kappa^1+K^2N_\kappa^2+K^3N_\kappa^3+K^4N_\kappa^4\right)\left(u_3^1\frac{\partial N_u^1}{\partial x_3}+u_3^2\frac{\partial N_u^2}{\partial x_3}+u_3^3\frac{\partial N_u^3}{\partial x_3}+u_3^4\frac{\partial N_u^4}{\partial x_3}\right) \\
r_{11\kappa} &= -\left(E^1N_\varepsilon^1+E^2N_\varepsilon^2+E^3N_\varepsilon^3+E^4N_\varepsilon^4\right) \qquad \text{(B.29)}
\end{aligned}
$$

Thus the vector coefficients $\left[f_{\kappa\Omega}^{i,j}\right]$ are

$$f_{\kappa\Omega}^{1,1}=N_\kappa^1\Upsilon_\kappa^{III};\quad f_{\kappa\Omega}^{2,1}=N_\kappa^2\Upsilon_\kappa^{III};\quad f_{\kappa\Omega}^{3,1}=N_\kappa^3\Upsilon_\kappa^{III};\quad f_{\kappa\Omega}^{4,1}=N_\kappa^4\Upsilon_\kappa^{III} \qquad \text{(B.30)}$$

The 4×1 forcing vector for the turbulent kinetic energy is given as

$$\mathbf{f}_{\kappa\Gamma}=\frac{1}{Re}\left(\mu+\frac{\mu_t}{\sigma_\kappa}\right)\int_\Gamma\left[f_{\kappa\Gamma}^{i,j}\right]d\Gamma=\int_\Gamma \mathbf{N}_\kappa{}^T t_\kappa d\Gamma \qquad \text{(B.31)}$$

where the vector coefficients $\left[f_{\kappa\Gamma}^{i,j}\right]$ are

$$\begin{aligned}
f_{\kappa\Gamma}^{1,1} &= N_\kappa^1\left(\kappa^1\frac{\partial N_\kappa^1}{\partial x_1}+\kappa^2\frac{\partial N_\kappa^2}{\partial x_1}+\kappa^3\frac{\partial N_\kappa^3}{\partial x_1}+\kappa^4\frac{\partial N_\kappa^4}{\partial x_1}\right)\hat{n}_{x_1}+ \\
&+ N_\kappa^1\left(\kappa^1\frac{\partial N_\kappa^1}{\partial x_2}+\kappa^2\frac{\partial N_\kappa^2}{\partial x_2}+\kappa^3\frac{\partial N_\kappa^3}{\partial x_2}+\kappa^4\frac{\partial N_\kappa^4}{\partial x_2}\right)\hat{n}_{x_2}+ \\
&+ N_\kappa^1\left(\kappa^1\frac{\partial N_\kappa^1}{\partial x_3}+\kappa^2\frac{\partial N_\kappa^2}{\partial x_3}+\kappa^3\frac{\partial N_\kappa^3}{\partial x_3}+\kappa^4\frac{\partial N_\kappa^4}{\partial x_3}\right)\hat{n}_{x_3} \\
f_{\kappa\Gamma}^{2,1} &= N_\kappa^2\left(\kappa^1\frac{\partial N_\kappa^1}{\partial x_1}+\kappa^2\frac{\partial N_\kappa^2}{\partial x_1}+\kappa^3\frac{\partial N_\kappa^3}{\partial x_1}+\kappa^4\frac{\partial N_\kappa^4}{\partial x_1}\right)\hat{n}_{x_1}+ \\
&+ N_\kappa^2\left(\kappa^1\frac{\partial N_\kappa^1}{\partial x_2}+\kappa^2\frac{\partial N_\kappa^2}{\partial x_2}+\kappa^3\frac{\partial N_\kappa^3}{\partial x_2}+\kappa^4\frac{\partial N_\kappa^4}{\partial x_2}\right)\hat{n}_{x_2}+ \\
&+ N_\kappa^2\left(\kappa^1\frac{\partial N_\kappa^1}{\partial x_3}+\kappa^2\frac{\partial N_\kappa^2}{\partial x_3}+\kappa^3\frac{\partial N_\kappa^3}{\partial x_3}+\kappa^4\frac{\partial N_\kappa^4}{\partial x_3}\right)\hat{n}_{x_3} \\
f_{\kappa\Gamma}^{3,1} &= N_\kappa^3\left(\kappa^1\frac{\partial N_\kappa^1}{\partial x_1}+\kappa^2\frac{\partial N_\kappa^2}{\partial x_1}+\kappa^3\frac{\partial N_\kappa^3}{\partial x_1}+\kappa^4\frac{\partial N_\kappa^4}{\partial x_1}\right)\hat{n}_{x_1}+ \\
&+ N_\kappa^3\left(\kappa^1\frac{\partial N_\kappa^1}{\partial x_2}+\kappa^2\frac{\partial N_\kappa^2}{\partial x_2}+\kappa^3\frac{\partial N_\kappa^3}{\partial x_2}+\kappa^4\frac{\partial N_\kappa^4}{\partial x_2}\right)\hat{n}_{x_2}+ \\
&+ N_\kappa^3\left(\kappa^1\frac{\partial N_\kappa^1}{\partial x_3}+\kappa^2\frac{\partial N_\kappa^2}{\partial x_3}+\kappa^3\frac{\partial N_\kappa^3}{\partial x_3}+\kappa^4\frac{\partial N_\kappa^4}{\partial x_3}\right)\hat{n}_{x_3} \\
f_{\kappa\Gamma}^{4,1} &= N_\kappa^4\left(\kappa^1\frac{\partial N_\kappa^1}{\partial x_1}+\kappa^2\frac{\partial N_\kappa^2}{\partial x_1}+\kappa^3\frac{\partial N_\kappa^3}{\partial x_1}+\kappa^4\frac{\partial N_\kappa^4}{\partial x_1}\right)\hat{n}_{x_1}+ \\
&+ N_\kappa^4\left(\kappa^1\frac{\partial N_\kappa^1}{\partial x_2}+\kappa^2\frac{\partial N_\kappa^2}{\partial x_2}+\kappa^3\frac{\partial N_\kappa^3}{\partial x_2}+\kappa^4\frac{\partial N_\kappa^4}{\partial x_2}\right)\hat{n}_{x_2}+ \\
&+ N_\kappa^4\left(\kappa^1\frac{\partial N_\kappa^1}{\partial x_3}+\kappa^2\frac{\partial N_\kappa^2}{\partial x_3}+\kappa^3\frac{\partial N_\kappa^3}{\partial x_3}+\kappa^4\frac{\partial N_\kappa^4}{\partial x_3}\right)\hat{n}_{x_3} \qquad \text{(B.32)}
\end{aligned}$$

The 4×4 symmetric convection matrix of the stabilization for the turbulent kinetic energy is given as

$$\mathbf{K}_{\mathbf{u}\kappa} = -\frac{1}{2}\int_\Omega \left[K_{u\kappa}^{i,j}\right] d\Omega = -\frac{1}{2}\int_\Omega (\nabla^T(\mathbf{u}\mathbf{N}_\kappa))^T(\nabla^T(\mathbf{u}\mathbf{N}_\kappa))d\Omega \qquad \text{(B.33)}$$

where the matrix coefficients $\left[K_{u\kappa}^{i,j}\right]$ are

$$
\begin{aligned}
K_{u\kappa}^{1,1} &= \left(\frac{\partial u_1 N_\kappa^1}{\partial x_1} + \frac{\partial u_2 N_\kappa^1}{\partial x_2} + \frac{\partial u_3 N_\kappa^1}{\partial x_3}\right)^2; \quad K_{u\kappa}^{2,2} = \left(\frac{\partial u_1 N_\kappa^2}{\partial x_1} + \frac{\partial u_2 N_\kappa^2}{\partial x_2} + \frac{\partial u_3 N_\kappa^2}{\partial x_3}\right)^2 \\
K_{u\kappa}^{3,3} &= \left(\frac{\partial u_1 N_\kappa^3}{\partial x_1} + \frac{\partial u_2 N_\kappa^3}{\partial x_2} + \frac{\partial u_3 N_\kappa^3}{\partial x_3}\right)^2; \quad K_{u\kappa}^{4,4} = \left(\frac{\partial u_1 N_\kappa^4}{\partial x_1} + \frac{\partial u_2 N_\kappa^4}{\partial x_2} + \frac{\partial u_3 N_\kappa^4}{\partial x_3}\right)^2 \\
K_{u\kappa}^{1,2} = K_{u\kappa}^{2,1} &= \left(\frac{\partial u_1 N_\kappa^1}{\partial x_1} + \frac{\partial u_2 N_\kappa^1}{\partial x_2} + \frac{\partial u_3 N_\kappa^1}{\partial x_3}\right)\left(\frac{\partial u_1 N_\kappa^2}{\partial x_1} + \frac{\partial u_2 N_\kappa^2}{\partial x_2} + \frac{\partial u_3 N_\kappa^2}{\partial x_3}\right) \\
K_{u\kappa}^{1,3} = K_{u\kappa}^{3,1} &= \left(\frac{\partial u_1 N_\kappa^1}{\partial x_1} + \frac{\partial u_2 N_\kappa^1}{\partial x_2} + \frac{\partial u_3 N_\kappa^1}{\partial x_3}\right)\left(\frac{\partial u_1 N_\kappa^3}{\partial x_1} + \frac{\partial u_2 N_\kappa^3}{\partial x_2} + \frac{\partial u_3 N_\kappa^3}{\partial x_3}\right) \\
K_{u\kappa}^{1,4} = K_{u\kappa}^{4,1} &= \left(\frac{\partial u_1 N_\kappa^1}{\partial x_1} + \frac{\partial u_2 N_\kappa^1}{\partial x_2} + \frac{\partial u_3 N_\kappa^1}{\partial x_3}\right)\left(\frac{\partial u_1 N_\kappa^4}{\partial x_1} + \frac{\partial u_2 N_\kappa^4}{\partial x_2} + \frac{\partial u_3 N_\kappa^4}{\partial x_3}\right) \\
K_{u\kappa}^{2,3} = K_{u\kappa}^{3,2} &= \left(\frac{\partial u_1 N_\kappa^2}{\partial x_1} + \frac{\partial u_2 N_\kappa^2}{\partial x_2} + \frac{\partial u_3 N_\kappa^2}{\partial x_3}\right)\left(\frac{\partial u_1 N_\kappa^3}{\partial x_1} + \frac{\partial u_2 N_\kappa^3}{\partial x_2} + \frac{\partial u_3 N_\kappa^3}{\partial x_3}\right) \\
K_{u\kappa}^{2,4} = K_{u\kappa}^{4,2} &= \left(\frac{\partial u_1 N_\kappa^2}{\partial x_1} + \frac{\partial u_2 N_\kappa^2}{\partial x_2} + \frac{\partial u_3 N_\kappa^2}{\partial x_3}\right)\left(\frac{\partial u_1 N_\kappa^4}{\partial x_1} + \frac{\partial u_2 N_\kappa^4}{\partial x_2} + \frac{\partial u_3 N_\kappa^4}{\partial x_3}\right) \\
K_{u\kappa}^{3,4} = K_{u\kappa}^{4,3} &= \left(\frac{\partial u_1 N_\kappa^3}{\partial x_1} + \frac{\partial u_2 N_\kappa^3}{\partial x_2} + \frac{\partial u_3 N_\kappa^3}{\partial x_3}\right)\left(\frac{\partial u_1 N_\kappa^4}{\partial x_1} + \frac{\partial u_2 N_\kappa^4}{\partial x_2} + \frac{\partial u_3 N_\kappa^4}{\partial x_3}\right)
\end{aligned}
\tag{B.34}
$$

The 4×4 symmetric, lumped mass matrix for the dissipation rate is given as

$$
\mathbf{M}_\varepsilon = \int_\Omega \left[M_\varepsilon^{i,j}\right] d\Omega = \int_\Omega \mathbf{N}_\varepsilon{}^T \mathbf{N}_\varepsilon d\Omega \tag{B.35}
$$

where the matrix coefficients $\left[M_\varepsilon^{i,j}\right]$ are

$$
\begin{aligned}
&M_\varepsilon^{1,1} = N_\varepsilon^1 N_\varepsilon^1; \quad M_\varepsilon^{2,2} = N_\varepsilon^2 N_\varepsilon^2; \quad M_\varepsilon^{3,3} = N_\varepsilon^3 N_\varepsilon^3; \quad M_\varepsilon^{4,4} = N_\varepsilon^4 N_\varepsilon^4 \\
&M_\varepsilon^{1,2} = M_\varepsilon^{2,1} = N_\varepsilon^1 N_\varepsilon^2; \quad M_\varepsilon^{1,3} = M_\varepsilon^{3,1} = N_\varepsilon^1 N_\varepsilon^3; \quad M_\varepsilon^{1,4} = M_\varepsilon^{4,1} = N_\varepsilon^1 N_\varepsilon^4 \\
&M_\varepsilon^{2,3} = M_\varepsilon^{3,2} = N_\varepsilon^2 N_\varepsilon^3; \quad M_\varepsilon^{2,4} = M_\varepsilon^{4,2} = N_\varepsilon^2 N_\varepsilon^4; \quad M_\varepsilon^{3,4} = M_\varepsilon^{4,3} = N_\varepsilon^3 N_\varepsilon^4
\end{aligned}
\tag{B.36}
$$

The 4×4 convection matrix for the dissipation rate is given as

$$
\mathbf{C}_\varepsilon = \int_\Omega \left[C_\varepsilon^{i,j}\right] d\Omega = \int_\Omega \mathbf{N}_\varepsilon{}^T (\nabla^T (\mathbf{u}\mathbf{N}_\varepsilon)) d\Omega \tag{B.37}
$$

where the matrix coefficients $\left[C_\varepsilon^{i,j}\right]$ are

$$
\begin{aligned}
C_\varepsilon^{1,1} &= N_\varepsilon^1\left(\frac{\partial u_1 N_\varepsilon^1}{\partial x_1}+\frac{\partial u_2 N_\varepsilon^1}{\partial x_2}+\frac{\partial u_3 N_\varepsilon^1}{\partial x_3}\right); \quad C_\varepsilon^{2,2} = N_\varepsilon^2\left(\frac{\partial u_1 N_\varepsilon^2}{\partial x_1}+\frac{\partial u_2 N_\varepsilon^2}{\partial x_2}+\frac{\partial u_3 N_\varepsilon^2}{\partial x_3}\right)\\
C_\varepsilon^{3,3} &= N_\varepsilon^3\left(\frac{\partial u_1 N_\varepsilon^3}{\partial x_1}+\frac{\partial u_2 N_\varepsilon^3}{\partial x_2}+\frac{\partial u_3 N_\varepsilon^3}{\partial x_3}\right); \quad C_\varepsilon^{4,4} = N_\varepsilon^4\left(\frac{\partial u_1 N_\varepsilon^4}{\partial x_1}+\frac{\partial u_2 N_\varepsilon^4}{\partial x_2}+\frac{\partial u_3 N_\varepsilon^4}{\partial x_3}\right)\\
C_\varepsilon^{1,2} &= N_\varepsilon^1\left(\frac{\partial u_1 N_\varepsilon^2}{\partial x_1}+\frac{\partial u_2 N_\varepsilon^2}{\partial x_2}+\frac{\partial u_3 N_\varepsilon^2}{\partial x_3}\right); \quad C_\varepsilon^{2,1} = N_\varepsilon^2\left(\frac{\partial u_1 N_\varepsilon^1}{\partial x_1}+\frac{\partial u_2 N_\varepsilon^1}{\partial x_2}+\frac{\partial u_3 N_\varepsilon^1}{\partial x_3}\right)\\
C_\varepsilon^{1,3} &= N_\varepsilon^1\left(\frac{\partial u_1 N_\varepsilon^3}{\partial x_1}+\frac{\partial u_2 N_\varepsilon^3}{\partial x_2}+\frac{\partial u_3 N_\varepsilon^3}{\partial x_3}\right); \quad C_\varepsilon^{3,1} = N_\varepsilon^3\left(\frac{\partial u_1 N_\varepsilon^1}{\partial x_1}+\frac{\partial u_2 N_\varepsilon^1}{\partial x_2}+\frac{\partial u_3 N_\varepsilon^1}{\partial x_3}\right)\\
C_\varepsilon^{1,4} &= N_\varepsilon^1\left(\frac{\partial u_1 N_\varepsilon^4}{\partial x_1}+\frac{\partial u_2 N_\varepsilon^4}{\partial x_2}+\frac{\partial u_3 N_\varepsilon^4}{\partial x_3}\right); \quad C_\varepsilon^{4,1} = N_\varepsilon^4\left(\frac{\partial u_1 N_\varepsilon^1}{\partial x_1}+\frac{\partial u_2 N_\varepsilon^1}{\partial x_2}+\frac{\partial u_3 N_\varepsilon^1}{\partial x_3}\right)\\
C_\varepsilon^{2,3} &= N_\varepsilon^2\left(\frac{\partial u_1 N_\varepsilon^3}{\partial x_1}+\frac{\partial u_2 N_\varepsilon^3}{\partial x_2}+\frac{\partial u_3 N_\varepsilon^3}{\partial x_3}\right); \quad C_\varepsilon^{3,2} = N_\varepsilon^3\left(\frac{\partial u_1 N_\varepsilon^2}{\partial x_1}+\frac{\partial u_2 N_\varepsilon^2}{\partial x_2}+\frac{\partial u_3 N_\varepsilon^2}{\partial x_3}\right)\\
C_\varepsilon^{2,4} &= N_\varepsilon^2\left(\frac{\partial u_1 N_\varepsilon^4}{\partial x_1}+\frac{\partial u_2 N_\varepsilon^4}{\partial x_2}+\frac{\partial u_3 N_\varepsilon^4}{\partial x_3}\right); \quad C_\varepsilon^{4,2} = N_\varepsilon^4\left(\frac{\partial u_1 N_\varepsilon^2}{\partial x_1}+\frac{\partial u_2 N_\varepsilon^2}{\partial x_2}+\frac{\partial u_3 N_\varepsilon^2}{\partial x_3}\right)\\
C_\varepsilon^{3,4} &= N_\varepsilon^3\left(\frac{\partial u_1 N_\varepsilon^4}{\partial x_1}+\frac{\partial u_2 N_\varepsilon^4}{\partial x_2}+\frac{\partial u_3 N_\varepsilon^4}{\partial x_3}\right); \quad C_\varepsilon^{4,3} = N_\varepsilon^4\left(\frac{\partial u_1 N_\varepsilon^3}{\partial x_1}+\frac{\partial u_2 N_\varepsilon^3}{\partial x_2}+\frac{\partial u_3 N_\varepsilon^3}{\partial x_3}\right)
\end{aligned}
\tag{B.38}
$$

The 4×4 symmetric diffusion matrix for the dissipation rate is given as

$$
\mathbf{K}_\varepsilon = \frac{1}{Re}\left(\mu + \frac{\mu_t}{\sigma_\varepsilon}\right)\int_\Omega [K_\varepsilon^{i,j}]\, d\Omega = \int_\Omega (\nabla \mathbf{N}_\varepsilon)^T \left(\frac{\mu_t + \sigma_\varepsilon \mu}{\sigma_\varepsilon Re}\right)\nabla \mathbf{N}_\varepsilon d\Omega \tag{B.39}
$$

where the matrix coefficients $\left[K_\varepsilon^{i,j}\right]$ are

$$
\begin{aligned}
K_\varepsilon^{1,1} &= \left(\frac{\partial N_\varepsilon^1}{\partial x_1}\right)^2+\left(\frac{\partial N_\varepsilon^1}{\partial x_2}\right)^2+\left(\frac{\partial N_\varepsilon^1}{\partial x_3}\right)^2; \quad K_\varepsilon^{2,2} = \left(\frac{\partial N_\varepsilon^2}{\partial x_1}\right)^2+\left(\frac{\partial N_\varepsilon^2}{\partial x_2}\right)^2+\left(\frac{\partial N_\varepsilon^2}{\partial x_3}\right)^2\\
K_\varepsilon^{3,3} &= \left(\frac{\partial N_\varepsilon^3}{\partial x_1}\right)^2+\left(\frac{\partial N_\varepsilon^3}{\partial x_2}\right)^2+\left(\frac{\partial N_\varepsilon^3}{\partial x_3}\right)^2; \quad K_\varepsilon^{4,4} = \left(\frac{\partial N_\varepsilon^4}{\partial x_1}\right)^2+\left(\frac{\partial N_\varepsilon^4}{\partial x_2}\right)^2+\left(\frac{\partial N_\varepsilon^4}{\partial x_3}\right)^2\\
K_\varepsilon^{1,2} &= K_\varepsilon^{2,1} = \frac{\partial N_\varepsilon^1}{\partial x_1}\frac{\partial N_\varepsilon^2}{\partial x_1}+\frac{\partial N_\varepsilon^1}{\partial x_2}\frac{\partial N_\varepsilon^2}{\partial x_2}+\frac{\partial N_\varepsilon^1}{\partial x_3}\frac{\partial N_\varepsilon^2}{\partial x_3}\\
K_\varepsilon^{1,3} &= K_\varepsilon^{3,1} = \frac{\partial N_\varepsilon^1}{\partial x_1}\frac{\partial N_\varepsilon^3}{\partial x_1}+\frac{\partial N_\varepsilon^1}{\partial x_2}\frac{\partial N_\varepsilon^3}{\partial x_2}+\frac{\partial N_\varepsilon^1}{\partial x_3}\frac{\partial N_\varepsilon^3}{\partial x_3}
\end{aligned}
$$

$$K_\varepsilon^{1,4} = K_\varepsilon^{4,1} = \frac{\partial N_\varepsilon^1}{\partial x_1}\frac{\partial N_\varepsilon^4}{\partial x_1} + \frac{\partial N_\varepsilon^1}{\partial x_2}\frac{\partial N_\varepsilon^4}{\partial x_2} + \frac{\partial N_\varepsilon^1}{\partial x_3}\frac{\partial N_\varepsilon^4}{\partial x_3}$$

$$K_\varepsilon^{2,3} = K_\varepsilon^{3,2} = \frac{\partial N_\varepsilon^2}{\partial x_1}\frac{\partial N_\varepsilon^3}{\partial x_1} + \frac{\partial N_\varepsilon^2}{\partial x_2}\frac{\partial N_\varepsilon^3}{\partial x_2} + \frac{\partial N_\varepsilon^2}{\partial x_3}\frac{\partial N_\varepsilon^3}{\partial x_3}$$

$$K_\varepsilon^{2,4} = K_\varepsilon^{4,2} = \frac{\partial N_\varepsilon^2}{\partial x_1}\frac{\partial N_\varepsilon^4}{\partial x_1} + \frac{\partial N_\varepsilon^2}{\partial x_2}\frac{\partial N_\varepsilon^4}{\partial x_2} + \frac{\partial N_\varepsilon^2}{\partial x_3}\frac{\partial N_\varepsilon^4}{\partial x_3}$$

$$K_\varepsilon^{3,4} = K_\varepsilon^{4,3} = \frac{\partial N_\varepsilon^3}{\partial x_1}\frac{\partial N_\varepsilon^4}{\partial x_1} + \frac{\partial N_\varepsilon^3}{\partial x_2}\frac{\partial N_\varepsilon^4}{\partial x_2} + \frac{\partial N_\varepsilon^3}{\partial x_3}\frac{\partial N_\varepsilon^4}{\partial x_3} \tag{B.40}$$

The 4×1 vector based on both the generation and source terms of the dissipation rate equation is given as

$$\mathbf{f}_{\varepsilon\Omega} = \frac{E}{K}\int_\Omega \left[f_{\varepsilon\Omega}^{i,j}\right] d\Omega = \int_\Omega \mathbf{N}_\varepsilon{}^T \frac{E}{K}\Upsilon_\varepsilon^{III} d\Omega = \int_\Omega \mathbf{N}_\varepsilon{}^T \frac{E}{K}\left[c_{\varepsilon 1}\tau_{ij}^R \partial_j u_i - c_{\varepsilon 2}\mathbf{N}_\varepsilon \tilde{\mathbf{E}}\right] d\Omega \tag{B.41}$$

where $\Upsilon_\varepsilon^{III} = r_{1\varepsilon} + r_{2\varepsilon} + r_{3\varepsilon} + r_{4\varepsilon} + r_{5\varepsilon} + r_{6\varepsilon} + r_{7\varepsilon} + r_{8\varepsilon} + r_{9\varepsilon} + r_{10\varepsilon} + r_{11\varepsilon}$ may be respectively expressed

$$\begin{aligned}
r_{1\varepsilon} &= \frac{4c_{\varepsilon 1}\mu_t}{3Re}\left(u_1^1\frac{\partial N_u^1}{\partial x_1} + u_1^2\frac{\partial N_u^2}{\partial x_1} + u_1^3\frac{\partial N_u^3}{\partial x_1} + u_1^4\frac{\partial N_u^4}{\partial x_1}\right)^2 - \\
&- \frac{2c_{\varepsilon 1}\mu_t}{3Re}\left(u_2^1\frac{\partial N_u^1}{\partial x_2} + u_2^2\frac{\partial N_u^2}{\partial x_2} + u_2^3\frac{\partial N_u^3}{\partial x_2} + u_2^4\frac{\partial N_u^4}{\partial x_2}\right) \\
&\quad \left(u_1^1\frac{\partial N_u^1}{\partial x_1} + u_1^2\frac{\partial N_u^2}{\partial x_1} + u_1^3\frac{\partial N_u^3}{\partial x_1} + u_1^4\frac{\partial N_u^4}{\partial x_1}\right) - \\
&- \frac{2c_{\varepsilon 1}\mu_t}{3Re}\left(u_3^1\frac{\partial N_u^1}{\partial x_3} + u_3^2\frac{\partial N_u^2}{\partial x_3} + u_3^3\frac{\partial N_u^3}{\partial x_3} + u_3^4\frac{\partial N_u^4}{\partial x_3}\right) \\
&\quad \left(u_1^1\frac{\partial N_u^1}{\partial x_1} + u_1^2\frac{\partial N_u^2}{\partial x_1} + u_1^3\frac{\partial N_u^3}{\partial x_1} + u_1^4\frac{\partial N_u^4}{\partial x_1}\right) \\
r_{2\varepsilon} &= \frac{4c_{\varepsilon 1}\mu_t}{3Re}\left(u_2^1\frac{\partial N_u^1}{\partial x_2} + u_2^2\frac{\partial N_u^2}{\partial x_2} + u_2^3\frac{\partial N_u^3}{\partial x_2} + u_2^4\frac{\partial N_u^4}{\partial x_2}\right)^2 - \\
&- \frac{2c_{\varepsilon 1}\mu_t}{3Re}\left(u_3^1\frac{\partial N_u^1}{\partial x_3} + u_3^2\frac{\partial N_u^2}{\partial x_3} + u_3^3\frac{\partial N_u^3}{\partial x_3} + u_3^4\frac{\partial N_u^4}{\partial x_3}\right) \\
&\quad \left(u_2^1\frac{\partial N_u^1}{\partial x_2} + u_2^2\frac{\partial N_u^2}{\partial x_2} + u_2^3\frac{\partial N_u^3}{\partial x_2} + u_2^4\frac{\partial N_u^4}{\partial x_2}\right) -
\end{aligned}$$

$$
\begin{aligned}
& - \frac{2c_{\varepsilon 1}\mu_t}{3Re}\left(u_1^1\frac{\partial N_u^1}{\partial x_1} + u_1^2\frac{\partial N_u^2}{\partial x_1} + u_1^3\frac{\partial N_u^3}{\partial x_1} + u_1^4\frac{\partial N_u^4}{\partial x_1}\right) \\
& \quad \left(u_2^1\frac{\partial N_u^1}{\partial x_2} + u_2^2\frac{\partial N_u^2}{\partial x_2} + u_2^3\frac{\partial N_u^3}{\partial x_2} + u_2^4\frac{\partial N_u^4}{\partial x_2}\right) \\
r_{3\varepsilon} &= \frac{4c_{\varepsilon 1}\mu_t}{3Re}\left(u_3^1\frac{\partial N_u^1}{\partial x_3} + u_3^2\frac{\partial N_u^2}{\partial x_3} + u_3^3\frac{\partial N_u^3}{\partial x_3} + u_3^4\frac{\partial N_u^4}{\partial x_3}\right)^2 - \\
& - \frac{2c_{\varepsilon 1}\mu_t}{3Re}\left(u_1^1\frac{\partial N_u^1}{\partial x_1} + u_1^2\frac{\partial N_u^2}{\partial x_1} + u_1^3\frac{\partial N_u^3}{\partial x_1} + u_1^4\frac{\partial N_u^4}{\partial x_1}\right) \\
& \quad \left(u_3^1\frac{\partial N_u^1}{\partial x_3} + u_3^2\frac{\partial N_u^2}{\partial x_3} + u_3^3\frac{\partial N_u^3}{\partial x_3} + u_3^4\frac{\partial N_u^4}{\partial x_3}\right) - \\
& - \frac{2c_{\varepsilon 1}\mu_t}{3Re}\left(u_2^1\frac{\partial N_u^1}{\partial x_2} + u_2^2\frac{\partial N_u^2}{\partial x_2} + u_2^3\frac{\partial N_u^3}{\partial x_2} + u_2^4\frac{\partial N_u^4}{\partial x_2}\right) \\
& \quad \left(u_3^1\frac{\partial N_u^1}{\partial x_3} + u_3^2\frac{\partial N_u^2}{\partial x_3} + u_3^3\frac{\partial N_u^3}{\partial x_3} + u_3^4\frac{\partial N_u^4}{\partial x_3}\right) \\
r_{4\varepsilon} &= \frac{c_{\varepsilon 1}\mu_t}{Re}\left(u_1^1\frac{\partial N_u^1}{\partial x_2} + u_1^2\frac{\partial N_u^2}{\partial x_2} + u_1^3\frac{\partial N_u^3}{\partial x_2} + u_1^4\frac{\partial N_u^4}{\partial x_2}\right)^2 + \\
& + \frac{c_{\varepsilon 1}\mu_t}{Re}\left(u_2^1\frac{\partial N_u^1}{\partial x_1} + u_2^2\frac{\partial N_u^2}{\partial x_1} + u_2^3\frac{\partial N_u^3}{\partial x_1} + u_2^4\frac{\partial N_u^4}{\partial x_1}\right) \\
& \quad \left(u_1^1\frac{\partial N_u^1}{\partial x_2} + u_1^2\frac{\partial N_u^2}{\partial x_2} + u_1^3\frac{\partial N_u^3}{\partial x_2} + u_1^4\frac{\partial N_u^4}{\partial x_2}\right) \\
r_{5\varepsilon} &= \frac{c_{\varepsilon 1}\mu_t}{Re}\left(u_2^1\frac{\partial N_u^1}{\partial x_1} + u_2^2\frac{\partial N_u^2}{\partial x_1} + u_2^3\frac{\partial N_u^3}{\partial x_1} + u_2^4\frac{\partial N_u^4}{\partial x_1}\right)^2 + \\
& + \frac{c_{\varepsilon 1}\mu_t}{Re}\left(u_1^1\frac{\partial N_u^1}{\partial x_2} + u_1^2\frac{\partial N_u^2}{\partial x_2} + u_1^3\frac{\partial N_u^3}{\partial x_2} + u_1^4\frac{\partial N_u^4}{\partial x_2}\right) \\
& \quad \left(u_2^1\frac{\partial N_u^1}{\partial x_1} + u_2^2\frac{\partial N_u^2}{\partial x_1} + u_2^3\frac{\partial N_u^3}{\partial x_1} + u_2^4\frac{\partial N_u^4}{\partial x_1}\right) \\
r_{6\varepsilon} &= \frac{c_{\varepsilon 1}\mu_t}{Re}\left(u_1^1\frac{\partial N_u^1}{\partial x_3} + u_1^2\frac{\partial N_u^2}{\partial x_3} + u_1^3\frac{\partial N_u^3}{\partial x_3} + u_1^4\frac{\partial N_u^4}{\partial x_3}\right)^2 + \\
& + \frac{c_{\varepsilon 1}\mu_t}{Re}\left(u_3^1\frac{\partial N_u^1}{\partial x_1} + u_3^2\frac{\partial N_u^2}{\partial x_1} + u_3^3\frac{\partial N_u^3}{\partial x_1} + u_3^4\frac{\partial N_u^4}{\partial x_1}\right) \\
& \quad \left(u_1^1\frac{\partial N_u^1}{\partial x_3} + u_1^2\frac{\partial N_u^2}{\partial x_3} + u_1^3\frac{\partial N_u^3}{\partial x_3} + u_1^4\frac{\partial N_u^4}{\partial x_3}\right) \\
r_{7\varepsilon} &= \frac{c_{\varepsilon 1}\mu_t}{Re}\left(u_3^1\frac{\partial N_u^1}{\partial x_1} + u_3^2\frac{\partial N_u^2}{\partial x_1} + u_3^3\frac{\partial N_u^3}{\partial x_1} + u_3^4\frac{\partial N_u^4}{\partial x_1}\right)^2 + \\
& + \frac{c_{\varepsilon 1}\mu_t}{Re}\left(u_1^1\frac{\partial N_u^1}{\partial x_3} + u_1^2\frac{\partial N_u^2}{\partial x_3} + u_1^3\frac{\partial N_u^3}{\partial x_3} + u_1^4\frac{\partial N_u^4}{\partial x_3}\right) \\
& \quad \left(u_3^1\frac{\partial N_u^1}{\partial x_1} + u_3^2\frac{\partial N_u^2}{\partial x_1} + u_3^3\frac{\partial N_u^3}{\partial x_1} + u_3^4\frac{\partial N_u^4}{\partial x_1}\right)
\end{aligned}
$$

$$\begin{aligned}
r_{8\varepsilon} &= \frac{c_{\varepsilon 1}\mu_t}{Re}\left(u_2^1\frac{\partial N_u^1}{\partial x_3}+u_2^2\frac{\partial N_u^2}{\partial x_3}+u_2^3\frac{\partial N_u^3}{\partial x_3}+u_2^4\frac{\partial N_u^4}{\partial x_3}\right)^2+\\
&+ \frac{c_{\varepsilon 1}\mu_t}{Re}\left(u_3^1\frac{\partial N_u^1}{\partial x_2}+u_3^2\frac{\partial N_u^2}{\partial x_2}+u_3^3\frac{\partial N_u^3}{\partial x_2}+u_3^4\frac{\partial N_u^4}{\partial x_2}\right)\\
&\quad \left(u_2^1\frac{\partial N_u^1}{\partial x_3}+u_2^2\frac{\partial N_u^2}{\partial x_3}+u_2^3\frac{\partial N_u^3}{\partial x_3}+u_2^4\frac{\partial N_u^4}{\partial x_3}\right)\\
r_{9\varepsilon} &= \frac{c_{\varepsilon 1}\mu_t}{Re}\left(u_3^1\frac{\partial N_u^1}{\partial x_2}+u_3^2\frac{\partial N_u^2}{\partial x_2}+u_3^3\frac{\partial N_u^3}{\partial x_2}+u_3^4\frac{\partial N_u^4}{\partial x_2}\right)^2+\\
&+ \frac{c_{\varepsilon 1}\mu_t}{Re}\left(u_2^1\frac{\partial N_u^1}{\partial x_3}+u_2^2\frac{\partial N_u^2}{\partial x_3}+u_2^3\frac{\partial N_u^3}{\partial x_3}+u_2^4\frac{\partial N_u^4}{\partial x_3}\right)\\
&\quad \left(u_3^1\frac{\partial N_u^1}{\partial x_2}+u_3^2\frac{\partial N_u^2}{\partial x_2}+u_3^3\frac{\partial N_u^3}{\partial x_2}+u_3^4\frac{\partial N_u^4}{\partial x_2}\right)\\
r_{10\varepsilon} &= -\frac{2c_{\varepsilon 1}}{3}\left(K^1N_\varepsilon^1+K^2N_\varepsilon^2+K^3N_\varepsilon^3+K^4N_\varepsilon^4\right)\\
&\quad \left(u_1^1\frac{\partial N_u^1}{\partial x_1}+u_1^2\frac{\partial N_u^2}{\partial x_1}+u_1^3\frac{\partial N_u^3}{\partial x_1}+u_1^4\frac{\partial N_u^4}{\partial x_1}\right)-\\
&- \frac{2c_{\varepsilon 1}}{3}\left(K^1N_\varepsilon^1+K^2N_\varepsilon^2+K^3N_\varepsilon^3+K^4N_\varepsilon^4\right)\left(u_2^1\frac{\partial N_u^1}{\partial x_2}+u_2^2\frac{\partial N_u^2}{\partial x_2}+u_2^3\frac{\partial N_u^3}{\partial x_2}+u_2^4\frac{\partial N_u^4}{\partial x_2}\right)-\\
&- \frac{2c_{\varepsilon 1}}{3}\left(K^1N_\varepsilon^1+K^2N_\varepsilon^2+K^3N_\varepsilon^3+K^4N_\varepsilon^4\right)\left(u_3^1\frac{\partial N_u^1}{\partial x_3}+u_3^2\frac{\partial N_u^2}{\partial x_3}+u_3^3\frac{\partial N_u^3}{\partial x_3}+u_3^4\frac{\partial N_u^4}{\partial x_3}\right)\\
r_{11\varepsilon} &= -c_{\varepsilon 2}\left(E^1N_\varepsilon^1+E^2N_\varepsilon^2+E^3N_\varepsilon^3+E^4N_\varepsilon^4\right) \qquad \text{(B.42)}
\end{aligned}$$

Thus the vector coefficients $\left[f_{\varepsilon\Omega}^{i,j}\right]$ are

$$f_{\varepsilon\Omega}^{1,1}=N_\varepsilon^1\Upsilon_\varepsilon^{III};\quad f_{\varepsilon\Omega}^{2,1}=N_\varepsilon^2\Upsilon_\varepsilon^{III};\quad f_{\varepsilon\Omega}^{3,1}=N_\varepsilon^3\Upsilon_\varepsilon^{III};\quad f_{\varepsilon\Omega}^{4,1}=N_\varepsilon^4\Upsilon_\varepsilon^{III} \qquad \text{(B.43)}$$

The 4×1 forcing vector for the dissipation rate is given as

$$\mathbf{f}_{\varepsilon\Gamma}=\frac{1}{Re}\left(\mu+\frac{\mu_t}{\sigma_\varepsilon}\right)\int_\Gamma\left[f_{\varepsilon\Gamma}^{i,j}\right]d\Gamma=\int_\Gamma \mathbf{N}_\varepsilon{}^T t_\varepsilon d\Gamma \qquad \text{(B.44)}$$

where the vector coefficients $\left[f_{\varepsilon\Gamma}^{i,j}\right]$ are

$$f_{\varepsilon\Gamma}^{1,1} = N_\varepsilon^1\left(\varepsilon^1\frac{\partial N_\varepsilon^1}{\partial x_1}+\varepsilon^2\frac{\partial N_\varepsilon^2}{\partial x_1}+\varepsilon^3\frac{\partial N_\varepsilon^3}{\partial x_1}+\varepsilon^4\frac{\partial N_\varepsilon^4}{\partial x_1}\right)\hat{n}_{x_1}+$$

$$
\begin{aligned}
& + \quad N_\varepsilon^1 \left(\varepsilon^1 \frac{\partial N_\varepsilon^1}{\partial x_2} + \varepsilon^2 \frac{\partial N_\varepsilon^2}{\partial x_2} + \varepsilon^3 \frac{\partial N_\varepsilon^3}{\partial x_2} + \varepsilon^4 \frac{\partial N_\varepsilon^4}{\partial x_2} \right) \hat{n}_{x_2} + \\
& + \quad N_\varepsilon^1 \left(\varepsilon^1 \frac{\partial N_\varepsilon^1}{\partial x_3} + \varepsilon^2 \frac{\partial N_\varepsilon^2}{\partial x_3} + \varepsilon^3 \frac{\partial N_\varepsilon^3}{\partial x_3} + \varepsilon^4 \frac{\partial N_\varepsilon^4}{\partial x_3} \right) \hat{n}_{x_3} \\
f_{\varepsilon\Gamma}^{2,1} & = \quad N_\varepsilon^2 \left(\varepsilon^1 \frac{\partial N_\varepsilon^1}{\partial x_1} + \varepsilon^2 \frac{\partial N_\varepsilon^2}{\partial x_1} + \varepsilon^3 \frac{\partial N_\varepsilon^3}{\partial x_1} + \varepsilon^4 \frac{\partial N_\varepsilon^4}{\partial x_1} \right) \hat{n}_{x_1} + \\
& + \quad N_\varepsilon^2 \left(\varepsilon^1 \frac{\partial N_\varepsilon^1}{\partial x_2} + \varepsilon^2 \frac{\partial N_\varepsilon^2}{\partial x_2} + \varepsilon^3 \frac{\partial N_\varepsilon^3}{\partial x_2} + \varepsilon^4 \frac{\partial N_\varepsilon^4}{\partial x_2} \right) \hat{n}_{x_2} + \\
& + \quad N_\varepsilon^2 \left(\varepsilon^1 \frac{\partial N_\varepsilon^1}{\partial x_3} + \varepsilon^2 \frac{\partial N_\varepsilon^2}{\partial x_3} + \varepsilon^3 \frac{\partial N_\varepsilon^3}{\partial x_3} + \varepsilon^4 \frac{\partial N_\varepsilon^4}{\partial x_3} \right) \hat{n}_{x_3} \\
f_{\varepsilon\Gamma}^{3,1} & = \quad N_\varepsilon^3 \left(\varepsilon^1 \frac{\partial N_\varepsilon^1}{\partial x_1} + \varepsilon^2 \frac{\partial N_\varepsilon^2}{\partial x_1} + \varepsilon^3 \frac{\partial N_\varepsilon^3}{\partial x_1} + \varepsilon^4 \frac{\partial N_\varepsilon^4}{\partial x_1} \right) \hat{n}_{x_1} + \\
& + \quad N_\varepsilon^3 \left(\varepsilon^1 \frac{\partial N_\varepsilon^1}{\partial x_2} + \varepsilon^2 \frac{\partial N_\varepsilon^2}{\partial x_2} + \varepsilon^3 \frac{\partial N_\varepsilon^3}{\partial x_2} + \varepsilon^4 \frac{\partial N_\varepsilon^4}{\partial x_2} \right) \hat{n}_{x_2} + \\
& + \quad N_\varepsilon^3 \left(\varepsilon^1 \frac{\partial N_\varepsilon^1}{\partial x_3} + \varepsilon^2 \frac{\partial N_\varepsilon^2}{\partial x_3} + \varepsilon^3 \frac{\partial N_\varepsilon^3}{\partial x_3} + \varepsilon^4 \frac{\partial N_\varepsilon^4}{\partial x_3} \right) \hat{n}_{x_3} \\
f_{\varepsilon\Gamma}^{4,1} & = \quad N_\varepsilon^4 \left(\varepsilon^1 \frac{\partial N_\varepsilon^1}{\partial x_1} + \varepsilon^2 \frac{\partial N_\varepsilon^2}{\partial x_1} + \varepsilon^3 \frac{\partial N_\varepsilon^3}{\partial x_1} + \varepsilon^4 \frac{\partial N_\varepsilon^4}{\partial x_1} \right) \hat{n}_{x_1} + \\
& + \quad N_\varepsilon^4 \left(\varepsilon^1 \frac{\partial N_\varepsilon^1}{\partial x_2} + \varepsilon^2 \frac{\partial N_\varepsilon^2}{\partial x_2} + \varepsilon^3 \frac{\partial N_\varepsilon^3}{\partial x_2} + \varepsilon^4 \frac{\partial N_\varepsilon^4}{\partial x_2} \right) \hat{n}_{x_2} + \\
& + \quad N_\varepsilon^4 \left(\varepsilon^1 \frac{\partial N_\varepsilon^1}{\partial x_3} + \varepsilon^2 \frac{\partial N_\varepsilon^2}{\partial x_3} + \varepsilon^3 \frac{\partial N_\varepsilon^3}{\partial x_3} + \varepsilon^4 \frac{\partial N_\varepsilon^4}{\partial x_3} \right) \hat{n}_{x_3} \qquad \text{(B.45)}
\end{aligned}
$$

The 4×4 symmetric convection matrix of the stabilization for the dissipation rate is given as

$$
\mathbf{K}_{\mathbf{u}\varepsilon} = -\frac{1}{2} \int_\Omega \left[K_{u\varepsilon}^{i,j} \right] d\Omega = -\frac{1}{2} \int_\Omega (\nabla^T (\mathbf{u}\mathbf{N}_\varepsilon))^T (\nabla^T (\mathbf{u}\mathbf{N}_\varepsilon)) d\Omega \qquad \text{(B.46)}
$$

where the matrix coefficients $\left[K_{u\varepsilon}^{i,j} \right]$ are

$$
\begin{aligned}
K_{u\varepsilon}^{1,1} &= \left(\frac{\partial u_1 N_\varepsilon^1}{\partial x_1} + \frac{\partial u_2 N_\varepsilon^1}{\partial x_2} + \frac{\partial u_3 N_\varepsilon^1}{\partial x_3} \right)^2; \quad K_{u\varepsilon}^{2,2} = \left(\frac{\partial u_1 N_\varepsilon^2}{\partial x_1} + \frac{\partial u_2 N_\varepsilon^2}{\partial x_2} + \frac{\partial u_3 N_\varepsilon^2}{\partial x_3} \right)^2 \\
K_{u\varepsilon}^{3,3} &= \left(\frac{\partial u_1 N_\varepsilon^3}{\partial x_1} + \frac{\partial u_2 N_\varepsilon^3}{\partial x_2} + \frac{\partial u_3 N_\varepsilon^3}{\partial x_3} \right)^2; \quad K_{u\varepsilon}^{4,4} = \left(\frac{\partial u_1 N_\varepsilon^4}{\partial x_1} + \frac{\partial u_2 N_\varepsilon^4}{\partial x_2} + \frac{\partial u_3 N_\varepsilon^4}{\partial x_3} \right)^2 \\
K_{u\varepsilon}^{1,2} = K_{u\varepsilon}^{2,1} &= \left(\frac{\partial u_1 N_\varepsilon^1}{\partial x_1} + \frac{\partial u_2 N_\varepsilon^1}{\partial x_2} + \frac{\partial u_3 N_\varepsilon^1}{\partial x_3} \right) \left(\frac{\partial u_1 N_\varepsilon^2}{\partial x_1} + \frac{\partial u_2 N_\varepsilon^2}{\partial x_2} + \frac{\partial u_3 N_\varepsilon^2}{\partial x_3} \right)
\end{aligned}
$$

$$K_{u\varepsilon}^{1,3} = K_{u\varepsilon}^{3,1} = \left(\frac{\partial u_1 N_\varepsilon^1}{\partial x_1} + \frac{\partial u_2 N_\varepsilon^1}{\partial x_2} + \frac{\partial u_3 N_\varepsilon^1}{\partial x_3}\right)\left(\frac{\partial u_1 N_\varepsilon^3}{\partial x_1} + \frac{\partial u_2 N_\varepsilon^3}{\partial x_2} + \frac{\partial u_3 N_\varepsilon^3}{\partial x_3}\right)$$
$$K_{u\varepsilon}^{1,4} = K_{u\varepsilon}^{4,1} = \left(\frac{\partial u_1 N_\varepsilon^1}{\partial x_1} + \frac{\partial u_2 N_\varepsilon^1}{\partial x_2} + \frac{\partial u_3 N_\varepsilon^1}{\partial x_3}\right)\left(\frac{\partial u_1 N_\varepsilon^4}{\partial x_1} + \frac{\partial u_2 N_\varepsilon^4}{\partial x_2} + \frac{\partial u_3 N_\varepsilon^4}{\partial x_3}\right)$$
$$K_{u\varepsilon}^{2,3} = K_{u\varepsilon}^{3,2} = \left(\frac{\partial u_1 N_\varepsilon^2}{\partial x_1} + \frac{\partial u_2 N_\varepsilon^2}{\partial x_2} + \frac{\partial u_3 N_\varepsilon^2}{\partial x_3}\right)\left(\frac{\partial u_1 N_\varepsilon^3}{\partial x_1} + \frac{\partial u_2 N_\varepsilon^3}{\partial x_2} + \frac{\partial u_3 N_\varepsilon^3}{\partial x_3}\right)$$
$$K_{u\varepsilon}^{2,4} = K_{u\varepsilon}^{4,2} = \left(\frac{\partial u_1 N_\varepsilon^2}{\partial x_1} + \frac{\partial u_2 N_\varepsilon^2}{\partial x_2} + \frac{\partial u_3 N_\varepsilon^2}{\partial x_3}\right)\left(\frac{\partial u_1 N_\varepsilon^4}{\partial x_1} + \frac{\partial u_2 N_\varepsilon^4}{\partial x_2} + \frac{\partial u_3 N_\varepsilon^4}{\partial x_3}\right)$$
$$K_{u\varepsilon}^{3,4} = K_{u\varepsilon}^{4,3} = \left(\frac{\partial u_1 N_\varepsilon^3}{\partial x_1} + \frac{\partial u_2 N_\varepsilon^3}{\partial x_2} + \frac{\partial u_3 N_\varepsilon^3}{\partial x_3}\right)\left(\frac{\partial u_1 N_\varepsilon^4}{\partial x_1} + \frac{\partial u_2 N_\varepsilon^4}{\partial x_2} + \frac{\partial u_3 N_\varepsilon^4}{\partial x_3}\right) \tag{B.47}$$

The 4 × 4 symmetric, lumped mass matrix for the modified turbulent eddy kinematic viscosity is given as

$$\mathbf{M}_{\hat{\nu}} = \int_\Omega \left[M_{\hat{\nu}}^{i,j}\right] d\Omega = \int_\Omega \mathbf{N}_{\hat{\nu}}{}^T \mathbf{N}_{\hat{\nu}} d\Omega \tag{B.48}$$

where the matrix coefficients $\left[M_{\hat{\nu}}^{i,j}\right]$ are

$$M_{\hat{\nu}}^{1,1} = N_{\hat{\nu}}^1 N_{\hat{\nu}}^1; \quad M_{\hat{\nu}}^{2,2} = N_{\hat{\nu}}^2 N_{\hat{\nu}}^2; \quad M_{\hat{\nu}}^{3,3} = N_{\hat{\nu}}^3 N_{\hat{\nu}}^3; \quad M_{\hat{\nu}}^{4,4} = N_{\hat{\nu}}^4 N_{\hat{\nu}}^4$$
$$M_{\hat{\nu}}^{1,2} = M_{\hat{\nu}}^{2,1} = N_{\hat{\nu}}^1 N_{\hat{\nu}}^2; \quad M_{\hat{\nu}}^{1,3} = M_{\hat{\nu}}^{3,1} = N_{\hat{\nu}}^1 N_{\hat{\nu}}^3; \quad M_{\hat{\nu}}^{1,4} = M_{\hat{\nu}}^{4,1} = N_{\hat{\nu}}^1 N_{\hat{\nu}}^4$$
$$M_{\hat{\nu}}^{2,3} = M_{\hat{\nu}}^{3,2} = N_{\hat{\nu}}^2 N_{\hat{\nu}}^3; \quad M_{\hat{\nu}}^{2,4} = M_{\hat{\nu}}^{4,2} = N_{\hat{\nu}}^2 N_{\hat{\nu}}^4; \quad M_{\hat{\nu}}^{3,4} = M_{\hat{\nu}}^{4,3} = N_{\hat{\nu}}^3 N_{\hat{\nu}}^4 \tag{B.49}$$

The 4 × 4 convection matrix for the modified turbulent eddy kinematic viscosity is given as

$$\mathbf{C}_{\hat{\nu}} = \int_\Omega \left[C_{\hat{\nu}}^{i,j}\right] d\Omega = \int_\Omega \mathbf{N}_{\hat{\nu}}{}^T (\nabla^T (\mathbf{u}\mathbf{N}_{\hat{\nu}})) d\Omega \tag{B.50}$$

where the matrix coefficients $\left[C_{\hat{\nu}}^{i,j}\right]$ are

$$C_{\hat{\nu}}^{1,1} = N_{\hat{\nu}}^1 \left(\frac{\partial u_1 N_{\hat{\nu}}^1}{\partial x_1} + \frac{\partial u_2 N_{\hat{\nu}}^1}{\partial x_2} + \frac{\partial u_3 N_{\hat{\nu}}^1}{\partial x_3}\right); \quad C_{\hat{\nu}}^{2,2} = N_{\hat{\nu}}^2 \left(\frac{\partial u_1 N_{\hat{\nu}}^2}{\partial x_1} + \frac{\partial u_2 N_{\hat{\nu}}^2}{\partial x_2} + \frac{\partial u_3 N_{\hat{\nu}}^2}{\partial x_3}\right)$$
$$C_{\hat{\nu}}^{3,3} = N_{\hat{\nu}}^3 \left(\frac{\partial u_1 N_{\hat{\nu}}^3}{\partial x_1} + \frac{\partial u_2 N_{\hat{\nu}}^3}{\partial x_2} + \frac{\partial u_3 N_{\hat{\nu}}^3}{\partial x_3}\right); \quad C_{\hat{\nu}}^{4,4} = N_{\hat{\nu}}^4 \left(\frac{\partial u_1 N_{\hat{\nu}}^4}{\partial x_1} + \frac{\partial u_2 N_{\hat{\nu}}^4}{\partial x_2} + \frac{\partial u_3 N_{\hat{\nu}}^4}{\partial x_3}\right)$$

$$C_{\hat{\nu}}^{1,2} = N_{\hat{\nu}}^1\left(\frac{\partial u_1 N_{\hat{\nu}}^2}{\partial x_1} + \frac{\partial u_2 N_{\hat{\nu}}^2}{\partial x_2} + \frac{\partial u_3 N_{\hat{\nu}}^2}{\partial x_3}\right); \quad C_{\hat{\nu}}^{2,1} = N_{\hat{\nu}}^2\left(\frac{\partial u_1 N_{\hat{\nu}}^1}{\partial x_1} + \frac{\partial u_2 N_{\hat{\nu}}^1}{\partial x_2} + \frac{\partial u_3 N_{\hat{\nu}}^1}{\partial x_3}\right)$$
$$C_{\hat{\nu}}^{1,3} = N_{\hat{\nu}}^1\left(\frac{\partial u_1 N_{\hat{\nu}}^3}{\partial x_1} + \frac{\partial u_2 N_{\hat{\nu}}^3}{\partial x_2} + \frac{\partial u_3 N_{\hat{\nu}}^3}{\partial x_3}\right); \quad C_{\hat{\nu}}^{3,1} = N_{\hat{\nu}}^3\left(\frac{\partial u_1 N_{\hat{\nu}}^1}{\partial x_1} + \frac{\partial u_2 N_{\hat{\nu}}^1}{\partial x_2} + \frac{\partial u_3 N_{\hat{\nu}}^1}{\partial x_3}\right)$$
$$C_{\hat{\nu}}^{1,4} = N_{\hat{\nu}}^1\left(\frac{\partial u_1 N_{\hat{\nu}}^4}{\partial x_1} + \frac{\partial u_2 N_{\hat{\nu}}^4}{\partial x_2} + \frac{\partial u_3 N_{\hat{\nu}}^4}{\partial x_3}\right); \quad C_{\hat{\nu}}^{4,1} = N_{\hat{\nu}}^4\left(\frac{\partial u_1 N_{\hat{\nu}}^1}{\partial x_1} + \frac{\partial u_2 N_{\hat{\nu}}^1}{\partial x_2} + \frac{\partial u_3 N_{\hat{\nu}}^1}{\partial x_3}\right)$$
$$C_{\hat{\nu}}^{2,3} = N_{\hat{\nu}}^2\left(\frac{\partial u_1 N_{\hat{\nu}}^3}{\partial x_1} + \frac{\partial u_2 N_{\hat{\nu}}^3}{\partial x_2} + \frac{\partial u_3 N_{\hat{\nu}}^3}{\partial x_3}\right); \quad C_{\hat{\nu}}^{3,2} = N_{\hat{\nu}}^3\left(\frac{\partial u_1 N_{\hat{\nu}}^2}{\partial x_1} + \frac{\partial u_2 N_{\hat{\nu}}^2}{\partial x_2} + \frac{\partial u_3 N_{\hat{\nu}}^2}{\partial x_3}\right)$$
$$C_{\hat{\nu}}^{2,4} = N_{\hat{\nu}}^2\left(\frac{\partial u_1 N_{\hat{\nu}}^4}{\partial x_1} + \frac{\partial u_2 N_{\hat{\nu}}^4}{\partial x_2} + \frac{\partial u_3 N_{\hat{\nu}}^4}{\partial x_3}\right); \quad C_{\hat{\nu}}^{4,2} = N_{\hat{\nu}}^4\left(\frac{\partial u_1 N_{\hat{\nu}}^2}{\partial x_1} + \frac{\partial u_2 N_{\hat{\nu}}^2}{\partial x_2} + \frac{\partial u_3 N_{\hat{\nu}}^2}{\partial x_3}\right)$$
$$C_{\hat{\nu}}^{3,4} = N_{\hat{\nu}}^3\left(\frac{\partial u_1 N_{\hat{\nu}}^4}{\partial x_1} + \frac{\partial u_2 N_{\hat{\nu}}^4}{\partial x_2} + \frac{\partial u_3 N_{\hat{\nu}}^4}{\partial x_3}\right); \quad C_{\hat{\nu}}^{4,3} = N_{\hat{\nu}}^4\left(\frac{\partial u_1 N_{\hat{\nu}}^3}{\partial x_1} + \frac{\partial u_2 N_{\hat{\nu}}^3}{\partial x_2} + \frac{\partial u_3 N_{\hat{\nu}}^3}{\partial x_3}\right)$$

(B.51)

The 4 × 4 symmetric matrix resulted from first diffusion term in the modified turbulent eddy kinematic viscosity equation is given as

$$\mathbf{K}_{\hat{\nu}} = \frac{\nu + \hat{\nu}}{\sigma_{\hat{\nu}} Re}\int_\Omega \left[K_{\hat{\nu}}^{i,j}\right] d\Omega = \int_\Omega (\nabla \mathbf{N}_{\hat{\nu}})^T \left(\frac{\nu + \hat{\nu}}{\sigma_{\hat{\nu}} Re}\right) \nabla \mathbf{N}_{\hat{\nu}} d\Omega \tag{B.52}$$

where the matrix coefficients $\left[K_{\hat{\nu}}^{i,j}\right]$ are

$$K_{\hat{\nu}}^{1,1} = \left(\frac{\partial N_{\hat{\nu}}^1}{\partial x_1}\right)^2 + \left(\frac{\partial N_{\hat{\nu}}^1}{\partial x_2}\right)^2 + \left(\frac{\partial N_{\hat{\nu}}^1}{\partial x_3}\right)^2; \quad K_{\hat{\nu}}^{2,2} = \left(\frac{\partial N_{\hat{\nu}}^2}{\partial x_1}\right)^2 + \left(\frac{\partial N_{\hat{\nu}}^2}{\partial x_2}\right)^2 + \left(\frac{\partial N_{\hat{\nu}}^2}{\partial x_3}\right)^2$$
$$K_{\hat{\nu}}^{3,3} = \left(\frac{\partial N_{\hat{\nu}}^3}{\partial x_1}\right)^2 + \left(\frac{\partial N_{\hat{\nu}}^3}{\partial x_2}\right)^2 + \left(\frac{\partial N_{\hat{\nu}}^3}{\partial x_3}\right)^2; \quad K_{\hat{\nu}}^{4,4} = \left(\frac{\partial N_{\hat{\nu}}^4}{\partial x_1}\right)^2 + \left(\frac{\partial N_{\hat{\nu}}^4}{\partial x_2}\right)^2 + \left(\frac{\partial N_{\hat{\nu}}^4}{\partial x_3}\right)^2$$
$$K_{\hat{\nu}}^{1,2} = K_{\hat{\nu}}^{2,1} = \frac{\partial N_{\hat{\nu}}^1}{\partial x_1}\frac{\partial N_{\hat{\nu}}^2}{\partial x_1} + \frac{\partial N_{\hat{\nu}}^1}{\partial x_2}\frac{\partial N_{\hat{\nu}}^2}{\partial x_2} + \frac{\partial N_{\hat{\nu}}^1}{\partial x_3}\frac{\partial N_{\hat{\nu}}^2}{\partial x_3}$$
$$K_{\hat{\nu}}^{1,3} = K_{\hat{\nu}}^{3,1} = \frac{\partial N_{\hat{\nu}}^1}{\partial x_1}\frac{\partial N_{\hat{\nu}}^3}{\partial x_1} + \frac{\partial N_{\hat{\nu}}^1}{\partial x_2}\frac{\partial N_{\hat{\nu}}^3}{\partial x_2} + \frac{\partial N_{\hat{\nu}}^1}{\partial x_3}\frac{\partial N_{\hat{\nu}}^3}{\partial x_3}$$
$$K_{\hat{\nu}}^{1,4} = K_{\hat{\nu}}^{4,1} = \frac{\partial N_{\hat{\nu}}^1}{\partial x_1}\frac{\partial N_{\hat{\nu}}^4}{\partial x_1} + \frac{\partial N_{\hat{\nu}}^1}{\partial x_2}\frac{\partial N_{\hat{\nu}}^4}{\partial x_2} + \frac{\partial N_{\hat{\nu}}^1}{\partial x_3}\frac{\partial N_{\hat{\nu}}^4}{\partial x_3}$$
$$K_{\hat{\nu}}^{2,3} = K_{\hat{\nu}}^{3,2} = \frac{\partial N_{\hat{\nu}}^2}{\partial x_1}\frac{\partial N_{\hat{\nu}}^3}{\partial x_1} + \frac{\partial N_{\hat{\nu}}^2}{\partial x_2}\frac{\partial N_{\hat{\nu}}^3}{\partial x_2} + \frac{\partial N_{\hat{\nu}}^2}{\partial x_3}\frac{\partial N_{\hat{\nu}}^3}{\partial x_3}$$
$$K_{\hat{\nu}}^{2,4} = K_{\hat{\nu}}^{4,2} = \frac{\partial N_{\hat{\nu}}^2}{\partial x_1}\frac{\partial N_{\hat{\nu}}^4}{\partial x_1} + \frac{\partial N_{\hat{\nu}}^2}{\partial x_2}\frac{\partial N_{\hat{\nu}}^4}{\partial x_2} + \frac{\partial N_{\hat{\nu}}^2}{\partial x_3}\frac{\partial N_{\hat{\nu}}^4}{\partial x_3}$$
$$K_{\hat{\nu}}^{3,4} = K_{\hat{\nu}}^{4,3} = \frac{\partial N_{\hat{\nu}}^3}{\partial x_1}\frac{\partial N_{\hat{\nu}}^4}{\partial x_1} + \frac{\partial N_{\hat{\nu}}^3}{\partial x_2}\frac{\partial N_{\hat{\nu}}^4}{\partial x_2} + \frac{\partial N_{\hat{\nu}}^3}{\partial x_3}\frac{\partial N_{\hat{\nu}}^4}{\partial x_3}$$

(B.53)

The 4×1 vector resulted from second diffusion term in the modified turbulent eddy kinematic viscosity equation is given as

$$\mathbf{f}_{\hat{\nu}\boldsymbol{\Omega}} = \frac{c_{b2}}{\sigma_{\hat{\nu}} Re} \int_{\Omega} \left[f_{\hat{\nu}\Omega}^{i,j} \right] d\Omega = \int_{\Omega} \mathbf{N}_{\hat{\nu}}{}^{T} \left(\frac{c_{b2}}{\sigma_{\hat{\nu}} Re} \right) (\partial_i \hat{\nu})^2 d\Omega \qquad \text{(B.54)}$$

where the vector coefficients $\left[f_{\hat{\nu}\Omega}^{i,j} \right]$ are

$$\begin{aligned}
f_{\hat{\nu}\Omega}^{1,1} &= N_{\hat{\nu}}^{1} \left(\hat{\nu}^{1} \frac{\partial N_{\hat{\nu}}^{1}}{\partial x_1} + \hat{\nu}^{2} \frac{\partial N_{\hat{\nu}}^{2}}{\partial x_1} + \hat{\nu}^{3} \frac{\partial N_{\hat{\nu}}^{3}}{\partial x_1} + \hat{\nu}^{4} \frac{\partial N_{\hat{\nu}}^{4}}{\partial x_1} \right)^2 + \\
&+ N_{\hat{\nu}}^{1} \left(\hat{\nu}^{1} \frac{\partial N_{\hat{\nu}}^{1}}{\partial x_2} + \hat{\nu}^{2} \frac{\partial N_{\hat{\nu}}^{2}}{\partial x_2} + \hat{\nu}^{3} \frac{\partial N_{\hat{\nu}}^{3}}{\partial x_2} + \hat{\nu}^{4} \frac{\partial N_{\hat{\nu}}^{4}}{\partial x_2} \right)^2 + \\
&+ N_{\hat{\nu}}^{1} \left(\hat{\nu}^{1} \frac{\partial N_{\hat{\nu}}^{1}}{\partial x_3} + \hat{\nu}^{2} \frac{\partial N_{\hat{\nu}}^{2}}{\partial x_3} + \hat{\nu}^{3} \frac{\partial N_{\hat{\nu}}^{3}}{\partial x_3} + \hat{\nu}^{4} \frac{\partial N_{\hat{\nu}}^{4}}{\partial x_3} \right)^2 \\
f_{\hat{\nu}\Omega}^{2,1} &= N_{\hat{\nu}}^{2} \left(\hat{\nu}^{1} \frac{\partial N_{\hat{\nu}}^{1}}{\partial x_1} + \hat{\nu}^{2} \frac{\partial N_{\hat{\nu}}^{2}}{\partial x_1} + \hat{\nu}^{3} \frac{\partial N_{\hat{\nu}}^{3}}{\partial x_1} + \hat{\nu}^{4} \frac{\partial N_{\hat{\nu}}^{4}}{\partial x_1} \right)^2 + \\
&+ N_{\hat{\nu}}^{2} \left(\hat{\nu}^{1} \frac{\partial N_{\hat{\nu}}^{1}}{\partial x_2} + \hat{\nu}^{2} \frac{\partial N_{\hat{\nu}}^{2}}{\partial x_2} + \hat{\nu}^{3} \frac{\partial N_{\hat{\nu}}^{3}}{\partial x_2} + \hat{\nu}^{4} \frac{\partial N_{\hat{\nu}}^{4}}{\partial x_2} \right)^2 + \\
&+ N_{\hat{\nu}}^{2} \left(\hat{\nu}^{1} \frac{\partial N_{\hat{\nu}}^{1}}{\partial x_3} + \hat{\nu}^{2} \frac{\partial N_{\hat{\nu}}^{2}}{\partial x_3} + \hat{\nu}^{3} \frac{\partial N_{\hat{\nu}}^{3}}{\partial x_3} + \hat{\nu}^{4} \frac{\partial N_{\hat{\nu}}^{4}}{\partial x_3} \right)^2 \\
f_{\hat{\nu}\Omega}^{3,1} &= N_{\hat{\nu}}^{3} \left(\hat{\nu}^{1} \frac{\partial N_{\hat{\nu}}^{1}}{\partial x_1} + \hat{\nu}^{2} \frac{\partial N_{\hat{\nu}}^{2}}{\partial x_1} + \hat{\nu}^{3} \frac{\partial N_{\hat{\nu}}^{3}}{\partial x_1} + \hat{\nu}^{4} \frac{\partial N_{\hat{\nu}}^{4}}{\partial x_1} \right)^2 + \\
&+ N_{\hat{\nu}}^{3} \left(\hat{\nu}^{1} \frac{\partial N_{\hat{\nu}}^{1}}{\partial x_2} + \hat{\nu}^{2} \frac{\partial N_{\hat{\nu}}^{2}}{\partial x_2} + \hat{\nu}^{3} \frac{\partial N_{\hat{\nu}}^{3}}{\partial x_2} + \hat{\nu}^{4} \frac{\partial N_{\hat{\nu}}^{4}}{\partial x_2} \right)^2 + \\
&+ N_{\hat{\nu}}^{3} \left(\hat{\nu}^{1} \frac{\partial N_{\hat{\nu}}^{1}}{\partial x_3} + \hat{\nu}^{2} \frac{\partial N_{\hat{\nu}}^{2}}{\partial x_3} + \hat{\nu}^{3} \frac{\partial N_{\hat{\nu}}^{3}}{\partial x_3} + \hat{\nu}^{4} \frac{\partial N_{\hat{\nu}}^{4}}{\partial x_3} \right)^2 \\
f_{\hat{\nu}\Omega}^{4,1} &= N_{\hat{\nu}}^{4} \left(\hat{\nu}^{1} \frac{\partial N_{\hat{\nu}}^{1}}{\partial x_1} + \hat{\nu}^{2} \frac{\partial N_{\hat{\nu}}^{2}}{\partial x_1} + \hat{\nu}^{3} \frac{\partial N_{\hat{\nu}}^{3}}{\partial x_1} + \hat{\nu}^{4} \frac{\partial N_{\hat{\nu}}^{4}}{\partial x_1} \right)^2 + \\
&+ N_{\hat{\nu}}^{4} \left(\hat{\nu}^{1} \frac{\partial N_{\hat{\nu}}^{1}}{\partial x_2} + \hat{\nu}^{2} \frac{\partial N_{\hat{\nu}}^{2}}{\partial x_2} + \hat{\nu}^{3} \frac{\partial N_{\hat{\nu}}^{3}}{\partial x_2} + \hat{\nu}^{4} \frac{\partial N_{\hat{\nu}}^{4}}{\partial x_2} \right)^2 + \\
&+ N_{\hat{\nu}}^{4} \left(\hat{\nu}^{1} \frac{\partial N_{\hat{\nu}}^{1}}{\partial x_3} + \hat{\nu}^{2} \frac{\partial N_{\hat{\nu}}^{2}}{\partial x_3} + \hat{\nu}^{3} \frac{\partial N_{\hat{\nu}}^{3}}{\partial x_3} + \hat{\nu}^{4} \frac{\partial N_{\hat{\nu}}^{4}}{\partial x_3} \right)^2 \qquad \text{(B.55)}
\end{aligned}$$

The 4×1 vector based on both the production and destruction terms of the modified turbulent eddy kinematic viscosity equation is given as

$$\mathbf{f}_{\hat{\nu}\Omega^*} = \left(c_{b1}\hat{S} - \frac{c_{w1}f_w}{Re}\frac{\hat{\nu}}{y^2}\right)\int_\Omega \left[f^{i,j}_{\hat{\nu}\Omega^*}\right] d\Omega = \int_\Omega \mathbf{N}_{\hat{\nu}}{}^T\left(c_{b1}\hat{S} - \frac{c_{w1}f_w}{Re}\frac{\hat{\nu}}{y^2}\right)\mathbf{N}_{\hat{\nu}}\tilde{\hat{\nu}}d\Omega \quad \text{(B.56)}$$

where the vector coefficients $\left[f^{i,j}_{\hat{\nu}\Omega^*}\right]$ are

$$\begin{aligned}
f^{1,1}_{\hat{\nu}\Omega^*} &= N^1_{\hat{\nu}}\left(\hat{\nu}^1 N^1_{\hat{\nu}} + \hat{\nu}^2 N^2_{\hat{\nu}} + \hat{\nu}^3 N^3_{\hat{\nu}} + \hat{\nu}^4 N^4_{\hat{\nu}}\right)\\
f^{2,1}_{\hat{\nu}\Omega^*} &= N^2_{\hat{\nu}}\left(\hat{\nu}^1 N^1_{\hat{\nu}} + \hat{\nu}^2 N^2_{\hat{\nu}} + \hat{\nu}^3 N^3_{\hat{\nu}} + \hat{\nu}^4 N^4_{\hat{\nu}}\right)\\
f^{3,1}_{\hat{\nu}\Omega^*} &= N^3_{\hat{\nu}}\left(\hat{\nu}^1 N^1_{\hat{\nu}} + \hat{\nu}^2 N^2_{\hat{\nu}} + \hat{\nu}^3 N^3_{\hat{\nu}} + \hat{\nu}^4 N^4_{\hat{\nu}}\right)\\
f^{4,1}_{\hat{\nu}\Omega^*} &= N^4_{\hat{\nu}}\left(\hat{\nu}^1 N^1_{\hat{\nu}} + \hat{\nu}^2 N^2_{\hat{\nu}} + \hat{\nu}^3 N^3_{\hat{\nu}} + \hat{\nu}^4 N^4_{\hat{\nu}}\right) \qquad \text{(B.57)}
\end{aligned}$$

The 4 × 1 forcing vector for the modified turbulent eddy kinematic viscosity is given as

$$\mathbf{f}_{\hat{\nu}\Gamma} = \frac{\nu + \hat{\nu}}{\sigma_{\hat{\nu}} Re}\int_\Gamma \left[f^{i,j}_{\hat{\nu}\Gamma}\right] d\Gamma = \int_\Gamma \mathbf{N}_{\hat{\nu}}{}^T t_{\hat{\nu}} d\Gamma \qquad \text{(B.58)}$$

where the vector coefficients $\left[f^{i,j}_{\hat{\nu}\Gamma}\right]$ are

$$\begin{aligned}
f^{1,1}_{\hat{\nu}\Gamma} &= N^1_{\hat{\nu}}\left(\hat{\nu}^1\frac{\partial N^1_{\hat{\nu}}}{\partial x_1} + \hat{\nu}^2\frac{\partial N^2_{\hat{\nu}}}{\partial x_1} + \hat{\nu}^3\frac{\partial N^3_{\hat{\nu}}}{\partial x_1} + \hat{\nu}^4\frac{\partial N^4_{\hat{\nu}}}{\partial x_1}\right)\hat{n}_{x_1} +\\
&+ N^1_{\hat{\nu}}\left(\hat{\nu}^1\frac{\partial N^1_{\hat{\nu}}}{\partial x_2} + \hat{\nu}^2\frac{\partial N^2_{\hat{\nu}}}{\partial x_2} + \hat{\nu}^3\frac{\partial N^3_{\hat{\nu}}}{\partial x_2} + \hat{\nu}^4\frac{\partial N^4_{\hat{\nu}}}{\partial x_2}\right)\hat{n}_{x_2} +\\
&+ N^1_{\hat{\nu}}\left(\hat{\nu}^1\frac{\partial N^1_{\hat{\nu}}}{\partial x_3} + \hat{\nu}^2\frac{\partial N^2_{\hat{\nu}}}{\partial x_3} + \hat{\nu}^3\frac{\partial N^3_{\hat{\nu}}}{\partial x_3} + \hat{\nu}^4\frac{\partial N^4_{\hat{\nu}}}{\partial x_3}\right)\hat{n}_{x_3}\\
f^{2,1}_{\hat{\nu}\Gamma} &= N^2_{\hat{\nu}}\left(\hat{\nu}^1\frac{\partial N^1_{\hat{\nu}}}{\partial x_1} + \hat{\nu}^2\frac{\partial N^2_{\hat{\nu}}}{\partial x_1} + \hat{\nu}^3\frac{\partial N^3_{\hat{\nu}}}{\partial x_1} + \hat{\nu}^4\frac{\partial N^4_{\hat{\nu}}}{\partial x_1}\right)\hat{n}_{x_1} +\\
&+ N^2_{\hat{\nu}}\left(\hat{\nu}^1\frac{\partial N^1_{\hat{\nu}}}{\partial x_2} + \hat{\nu}^2\frac{\partial N^2_{\hat{\nu}}}{\partial x_2} + \hat{\nu}^3\frac{\partial N^3_{\hat{\nu}}}{\partial x_2} + \hat{\nu}^4\frac{\partial N^4_{\hat{\nu}}}{\partial x_2}\right)\hat{n}_{x_2} +\\
&+ N^2_{\hat{\nu}}\left(\hat{\nu}^1\frac{\partial N^1_{\hat{\nu}}}{\partial x_3} + \hat{\nu}^2\frac{\partial N^2_{\hat{\nu}}}{\partial x_3} + \hat{\nu}^3\frac{\partial N^3_{\hat{\nu}}}{\partial x_3} + \hat{\nu}^4\frac{\partial N^4_{\hat{\nu}}}{\partial x_3}\right)\hat{n}_{x_3}\\
f^{3,1}_{\hat{\nu}\Gamma} &= N^3_{\hat{\nu}}\left(\hat{\nu}^1\frac{\partial N^1_{\hat{\nu}}}{\partial x_1} + \hat{\nu}^2\frac{\partial N^2_{\hat{\nu}}}{\partial x_1} + \hat{\nu}^3\frac{\partial N^3_{\hat{\nu}}}{\partial x_1} + \hat{\nu}^4\frac{\partial N^4_{\hat{\nu}}}{\partial x_1}\right)\hat{n}_{x_1} +\\
&+ N^3_{\hat{\nu}}\left(\hat{\nu}^1\frac{\partial N^1_{\hat{\nu}}}{\partial x_2} + \hat{\nu}^2\frac{\partial N^2_{\hat{\nu}}}{\partial x_2} + \hat{\nu}^3\frac{\partial N^3_{\hat{\nu}}}{\partial x_2} + \hat{\nu}^4\frac{\partial N^4_{\hat{\nu}}}{\partial x_2}\right)\hat{n}_{x_2} +
\end{aligned}$$

$$
\begin{aligned}
& + \quad N_{\hat{\nu}}^{3}\left(\hat{\nu}^{1}\frac{\partial N_{\hat{\nu}}^{1}}{\partial x_{3}}+\hat{\nu}^{2}\frac{\partial N_{\hat{\nu}}^{2}}{\partial x_{3}}+\hat{\nu}^{3}\frac{\partial N_{\hat{\nu}}^{3}}{\partial x_{3}}+\hat{\nu}^{4}\frac{\partial N_{\hat{\nu}}^{4}}{\partial x_{3}}\right)\hat{n}_{x_{3}} \\
f_{\hat{\nu}\Gamma}^{4,1} &= N_{\hat{\nu}}^{4}\left(\hat{\nu}^{1}\frac{\partial N_{\hat{\nu}}^{1}}{\partial x_{1}}+\hat{\nu}^{2}\frac{\partial N_{\hat{\nu}}^{2}}{\partial x_{1}}+\hat{\nu}^{3}\frac{\partial N_{\hat{\nu}}^{3}}{\partial x_{1}}+\hat{\nu}^{4}\frac{\partial N_{\hat{\nu}}^{4}}{\partial x_{1}}\right)\hat{n}_{x_{1}}+ \\
&+ N_{\hat{\nu}}^{4}\left(\hat{\nu}^{1}\frac{\partial N_{\hat{\nu}}^{1}}{\partial x_{2}}+\hat{\nu}^{2}\frac{\partial N_{\hat{\nu}}^{2}}{\partial x_{2}}+\hat{\nu}^{3}\frac{\partial N_{\hat{\nu}}^{3}}{\partial x_{2}}+\hat{\nu}^{4}\frac{\partial N_{\hat{\nu}}^{4}}{\partial x_{2}}\right)\hat{n}_{x_{2}}+ \\
&+ N_{\hat{\nu}}^{4}\left(\hat{\nu}^{1}\frac{\partial N_{\hat{\nu}}^{1}}{\partial x_{3}}+\hat{\nu}^{2}\frac{\partial N_{\hat{\nu}}^{2}}{\partial x_{3}}+\hat{\nu}^{3}\frac{\partial N_{\hat{\nu}}^{3}}{\partial x_{3}}+\hat{\nu}^{4}\frac{\partial N_{\hat{\nu}}^{4}}{\partial x_{3}}\right)\hat{n}_{x_{3}} \qquad \text{(B.59)}
\end{aligned}
$$

The 4×4 symmetric convection matrix of the stabilization for the modified turbulent eddy kinematic viscosity is given as

$$
\mathbf{K}_{\mathbf{u}\hat{\nu}} = -\frac{1}{2}\int_{\Omega}\left[K_{u\hat{\nu}}^{i,j}\right]d\Omega = -\frac{1}{2}\int_{\Omega}(\nabla^{T}(\mathbf{u}\mathbf{N}_{\hat{\nu}}))^{T}(\nabla^{T}(\mathbf{u}\mathbf{N}_{\hat{\nu}}))d\Omega \qquad \text{(B.60)}
$$

where the matrix coefficients $\left[K_{u\hat{\nu}}^{i,j}\right]$ are

$$
\begin{aligned}
K_{u\hat{\nu}}^{1,1} &= \left(\frac{\partial u_1 N_{\hat{\nu}}^{1}}{\partial x_1}+\frac{\partial u_2 N_{\hat{\nu}}^{1}}{\partial x_2}+\frac{\partial u_3 N_{\hat{\nu}}^{1}}{\partial x_3}\right)^2; \quad K_{u\hat{\nu}}^{2,2} = \left(\frac{\partial u_1 N_{\hat{\nu}}^{2}}{\partial x_1}+\frac{\partial u_2 N_{\hat{\nu}}^{2}}{\partial x_2}+\frac{\partial u_3 N_{\hat{\nu}}^{2}}{\partial x_3}\right)^2 \\
K_{u\hat{\nu}}^{3,3} &= \left(\frac{\partial u_1 N_{\hat{\nu}}^{3}}{\partial x_1}+\frac{\partial u_2 N_{\hat{\nu}}^{3}}{\partial x_2}+\frac{\partial u_3 N_{\hat{\nu}}^{3}}{\partial x_3}\right)^2; \quad K_{u\hat{\nu}}^{4,4} = \left(\frac{\partial u_1 N_{\hat{\nu}}^{4}}{\partial x_1}+\frac{\partial u_2 N_{\hat{\nu}}^{4}}{\partial x_2}+\frac{\partial u_3 N_{\hat{\nu}}^{4}}{\partial x_3}\right)^2 \\
K_{u\hat{\nu}}^{1,2} = K_{u\hat{\nu}}^{2,1} &= \left(\frac{\partial u_1 N_{\hat{\nu}}^{1}}{\partial x_1}+\frac{\partial u_2 N_{\hat{\nu}}^{1}}{\partial x_2}+\frac{\partial u_3 N_{\hat{\nu}}^{1}}{\partial x_3}\right)\left(\frac{\partial u_1 N_{\hat{\nu}}^{2}}{\partial x_1}+\frac{\partial u_2 N_{\hat{\nu}}^{2}}{\partial x_2}+\frac{\partial u_3 N_{\hat{\nu}}^{2}}{\partial x_3}\right) \\
K_{u\hat{\nu}}^{1,3} = K_{u\hat{\nu}}^{3,1} &= \left(\frac{\partial u_1 N_{\hat{\nu}}^{1}}{\partial x_1}+\frac{\partial u_2 N_{\hat{\nu}}^{1}}{\partial x_2}+\frac{\partial u_3 N_{\hat{\nu}}^{1}}{\partial x_3}\right)\left(\frac{\partial u_1 N_{\hat{\nu}}^{3}}{\partial x_1}+\frac{\partial u_2 N_{\hat{\nu}}^{3}}{\partial x_2}+\frac{\partial u_3 N_{\hat{\nu}}^{3}}{\partial x_3}\right) \\
K_{u\hat{\nu}}^{1,4} = K_{u\hat{\nu}}^{4,1} &= \left(\frac{\partial u_1 N_{\hat{\nu}}^{1}}{\partial x_1}+\frac{\partial u_2 N_{\hat{\nu}}^{1}}{\partial x_2}+\frac{\partial u_3 N_{\hat{\nu}}^{1}}{\partial x_3}\right)\left(\frac{\partial u_1 N_{\hat{\nu}}^{4}}{\partial x_1}+\frac{\partial u_2 N_{\hat{\nu}}^{4}}{\partial x_2}+\frac{\partial u_3 N_{\hat{\nu}}^{4}}{\partial x_3}\right) \\
K_{u\hat{\nu}}^{2,3} = K_{u\hat{\nu}}^{3,2} &= \left(\frac{\partial u_1 N_{\hat{\nu}}^{2}}{\partial x_1}+\frac{\partial u_2 N_{\hat{\nu}}^{2}}{\partial x_2}+\frac{\partial u_3 N_{\hat{\nu}}^{2}}{\partial x_3}\right)\left(\frac{\partial u_1 N_{\hat{\nu}}^{3}}{\partial x_1}+\frac{\partial u_2 N_{\hat{\nu}}^{3}}{\partial x_2}+\frac{\partial u_3 N_{\hat{\nu}}^{3}}{\partial x_3}\right) \\
K_{u\hat{\nu}}^{2,4} = K_{u\hat{\nu}}^{4,2} &= \left(\frac{\partial u_1 N_{\hat{\nu}}^{2}}{\partial x_1}+\frac{\partial u_2 N_{\hat{\nu}}^{2}}{\partial x_2}+\frac{\partial u_3 N_{\hat{\nu}}^{2}}{\partial x_3}\right)\left(\frac{\partial u_1 N_{\hat{\nu}}^{4}}{\partial x_1}+\frac{\partial u_2 N_{\hat{\nu}}^{4}}{\partial x_2}+\frac{\partial u_3 N_{\hat{\nu}}^{4}}{\partial x_3}\right) \\
K_{u\hat{\nu}}^{3,4} = K_{u\hat{\nu}}^{4,3} &= \left(\frac{\partial u_1 N_{\hat{\nu}}^{3}}{\partial x_1}+\frac{\partial u_2 N_{\hat{\nu}}^{3}}{\partial x_2}+\frac{\partial u_3 N_{\hat{\nu}}^{3}}{\partial x_3}\right)\left(\frac{\partial u_1 N_{\hat{\nu}}^{4}}{\partial x_1}+\frac{\partial u_2 N_{\hat{\nu}}^{4}}{\partial x_2}+\frac{\partial u_3 N_{\hat{\nu}}^{4}}{\partial x_3}\right)
\end{aligned}
$$

(B.61)

Appendix C

Jacobian matrix of the transformations

The transformation of a triangular or tetrahedral element of a finite element mesh to a regularly shaped element is solely for the purpose of numerically evaluating the integrals. Thus when a typical element of a finite element mesh is transformed from the global coordinates to the local coordinates of the elements, the weak form of the integral equations for applying the standard Galerkin approximation must also be expressed in terms of the local coordinates.

C.1 Area coordinates

Cartesian directions are not convenient in the triangule while these are not parallel to the side of a triangular element. However, it is easy to construct that an definition of three non-dimensionalized coordinates L^i, which relate respectively to the sides opposite nodes, such that

$$L^i = \frac{A^i}{A}; \quad A = \sum_{i=1}^{3} A^i \tag{C.1}$$

where A^i is the triangle formed by the other nodes (except node i) and an arbitrary point in the element. A is the total area of the local element. It is obvious that each individually gives unity at one node, zero at others and varies linearly in the element such that $L^1+L^2+L^3 = 1$.

The shape functions are simply the area coordinate, i.e.

$$N^1 = L^1; \quad N^2 = L^2; \quad N^3 = L^3 \tag{C.2}$$

where the shape functions N^1, N^2 and N^3 are non-dimensional coordinates system (ξ, η)

$$N^1 = 1 - \xi - \eta; \quad N^2 = \xi; \quad N^3 = \eta \tag{C.3}$$

The transformation between (x, y) and (ξ, η) is accomplished by a coordinate transformation of the form [161]

$$\begin{aligned} x_1(\xi,\eta) &= \sum_{i=1}^{3} x_1^i N^i = x_1^1 + (x_1^2 - x_1^1)\xi + (x_1^3 - x_1^1)\eta \\ x_2(\xi,\eta) &= \sum_{i=1}^{3} x_2^i N^i = x_2^1 + (x_2^2 - x_2^1)\xi + (x_2^3 - x_2^1)\eta \end{aligned} \tag{C.4}$$

Because the interpolation functions $N^i(\xi, \eta)$ can be expressed in terms of the local coordinates ξ and η, using the chain rule of partial differentiation

$$\begin{aligned} \frac{\partial N^i}{\partial \xi} &= \frac{\partial N^i}{\partial x_1}\frac{\partial x_1}{\partial \xi} + \frac{\partial N^i}{\partial x_2}\frac{\partial x_2}{\partial \xi} \\ \frac{\partial N^i}{\partial \eta} &= \frac{\partial N^i}{\partial x_1}\frac{\partial x_1}{\partial \eta} + \frac{\partial N^i}{\partial x_2}\frac{\partial x_2}{\partial \eta} \end{aligned} \tag{C.5}$$

and the matrix formulation is

$$\begin{bmatrix} \frac{\partial N^1}{\partial \xi} & \frac{\partial N^2}{\partial \xi} & \frac{\partial N^3}{\partial \xi} \\ \frac{\partial N^1}{\partial \eta} & \frac{\partial N^2}{\partial \eta} & \frac{\partial N^3}{\partial \eta} \end{bmatrix} = \begin{bmatrix} \frac{\partial x_1}{\partial \xi} & \frac{\partial x_2}{\partial \xi} \\ \frac{\partial x_1}{\partial \eta} & \frac{\partial x_2}{\partial \eta} \end{bmatrix} \begin{bmatrix} \frac{\partial N^1}{\partial x_1} & \frac{\partial N^2}{\partial x_1} & \frac{\partial N^3}{\partial x_1} \\ \frac{\partial N^1}{\partial x_2} & \frac{\partial N^2}{\partial x_2} & \frac{\partial N^3}{\partial x_2} \end{bmatrix} \tag{C.6}$$

which gives the relation between the derivatives of N^i with respect to the global and local coordinates. However, the Jacobian matrix of the transformation is

$$\mathbf{J} = \begin{bmatrix} \frac{\partial x_1}{\partial \xi} & \frac{\partial x_2}{\partial \xi} \\ \frac{\partial x_1}{\partial \eta} & \frac{\partial x_2}{\partial \eta} \end{bmatrix} = \begin{bmatrix} x_1^2 - x_1^1 & x_2^2 - x_2^1 \\ x_1^3 - x_1^1 & x_2^3 - x_2^1 \end{bmatrix} \tag{C.7}$$

In order to compute the global derivatives of N^i with respect to x_1 and x_2, it have to invert the Jacobian matrix. The determinant **J**−the Jacobian−is non-negative at every point (ξ, η) in finite element domain for $\mathbf{J}^{-1}$ existence, i.e.

$$det(\mathbf{J}) = \frac{\partial x_1}{\partial \xi}\frac{\partial x_2}{\partial \eta} - \frac{\partial x_1}{\partial \eta}\frac{\partial x_2}{\partial \xi} > 0 \tag{C.8}$$

where the functions $\xi = \xi(x, y)$ and $\eta = \eta(x, y)$ are continuous, differentiable and invertible. However, the Jacobian matrix **J** must be nonsingular.

Hence, the global derivatives of N^i can be easily evaluated

$$\begin{aligned}
\frac{\partial N^1}{\partial x_1} &= \frac{x_2^2 - x_2^3}{(x_1^2 - x_1^1)(x_2^3 - x_2^1) - (x_1^3 - x_1^1)(x_2^2 - x_2^1)} \\
\frac{\partial N^2}{\partial x_1} &= \frac{x_2^3 - x_2^1}{(x_1^2 - x_1^1)(x_2^3 - x_2^1) - (x_1^3 - x_1^1)(x_2^2 - x_2^1)} \\
\frac{\partial N^3}{\partial x_1} &= -\left(\frac{\partial N^1}{\partial x_1} + \frac{\partial N^2}{\partial x_1}\right) = \frac{-x_2^2 + x_2^1}{(x_1^2 - x_1^1)(x_2^3 - x_2^1) - (x_1^3 - x_1^1)(x_2^2 - x_2^1)} \\
\frac{\partial N^1}{\partial x_2} &= \frac{x_1^3 - x_1^2}{(x_1^2 - x_1^1)(x_2^3 - x_2^1) - (x_1^3 - x_1^1)(x_2^2 - x_2^1)} \\
\frac{\partial N^2}{\partial x_2} &= \frac{-x_1^3 + x_1^1}{(x_1^2 - x_1^1)(x_2^3 - x_2^1) - (x_1^3 - x_1^1)(x_2^2 - x_2^1)} \\
\frac{\partial N^3}{\partial x_2} &= -\left(\frac{\partial N^1}{\partial x_2} + \frac{\partial N^2}{\partial x_2}\right) = \frac{x_1^2 - x_1^1}{(x_1^2 - x_1^1)(x_2^3 - x_2^1) - (x_1^3 - x_1^1)(x_2^2 - x_2^1)}
\end{aligned} \tag{C.9}$$

C.2 Volume coordinates

$$M^i = \frac{V^i}{V}; \quad V = \sum_{i=1}^{4} V^i \tag{C.10}$$

where V^i is the tetrahedron formed by the other nodes (except node i) and an arbitrary point in the element. V is the total volume of the local element. $M^1 + M^2 + M^3 + M^4 = 1$.

The shape functions are expressed as

$$N^1 = M^1; \quad N^2 = M^2; \quad N^3 = M^3; \quad N^4 = M^4 \tag{C.11}$$

where the shape functions N^1, N^2, N^3 and N^4 identify non-dimensional coordinates system (ξ, η, ζ)

$$N^1 = 1 - \xi - \eta - \zeta; \quad N^2 = \xi; \quad N^3 = \eta; \quad N^4 = \zeta \tag{C.12}$$

A coordinate transformation of the form can be written as

$$\begin{aligned}
x_1(\xi,\eta,\zeta) &= \sum_{i=1}^{4} x_1^i N^i = x_1^1 + (x_1^2 - x_1^1)\xi + (x_1^3 - x_1^1)\eta + (x_1^4 - x_1^1)\zeta \\
x_2(\xi,\eta,\zeta) &= \sum_{i=1}^{4} x_2^i N^i = x_2^1 + (x_2^2 - x_2^1)\xi + (x_2^3 - x_2^1)\eta + (x_2^4 - x_2^1)\zeta \\
x_3(\xi,\eta,\zeta) &= \sum_{i=1}^{4} x_3^i N^i = x_3^1 + (x_3^2 - x_3^1)\xi + (x_3^3 - x_3^1)\eta + (x_3^4 - x_3^1)\zeta
\end{aligned} \tag{C.13}$$

The derivatives of interpolation functions N^i relate to the local coordinates (ξ,η,ζ) and the global coordinates (ξ,η,ζ), i.e.

$$\begin{aligned}
\frac{\partial N^i}{\partial \xi} &= \frac{\partial N^i}{\partial x_1}\frac{\partial x_1}{\partial \xi} + \frac{\partial N^i}{\partial x_2}\frac{\partial x_2}{\partial \xi} + \frac{\partial N^i}{\partial x_3}\frac{\partial x_3}{\partial \xi} \\
\frac{\partial N^i}{\partial \eta} &= \frac{\partial N^i}{\partial x_1}\frac{\partial x_1}{\partial \eta} + \frac{\partial N^i}{\partial x_2}\frac{\partial x_2}{\partial \eta} + \frac{\partial N^i}{\partial x_3}\frac{\partial x_3}{\partial \eta} \\
\frac{\partial N^i}{\partial \zeta} &= \frac{\partial N^i}{\partial x_1}\frac{\partial x_1}{\partial \zeta} + \frac{\partial N^i}{\partial x_2}\frac{\partial x_2}{\partial \zeta} + \frac{\partial N^i}{\partial x_3}\frac{\partial x_3}{\partial \zeta}
\end{aligned} \tag{C.14}$$

and the matrix formulation is

$$\begin{bmatrix} \frac{\partial N^1}{\partial \xi} & \frac{\partial N^2}{\partial \xi} & \frac{\partial N^3}{\partial \xi} & \frac{\partial N^4}{\partial \xi} \\ \frac{\partial N^1}{\partial \eta} & \frac{\partial N^2}{\partial \eta} & \frac{\partial N^3}{\partial \eta} & \frac{\partial N^4}{\partial \eta} \\ \frac{\partial N^1}{\partial \zeta} & \frac{\partial N^2}{\partial \zeta} & \frac{\partial N^3}{\partial \zeta} & \frac{\partial N^4}{\partial \zeta} \end{bmatrix} = \begin{bmatrix} \frac{\partial x_1}{\partial \xi} & \frac{\partial x_2}{\partial \xi} & \frac{\partial x_3}{\partial \xi} \\ \frac{\partial x_1}{\partial \eta} & \frac{\partial x_2}{\partial \eta} & \frac{\partial x_3}{\partial \eta} \\ \frac{\partial x_1}{\partial \zeta} & \frac{\partial x_2}{\partial \zeta} & \frac{\partial x_3}{\partial \zeta} \end{bmatrix} \begin{bmatrix} \frac{\partial N^1}{\partial x_1} & \frac{\partial N^2}{\partial x_1} & \frac{\partial N^3}{\partial x_1} & \frac{\partial N^4}{\partial x_1} \\ \frac{\partial N^1}{\partial x_2} & \frac{\partial N^2}{\partial x_2} & \frac{\partial N^3}{\partial x_2} & \frac{\partial N^4}{\partial x_2} \\ \frac{\partial N^1}{\partial x_3} & \frac{\partial N^2}{\partial x_3} & \frac{\partial N^3}{\partial x_3} & \frac{\partial N^4}{\partial x_3} \end{bmatrix} \tag{C.15}$$

The Jacobian matrix of the transformation for the tetrahedral element 4 nodes is

$$\mathbf{J} = \begin{bmatrix} \frac{\partial x_1}{\partial \xi} & \frac{\partial x_2}{\partial \xi} & \frac{\partial x_3}{\partial \xi} \\ \frac{\partial x_1}{\partial \eta} & \frac{\partial x_2}{\partial \eta} & \frac{\partial x_3}{\partial \eta} \\ \frac{\partial x_1}{\partial \zeta} & \frac{\partial x_2}{\partial \zeta} & \frac{\partial x_3}{\partial \zeta} \end{bmatrix} = \begin{bmatrix} x_1^2 - x_1^1 & x_2^2 - x_2^1 & x_3^2 - x_3^1 \\ x_1^3 - x_1^1 & x_2^3 - x_2^1 & x_3^3 - x_3^1 \\ x_1^4 - x_1^1 & x_2^4 - x_2^1 & x_3^4 - x_3^1 \end{bmatrix} \tag{C.16}$$

As mentioned before, invert the Jacobian matrix have to non-negative at every point (ξ, η, ζ) in finite element domain, i.e.

$$\begin{aligned} det(\mathbf{J}) &= \left(x_1^2 - x_1^1\right)\left(x_2^3 - x_2^1\right)\left(x_3^4 - x_3^1\right) + \left(x_1^3 - x_1^1\right)\left(x_2^4 - x_2^1\right)\left(x_3^2 - x_3^1\right) + \\ &+ \left(x_1^4 - x_1^1\right)\left(x_2^2 - x_2^1\right)\left(x_3^3 - x_3^1\right) - \left(x_1^4 - x_1^1\right)\left(x_2^3 - x_2^1\right)\left(x_3^2 - x_3^1\right) - \\ &- \left(x_1^3 - x_1^1\right)\left(x_2^2 - x_2^1\right)\left(x_3^4 - x_3^1\right) - \left(x_1^2 - x_1^1\right)\left(x_2^4 - x_2^1\right)\left(x_3^3 - x_3^1\right) > 0 \qquad \text{(C.17)} \end{aligned}$$

However, the global derivatives of N^i are

$$\begin{aligned} \frac{\partial N^1}{\partial x_1} &= -\left[(x_2^3 - x_2^1)(x_3^4 - x_3^1) - (x_2^4 - x_2^1)(x_3^3 - x_3^1)\right]/det(\mathbf{J}) - \\ &- \left[(x_2^4 - x_2^1)(x_3^2 - x_3^1) - (x_2^2 - x_2^1)(x_3^4 - x_3^1)\right]/det(\mathbf{J}) - \\ &- \left[(x_2^2 - x_2^1)(x_3^3 - x_3^1) - (x_2^3 - x_2^1)(x_3^2 - x_3^1)\right]/det(\mathbf{J}) \\ \frac{\partial N^2}{\partial x_1} &= \left[(x_2^3 - x_2^1)(x_3^4 - x_3^1) - (x_2^4 - x_2^1)(x_3^3 - x_3^1)\right]/det(\mathbf{J}) \\ \frac{\partial N^3}{\partial x_1} &= \left[(x_2^4 - x_2^1)(x_3^2 - x_3^1) - (x_2^2 - x_2^1)(x_3^4 - x_3^1)\right]/det(\mathbf{J}) \\ \frac{\partial N^4}{\partial x_1} &= \left[(x_2^2 - x_2^1)(x_3^3 - x_3^1) - (x_2^3 - x_2^1)(x_3^2 - x_3^1)\right]/det(\mathbf{J}) \\ \frac{\partial N^1}{\partial x_2} &= -\left[(x_1^4 - x_1^1)(x_3^3 - x_3^1) - (x_1^3 - x_1^1)(x_3^4 - x_3^1)\right]/det(\mathbf{J}) - \\ &- \left[(x_1^2 - x_1^1)(x_3^4 - x_3^1) - (x_1^4 - x_1^1)(x_3^2 - x_3^1)\right]/det(\mathbf{J}) - \\ &- \left[(x_1^3 - x_1^1)(x_3^2 - x_3^1) - (x_1^2 - x_1^1)(x_3^3 - x_3^1)\right]/det(\mathbf{J}) \\ \frac{\partial N^2}{\partial x_2} &= \left[(x_1^4 - x_1^1)(x_3^3 - x_3^1) - (x_1^3 - x_1^1)(x_3^4 - x_3^1)\right]/det(\mathbf{J}) \\ \frac{\partial N^3}{\partial x_2} &= \left[(x_1^2 - x_1^1)(x_3^4 - x_3^1) - (x_1^4 - x_1^1)(x_3^2 - x_3^1)\right]/det(\mathbf{J}) \\ \frac{\partial N^4}{\partial x_2} &= \left[(x_1^3 - x_1^1)(x_3^2 - x_3^1) - (x_1^2 - x_1^1)(x_3^3 - x_3^1)\right]/det(\mathbf{J}) \\ \frac{\partial N^1}{\partial x_3} &= -\left[(x_1^3 - x_1^1)(x_2^4 - x_2^1) - (x_1^4 - x_1^1)(x_2^3 - x_2^1)\right]/det(\mathbf{J}) - \\ &- \left[(x_1^4 - x_1^1)(x_2^2 - x_2^1) - (x_1^2 - x_1^1)(x_2^4 - x_2^1)\right]/det(\mathbf{J}) - \\ &- \left[(x_1^2 - x_1^1)(x_2^3 - x_2^1) - (x_1^3 - x_1^1)(x_2^2 - x_2^1)\right]/det(\mathbf{J}) \end{aligned}$$

$$
\begin{aligned}
\frac{\partial N^2}{\partial x_3} &= \left[(x_1^3 - x_1^1)(x_2^4 - x_2^1) - (x_1^4 - x_1^1)(x_2^3 - x_2^1)\right] / det(\mathbf{J}) \\
\frac{\partial N^3}{\partial x_3} &= \left[(x_1^4 - x_1^1)(x_2^2 - x_2^1) - (x_1^2 - x_1^1)(x_2^4 - x_2^1)\right] / det(\mathbf{J}) \\
\frac{\partial N^4}{\partial x_3} &= \left[(x_1^2 - x_1^1)(x_2^3 - x_2^1) - (x_1^3 - x_1^1)(x_2^2 - x_2^1)\right] / det(\mathbf{J}) \qquad \text{(C.18)}
\end{aligned}
$$

Appendix D

The nonlinear $\kappa - \varepsilon$ model

It is well known that the nonlinear $\kappa - \varepsilon$ model can take into account the anisotropy of turbulence with less CPU time and computer memory than LES formulation [84]. Also, the linear $\kappa - \varepsilon$ does not perform well for near-wall predictions of high Reynolds number flows and may not predict turbulent flow fields where the anisotropy plays an important part. The nonlinear $\kappa - \varepsilon$ model, unlike the linear one, does not use Boussinesq assumption for Reynolds stresses. It was originally derived from a solution of the transport equation of the Reynolds stress tensor $\overline{u_i'u_j'}$. By making use of compactness in Cartesian tensor notation, Equation (2.31) may be written as

$$\frac{D\overline{u_i'u_j'}}{Dt} = G_{ij} + \Phi_{ij} - \varepsilon_{ij} + d_{ij}^t + d_{ij}^\nu \tag{D.1}$$

where

$$G_{ij} \equiv -\left\{\overline{u_i'u_k'}\frac{\partial \bar{u}_j}{\partial x_k} + \overline{u_j'u_k'}\frac{\partial \bar{u}_i}{\partial x_k}\right\} \tag{D.2}$$

$$\Phi_{ij} \equiv \overline{\frac{p'}{\rho}\left(\frac{\partial u_i'}{\partial x_j} + \frac{\partial u_j'}{\partial x_i}\right)} \tag{D.3}$$

$$\varepsilon_{ij} \equiv 2\nu\overline{\frac{\partial u_i'}{\partial x_k}\frac{\partial u_j'}{\partial x_k}} \tag{D.4}$$

$$d_{ij}^t \equiv -\frac{\partial}{\partial x_k}\left(\overline{u_i'u_j'u_k'} + \frac{\overline{p'u_i'}}{\rho}\delta_{jk} + \frac{\overline{p'u_j'}}{\rho}\delta_{ik}\right) \quad \text{(D.5)}$$

$$d_{ij}^\nu \equiv \nu\nabla^2\overline{u_i'u_j'} = \nu\frac{\partial^2\overline{u_i'u_j'}}{\partial x_k^2} \quad \text{(D.6)}$$

are, respectively, the shear stress generation, the pressure-strain correlation, the dissipative correlation of second-rank tensor, the turbulent stress diffusion, and the viscous diffusion.

For turbulent incompressible flows, the derivation of algebraic stress models are used by the basic equilibrium hypothesis which satisfies the following constrains [98]

$$\frac{Db_{ij}}{Dt} = 0 \quad \text{(D.7)}$$

$$d_{ij}^t + d_{ij}^\nu = 0 \quad \text{(D.8)}$$

where b_{ij} is the normalized Reynolds stress anisotropy tensor, i.e.

$$b_{ij} \equiv \frac{\overline{u_i'u_j'} - \frac{1}{3}\overline{u_i'u_i'}\delta_{ij}}{\overline{u_i'u_i'}} \quad \text{(D.9)}$$

It follows first equilibrium hypothesis from Equation (D.7) that

$$\frac{D\overline{u_i'u_j'}}{Dt} + \frac{\overline{u_i'u_i'}}{2}\overline{u_i'u_j'}\frac{D}{Dt}\frac{2}{\overline{u_i'u_i'}} = 0 \quad \text{(D.10)}$$

and, hence, by making use of the product rule of the derivative with the turbulent kinetic energy equation of isotropic tensors of rank 2 by the Equation (2.15), we obtain

$$\frac{D\overline{u_i'u_j'}}{Dt} = \frac{2\overline{u_i'u_j'}}{\overline{u_i'u_i'}}\left[-\frac{\partial}{\partial x_j}\left(\frac{\overline{u_j'u_i'u_i'}}{2}\right) - \frac{\partial}{\partial x_i}\left(\frac{\overline{u_i'p'}}{\rho}\right) + \frac{\partial}{\partial x_j}\left(\overline{\nu u_i'\frac{\partial u_i'}{\partial x_j}}\right) - \overline{u_i'u_j'}\frac{\partial \bar{u}_i}{\partial x_j} - \nu\overline{\frac{\partial u_i'}{\partial x_j}\frac{\partial u_i'}{\partial x_j}}\right] \quad \text{(D.11)}$$

The dissipation rate tensor ε_{ij} can be split into isotropic part $(1/3)\varepsilon_{ii}\delta_{ij}$ and deviatoric part ε_{ij}^D. By substituting Equation (D.11) and second equilibrium hypothesis Equation (D.8) into Equation (D.1) and neglecting diffusion process, it yields the equilibrium formulation of the Reynolds stress:

$$\left(P_{ij} - \frac{\varepsilon_{ii}}{2}\right)\left(\frac{2\overline{u_i'u_j'}}{\overline{u_i'u_i'}} - \frac{2}{3}\delta_{ij}\right) = -\frac{\overline{u_i'u_i'}}{3}\left(\frac{\partial \bar{u}_i}{\partial x_j} + \frac{\partial \bar{u}_j}{\partial x_i}\right) +$$
$$+ \frac{\overline{u_m'u_n'}}{3}\left(\frac{\partial \bar{u}_m}{\partial x_n} + \frac{\partial \bar{u}_n}{\partial x_m}\right)\delta_{mn} - \frac{\overline{u_i'u_i'}}{9}\delta_{mn}\left(\frac{\partial \bar{u}_m}{\partial x_n} + \frac{\partial \bar{u}_n}{\partial x_m}\right)\delta_{ij} -$$
$$- \overline{u_i'u_k'}\frac{\partial \bar{u}_j}{\partial x_k} - \overline{u_j'u_k'}\frac{\partial \bar{u}_i}{\partial x_k} + \frac{\overline{u_i'u_i'}}{3}\delta_{ik}\frac{\partial \bar{u}_j}{\partial x_k} + \frac{\overline{u_i'u_i'}}{3}\delta_{jk}\frac{\partial \bar{u}_i}{\partial x_k} +$$
$$+ \Phi_{ij} - \varepsilon_{ij}^D \qquad \text{(D.12)}$$

where $P_{ij} \equiv -\overline{u_i'u_j'}\partial \bar{u}_i/\partial x_j$ is the production of turbulent kinetic energy and ε_{ii} is the scalar turbulent dissipation rate. Equation (D.12) reduces to the simpler form if Equation (D.9) is substituted

$$\left(P_{ij} - \frac{\varepsilon_{ii}}{2}\right) b_{ij} = -\frac{2}{3}\kappa S_{ij} - \kappa\left(b_{ik}S_{jk} + b_{jk}S_{ik} - \frac{2}{3}b_{mn}S_{mn}\delta_{ij}\right) - \kappa\left(b_{ik}\Omega_{jk} + b_{jk}\Omega_{ik}\right) + \frac{\Pi_{ij}}{2} \qquad \text{(D.13)}$$

where $\Pi_{ij} = \Phi_{ij} - \varepsilon_{ij}^D$ and $\kappa = \overline{u_i'u_i'}/2$ is the turbulent kinetic energy. The mean strain-rate tensor is S_{ij} and Ω_{ij} is the mean vorticity tensor, giving respectively

$$S_{ij} \equiv \frac{1}{2}\left(\frac{\partial \bar{u}_i}{\partial x_j} + \frac{\partial \bar{u}_j}{\partial x_i}\right); \quad \Omega_{ij} \equiv \frac{1}{2}\left(\frac{\partial \bar{u}_i}{\partial x_j} - \frac{\partial \bar{u}_j}{\partial x_i}\right) \qquad \text{(D.14)}$$

In all of the second-order closure models, Π_{ij} is modelled and the most general form which is tensorially linear in the normalized Reynolds stress anisotropy tensor b_{ij} is given by Speziale et al. [162] as

$$\Pi_{ij} = \gamma_1\epsilon b_{ij} + \gamma_2\epsilon\left(b_{ik}b_{kj} - \frac{1}{3}b_{mn}b_{mn}\delta_{ij}\right) + \gamma_3\kappa S_{ij} +$$
$$+ \gamma_4\kappa\left(b_{ik}S_{jk} + b_{jk}S_{ik} - \frac{2}{3}b_{mn}S_{mn}\delta_{ij}\right) + \gamma_5\kappa\left(b_{ik}b_{kl}S_{jl} + b_{jk}b_{kl}S_{il} - \frac{2}{3}b_{lm}b_{mn}S_{nl}\delta_{ij}\right) +$$
$$+ \gamma_6\kappa\left(b_{ik}\Omega_{jk} + b_{jk}\Omega_{ik}\right) + \gamma_7\kappa\left(b_{ik}b_{kl}\Omega_{jl} + b_{jk}b_{kl}\Omega_{il}\right) \qquad \text{(D.15)}$$

where $\epsilon = \varepsilon_{ii}/2$ and $\gamma_1, \gamma_2, ..., \gamma_7$ are constants.

Continuing in this way, the anisotropy b_{ij} may be expressed as the tensor polynomial. It includes functions of a deviatoric symmetric and an antisymmetric tensor and the coefficients of the irreducible invariants to obtain a nonlinear turbulent eddy kinematic viscosity form by using the Cayley-Hamilton theorem [92, 98, 163].

The nonlinear form of a cubic relation between the mean strain-rate tensor and the mean vorticity tensor for the Reynolds stresses is normally used [99], i.e.

$$\begin{aligned}
\tau_{ij}^{R} &= -\rho\overline{u_i'u_j'} \\
&= -\frac{2}{3}\rho\kappa\delta_{ij} + \underbrace{\rho\nu_t S_{ij}}_{Linear\ \ term} - \\
&- \underbrace{\frac{\rho\kappa\nu_t}{\varepsilon}\left(\alpha_1\Xi_1 + \alpha_2\Xi_2 + \alpha_3\Xi_3 + \alpha_4\Xi_4 + \alpha_5\Xi_5 + \alpha_6\Xi_6 + \alpha_7\Xi_7\right)}_{Cubic\ \ term}
\end{aligned} \qquad \text{(D.16)}$$

where the constitutive time-averaging stress/vorticity terms are

$$\begin{aligned}
\Xi_1 &= \Omega_{ik}S_{jk} + \Omega_{jk}S_{ik} \\
\Xi_2 &= S_{ik}S_{jk} - \frac{1}{3}S_{kl}S_{kl}\delta_{ij} \\
\Xi_3 &= \Omega_{ik}\Omega_{jk} - \frac{1}{3}\Omega_{kl}\Omega_{kl}\delta_{ij} \\
\Xi_4 &= S_{ki}S_{kl}\Omega_{lj} + S_{kj}S_{kl}\Omega_{li} \\
\Xi_5 &= \Omega_{il}\Omega_{lm}S_{mj} + S_{il}\Omega_{lm}\Omega_{mj} - \frac{2}{3}S_{lm}\Omega_{mn}\Omega_{nl}\delta_{ij} \\
\Xi_6 &= S_{ij}S_{kl}S_{kl} \\
\Xi_7 &= S_{ij}\Omega_{kl}\Omega_{kl}
\end{aligned} \qquad \text{(D.17)}$$

Thus the components of Reynolds stresses of three-dimensional turbulent flow are given as

$$
\begin{aligned}
\tau_{11}^R &= -\rho\overline{u_1'u_1'} \\
&= -(2/3)\rho\kappa + \mu_t S_{11} - (2\alpha_1\mu_t\kappa/\varepsilon)\left(\Omega_{12}S_{12} + \Omega_{13}S_{13}\right) - \\
&- \left(\alpha_2\mu_t\kappa/\varepsilon\right)\left[(2/3)\left(S_{11}S_{11} - S_{23}S_{23}\right) + (1/3)\left(S_{12}S_{12} + S_{13}S_{13} - S_{22}S_{22} - S_{33}S_{33}\right)\right] - \\
&- \left(\alpha_3\mu_t\kappa/\varepsilon\right)\left[(2/3)\Omega_{23}\Omega_{32} + (1/3)\left(\Omega_{12}\Omega_{12} + \Omega_{13}\Omega_{13}\right)\right] - \\
&- \left(2\alpha_4\mu_t\kappa^2/\varepsilon^2\right)\left[\Omega_{21}\left(S_{11}S_{12} + S_{21}S_{22} + S_{31}S_{32}\right) + \Omega_{31}\left(S_{11}S_{13} + S_{21}S_{23} + S_{31}S_{33}\right)\right] - \\
&- \left(4\alpha_5\mu_t\kappa^2/3\varepsilon^2\right)\left(S_{11}\Omega_{12}\Omega_{21} + S_{11}\Omega_{13}\Omega_{31} + S_{23}\Omega_{12}\Omega_{13}\right) - \\
&- \left(2\alpha_5\mu_t\kappa^2/3\varepsilon^2\right)\left(S_{12}\Omega_{23}\Omega_{31} + S_{13}\Omega_{32}\Omega_{21} + S_{22}\Omega_{21}\Omega_{21}\right) - \\
&- \left(2\alpha_5\mu_t\kappa^2/3\varepsilon^2\right)\left(S_{22}\Omega_{23}\Omega_{23} + S_{33}\Omega_{31}\Omega_{31} + S_{33}\Omega_{32}\Omega_{32}\right) - \\
&- \left(\alpha_6\mu_t\kappa^2/\varepsilon^2\right)\left[S_{11}\left(S_{11}S_{11} + S_{22}S_{22} + S_{33}S_{33}\right) + 2S_{11}\left(S_{12}S_{12} + S_{13}S_{13} + S_{23}S_{23}\right)\right] - \\
&- \left(2\alpha_7\mu_t\kappa^2/\varepsilon^2\right)S_{11}\left(\Omega_{12}\Omega_{12} + \Omega_{13}\Omega_{13} + \Omega_{23}\Omega_{23}\right)
\end{aligned} \tag{D.18}
$$

$$
\begin{aligned}
\tau_{22}^R &= -\rho\overline{u_2'u_2'} \\
&= -(2/3)\rho\kappa + \mu_t S_{22} - (2\alpha_1\mu_t\kappa/\varepsilon)\left(\Omega_{21}S_{21} + \Omega_{23}S_{23}\right) - \\
&- \left(\alpha_2\mu_t\kappa/\varepsilon\right)\left[(2/3)\left(S_{22}S_{22} - S_{31}S_{31}\right) + (1/3)\left(S_{21}S_{21} + S_{23}S_{23} - S_{11}S_{11} - S_{33}S_{33}\right)\right] - \\
&- \left(\alpha_3\mu_t\kappa/\varepsilon\right)\left[(2/3)\Omega_{13}\Omega_{31} + (1/3)\left(\Omega_{21}\Omega_{21} + \Omega_{23}\Omega_{23}\right)\right] - \\
&- \left(2\alpha_4\mu_t\kappa^2/\varepsilon^2\right)\left[\Omega_{12}\left(S_{12}S_{11} + S_{22}S_{21} + S_{32}S_{31}\right) + \Omega_{32}\left(S_{12}S_{13} + S_{22}S_{23} + S_{32}S_{33}\right)\right] - \\
&- \left(4\alpha_5\mu_t\kappa^2/3\varepsilon^2\right)\left(S_{22}\Omega_{21}\Omega_{12} + S_{22}\Omega_{23}\Omega_{32} + S_{31}\Omega_{21}\Omega_{23}\right) - \\
&- \left(2\alpha_5\mu_t\kappa^2/3\varepsilon^2\right)\left(S_{21}\Omega_{13}\Omega_{32} + S_{23}\Omega_{31}\Omega_{12} + S_{11}\Omega_{12}\Omega_{12}\right) - \\
&- \left(2\alpha_5\mu_t\kappa^2/3\varepsilon^2\right)\left(S_{11}\Omega_{13}\Omega_{13} + S_{33}\Omega_{31}\Omega_{31} + S_{33}\Omega_{32}\Omega_{32}\right) - \\
&- \left(\alpha_6\mu_t\kappa^2/\varepsilon^2\right)\left[S_{22}\left(S_{11}S_{11} + S_{22}S_{22} + S_{33}S_{33}\right) + 2S_{22}\left(S_{21}S_{21} + S_{31}S_{31} + S_{32}S_{32}\right)\right] - \\
&- \left(2\alpha_7\mu_t\kappa^2/\varepsilon^2\right)S_{22}\left(\Omega_{12}\Omega_{12} + \Omega_{13}\Omega_{13} + \Omega_{23}\Omega_{23}\right)
\end{aligned} \tag{D.19}
$$

$$
\begin{aligned}
\tau_{33}^{R} &= -\rho\overline{u_3'u_3'} \\
&= -(2/3)\rho\kappa + \mu_t S_{33} - (2\alpha_1\mu_t\kappa/\varepsilon)\left(\Omega_{31}S_{31} + \Omega_{32}S_{32}\right) - \\
&- (\alpha_2\mu_t\kappa/\varepsilon)\left[(2/3)\left(S_{33}S_{33} - S_{21}S_{21}\right) + (1/3)\left(S_{31}S_{31} + S_{23}S_{23} - S_{11}S_{11} - S_{22}S_{22}\right)\right] - \\
&- (\alpha_3\mu_t\kappa/\varepsilon)\left[(2/3)\Omega_{12}\Omega_{21} + (1/3)\left(\Omega_{31}\Omega_{31} + \Omega_{32}\Omega_{32}\right)\right] - \\
&- \left(2\alpha_4\mu_t\kappa^2/\varepsilon^2\right)\left[\Omega_{13}\left(S_{13}S_{11} + S_{23}S_{21} + S_{33}S_{31}\right) + \Omega_{23}\left(S_{13}S_{12} + S_{23}S_{22} + S_{33}S_{32}\right)\right] - \\
&- \left(4\alpha_5\mu_t\kappa^2/3\varepsilon^2\right)\left(S_{33}\Omega_{31}\Omega_{13} + S_{33}\Omega_{32}\Omega_{23} + S_{12}\Omega_{31}\Omega_{32}\right) - \\
&- \left(2\alpha_5\mu_t\kappa^2/3\varepsilon^2\right)\left(S_{31}\Omega_{12}\Omega_{23} + S_{32}\Omega_{21}\Omega_{13} + S_{11}\Omega_{12}\Omega_{12}\right) - \\
&- \left(2\alpha_5\mu_t\kappa^2/3\varepsilon^2\right)\left(S_{11}\Omega_{13}\Omega_{13} + S_{22}\Omega_{21}\Omega_{21} + S_{22}\Omega_{23}\Omega_{23}\right) - \\
&- \left(\alpha_6\mu_t\kappa^2/\varepsilon^2\right)\left[S_{33}\left(S_{11}S_{11} + S_{22}S_{22} + S_{33}S_{33}\right) + 2S_{33}\left(S_{12}S_{12} + S_{13}S_{13} + S_{23}S_{23}\right)\right] - \\
&- \left(2\alpha_7\mu_t\kappa^2/\varepsilon^2\right)S_{33}\left(\Omega_{12}\Omega_{12} + \Omega_{13}\Omega_{13} + \Omega_{23}\Omega_{23}\right)
\end{aligned}
\tag{D.20}
$$

$$
\begin{aligned}
\tau_{12}^{R} &= -\rho\overline{u_1'u_2'} \\
&= \tau_{21}^{R} \\
&= \mu_t S_{12} - (\alpha_1\mu_t\kappa/\varepsilon)\left[\Omega_{12}\left(S_{22} - S_{11}\right) + \Omega_{13}S_{23} + \Omega_{23}S_{13}\right] - \\
&- (\alpha_2\mu_t\kappa/\varepsilon)\left(S_{11}S_{21} + S_{12}S_{22} + S_{13}S_{23}\right) - (\alpha_3\mu_t\kappa/\varepsilon)\,\Omega_{13}\Omega_{23} - \\
&- \left(\alpha_4\mu_t\kappa^2/\varepsilon^2\right)\Omega_{12}\left(S_{11}S_{11} + S_{31}S_{31} - S_{22}S_{22} - S_{32}S_{32}\right) - \\
&- \left(\alpha_4\mu_t\kappa^2/\varepsilon^2\right)\left[\Omega_{31}\left(S_{12}S_{13} + S_{22}S_{23} + S_{32}S_{33}\right) + \Omega_{32}\left(S_{11}S_{13} + S_{21}S_{23} + S_{31}S_{33}\right)\right] - \\
&- \left(\alpha_5\mu_t\kappa^2/\varepsilon^2\right)\left[S_{11}\Omega_{13}\Omega_{32} + S_{12}\left(2\Omega_{12}\Omega_{21} + \Omega_{13}\Omega_{31} + \Omega_{23}\Omega_{32}\right)\right] - \\
&- \left(\alpha_5\mu_t\kappa^2/\varepsilon^2\right)\left(S_{13}\Omega_{31}\Omega_{12} + S_{22}\Omega_{13}\Omega_{32} + S_{32}\Omega_{12}\Omega_{23}\right) - \\
&- \left(\alpha_6\mu_t\kappa^2/\varepsilon^2\right)\left[S_{12}\left(S_{11}S_{11} + S_{22}S_{22} + S_{33}S_{33} + 2S_{12}S_{12} + 2S_{13}S_{13} + 2S_{23}S_{23}\right)\right] - \\
&- \left(2\alpha_7\mu_t\kappa^2/\varepsilon^2\right)S_{12}\left(\Omega_{12}\Omega_{12} + \Omega_{13}\Omega_{13} + \Omega_{23}\Omega_{23}\right)
\end{aligned}
\tag{D.21}
$$

$$
\begin{aligned}
\tau_{13}^{R} &= -\rho\overline{u_1'u_3'} \\
&= \tau_{31}^{R} \\
&= \mu_t S_{13} - (\alpha_1\mu_t\kappa/\varepsilon)\left[\Omega_{13}\left(S_{33}-S_{11}\right)+\Omega_{12}S_{32}+\Omega_{32}S_{12}\right] - \\
&- (\alpha_2\mu_t\kappa/\varepsilon)\left(S_{11}S_{31}+S_{12}S_{32}+S_{13}S_{33}\right) - (\alpha_3\mu_t\kappa/\varepsilon)\,\Omega_{12}\Omega_{32} - \\
&- \left(\alpha_4\mu_t\kappa^2/\varepsilon^2\right)\Omega_{13}\left(S_{11}S_{11}+S_{21}S_{21}-S_{23}S_{23}-S_{33}S_{33}\right) - \\
&- \left(\alpha_4\mu_t\kappa^2/\varepsilon^2\right)\left[\Omega_{21}\left(S_{13}S_{12}+S_{23}S_{22}+S_{33}S_{32}\right)+\Omega_{23}\left(S_{11}S_{12}+S_{21}S_{22}+S_{31}S_{32}\right)\right] - \\
&- \left(\alpha_5\mu_t\kappa^2/\varepsilon^2\right)\left[S_{11}\Omega_{12}\Omega_{23}+S_{13}\left(2\Omega_{13}\Omega_{31}+\Omega_{12}\Omega_{21}+\Omega_{23}\Omega_{32}\right)\right] - \\
&- \left(\alpha_5\mu_t\kappa^2/\varepsilon^2\right)\left(S_{12}\Omega_{21}\Omega_{13}+S_{23}\Omega_{13}\Omega_{32}+S_{33}\Omega_{12}\Omega_{23}\right) - \\
&- \left(\alpha_6\mu_t\kappa^2/\varepsilon^2\right)\left[S_{13}\left(S_{11}S_{11}+S_{22}S_{22}+S_{33}S_{33}+2S_{12}S_{12}+2S_{13}S_{13}+2S_{23}S_{23}\right)\right] - \\
&- \left(2\alpha_7\mu_t\kappa^2/\varepsilon^2\right)S_{13}\left(\Omega_{12}\Omega_{12}+\Omega_{13}\Omega_{13}+\Omega_{23}\Omega_{23}\right) \qquad \text{(D.22)}
\end{aligned}
$$

$$
\begin{aligned}
\tau_{23}^{R} &= -\rho\overline{u_2'u_3'} \\
&= \tau_{32}^{R} \\
&= \mu_t S_{23} - (\alpha_1\mu_t\kappa/\varepsilon)\left[\Omega_{23}\left(S_{33}-S_{22}\right)+\Omega_{21}S_{31}+\Omega_{31}S_{21}\right] - \\
&- (\alpha_2\mu_t\kappa/\varepsilon)\left(S_{21}S_{31}+S_{22}S_{32}+S_{23}S_{33}\right) - (\alpha_3\mu_t\kappa/\varepsilon)\,\Omega_{21}\Omega_{31} - \\
&- \left(\alpha_4\mu_t\kappa^2/\varepsilon^2\right)\Omega_{23}\left(S_{22}S_{22}+S_{12}S_{12}-S_{13}S_{13}-S_{33}S_{33}\right) - \\
&- \left(\alpha_4\mu_t\kappa^2/\varepsilon^2\right)\left[\Omega_{12}\left(S_{13}S_{11}+S_{23}S_{21}+S_{33}S_{31}\right)+\Omega_{13}\left(S_{12}S_{11}+S_{22}S_{21}+S_{32}S_{31}\right)\right] - \\
&- \left(\alpha_5\mu_t\kappa^2/\varepsilon^2\right)\left[S_{22}\Omega_{21}\Omega_{13}+S_{23}\left(2\Omega_{23}\Omega_{32}+\Omega_{21}\Omega_{12}+\Omega_{31}\Omega_{13}\right)\right] - \\
&- \left(\alpha_5\mu_t\kappa^2/\varepsilon^2\right)\left(S_{21}\Omega_{12}\Omega_{23}+S_{13}\Omega_{23}\Omega_{31}+S_{33}\Omega_{21}\Omega_{13}\right) - \\
&- \left(\alpha_6\mu_t\kappa^2/\varepsilon^2\right)\left[S_{23}\left(S_{11}S_{11}+S_{22}S_{22}+S_{33}S_{33}+2S_{12}S_{12}+2S_{13}S_{13}+2S_{23}S_{23}\right)\right] - \\
&- \left(2\alpha_7\mu_t\kappa^2/\varepsilon^2\right)S_{23}\left(\Omega_{12}\Omega_{12}+\Omega_{13}\Omega_{13}+\Omega_{23}\Omega_{23}\right) \qquad \text{(D.23)}
\end{aligned}
$$

where μ_t is the turbulent eddy dynamic viscosity.

The coefficients used in Equation (D.16) are proposed by Kimura and Hosoda [84]

$$
\begin{aligned}
&\alpha_1 = c_3 - c_1; \quad \alpha_2 = c_1 + c_2 + c_3; \quad \alpha_3 = c_2 - c_1 - c_3; \\
&\alpha_4 = \alpha_5 = \alpha_6 = \alpha_7 = 0 \qquad \text{(D.24)}
\end{aligned}
$$

The coefficients, c_1, c_2, c_3, and c_μ are evaluated as follows:

$$c_1 = \frac{0.4}{1+0.01M^2}; \quad c_2 = 0; \quad c_3 = \frac{-0.13}{1+0.01M^2}; \quad c_\mu = min\left(0.09, \frac{0.3}{1+0.09M^2}\right) \tag{D.25}$$

where M=max$(\tilde{S}, \tilde{\Omega})$ and

$$\tilde{S} = \frac{\kappa}{\varepsilon}\sqrt{\frac{1}{2}\left(\frac{\partial \bar{u}_i}{\partial x_j} + \frac{\partial \bar{u}_j}{\partial x_i}\right)^2}; \quad \tilde{\Omega} = \frac{\kappa}{\varepsilon}\sqrt{\frac{1}{2}\left(\frac{\partial \bar{u}_i}{\partial x_j} - \frac{\partial \bar{u}_j}{\partial x_i}\right)^2} \tag{D.26}$$

Both nondimensional functions of the strain invariant $\tilde{S}$ and the vorticity invariant $\tilde{\Omega}$ were initially introduced by Pop [163].

Appendix E

Comparison between the single-processor and the parallel computing

E.1 Introduction

The multiprocessor and multicomputer based on multiple instruction stream, multiple data (MIMD) systems with both a shared-memory architecture and a distributed-memory architecture have had an explosive expansion in many areas of computational engineering. One of the message-passing programming paradigm, the Message-Passing Interface (MPI), is a standard library of subprograms used a distributed-memory method to write parallel programs binding for either Fortran or C languages [159, 160]. In this study the matrix free CBS-AC scheme has been implemented into a parallel environment with MPI model to test three-dimensional, steady and unsteady laminar flow past a stationary circular cylinder. The present results are compared against the numerically qualitative solutions by the single-processor system.

E.2 The Message-Passing Interface programming model

E.2.1 Starting and terminating communication

First preprocessor assigns `mpif.h` to definite for compiling an MPI library at every program. Then MPI routines can be employed in the program. In order to initialize the MPI identifier to lead to an error code, `MPI_INIT(ierror)` function must be called before any other MPI functions. At the end of MPI environment, the program terminates the MPI identifier must contain an error code using `MPI_FINALIZE(ierror)`.

For shutting down all the processes if any error occurs in the MPI environment, MPI function is written as

`MPI_ABORT    (communicator,ierror)`   (E.1)

All the MPI functions require the communicator to send message to each other in the communication domain for all the running processes. For this reason, the function, `MPI_COMM_WORLD` communicator, is to be performed in the executing program.

The parallel process have to determine its rank in the MPI implementation. Thus `MPI_COMM_RANK` function which ranges from zero to the size of `MPI_COMM_WORLD` minus one is asked to identify the rank of every process. For determining the number of processes to make executable MPI paradigm, `MPI_COMM_SIZE` is to be used in the communication domain.

There are several datatypes to determine which predefined type is needed for the MPI identifier to send message. It includes `MPI_DOUBLE_PRECISION`, `MPI_INTEGER`, `MPI_REAL8`, `MPI_CHARACTER`, `MPI_COMPLEX`, `MPI_LOGICAL` etc. However, each `MPI_datatype` can easily to correspond with Fortran data type.

E.2.2 Sending function and collectors for communication

There are two different ways of sending and receiving messages by MPI functions. The first command is to use tags to check enclosed messages on the typical message passing system. The exact syntax for sending and receiving MPI identifiers are, respectively, given as

MPI_SEND (buffer, reckoner, MPI_datatype, destination, tag, communicator, ierror)

MPI_RECV (buffer, reckoner, MPI_datatype, source, tag, communicator, stand, ierror) (E.2)

The function MPI_SEND sends the message put in the buffer area by the parameter buffer. The message are stored in the buffer area which depends on giving reckoner variable and choosing MPI_datatype. The destination of sending message whose rank of the process is determined by destination parameter. The message type is referenced by the integers tag of which standard value ranges from 0 to 32767. The MPI_COMM_WORLD function can be only used as the communicator for the message passing system in the communication domain. However, it should be noted that MPI_SEND uses the communicator arguments have to consistent with receiving function MPI_RECV. The source parameter serves as its identifier MPI_RECV for a message process to determine how many rank is needed. Any message is received and located in the buffer area does not exact same the amount of a message from the sending process. The tag of a receiving process is also employed with MPI_RECV to handle the number of messages. Since three information, source, tag and ierror, are necessary for return on the all processes, the stand parameter carries out this computation. All in all, both commands include error code in the ierror argument to detect any error occur in the MPI process.

The alternative pattern, MPI_BCAST function, sends the identified message to all the processes in the domain of collective communication. Its formulation of MPI paradigm can be written as

MPI_BCAST (buffer, reckoner, MPI_datatype, source, communicator, ierror) (E.3)

In the above MPI formulation the buffer area referenced by buffer allocates both sending and receiving messages based on available reckoner parameter and the data type is specified in the MPI environment. From the source process to any other process, the message is used to specify the only communicator MPI_COMM_WORLD with the rank of source. Since the collector MPI_BCAST does not use tag on all processes to recognize source and destination processes, every reckoner value and MPI_datatype must match on all the parallel process to return needed information, for instance source and ierror.

There are several operations undertaken to optimize MPI implementation. In this study, three predefined values i.e. MPI_SUM, MPI_MIN and MPI_MAX are, respectively, identified sum, minimum and maximum for performing MPI_REDUCE and MPI_ALLREDUCE functions. One of syntax of MPI subprogram is

$$\texttt{MPI\_REDUCE} \quad (\texttt{buffer\_send, buffer\_receve, reckoner, MPI\_datatype,} \\ \texttt{MPI\_operator, target, communicator, ierror}) \tag{E.4}$$

The reduction operation MPI_REDUCE provides the buffer memory to store sending messages in the buffer_send from each process and return the results via using MPI_operator computing in the buffer memory buffer_receve with the identified rank target on the process. The reckoner memory location and MPI_datatype are both used by buffer_send and buffer_receve parameters. However, MPI_COMM_WORLD communicator, MPI_operator reduction, MPI_datatype form with reckoner and target parameters have the same calculation on each process to be called by MPI_REDUCE.

In order to return the results toward original process, MPI_ALLREDUCE in the MPI library provides for its successive computation on the reduction operation. The function contains

$$\texttt{MPI\_ALLREDUCE} \quad (\texttt{buffer\_send, buffer\_receve, reckoner, MPI\_datatype,} \\ \texttt{MPI\_operator, communicator, ierror}) \tag{E.5}$$

In the above formulation since the reducing results return to all original processes, the rank referenced by target used for MPI_REDUCE is not needed any more with a call to MPI_ALLREDUCE.

One of basic communication operatior is known as all-to-all total exchange for the use of the design of data parallel model. The MPI implementation supplies two different forms to satisfy the process. The first form is only to be used in the same amount of message which have to send every process, i.e.

$$\texttt{MPI\_ALLTOALL} \quad (\texttt{buffer\_send}, \texttt{reckoner\_send}, \texttt{MPI\_datatype(send)}, \texttt{buffer\_receve}, \texttt{reckoner\_receve}, \texttt{MPI\_datatype(receve)}, \texttt{communicator}, \texttt{ierror}) \tag{E.6}$$

`MPI_ALLTOALL` determines how much large `reckoner_send` data stored in the `buffer_send` memory using the MPI data type send it to store in the buffer area `buffer_receve` by receving `MPI_datatype` in the communication domain `MPI_COMM_WORLD` via each parallel process. It is only to be called same amount of sequential data for every process.

If the MPI environment need to obtain different number of data from each calculating, then `MPI_ALLTOALLV` have to communicate this process. The function is given as

$$\texttt{MPI\_ALLTOALLV} \quad (\texttt{buffer\_send}, \texttt{reckoner\_send}, \texttt{shift\_send}, \texttt{MPI\_datatype(send)}, \texttt{buffer\_receve}, \texttt{reckoner\_receve}, \texttt{shift\_receve}, \texttt{MPI\_datatype(receve)}, \texttt{communicator}, \texttt{ierror}) \tag{E.7}$$

The positions of identified buffer area refer to `shift_send` as well as `shift_receve` for the interaction between sending and receving data on each process. Thus each process can send every other process the different quantity of computing data by using `MPI_ALLTOALLV`. From every other process, each process also receves the different quantity of computing data. However, the same number of processes in the `MPI_COMM_WORLD` communicator must be used for the several arrays of `reckoner_send`, `shift_send`, `reckoner_receve` and `shift_receve` parameters.

(a)
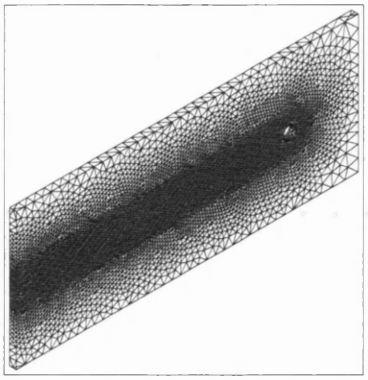
(b)
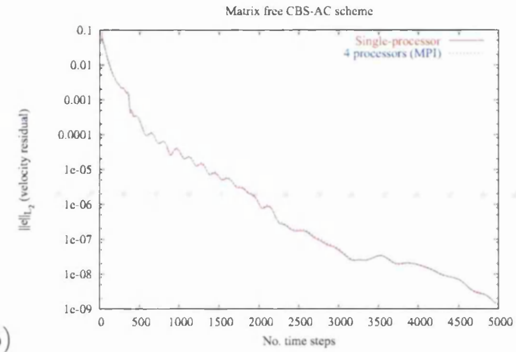

Figure E.1: Laminar flow around a circular cylinder. (a) Unstructured finite element meshes (Elements: 69948, Nodes: 17382); (b) Steady state convergence obtained at Re=20 using the matrix free CBS-AC scheme.

E.2.3 Data type constructors for communication

The MPI implementation provides derived data type for every process to construct individual data. Before any mechanism of derived data is employed in the communication domain, MPI program have to be committed and include error code to detect every process. Its syntax is

$$\texttt{MPI\_TYPE\_COMMIT} \quad (\texttt{datatype\_vector}, \texttt{ierror}) \tag{E.8}$$

In the above form the derived data type `datatype_vector` is employed by all `MPI_datatype` for the MPI system.

There are three data type constructors for communication, `MPI_TYPE_CONTIGUOUS`, `MPI_TYPE_VECTOR` and `MPI_TYPE_INDEXED`, to build the derived data type. In the present study, `MPI_TYPE_CONTIGUOUS` is only for the use of the MPI program. The formulation is given as

$$\texttt{MPI\_TYPE\_CONTIGUOUS} \quad (\texttt{reckoner}, \texttt{MPI\_datatype}, \texttt{datatype\_vector}, \texttt{ierror}) \tag{E.9}$$

The old data type `MPI_datatype` creates the vector to build the dervied type `datatype_vector` with a contiguous `reckoner` parameter in the function `MPI_TYPE_CONTIGUOUS`.

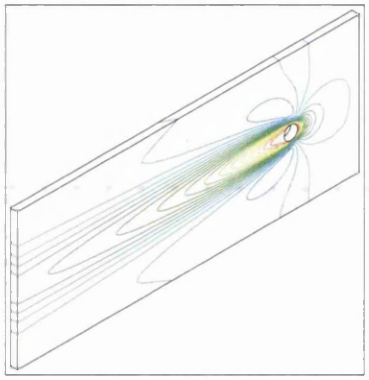

(a) u_1 velocity contours

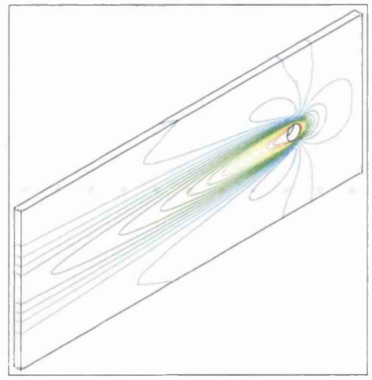

(b) u_1 velocity contours

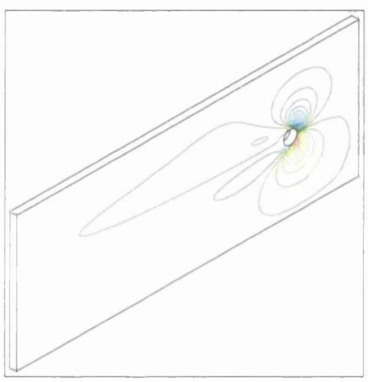

(c) u_3 velocity contours

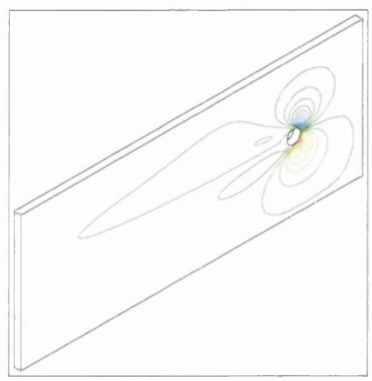

(d) u_3 velocity contours

Figure E.2: Steady laminar flow past a circular cylinder at Re=20 using the single-processor (left) and the 4 processors parallel computing (right) based on the matrix free CBS-AC scheme. (a) u_1 velocity contours. $u1_{min}$(red) = -0.022, $u1_{max}$(blue) = 1.336; (b) u_1 velocity contours. $u1_{min}$(red) = -0.022, $u1_{max}$(blue) = 1.335; (c) u_3 velocity contours. $u3_{min}$(red) = -0.535, $u3_{max}$(blue) = 0.626; (d) u_3 velocity contours. $u3_{min}$(red) = -0.535, $u3_{max}$(blue) = 0.627.

E.3 Three-dimensional laminar flow around a stationary circular cylinder

The primary objective of studying the low-Reynolds-number flow past a stationary circular cylinder here is to compare prediction of qualitative results from the single-processor and the

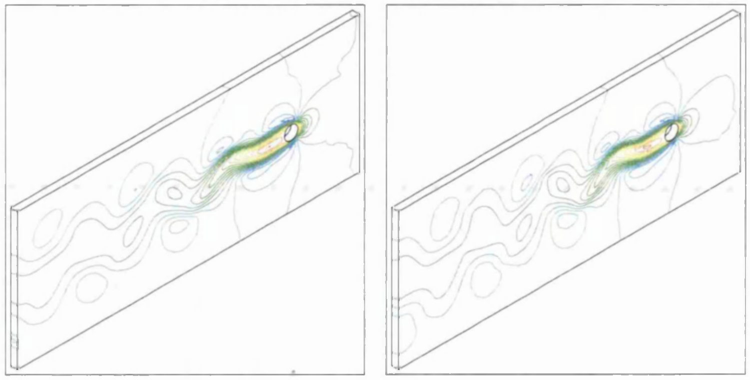

(a) u_1 velocity contours (b) u_1 velocity contours

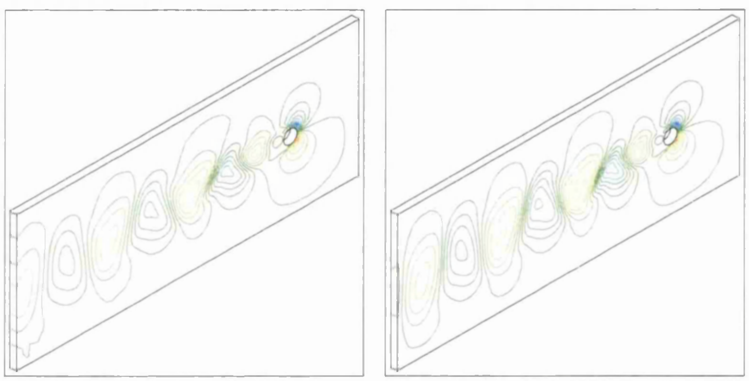

(c) u_3 velocity contours (d) u_3 velocity contours

Figure E.3: Unsteady laminar flow past a circular cylinder at Re=100 using the single-processor (left) and the 8 processors parallel computing based on the matrix free CBS-AC scheme. (a) u_1 velocity contours. $u_{1_{min}}$(red) = -0.186, $u_{1_{max}}$(blue) = 1.510; (b) u_1 velocity contours. $u_{1_{min}}$(red) = -0.206, $u_{1_{max}}$(blue) = 1.516; (c) u_3 velocity contours. $u_{3_{min}}$(red) = -0.696, $u_{3_{max}}$(blue) = 0.814; (d) u_3 velocity contours. $u_{3_{min}}$(red) = -0.692, $u_{3_{max}}$(blue) = 0.810.

parallel computing using the matrix free CBS-AC scheme. A constant horizontal-velocity was specified at the inflow and a no-slip condition was prescribed on the circular cylinder surface. All sides except exit are treated as symmetric planes.

For the low-Reynolds-number flow, the coarse mesh used is shown in Figure E.1(a).

This mesh was produced using the PSUE-II code.

Figure E.2 presents the qualitative solutions of the matrix free CBS-AC scheme using the single-processor and the parallel environment using 4 processors through the MPI library. These numerical results clearly show that all contours of the steady velocity field are identical.

The transient flow past a circular cylinder has been tested at the Reynolds number of 100. The matrix free CBS-AC scheme based on the dual time stepping procedure is employed with 8 processors on a parallel computing environment. Figure E.3 shows the qualitative comparison between the single-processor and parallel computing. As seen, the results are almost identical.

E.4 Summary

Steady and unsteady three-dimensional laminar flow around a circular cylinder has been performed in the parallel computing environment with message-passing interface (MPI) at the Reynolds number of 20 and 100. These qualitative results obtained are in agreement with numerical solutions from the single-processor calculation. It is noted that the matrix free CBS-AC scheme with the dual time stepping method is well suited for the MPI implementation.

Publication

[Journal papers]

1. Nithiarasu P, Liu CB. Steady and unsteady incompressible flow in a double driven cavity using the artificial compressibility (AC)-based characteristic-based split (CBS) scheme. *International Journal for Numerical Methods in Engineering* 2005; **63**(3):380–397.

2. Nithiarasu P, Liu CB. An artificial compressibility based Characteristic Based Split (CBS) scheme for steady and unsteady turbulent incompressible flows. *Computer Methods in Applied Mechanics and Engineering* (In press 2005)

3. Codina R, Coppola-Owen H, Nithiarasu P, Liu CB. Numerical comparison of CBS and SGS as stabilization techniques for the incompressible Navier-Stokes equations. *International Journal for Numerical Methods in Engineering* 2006; Special issue.

4. Liu CB, Nithiarasu P, Jones JW. Three dimensional RANS calculations on unstructured meshes using an explicit CBS scheme. *International Journal for Numerical Methods in Fluids* (to submit 2005)

5. Nithiarasu P, Liu CB. Laminar and turbulent flow calculations through a human upper airway using unstructured meshes. *Communications in numerical methods in engineering* 2006.

[Conference papers]

1. Liu CB, Nithiarasu P, Massarotti N. Incompressible turbulent flow calculations using the Characteristic Based Split (CBS) scheme on unstructured meshes. *The 11th Annual Association of Computational Methods in Engineering Conference*, ACME 2003, M.A. Wheel eds., University of Strathclyde, Glasgow, Scotland, UK, 24-25 April 2003; pp.161-164.

2. Liu CB, Nithiarasu P. Incompressible turbulent flow calculations using the explicit Characteristic Based Split (CBS) scheme on unstructured meshes. *The 4th European Congress on Computational Methods in Applied Sciences and Engineering*, ECCOMAS 2004, P. Neittaanmäki et al. eds., University of Jyväskylä, Jyväskylä, Finland, 24-28 July 2004.

3. Codina R, Coppola-Owem H, Nithiarasu P, Liu CB. Numerical comparison of CBS and SGS as stabilisation techniques for the incompressible Navier-Stokes equations. *The 4th European Congress on Computational Methods in Applied Sciences and Engineering*, ECCOMAS 2004, P. Neittaanmäki et al. eds., University of Jyväskylä, Jyväskylä, Finland, 24-28 July 2004.

4. Liu CB, Nithiarasu P. Explicit artificial compressibility based method using one and two equation turbulence models for incompressible flows. *The 13th Conference on Finite Elements for Flow Problems*, FEF05, University of Wales Swansea, Swansea, Wales, UK, 4-6 April 2005.